NASA Technical Memorandum 104617

Intercomparison of Hydrologic Processes in Global Climate Models

W. K.-M. Lau
Y. C. Sud
Goddard Space Flight Center
Greenbelt, Maryland

J.-H. Kim
Applied Research Corporation
Landover, Maryland

National Aeronautics and
Space Administration

Goddard Space Flight Center
Greenbelt, Maryland 20771
1995

This publication is available from the NASA Center for AeroSpace Information,
800 Elkridge Landing Road, Linthicum Heights, MD 21090-2934, (301) 621-0390.

Abstract

Preliminary results of the Atmospheric Model Intercomparison Project (AMIP) diagnostic subproject on "Intercomparison of Hydrologic Processes in Global Climate Models" are presented. The objective of the subproject is to evaluate the ability of atmospheric general circulation models (GCM) in simulating the global hydrologic cycle and to explore means of validating GCM precipitation and hydrologic processes with space-based and ground-based observations. Based on this evaluation, we hope to identify generic and/or specific strengths and weaknesses of the participating climate models which will help to formulate a strategy for model improvement.

In this report, we address the intercomparison of precipitation (P), evaporation (E), and surface hydrologic forcing (P-E) for 23 AMIP GCMs including relevant observations, over a variety of spatial and temporal scales. The intercomparison includes global and hemispheric means, latitudinal profiles, selected areal means for the tropics and extratropics, ocean and land, respectively. In addition, we have computed anomaly pattern correlations among models and observations for different seasons, harmonic analysis for annual and semiannual cycles, and rain-rate frequency distribution. We also compare the joint influence of temperature and precipitation on local climate using the Koeppen climate classification scheme.

Results show that the models collectively portray an Earthlike climate with respect to the observed land-only global mean surface temperature (=14.8 °C) and precipitation (=2.4 mm/day) to within 10%. The model consensus indicates a cold-wet bias of about 1.5 °C and 0.5 mm/day. Most of the models conserve atmospheric water up to about 5%. While most models show a rain-rate intensity distribution similar to that of the observed, almost all models underestimate the frequency of occurrence of light rain (<1 mm/day), suggesting some fundamental problems in the treatment of nonconvective rainfall in models. The major areas of deficiencies in global rainfall distribution are in the eastern Pacific Intertropical Convergence Zone (ITCZ), the South Pacific Convergence Zone (SPCZ), and the Asian monsoon. The main discrepancy in the ITCZ and the SPCZ is in the rainfall amount. In the Asian monsoon region, the problem seems to be more severe. None of the models are able to reproduce the East Asian monsoon rainbelt. Perhaps, not by happenstance, the disparities among observed estimates are also large in the above regions.

The model depiction of the hydrologic cycle tends to be more realistic where there is a strong annual cycle and where local moisture balance is the key operating mechanism, i.e., over large interior land mass in the extratropics. In regions of strong dynamical control (P-E >>0), i.e., over the tropical western Pacific, the monsoon region and the ITCZ, the differences among models tend to be large. In the interannual time scales, all models show enhanced rainfall prediction over the tropics because of sea surface temperature (SST) forcing, i.e., during El Niño Southern Oscilation (ENSO). However, the models do not show any useful skill for rainfall prediction in the extratropics from tropical SST forcing.

TABLE OF CONTENTS

1. Introduction

Under Atmospheric Model Intercomparison Project (AMIP), participating modeling groups carried out a 10-year integration (1979--1988) of atmospheric general circulation models (GCM) using daily sea surface temperature (SST) forcing derived from monthly mean observed SST field produced by Reynolds (1988). The goal of the project is to provide a common forum for global climate research groups to assess model capabilities, and to discuss and exchange information on all aspects of the model so as to determine the best strategy and priority for improving model performance (Gates, 1992). To diagnose the various aspects of the models, 27 diagnostic subprojects have been initiated. The following is a preliminary report for the subproject on "Hydrologic Processes in GCMs." This report is presented in the form of a technical report, which contains a large number of figures detailing the overall, as well as the individual, performance of the models in 15 key parameters and fields related to the regional and global hydrologic cycle. The discussion on each section will refer to sets of similar figures for each model and observation, if available. Figures will be numbered according to the section numbers. Appendices are given at the end for extended figure legends and for acronyms used for each model. The intent of this report is to provide readers and AMIP modelers, quick-look plots and easy reference to their own model performances in comparison with others, as well as available observations. For a description of the individual model characteristics, the readers are referred to Phillips (1994).

2. Global Temperature and Precipitation Relationship

The first step in the intercomparison is to determine whether the participating models are simulating an Earthlike climate as defined by the global mean surface temperature (T_S) and precipitation (P). Figure 1 shows the scattered plot of model global mean surface air temperature and precipitation over land and the one- (1-σ) and two- (2-σ) standard deviation limits spanned by the models. The land-only region is chosen because of more reliable observations of surface temperature and precipitation over land. The climatic state of the models and of the Earth is represented by a point in the T_S-P phase space. The global mean surface air temperature and precipitation show large variation among the models. The model mean surface temperature and rainfall over land is 13.4 ^{o}C and 2.7 mm/day with standard deviations 1.5 ^{o}C and 0.5 mm/day respectively. Compared with

the observed climatology of global surface temperature (= 14.8 ^{o}C) and precipitation (= 2.4 mm/day), it is fair to say that the models collectively are simulating Earthlike climates. As confirmed by subsequent analysis, models that lie outside the 2-σ limit (e.g., CSU and MGO, see Appendix A for model acronyms) have inherent inconsistencies in their representation of the global hydrologic cycle compared to observations. However, it does not imply that models lying within the 1-σ limit and/or close to the observed global climate state necessarily have a realistic distribution or evolution of the global hydrologic cycle.

Figure 1 also shows that the model's range can be as much as 6-7 ^{o}C in surface air temperature and up to 2.00 mm/day in precipitation. This is a substantial range that warrants attention, especially in the use of individual GCMs for global change scenarios relating to the global hydrologic cycle. The precipitation uncertainties alone can lead to approximately 60 Wm^{-2} differences in condensation heating. Errors of such magnitude can introduce large changes in the global circulation. Because these errors are often accompanied by other compensating errors, the circulation simulated by the GCMs may still be realistic in a broad scale sense, but the energy balance will not. Evidently, most models produce excessive precipitation and have lower surface temperature compared to those observed. This suggests a systematic cold-wet bias for most models. However, it must be remembered that the uncertainties in the observed global surface temperature and precipitation are also quite large.

3. Global Mean Precipitation (P)

Figure 2, top panel, shows the total global precipitation (70^{o} S to 70^{o} N) and its mean values over land and oceans, respectively, for each model and for different estimates based on observations. The variability among models (2.5 to 4.0 mm/day) is larger than observations (2.7 to 3.2 mm/day). This is true for both oceans and land. The global mean precipitation rate over the oceans is larger than that over land in the observation and in a majority of the models except DNM and GFD. However, most models, with the exception of DNM and CSI, show that the amplitude of the rainfall annual cycle is larger over land than over ocean (Figure 2, bottom panel). Here, the observations disagree among themselves, with JGR and MSU (see Appendix A for the definition of observation acronyms) showing larger annual cycles over land than over ocean, but the reverse for LWC and LWU. In general, the model annual cycles are much weaker than observed

annual cycles. Since the observed rainfall estimates differ as much as the models, at the present time, it is impossible to determine what the true magnitude of the annual cycle is.

4. Global Mean Evaporation (E)

The global mean evaporation shows large variations among the models (Figure 3, top panel). The range is 2.5-4.5 mm/day over the ocean and 1.5-2.5 mm/day over land. All models show that the annual variation is much stronger over land than over ocean. In large part, this is because of the same SST forcing is used for all models, so that the variability of ocean evaporation is constrained to follow the SST variation. However, most models have interactive land surface hydrology; therefore, the variability of land evaporation is much larger than that over the oceans (Figure 3, bottom panel).

5. Global Mean Evaporation Minus Precipitation (E-P)

The quantity E-P is a test of the conservation of water mass; by definition, this quantity should vanish when averaged over the globe for a long period. Figure 4.1 shows that most models have an approximate balance between global E and P. The differences over land, ocean, and hemispheric averages represent the degree of local water recycling over these spatial domains. Most models conserve water to within 5% of the total precipitation. Nonetheless, global conservation (error >5%) is apparently lacking in a few models (e.g., BMR, COL, SUN and UIU). On the average, all models show that the ocean (land) is a source (sink) of atmospheric moisture. During the entire 10-year period, the models show that the southern (northern) hemisphere generally is a source (sink) of atmospheric moisture, which implies that there is a net transport of atmospheric moisture from the southern to the northern hemisphere.

The E-P analysis is also carried out for all the four seasons (Figures 4.2 - 4.5). The models consistently show that the E-P imbalance (or the implied net transport of moisture) is always from ocean to land, and the amount is almost independent of the season. On the other hand, the northern and southern hemispheres reverse their roles as source and sink of atmospheric moisture as a function of the season. The moisture transport in all models except SUN is consistent from the winter hemisphere to the summer hemisphere. The strongest interhemispheric moisture transport occurs during summer (JJA) and the weakest

occurs in spring (MAM). While all models are consistent in depicting the direction of transport as a function of the season, the amount of transport varies greatly among them.

6. Normalized Rain-rate Frequency Distribution

The frequency distribution of the model rain rates is in general agreement with that of the observed (Figure 5.1). The distribution of the higher rain rates (monthly mean > 6-7 mm/day) is quite well modeled. Figures 5.2-5.3 shows that a common discrepancy among models is that they all underestimate the rain-rate frequency in the light rain category, i.e., 0-1 mm/day. This may be caused, in part, by sampling errors, but the magnitude of the discrepancy suggests that the differences are real. The systematic underestimates appear both over ocean and over land. The large and consistent differences suggest a fundamental deficiency in the representation of rainfall and moist processes in models. This deficiency may be related to the inadequate treatment of precipitation of the nonconvective type, i.e., mid- or low-level stratocumulus, shallow convection, and associated isolated showers, which are either absent or poorly represented in all models.

7. Zonal Precipitation

The AMIP models depict large variations in the zonal mean of precipitation as compared to the verification data (Figure 6.1). On the annual mean, most models agree well with the observations showing the equatorial ITCZ and the midlatitude maximum over the storm track latitudes. However, larger variations are found in the seasonal mean. In winter (DJF) (Figure 6.2), there is large variability among the models with respect to the magnitude and the location of the ITCZ. The observation shows a double maxima, with a minimum near the equator, but only a few of the models were able to reproduce this feature. All models fail to produce the high-latitude rainfall maximum over the southern oceans shown in the observations. However, this maximum in the observations is itself highly suspect because of the lack of in-situ observations and the difficulty of satellite rainfall algorithm to retrieve rainfall at high latitudes. In JJA (Figure 6.3), there is better agreement among models and observations in the position of the ITCZ. The models appear to produce a distinct subtropical minimum with a secondary maximum near 60^{o} N, while the observations suggest a broader shoulder in the rainfall profile in the subtropics and midlatitudes. These may be related to an overestimation of the effect of subsidence

associated with the northern summer monsoon meridional circulation. However, there is a major disagreement between MSU rainfall and the rest of the observations in the 30° N-60° N latitude belt over the northern Pacific, with the former indicating much higher rainfall in these latitudes. This is related to the different estimates of rainfall over the extratropical western Pacific associated with the *Mei-Yu* rainbelt in the East Asian monsoon (see discussion in Section 8).

8. Zonal Surface Hydrologic Forcing (P-E)

Over land, the models generally produce precipitation in excess of the observed (Figures 7.1-7.3). The excessive precipitation is generally accompanied by excessive evaporation; therefore, the P-E balance over land shows reasonable agreement with the estimated P-E (EST). Except for a few models, the 10-year annual mean P-E is positive over land, indicating that the land regions are sinks of atmospheric moisture. A negative P-E over land in the 10-year mean is physically unrealistic except for regions that gain water through river flow. Since river flow is not parameterized in any of the GCMs, negative P-E represents a continuous drying of the soil, which cannot be sustained because of the limited water-holding capacity of the soil. The excessive E and P over land appeared in the zonal averages may imply an excessively vigorous global hydrologic cycle. The excessive condensation heating of the atmosphere aloft, accompanied by the increased precipitation, however, is countered by an increase in net radiative cooling and a decrease in sensible heat flux at the surface, where the latter is caused by increased soil moisture and more evaporation. Thus, large E over land is accompanied by cooler land climate, as evidenced in the global mean land surface temperature (see Figure 1). It is clear that the diabatic heating errors are intertwined with complex energetics of the entire system. An improved precipitation simulation requires improvement in all the physical parameterizations which produce diabatic heating effects.

The water balance (P-E) over the ocean reflects the fresh water input in the deep tropics and at higher latitudes, which are supplied by evaporation over the subtropical oceans (Figure 7.4). Some of the fresh water flux into the tropics and higher latitudes are recycled through water transport by the oceanic circulation. As expected, the modeled seasonal average fields for DJF and JJA (Figures 7.5-7.6) and their departures from observations are much larger than the annual averages.

9. Precipitation Distribution

The global distribution of precipitation is shown in a three-panel plot containing yearly (ALL), winter (DJF) and summer (JJA) fields in Figures 8.1-8.4. There is considerable variability among the observed, as well as modeled, precipitation fields (Figures 8.1-8.3); however, this variability occurs at different locations in the observations vis-a-vis models. Some large differences among the corresponding observed fields (see for example, Jaeger (JGR) vs. MSU blended fields) must be taken into consideration in interpreting model performance. Figure 8.4 shows that the simulated precipitation in the spectral models shows serious spectral truncation noise which persists even in the 10-year average, e.g., DER and LMD. The grid point models such as GLA, GSF, UCL, and JMA, among others, produce much smoother rainfall fields.

As evident in the individual rainfall distribution in Figure 8.4, for many models, major deficiencies exist in the vicinity of mountains and regions of strong convection. The single-grid-point rain clusters, such as produced in COL, deserve a special attention; particularly in the DJF period over Eurasia. Overall, features that show the largest model-to-model variability, as well as disagreement among observations, are (i) the eastern tropical Pacific ITCZ, (ii) the SPCZ and (iii) the Asian monsoon rainfall. For the first two, most models are able to simulate the ITCZ and SPCZ in approximately the right locations so that the differences are mostly in the rainfall amount. This is an evidence that the model cumulus parameterizations are responding realistically to the tropical SST forcing to a first order. The low resolution in some models limits the better definition of the eastern Pacific ITCZ. For the Asian monsoon rainfall, the problem is more profound. Many models do not produce the rainfall maximum over western India and the Bay of Bengal. More seriously, none of the models is able to produce the East Asian *Mei-yu* rainbelt during JJA. This well-known feature is also absent in all climatologies, except those based on the MSU. Past studies of the East Asian monsoon (e.g., Lau and Li, 1984) indicate that the *Mei-yu* rainbelt arises from an anchoring of the stationary wave pattern with respect to the Tibetan plateau, providing favorable conditions for interaction between midlatitude baroclinic processes and tropical convection. It appears that most models fail to capture the physics of that particular interaction. It will be a major challenge for AMIP-like climate models to simulate regional features such as those discussed above. Arguably, most participating AMIP models are not yet ready for that.

10. Evaporation Distribution

The global evaporation field is shown in Figure 9. At the present time, this is essentially an unverifiable field. When the data assimilation products yield realistic moisture transports, the evaporation can be inferred from the sum of precipitation and vertically integrated moisture divergence. The other alternative is to calculate the surface hydrology and use the four-way balance among soil moisture, runoff, evapotranspiration, and precipitation. An interesting feature of the evapotranspiration field is the appearance of spectral truncation noise in the simulated evaporation, even over oceans, where smooth SST is prescribed. The most important feature is the increased evaporation over the Kuroshio region and the Gulf coast of North America during DJF. Another important feature is the increased evaporation over the northern Indian Ocean during JJA. These features are consistent with Oberhufer (1988), and the models are quite consistent in portraying these features.

11. East-West Excursion of Tropical Precipitation

Figure 10 shows the time-longitude cross-section of precipitation averaged between 10° S-10° N. This field shows a high degree of variability within and among models. The eastward excursion of the precipitation anomalies during the 1982-83 and 1986-87 ENSO is well captured by most, but not all, of the models. For models that produce the ENSO precipitation anomalies, the detailed evolution of the anomalies varies substantially among them. The ENSO signals are notably absent in the DNM and UIU and very weak in the GSF, MGO and MRI. In general, the year-to-year variabilities show major deficiencies compared to observations.

In the MSU rainfall, two convective zones -- one over the Indian Ocean (80° E-100° E) and one over the western Pacific (140° E-160° E) -- can be identified. Sandwiched between these two regions is an area of reduced rainfall over the maritime continent (110° E-130° E). Occurrences of rainfall over the maritime continent appear to be tied to eastward propagating features, which are most likely associated with the Madden and Julian Oscillation (MJO, see Lau and Chan, 1986). The suppressed convection/rainfall over the maritime continent is mimicked by most models. However, the suppression is too extreme and too regular in many models, i.e., BMR, COL, DNM, LMD, and SUN. This may be related to the excessive anchoring of the model precipitation to isolated land

masses along the equator, i.e., the longitudes of 100° E and 140° E. The appearance of artificial lines of rainfall on the time axis of the plots is also quite obvious in the above-mentioned models. The eastward propagating signals are poorly represented, and this may be related to the lack of realistic representation of MJO in many of the models. Models that have strong MJO (e.g., CSI and GLA) show eastward propagation resembling the MSU observation.

12. North-South Excursion of Asian Monsoon Precipitation

Compared to the east-west variation, the north-south excursion of Asian Monsoon (60° E-150° E) precipitation is well simulated by most of the models (Figure 11.1), even though considerable deficiencies can still be noted. An important feature in the meridional excursion is the hemispheric asymmetry, i.e., more rapid onset of the northern summer monsoon and the relatively slower evolution of the Australian monsoon. In a broad sense, this feature is captured by roughly half of the models. The northern summer monsoon is notably missing or very weak in a large number of models (e.g., CSI, CSU, LMD, NMC, SUN, UCL, and UIU). On the other hand, there are models that show a monsoon cycles that are too strong and regular compared with the observation (e.g., BMR, DER, GLA, NCA, and UKM). The latitudinal sections of precipitation from the equator to 60° N averaged between 120° E-150° E (Figure 11.2) show that none of the models produce the secondary rain maximum related to the extension of the monsoon trough or *Mei-yu* rain band over East Asia and the north-western Pacific. This is consistent with the discussion in Section 8.

13. Tropical Rainfall Anomaly Correlation

Figure 12 shows the anomaly correlation between the model simulated rainfall in the tropics (30° N - 30° S) with the observation based on MSU, for each of the 39 seasons over the 10-year period. Most models show an enhancement in rainfall prediction skill (correlation >0.4) in the tropics during the 1982-83 and the 1986-87 ENSO. During the non-ENSO periods, such as 1979-81 and 1984-85, the skills are notably low for all models. Operational models such as BMR, ECM, JMA, MPI, and UKM, show significantly better skills than the rest. Among the non-operational models, CNR, CSI, COL, GLA, and LMD models do quite well, even though the LMD has exhibited some

problems in other diagnostics. Interestingly, the cases of negative skills among all bar plots is not only quite low, but the magnitudes of such negative skills are quite small. Thus, a majority of the models produce some useful skills in the tropics. Nonetheless, a similar calculation (not shown) indicates that no useful rainfall prediction skills are found in the extratropics for all models .

14. Annual and Semiannual Harmonics

The vectors for annual and semiannual harmonics are plotted for nine chosen regions shown in Figures 13.1-13.5. In regions with strong annual cycle or monsoon characteristics, such as Amazon, Australia, East Asia, South Asia and the Sahel, the annual harmonics are reasonably simulated by most of the models (Figure 13.2). The phases of the annual cycle in these regions are predicted to within about 1 or 2 months of the observed. However, in the Mississippi basins and TOGA-COARE regions, there are major problems in the magnitude and the phase of the simulated annual cycle. The problems are more serious, especially in the latter, where deep tropical convection prevails. In general, we noted that in regions where a strong annual cycle is absent, the models tend to have more divergent behavior. The annual cycle for E-P (Figure 13.3) shows a closer agreement among models. The models disagree most in the Sahel and over the TOGA-COARE region.

The models also show large variability in the semiannual cycle in P and in E-P in all the above regions (Figure 13.4). Except over the Sahel, most models tend to overestimate the strength of the semiannual cycle. In the equatorial regions, the semiannual harmonic is related to the overhead passage of the Sun twice a year. In regions farther away from the equator, the semiannual harmonic may be simply a reflection of the asymmetric nature of the summer monsoon rainfall, i.e., rainfall occurs only during the summer months, while the remainding calendar months are dry. Compared to observations, the models appear to overemphasize the asymmetric aspect of the annual rainfall.

15. Moisture Recycling Over Continental Regions

The quantity, E-P can be used to infer the amount of moisture recycling within continental scale and large spatial domains. This quantity has been estimated from analysis

of observed precipitation in a surface hydrology model based on SiB (Liston et al., 1993). Figure 14 shows the time history of E-P of the 'observed' and that of each model for the AMIP integration period. In spite of the large degree of variability among models, most of the models are able to reproduce the annual variation in E-P. The following inference can be drawn regarding the role that each region plays in the variation of the global hydrologic cycle. All large tropical land masses (e.g., Amazon, East-Asia, and South-Asia) are moisture sinks (E-P<0). During the rainy season, E-P is large and negative, implying a net transport of moisture into the region and a large run-off from land to ocean, assuming that the land is well-saturated by the excessive rain. During the dry season, the land masses act as a moisture source, i.e., evapotranspiration exceeds precipitation. However, this supply is exceeded by the demand for moisture in the rainy season. Hence, regions with negative E-P are controlled by the atmosphere with strong remote forcing by monsoon dynamics involving large transport of moisture from the adjacent oceans. In contrast, the annual and long-term mean of E-P over Australia is close to zero, indicating that evaporation and soil moisture may play an important role in the regional recycling of moisture over this continent.

One of the most remarkable features is the agreement among models and observation in the annual variation of E-P over Europe. Here, the annual variation is almost perfectly sinusoidal, and the moisture sink and source are almost completely compensated within one annual cycle. This region is characterized by a strong control by the insolation and local energy balance. The interannual variability of E-P over this region is also very small. Other regions where local moisture recycling may be important are the Sahel and Siberia. Here, with a few exceptions, the model E-P estimates remain small throughout the year. The exceptions generally correspond to models that have problems in other aspects such as distribution and water balance. For example, the larger annual cycle of E-P depicted by SUN is apparently spurious, because of the nonconservation of water in the global mean (see Figure 4) and the unrealistic rainfall distribution, e.g., at high latitudes for that model (see Figure6). Over the tropical Pacific warm pool, i.e., the TOGA-COARE region, all models show a large E-P deficit, but the month-to-month variability does not show any agreement among models. As discussed earlier, the moisture needed to supply the heavy rainfall in this region has to be transported from the subtropical Pacific ocean and the Indian Ocean (see discussion for Figure 9). The lack of control by a strong annual cycle may contribute to the large model disparity.

16. Koeppen Climate Classifications

The joint distribution of observed and modeled surface air temperature and rainfall are presented in the form of maps according to the Koeppen climate classification (Figure 15). The detailed explanation for color codes is provided in the Appendix B. A simplified interpretation of the color code is as follows. The subtropical dry zones are indicated by bright yellow, the major desert climate by dark yellow or brown. The moist, tropical climate is indicated by a rich red tone while the rainy, midlatitude zones are shown in green and the frigid polar regions are in blue. On the broadest scale, most models are able to simulate the large-scale climate regimes quite well; however, the regional differences among models are substantial. For example, the north-south excursion of monsoon shows considerable deficiency in many models. The East-Asian and Indian monsoons also show major deficiencies. The extent of subtropical highs and desert climate over central Asia and that over the Australian continent varies greatly from model to model. There are many other interesting details in the Koeppen maps for each model, but they are outside the scope of the discussion in this report.

17. Summary

We have presented results of an intercomparison study of the global hydrologic cycle in 23 AMIP global climate models. The main results are summarized as follows:

- The models collectively portray an Earthlike climate with respect to the observed global surface temperature (=14.8 °C) and precipitation (2.4 mm/day) to within 10%. The model consensus indicates a cold-wet bias of about 1.5 °C and 0.5 mm/day.

- With the exception of a few, most models conserve atmospheric water to within 5% and consistently indicate the role of ocean (land) as moisture source (sink), and the southern (northern) hemisphere as moisture source (sink) on the long-term mean. The seasonal reversal of the northern (southern) hemisphere as a moisture source (sink) is also well simulated.

- While the overall model rain-rate frequency distributions resemble the observed, almost all models underestimate the frequency of occurrence of light rain (monthly mean<1 mm/day), compared to observations. This suggests that there may be fundamental problems in the treatment of nonconvective rainfall in the models.

- The main features of the global rainfall distribution are reproduced by most models. The most common problems are the presence of spectral rain (Gibbs phenomenon) or spurious grid-point scale heavy rain in a number of the models. The artificial anchoring of rainfall to topographic features in the maritime continent also appear to be a problem in many models.

- Models (as well as observations) differ greatly in the magnitude of the rainfall amount over the SPCZ and the eastern Pacific ITCZ. The definition of the latter is apparently limited by the low-resolution nature of most of the models. The model simulations of the magnitude and location of rainfall have the worst problem over the Asian monsoon region. Generally, models do not simulate well the northward migration of the convective zone. No models are able to reproduce the East Asian monsoon rainbelt over the subtropical western Pacific.

- In general, the model depiction of the hydrologic cycle tends to be more realistic where there is a strong annual cycle and where long-term local moisture balance is maintained, i.e., $(E-P) \approx 0$, over large interior land regions in the extratropics. In regions of strong dynamic control, i.e., $(E-P) \ll 0$, tropical western Pacific, monsoon regions, and ITCZ, the model differences are largest.

- In the interannual time scale, all models show enhanced rainfall prediction skill in the tropics because of SST forcing associated with ENSO. The models do not show any useful skill for rainfall prediction in the extratropics due to tropical SST forcing.

Because of the relatively large number of models participating in AMIP, the results may be considered more representative compared to previous studies where only a few models are intercompared. Still, the above results should not be generalized to the much larger population of models, in particular, those that did not participate in AMIP. Moreover, the strengths and weaknesses identified in the models should not be regarded as a permanent label for the individual models, since almost all the models are undergoing continuous improvement. In this regard, the above assessments can only be viewed as a snapshot of an evolving climate modeling community. The present intercomparison has identified specific, as well as generic, problems in simulating the global hydrologic cycle for the participating AMIP models. The more difficult tasks of matching the detailed representation of hydrologic processes in each model to its performance and coming up with ways of improvement still lie ahead. The AMIP project has provided a most important first step toward this goal.

Acknowledgements

This work is supported jointly by the NASA EOS Interdisciplinary Investigation and the Climate Dynamics and Modeling Program at Office of the Mission to Planet Earth. The Program for Climate Model Diagnostics and Intercomparison, Lawerence Livermore National Laboratory coordinated the model intercomparison activity and provided model output for this study. Figures in this technical memorandum are generated by GrADS courtesy of Brian Doty. Dr. Mike Fiorino provided the FORTRAN program and GrADS script for the Koeppen Climate Classification.

REFERENCE

Baumgartner, A. and E. Reichel, 1975, The World Water Balance, Elsevier, Amsterdam, 179 pp.

Gates, W. L., 1992, AMIP, The Atmospheric Model Intercomparison Project., *Bull. Amer. Meteor. Soc.*, **73**, 1962-1970.

Jaeger, L., 1976, Montatskarten des Niederschlages fur die ganze Erde, Ber. Dtsch. Wetterienst, **18**, 38 pp.

Kim, J.-H., and Y. C. Sud, 1993, Circulation and rainfall climatology of a 10-year (1979-1988) integration with the Goddard Laboratory for Atmospheres General Circulation Model, *NASA Technical Memorandum 104591*, 247 pp.

Lau, K. M., and M. T. Li , 1984, The monsoon of East Asia and its global associations - a survey, *Bull. Amer. Meteor. Soc.*, **65**, 114-125.

Lau, K. M., and P. H. Chan, 1986, The El Nino Southern Oscillation and the 40-50 day oscillation, a new perspective. *Bull. Amer. Meteor. Soc.*, **67**, 533-534.

Legates, D. R., and C. J. Wilmott, 1990, Mean seasonal and spatial variability in gauge corrected, global precipitation. *Int. J. Climat.*, **10**, 111-127.

Liston, G. E., Y. C. Sud, and G. K. Walker, 1993, Design of a Global Soil Moisture Initialization Procedure for the Simple Biosphere Model, *NASA Technical Memorandum 104590*, 130 pp.

Mintz, Y., and G. K. Walker, 1993, Global fields of soil moisture and land surface evapotranspiration derived from observed precipitation and surface air temperature. J. *Appl. Meteorol.*, **32**, No. 8, 1305-1334.

Oberhuber, J. M., 1988, The budgets of heat, buoyancy and turbulent kinetic energy at the surface of the global ocean, *in Report 15, Max Planck Inst. fur Meteorol.*, Hamburg, Germany.

Peixoto, J. P., and A. H. Oort, 1992, Physics of climate, *American Institute of Physics*, New York, 520 pp.

Peixoto, J. P., and M. A. Kettani, 1973, The control of the water cycle, *Sci. Am.* **228**, 46-61.

Phillips, T., 1994, A summary documentation of the AMIP models. *PCMDI Report No. 18*, 343 pp.

Reynold, R., 1988, A real-time global sea surface temperature analysis. *J. Climate*, **1**, 75-86.

Schemm, J., S. Schubert, J. Terry, and S. Bloom, 1992, Estimates of monthly mean soil moisture for 1979-1989. *NASA Technical Memorandum 104571*, 254 pp.

Spencer, R. W., 1993, Global oceanic precipitation from the MSU during 1979-91 and comparisons to other climatologies, *J. Climate*, **6**, 1301-1326.

Appendix A: Acronyms for AMIP Models and validation datasets

BMR: Bureau of Meteorology Research Centre
CCC: Canadian Centre for Climate Research
CNR: Centre National de Recherches Mitiorologiques
COL: Center for Ocean-Land-Atmosphere Studies
CSI: Commonwealth Scientific and Industrial Research Organization
CSU: Colorado State University
DER: Dynamical Extended Range Forecasting (at GFDL)
DNM: Department of Numerical Mathematics of the Russian Academy ofSciences
ECM: European Centre for Medium-Range Weather Forecasts
GFD: Geophysical Fluid Dynamics Laboratory
GLA: Goddard Laboratory for Atmospheres
GSF: Goddard Space Flight Center
JMA: Japan Meteorological Agency
LMD: Laboratoire de Mitiorologie Dynamique
MGO: Main Geophysical Observatory
MPI: Max-Planck-Institut fuer Meteorologie
MRI: Meteorological Research Institute (of Japan)
NCA: National Center for Atmospheric Research
NMC: National Meteorological Center
SUN: State University of New York at Albany
UCL: University of California, Los Angeles
UIU: University of Illinois
UKM: United Kingdom Meteorological Office

* Rainfall verification

JGR: Jaeger climatology, 12-month monthly mean
LWU: Lagates/Willmott climatology, uncorrected, 12-month monthly mean
LWC: Lagates/Willmott climatology, corrected, 12-month monthly mean
MSU: Microwave Sounding Unit version-1 rainfall over ocean blended with rain gauge data over land on 4x5 grid from January, 1979 to December, 1989.

Appendix B: Koeppen Climate Classification

Af is the tropical rainforest climate.
- The mean temperature of every month is above 18 °C (64 °F), and the climate is not **BS** or **BW** (see below).
- Every month has at least 6 cm of rain.

Am is the tropical rainforest/monsoon and trade wind climate.
- The mean temperature of every month is above 18 °C, and the climate is not **BS** or **BW**.
- The driest month has less than 6 cm of rain but greater than 10 - $pr_{tot}/25$, where pr_{tot} is the total annual rainfall in cm.

Aw is the wet dry tropical savanna climate.
- The mean temperature of every month is above 18 °C, and the climate is not **BS** or **BW**.
- The driest month has less than 6 cm of rain and less than 10 - $pr_{tot}/25$, where pr_{tot} is the total annual rainfall in cm.

BSh is the low-latitude and midlatitude, dry, hot steppe climate.
- The summer rain is ge 70 percent of the total rainfall and $2*T_{ave}+28 > Prtot(cm) > T_{ave}+14$; or the winter rain is ge 70 percent of the total and $2*T_{ave} > prtot(cm) > T_{ave}$. If neither summer rain nor winter rain dominates then $Tave+7 < prtot(cm) < 2*Tave+14$.
- The mean annual temperature is above 18 °C.

BSk is the dry, midlatitude, cold steppe climate.
- The summer rain is ge 70 percent of the total rainfall and $2*T_{ave}+28 > prtot(cm) > T_{ave}+14$; or the winter rain is > 70 percent of the total and $2*T_{ave} > prtot(cm) > T_{ave}$. If neither summer rain or winter rain dominates then $T_{ave}+7 < prtot(cm) < 2*T_{ave}+14$.
- The mean annual temperature is below 18 °C and the warmest month is above 0 °C.

BWh is the dry, tropical and subtropical, hot desert climate.
- The summer rain is ge 70 percent of the total rainfall and $prtot(cm) < T_{ave}+14$; or the winter rain is ge 70 percent of the total and $prtot(cm) < T_{ave}$. If neither summer rain nor winter rain dominates then $prtot(cm) < T_{ave}+7$.
- The mean annual temperature is above 18 °C.

BWk is the dry, midlatitude, cold desert climate.
- The summer rain is ge 70 percent of the total rainfall and $prtot(cm) < T_{ave}+14$; or the winter rain is ge 70 percent of the total and $prtot(cm) < T_{ave}$. If neither summer rain or winter rain dominates then $prtot(cm) < T_{ave}+7$.
- The mean annual temperature is below 18 °C and the warmest month is above 0 °C.

Cwa is mild tropical climate with wet summers and dry winters.
- Coldest month has an average temperature below 18 °C but above -3 °C, and at least 1 monthly mean is above 10 °C. - The wettest month of the summer has at least 10 times the precipitation of the driest month of the winter or at least 70 percent of the rain falls in the 6 summer months. - The warmest mean monthly temperature is above 22 °C, and at least 4 months have mean temperatures above 10 °C.

Cwb is mild tropical climate with wet summers and dry winters.
- Coldest month has an average temperature below 18 °C but above -3 °C, and at least 1 monthly mean is above 10 °C. - The wettest month of the summer has at least 10 times the precipitation of the driest month of the winter or at least 70 percent of the rain falls in the 6 summer months. - The warmest mean monthly temperature is below 22 °C, and at least 4 months have means above 10 °C.

Cwc is mild tropical climate with wet summers and dry winters.
- Coldest month has an average temperature below 18 °C but above -3 °C, and at least 1 monthly mean is above 10 °C. - The wettest month of the summer has at least 10 times the precipitation of the driest month of the winter or at least 70 percent of the rain falls in the 6 summer months. - The warmest mean monthly temperature is below 22 °C, and 1, 2, or 3 months have means above 10 °C.

Csa is the Mediterranean climate.
- Coldest month has an average temperature below 18 °C but above -3 °C, and at least 1 monthly mean is above 10 °C. - Precipitation of the driest month of summer is less than 3 cm; precipitation of the wettest winter month is at least 3 times as much as the driest month of the summer or at least 70 percent of the rain falls in the 6 winter months. - The warmest mean monthly temperature is above 22 °C and at least 4 months have mean temperatures above 10 °C.

Csb is the Mediterranean climate (marine west-coast climate).
- Coldest month has an average temperature below 18 °C but above -3 °C, and at least 1 monthly mean is above 10 °C. - Precipitation of the driest month of summer is less than 3 cm; precipitation of the wettest winter month is at least 3 times as much as the driest month of the summer or at least 70 percent of the rain falls in the 6 winter months. - The warmest mean monthly temperature is below 22 °C, and at least 4 months have means above 10 °C.

Csc is the Mediterranean climate.
- Coldest month has an average temperature below 18 °C but above -3 °C, and at least 1 monthly mean is above 10 °C. - Precipitation of the driest month of summer is less than 3 cm; precipitation of the wettest winter month is at least 3 times as much as the driest month of the summer or at least 70 percent of the rain falls in the 6 winter months. - The warmest mean monthly temperature is below 22 °C, and 1, 2, or 3 months have means above 10 °C.

Cfa is mild climate with no dry season (moist subtropical climate).
- Coldest month has an average temperature below 18 °C but above -3 °C, and at least 1 monthly mean is above 10 °C. - Precipitation is not dominant in the summer or winter months. - The warmest mean monthly temperature is above 22 °C and at least 4 months have averages above 10 °C.

Cfb is mild climate with no dry season (marine west-coast climate).
- Coldest month has an average temperature below 18 °C but above -3 °C, and at least 1 monthly mean is above 10 °C. - Precipitation is not dominant in the summer or winter months. - The warmest mean monthly temperature is below 22 °C, and at least 4 months have means above 10 °C.

Cfc is mild climate with no dry season (boreal forest climate).
- Coldest month has an average temperature below 18 °C but above -3 °C, and at least 1 monthly mean is above 10 °C. - Precipitation is not dominant in the summer or winter months. - The warmest mean monthly temperature is below 22 °C, and 1, 2, or 3 months have means above 10 °C.

Dwa is cold snowy-forest climate with dry winters.
- Coldest monthly mean is below -3 °C, and the warmest monthly mean is above 10 °C.
- The wettest month of the summer has at least 10 times the precipitation of the driest month of the winter or at least 70 percent of the rain falls in the 6 summer months. - The warmest mean monthly temperature is above 22 °C and at least 4 months have averages above 10 °C.

Dwb is cold snowy-forest climate with dry winters.
- Coldest monthly mean is below -3 °C, and the warmest monthly mean is above 10 °C.
- The wettest month of the summer has at least 10 times the precipitation of the driest month of the winter or at least 70 percent of the rain falls in the 6 summer months. - The warmest mean monthly temperature is below 22 °C, and at least 4 months have means above 10 °C.

Dwc is cold snowy-forest climate with dry winters.
- Coldest monthly mean is below -3 °C, and the warmest monthly mean is above 10 °C.
- The wettest month of the summer has at least 10 times the precipitation of the driest month of the winter or at least 70 percent of the rain falls in the 6 summer months. - The warmest mean monthly temperature is below 22 °C, and 1, 2, or 3 months have means above 10 °C.

Dwd is cold snowy-forest climate with dry winters.
- Coldest monthly mean is below -3 °C, and the warmest monthly mean is above 10 °C.
- The wettest month of the summer has at least 10 times the precipitation of the driest month of the winter or at least 70 percent of the rain falls in the 6 summer months. - The warmest mean monthly temperature is below -38 °C, and less than 4 months have means above 10 °C.

Dsa is a cold Mediterranean climate (a non-existent climate on Earth).
- Coldest monthly mean is below -3 °C, and the warmest monthly mean is above 10 °C.
- Precipitation of the driest month of summer is less than 3 cm; precipitation of the wettest winter month is at least 3 times as much as the driest month of the summer or at least 70 percent of the rain falls in the 6 winter months. - The warmest mean monthly temperature is above 22 °C and at least 4 months have averages above 10 °C.

Dsb is a cold Mediterranean climate (a non-existent climate on Earth).
- Coldest monthly mean is below -3 °C, and the warmest monthly mean is above 10 °C.
- Precipitation of the driest month of summer is less than 3 cm; precipitation of the wettest winter month is at least 3 times as much as the driest month of the summer or at least 70 percent of the rain falls in the 6 winter months. - The warmest mean monthly temperature is below 22 °C, and at least 4 months have means above 10 °C.

Dsc is a cold Mediterranean climate (a non-existent climate on Earth).
- Coldest monthly mean is below -3 °C, and the warmest monthly mean is above 10 °C.
- Precipitation of the driest month of summer is less than 3 cm; precipitation of the wettest winter month is at least 3 times as much as the driest month of the summer or at least 70 percent of the rain falls in the 6 winter months. - The warmest mean monthly temperature is below 22 °C, and 1, 2, or 3 months have means above 10 °C.

Dsd is a cold Mediterranean climate (a non-existent climate on Earth).
- Coldest monthly mean is below -3 °C, and the warmest monthly mean is above 10 °C.
- Precipitation of the driest month of summer is less than 3 cm; precipitation of the wettest winter month is at least 3 times as much as the driest month of the summer or at least 70 percent of the rain falls in the 6 winter months. - Coldest monthly mean is below -3 °C, and the warmest monthly mean is above 10 °C.
- The warmest mean monthly temperature is below -38 °C, and less than 4 months have means above 10 °C.

Dfa is cold snowy-forest climates with hot summers (moist continents).
- Coldest monthly mean is below -3 °C, and the warmest monthly mean is above 10 °C.
- Precipitation is not dominant in the summer or winter months. - The warmest mean monthly temperature is above 22 °C and at least 4 months have averages above 10 °C.

Dfb is cold snowy-forest climates with warm summers (moist continents).
- Coldest monthly mean is below -3 °C, and the warmest monthly mean is above 10 °C.
- Precipitation is not dominant in the summer or winter months. - The warmest mean monthly temperature is below 22 °C, and at least 4 months have means above 10 °C.

Dfc is cold snowy-forest climates with cool summers (high-latitudes).
- Coldest monthly mean is below -3 °C, and the warmest monthly mean is above 10 °C.
- Precipitation is not dominant in the summer or winter months. - The warmest mean monthly temperature is below 22 °C, and 1, 2, or 3 months have means above 10 °C.

Dfd is cold snowy-forest climates with cool summers (high-latitudes).
- Coldest monthly mean is below -3 °C, and the warmest monthly mean is above 10 °C.
- Precipitation is not dominant in the summer or winter months. - The warmest mean monthly temperature is below -38 °C, and less than 4 months have means above 10 °C.

ET is the polar tundra climate. The warmest mean monthly temperature is less than 10 °C but greater than 0 °C.

EF is the polar, perpetual frost (ice sheet) climate. The mean of every month is less than 0 °C.

FIGURE LEGENDS

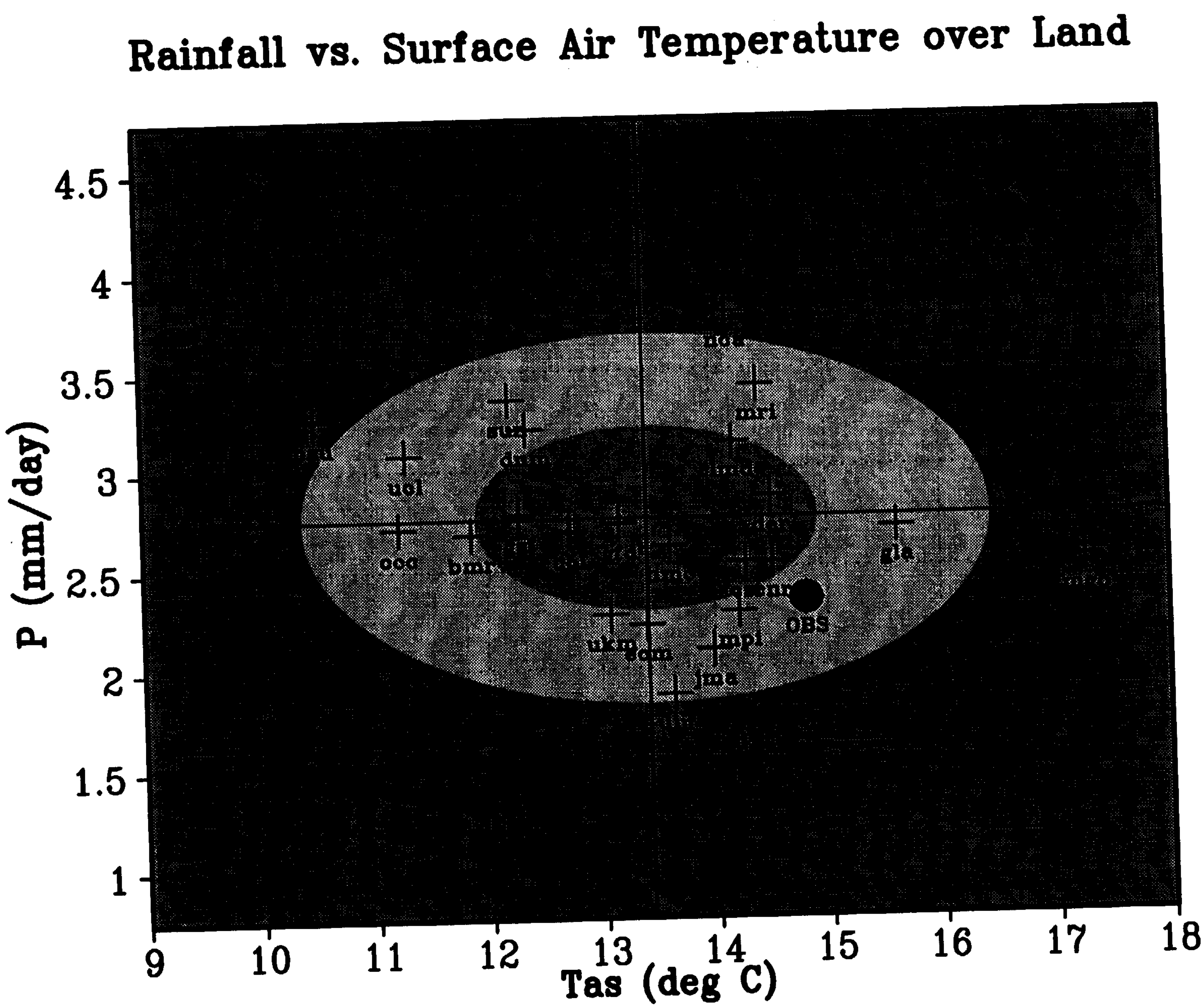
Rainfall vs. Surface Air Temperature over Land
P (mm/day)
4.5
4
3.5
3
2.5
2
1.5
1
9
10
11
12
13
14
15
16
17
18
Tas (deg C)
uol
ooc
mri
gla
OBS
mpi
jma
ukm

Figure 1

Total Precipitation

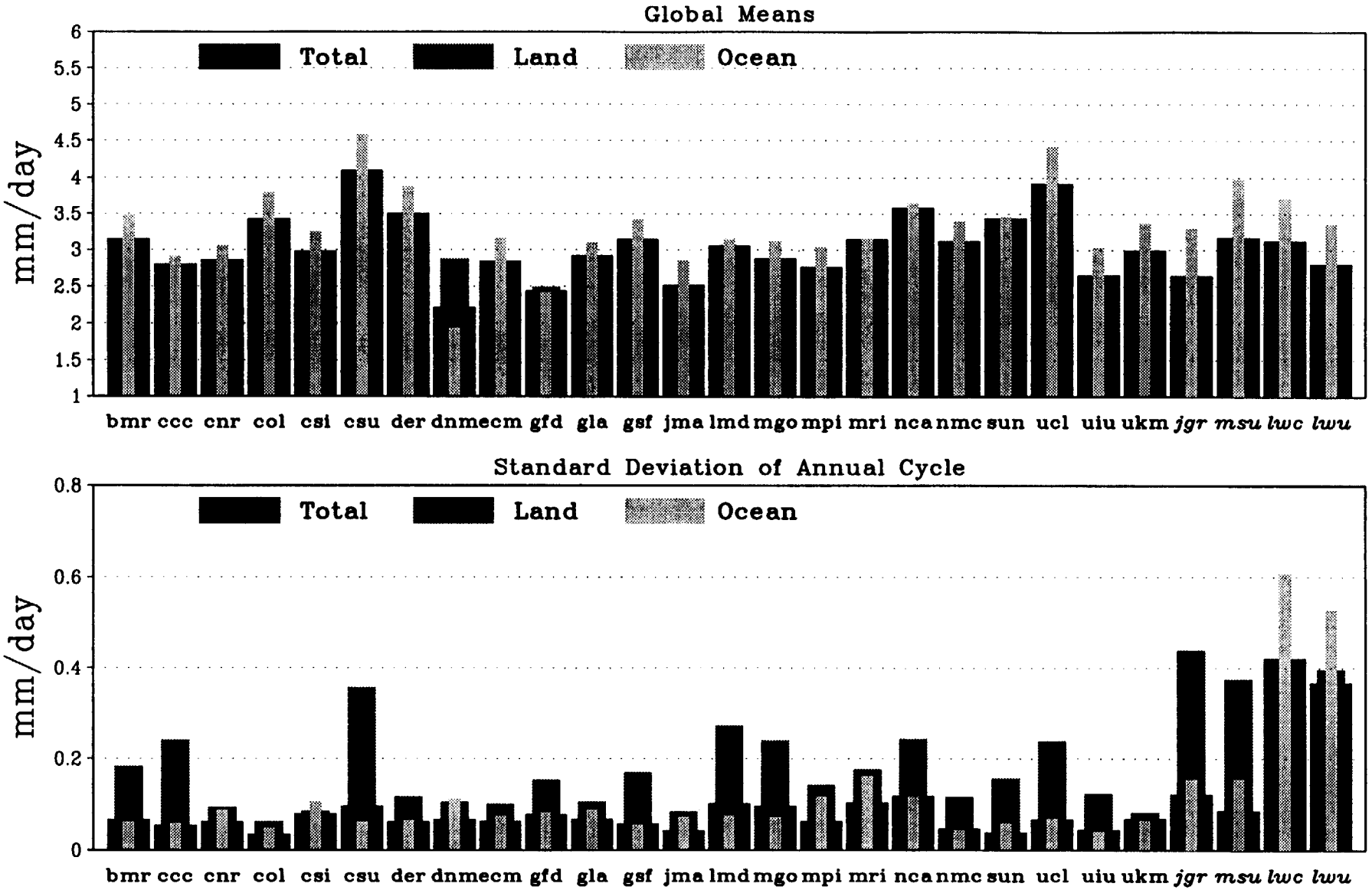

Figure 2

Evaporation

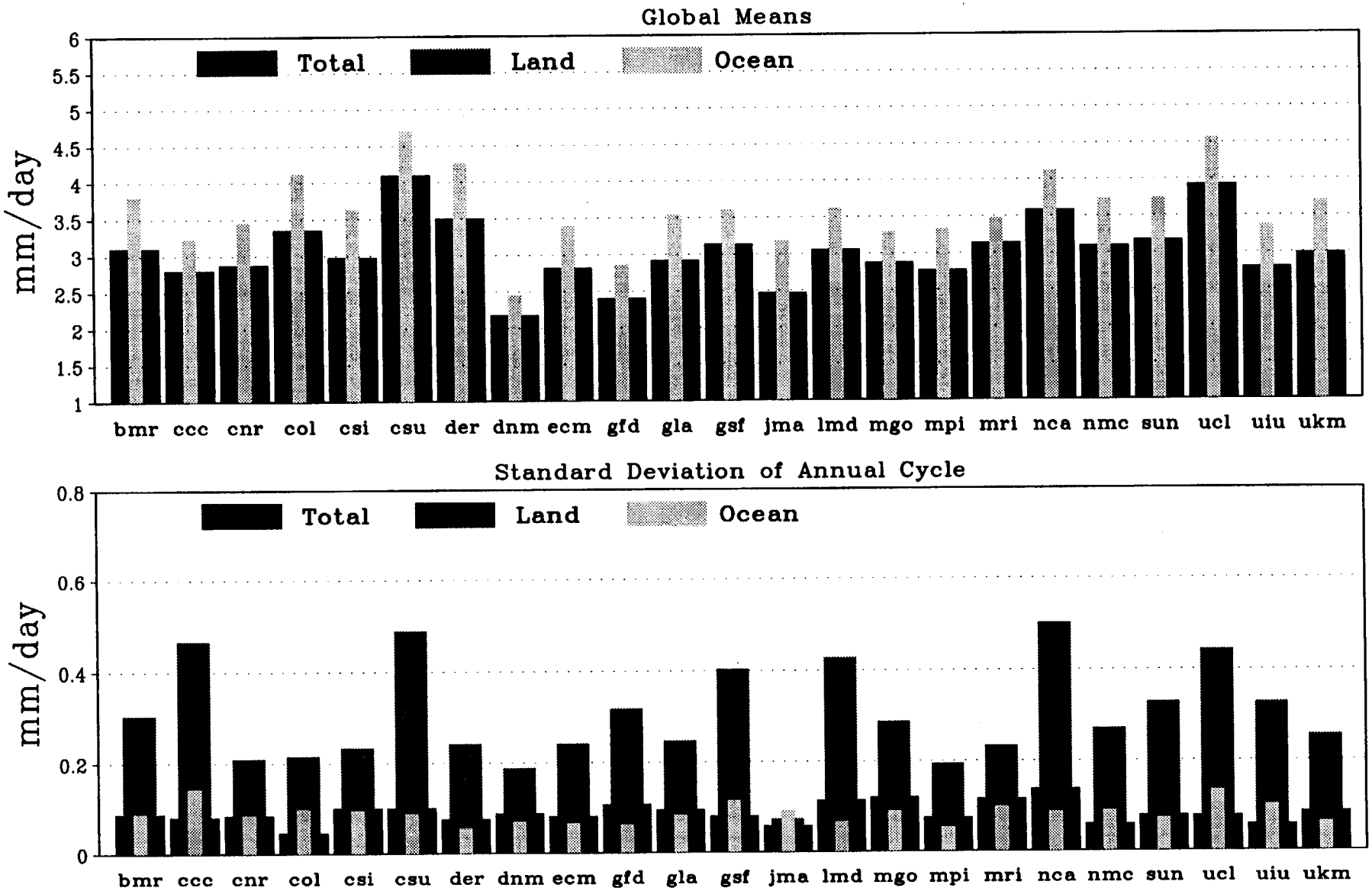

Figure 3

Amount of Water Exchanged (E−P), annual

P&K(Peixoto and Kettani, 1973), B&R(Baumgartner and Reichel, 1975)

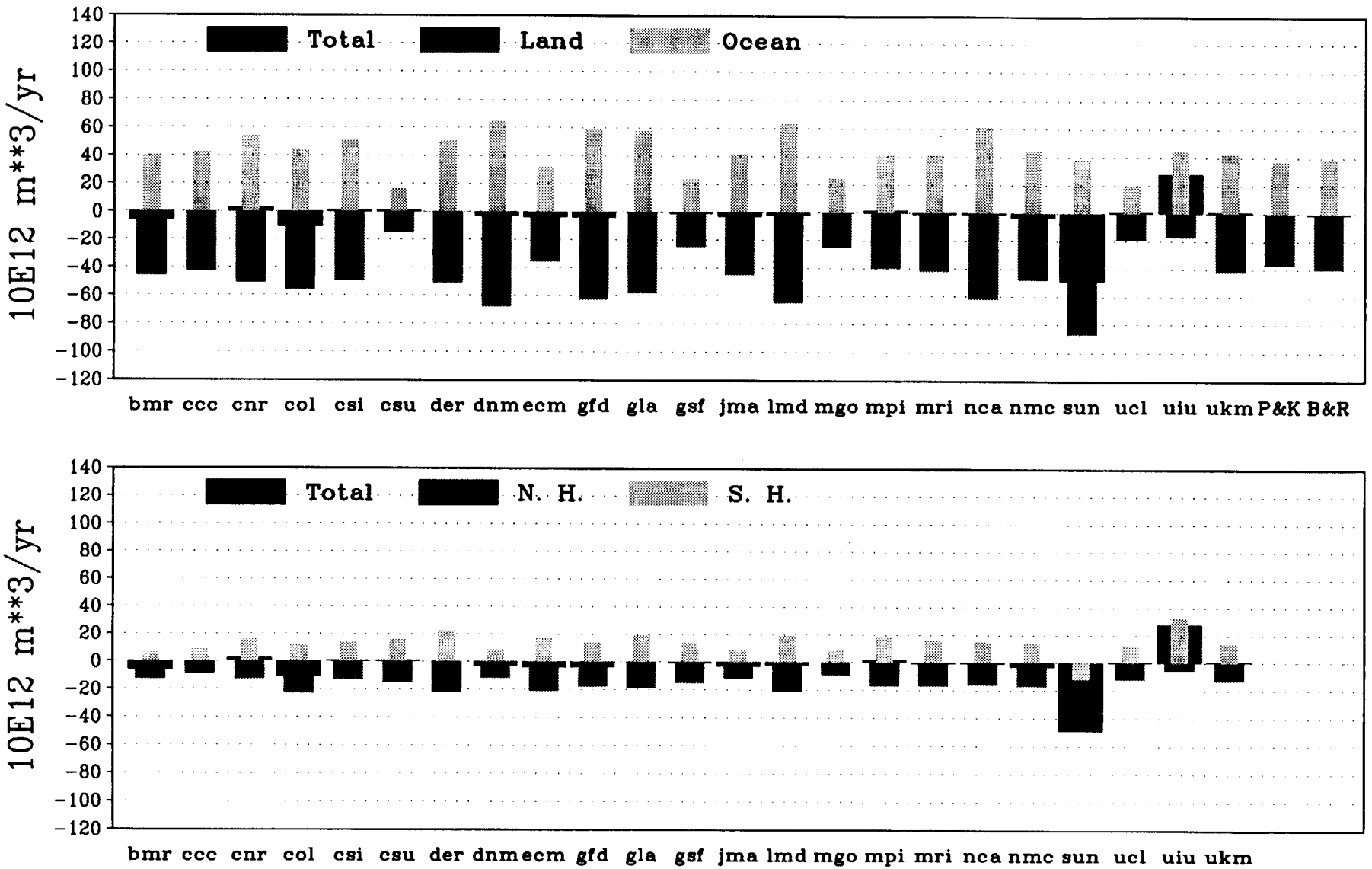

Figure 4.1

Amount of Water Exchanged (E−P), djf

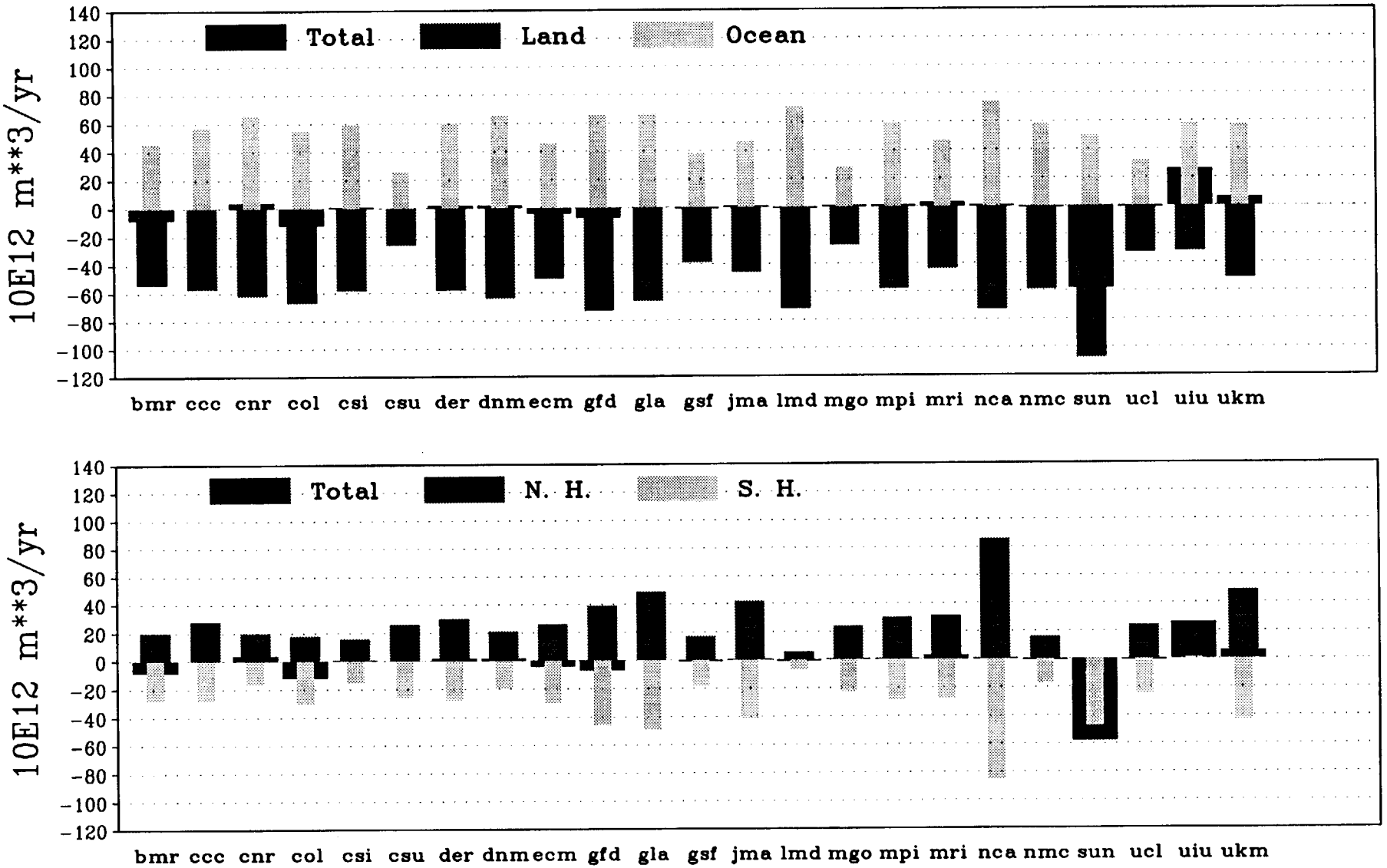

Figure 4.2

Amount of Water Exchanged (E−P), mam
10E12 m**3/yr
Total
Land
Ocean
140
120
100
80
60
40
20
0
−20
−40
−60
−80
−100
−120
bmr ccc cnr col csi csu der dnmecm gfd gla gsf jma lmd mgo mpi mri nca nmc sun ucl uiu ukm
10E12 m**3/yr
Total
N. H.
S. H.
140
120
100
80
60
40
20
0
−20
−40
−60
−80
−100
−120
bmr ccc cnr col csi csu der dnmecm gfd gla gsf jma lmd mgo mpi mri nca nmc sun ucl uiu ukm

Figure 4.3

Amount of Water Exchanged (E−P), jja

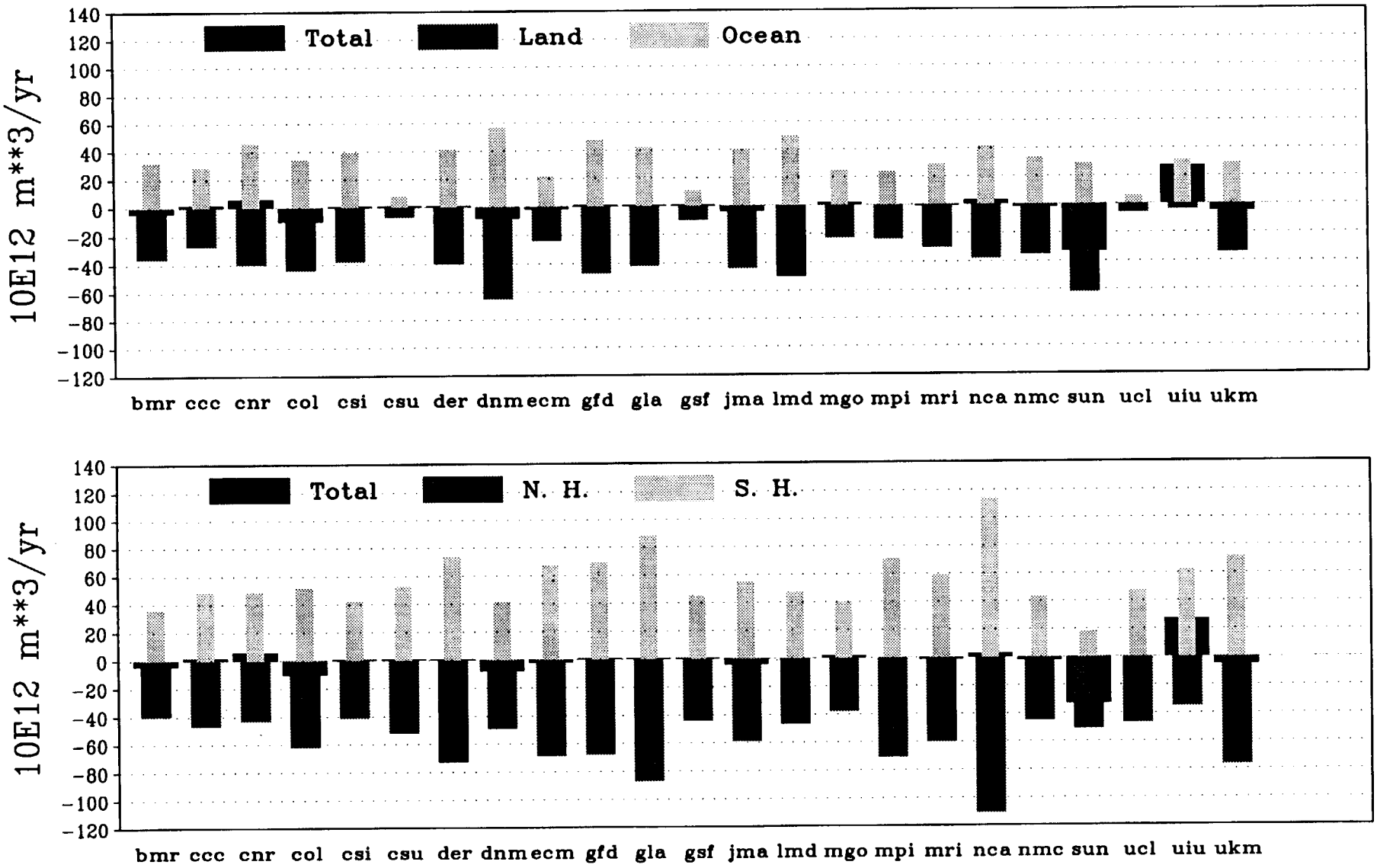

Figure 4.4

33

Amount of Water Exchanged (E−P), son

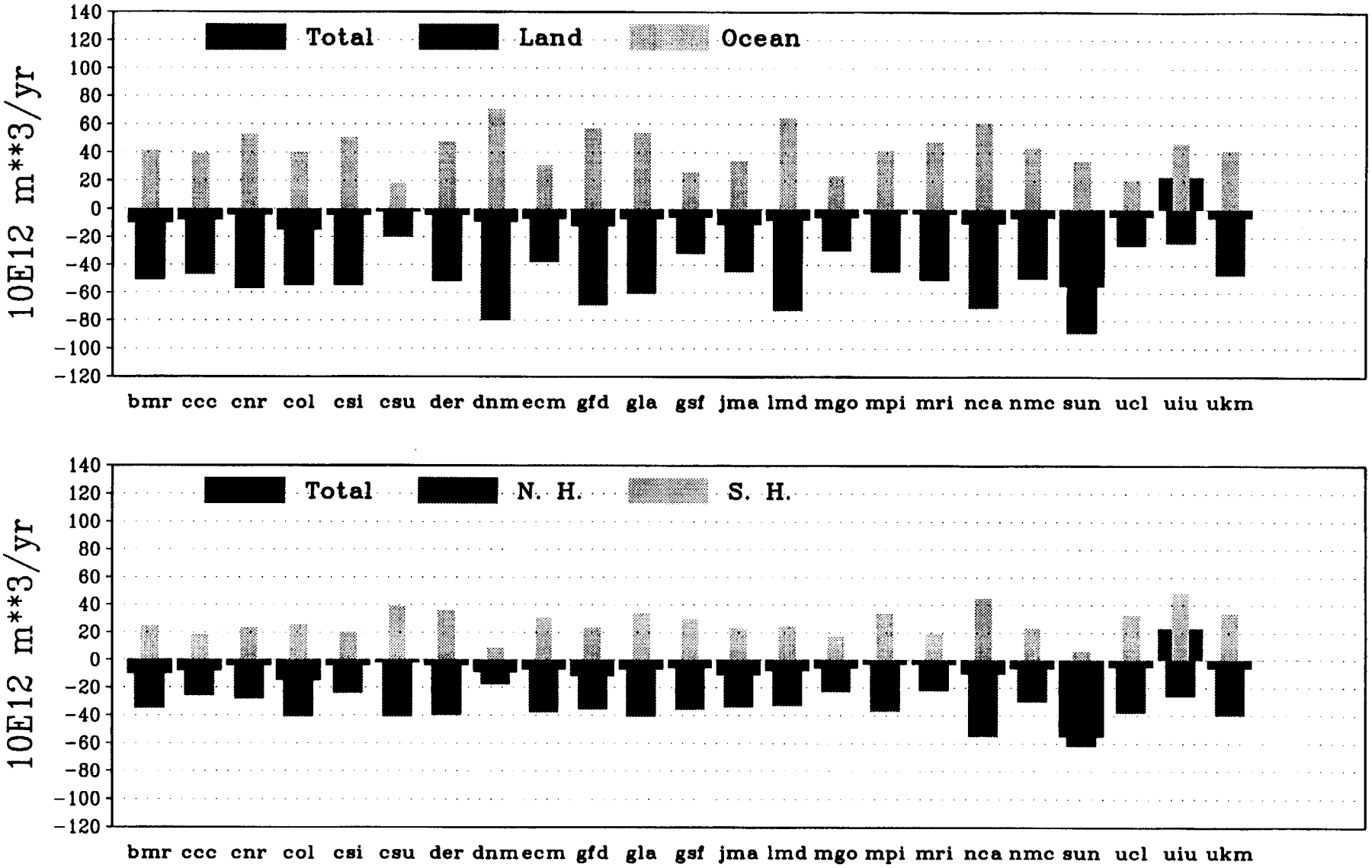

Figure 4.5

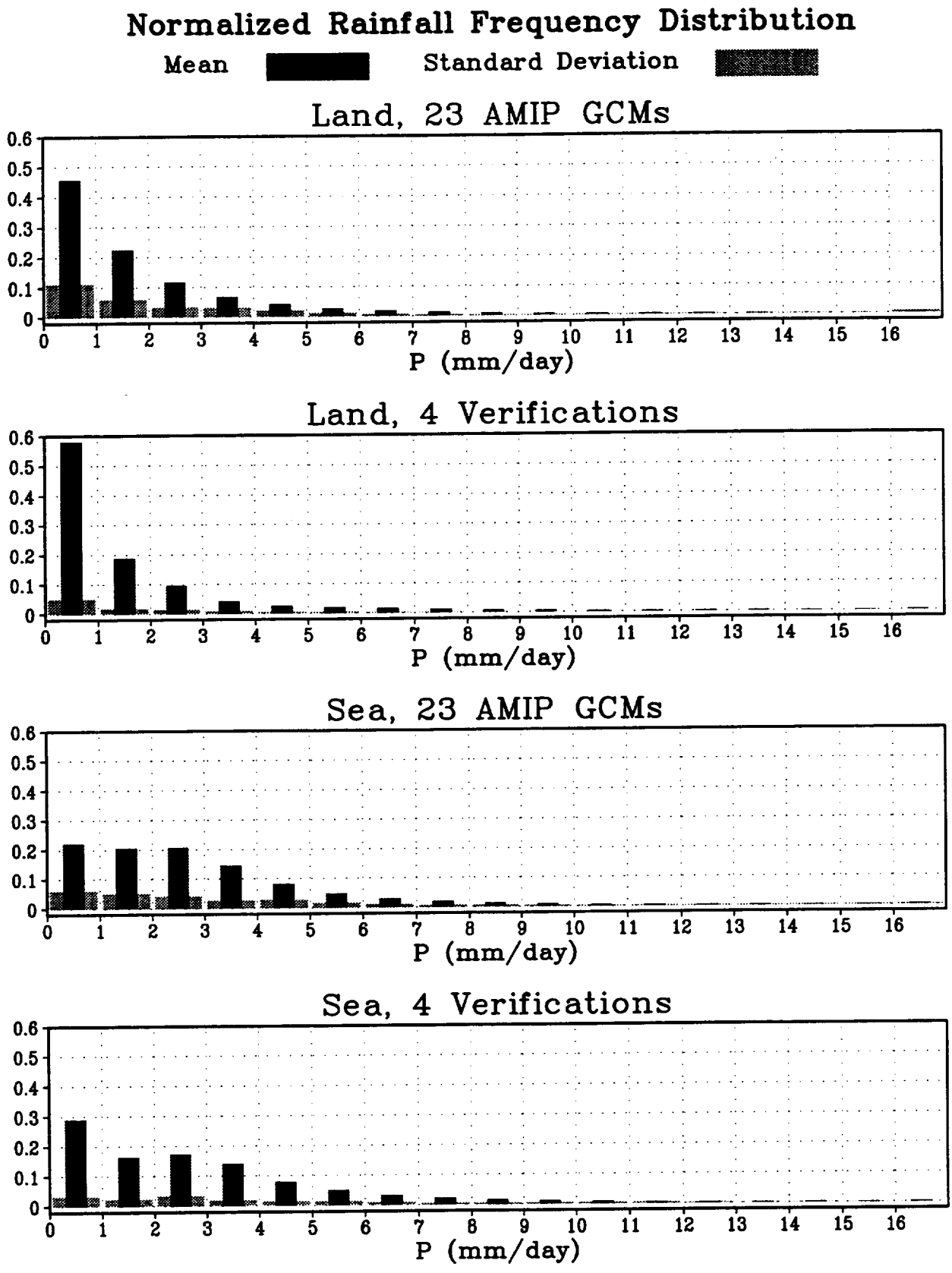
Normalized Rainfall Frequency Distribution
Mean
Standard Deviation
Land, 23 AMIP GCMs
Land, 4 Verifications
Sea, 23 AMIP GCMs
Sea, 4 Verifications
0.6
0.5
0.4
0.3
0.2
0.1
0
0 1 2 3 4 5 6 7 8 9 10 11 12 13 14 15 16
P (mm/day)

Figure 5.1

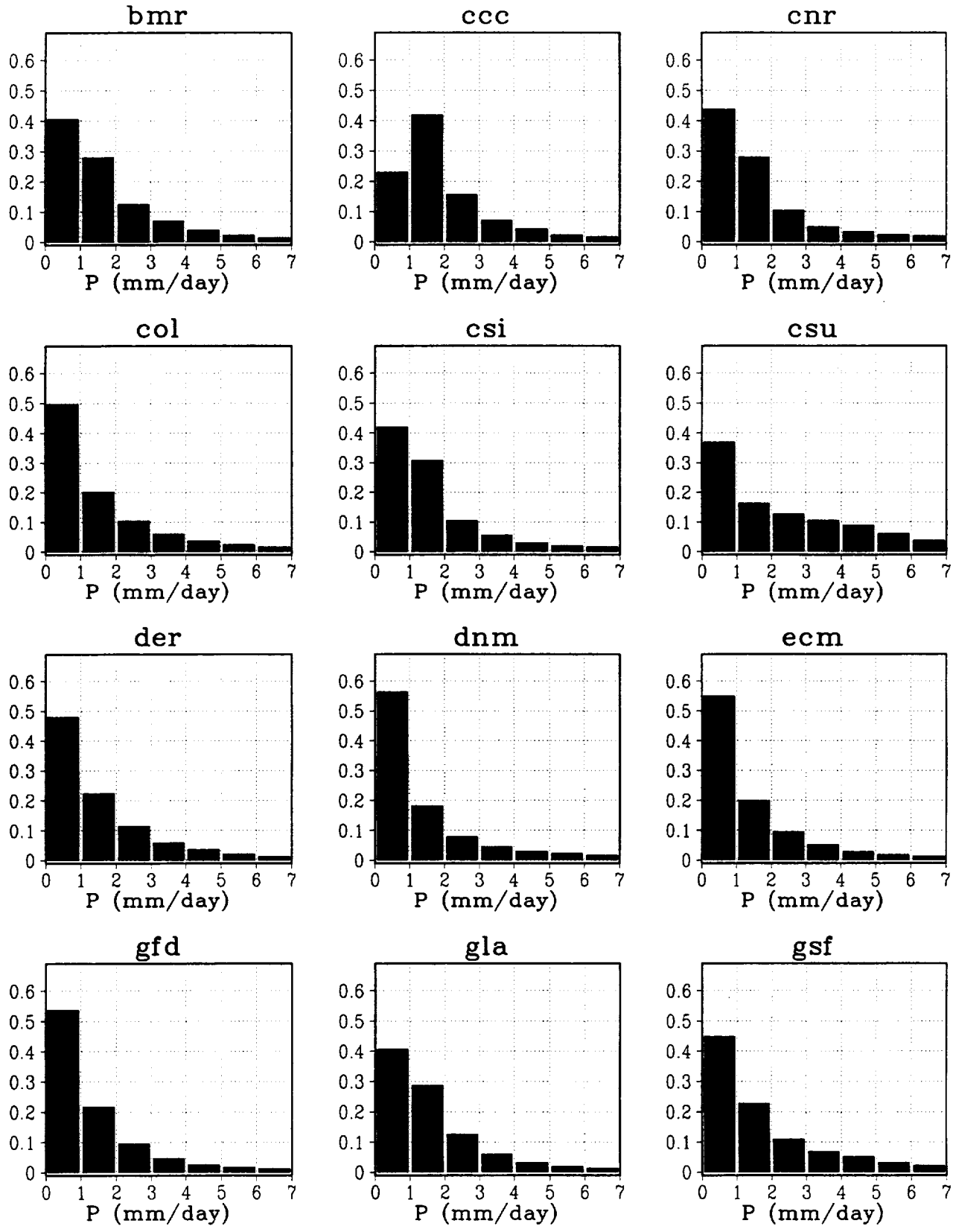
Normalized Rainfall Frequency Distribution
Land Points; AMIP GCMs and Rain Gauge
bmr
ccc
cnr
col
csi
csu
der
dnm
ecm
gfd
gla
gsf
0.6
0.5
0.4
0.3
0.2
0.1
0
0 1 2 3 4 5 6 7
P (mm/day)

Figure 5.2

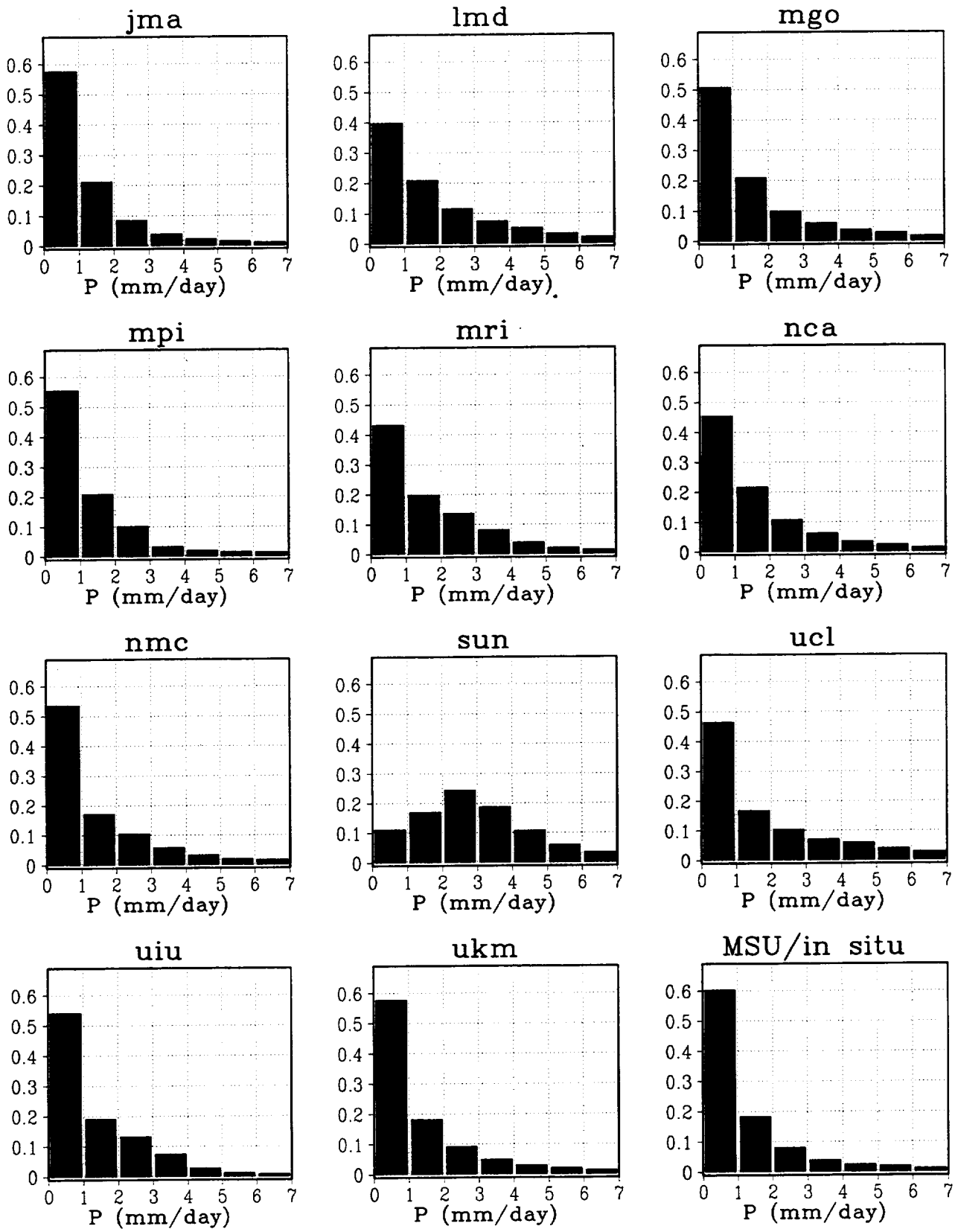

Figure 5.2 (continued)

Normalized Rainfall Frequency Distribution

Ocean Points; AMIP GCMs and MSU

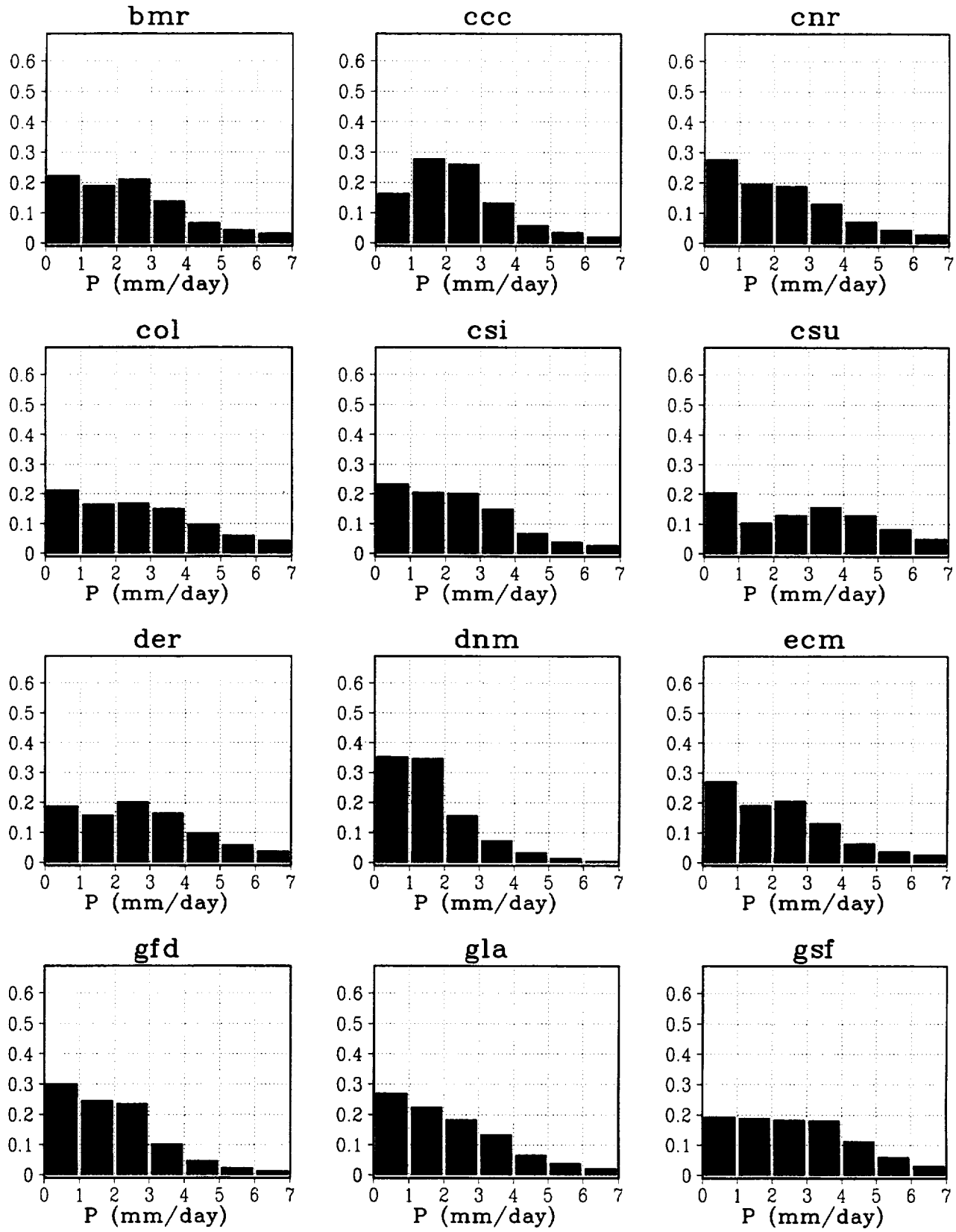

Figure 5.3

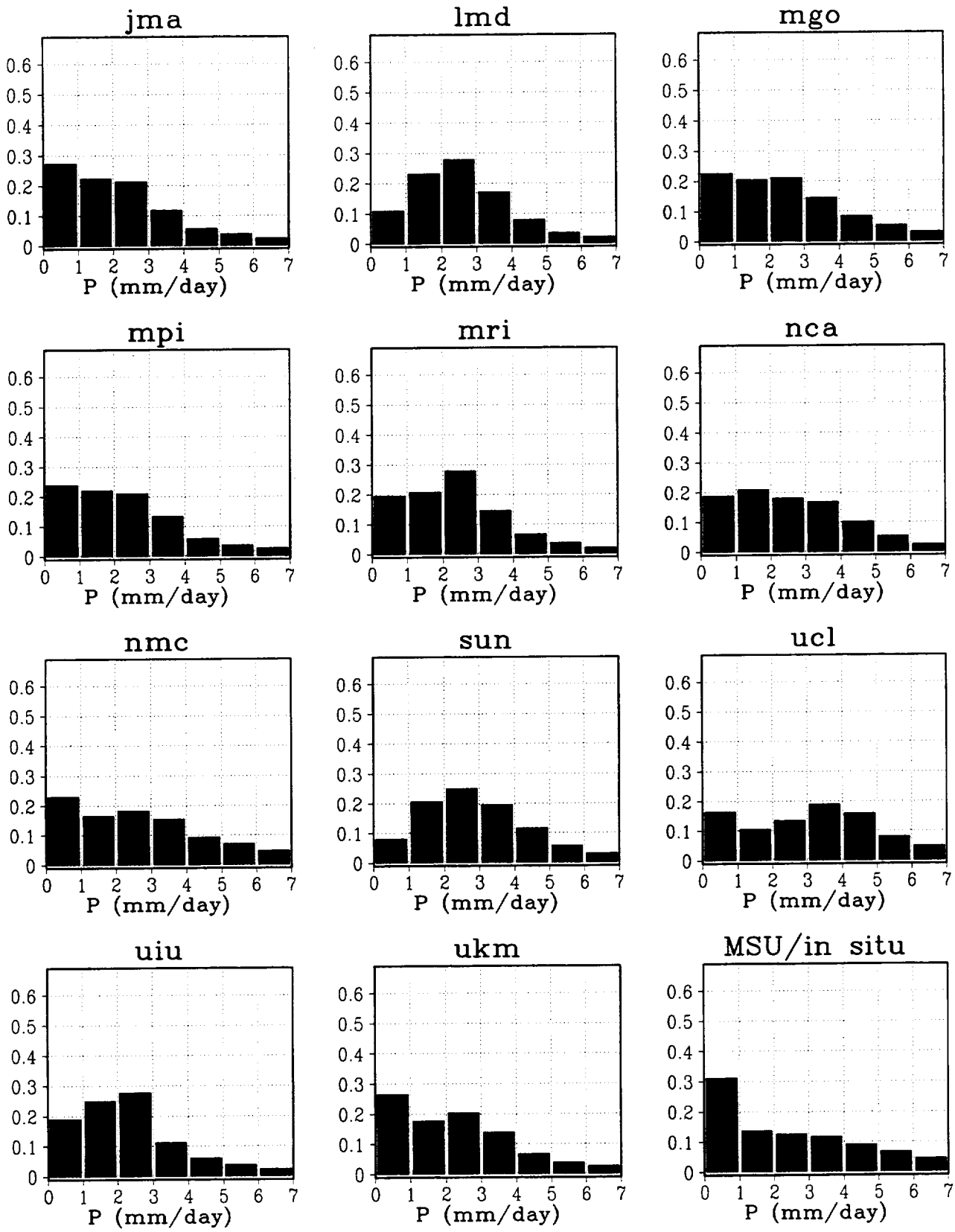

Figure 5.3 (continued)

Total Precipitation, Annual

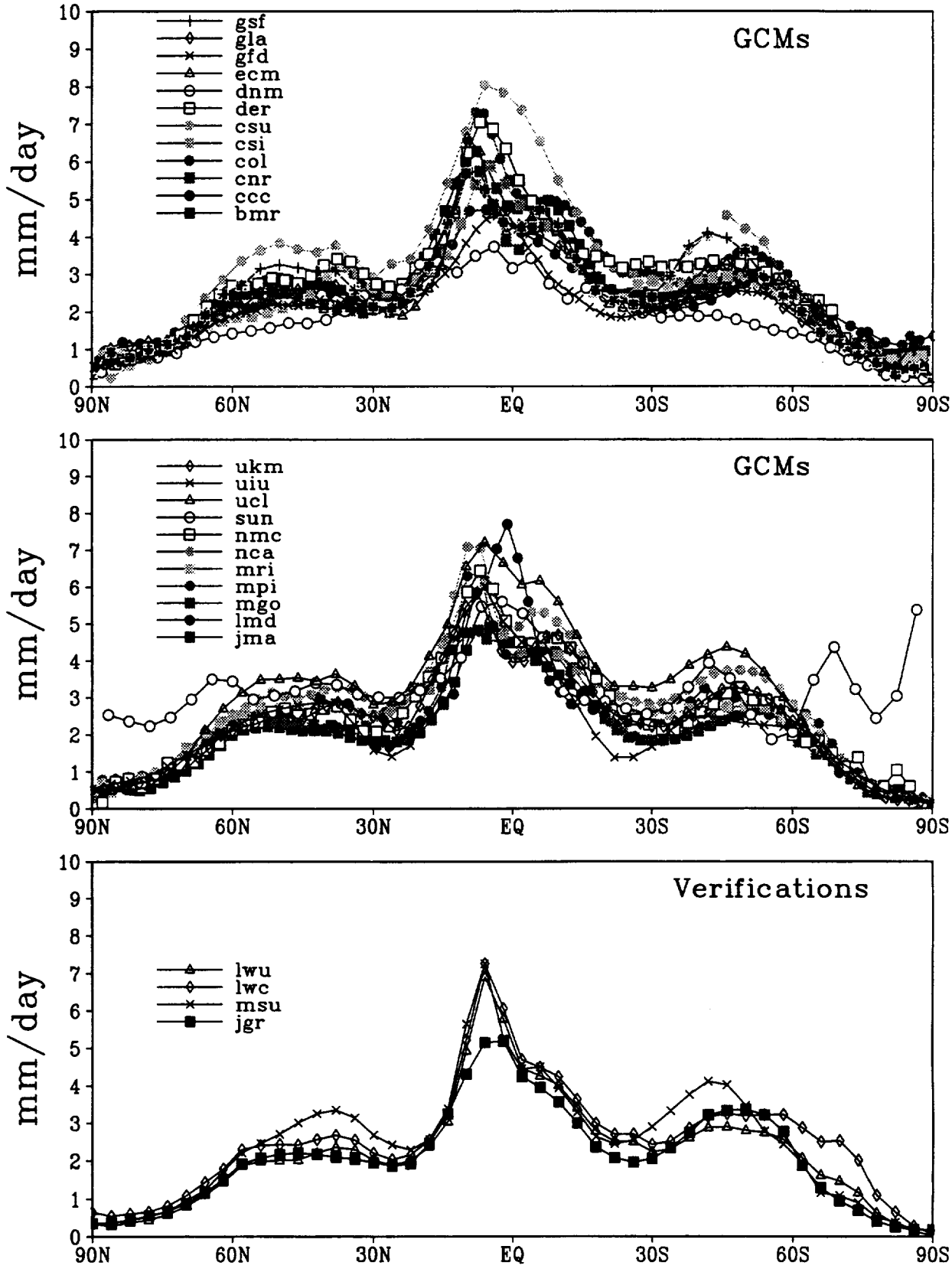

Figure 6.1

Total Precipitation, DJF

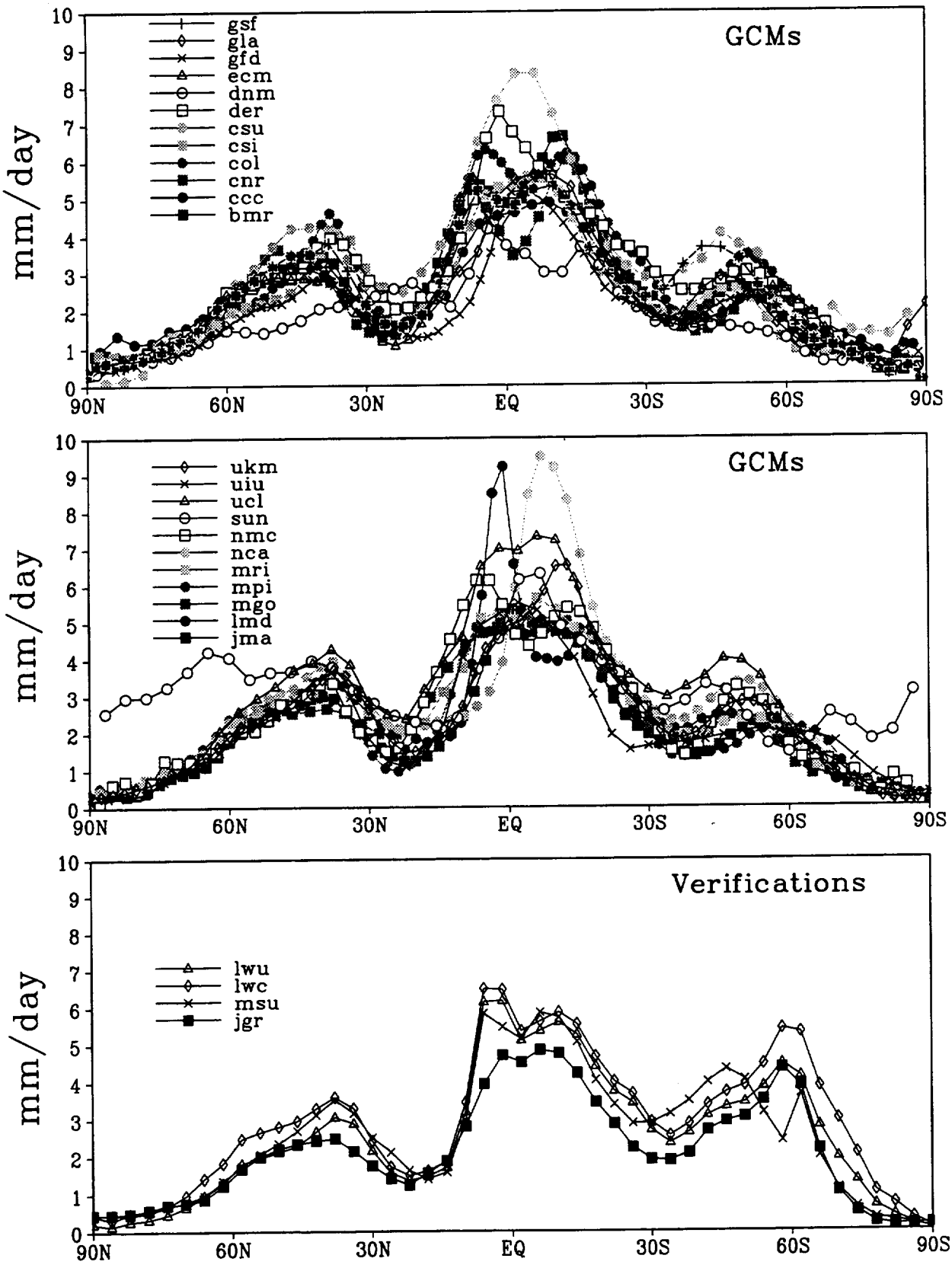

Figure 6.2

Total Precipitation, JJA

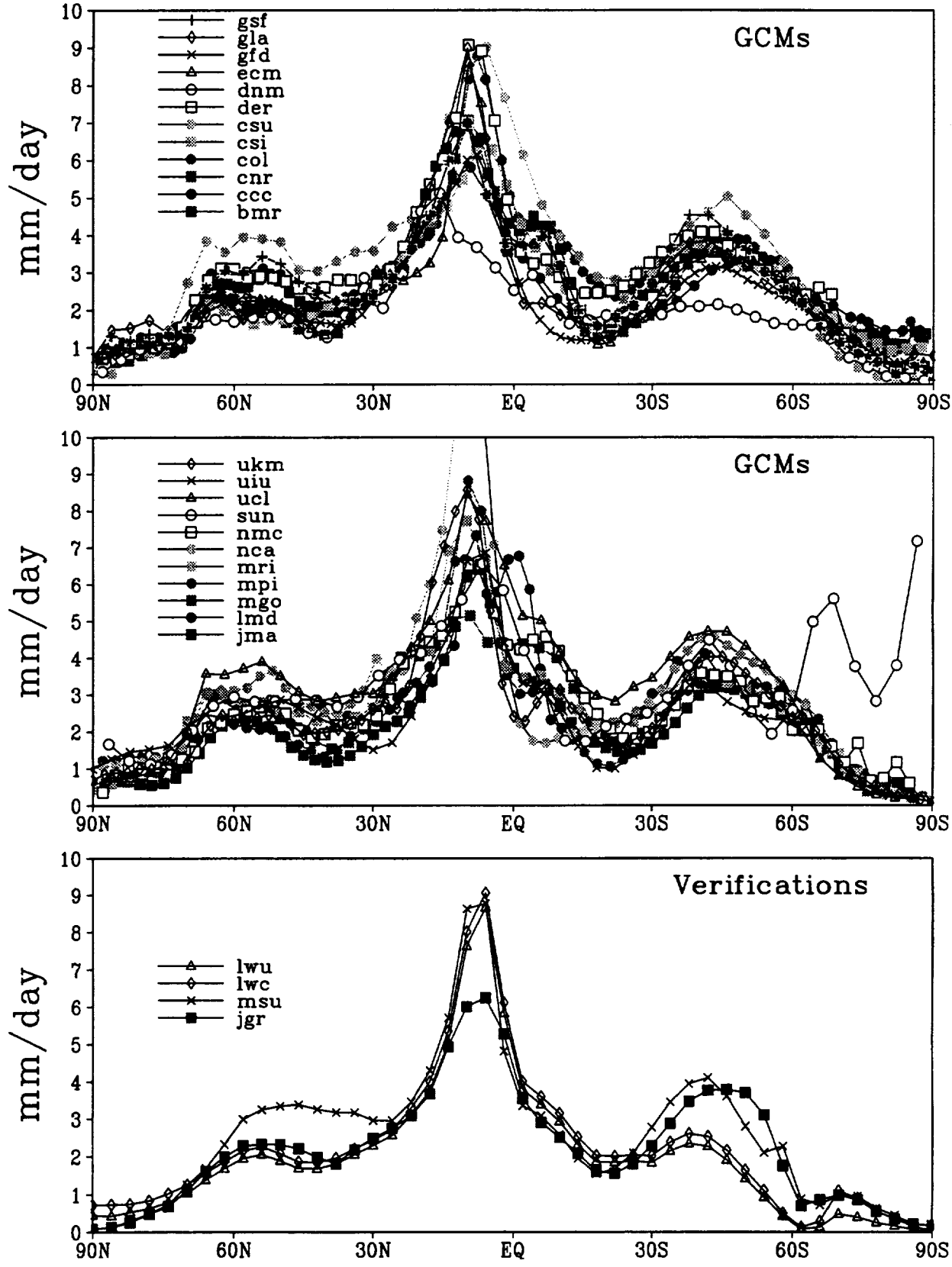

Figure 6.3

This page intentionally left blank.

Water Budget over Land, Annual

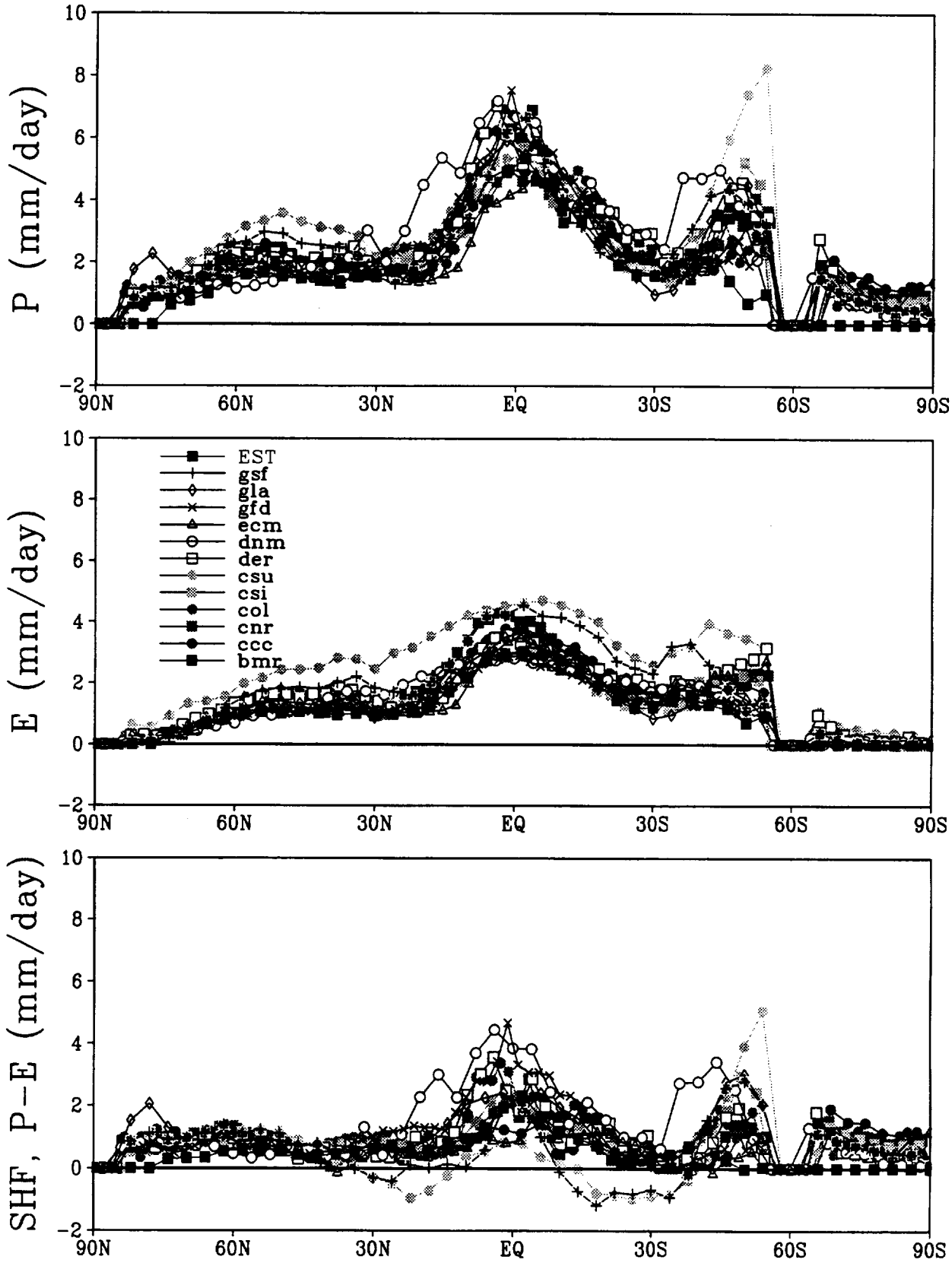

Figure 7.1

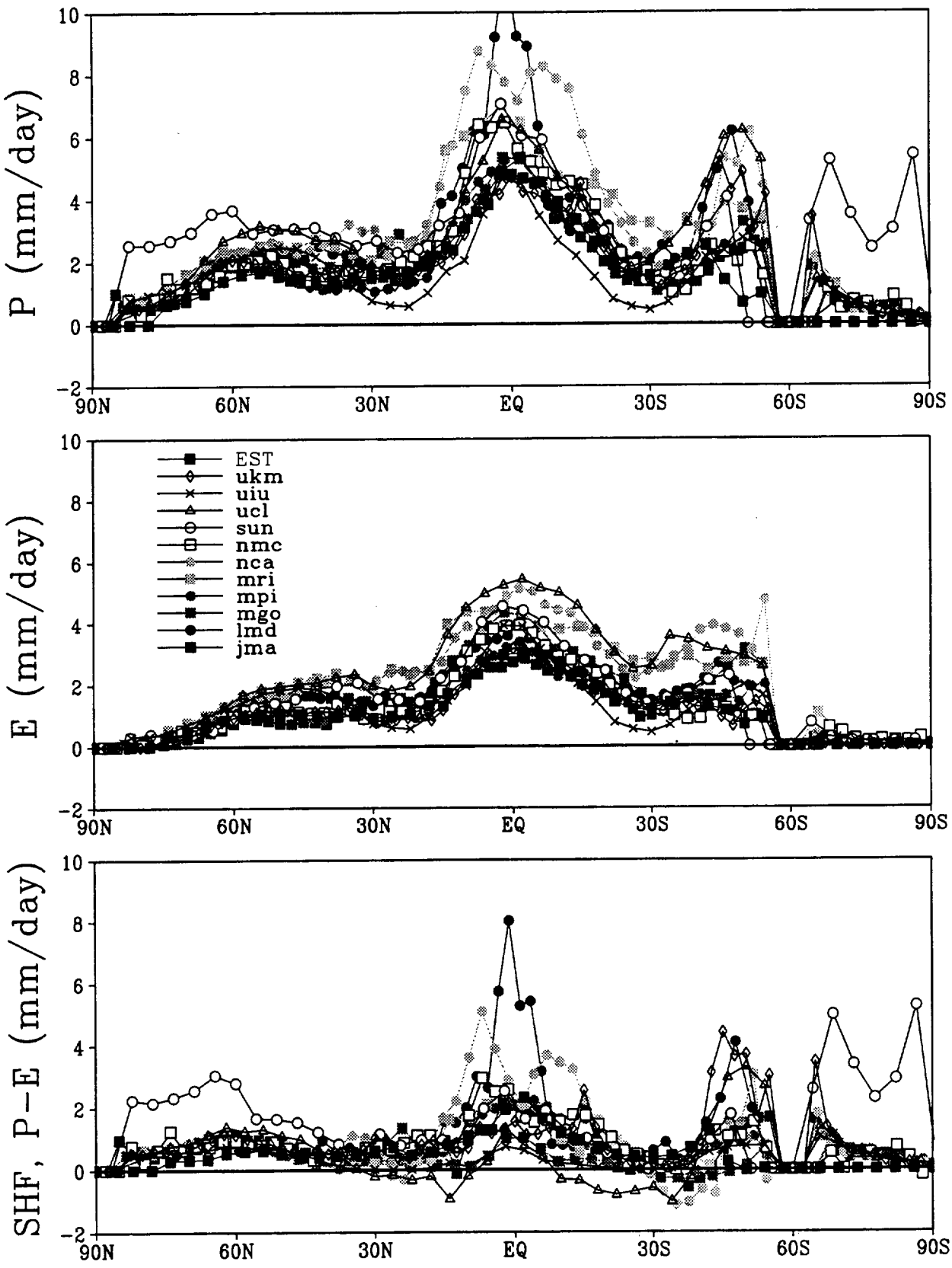

Figure 7.1 (continued)

Water Budget over Land, DJF

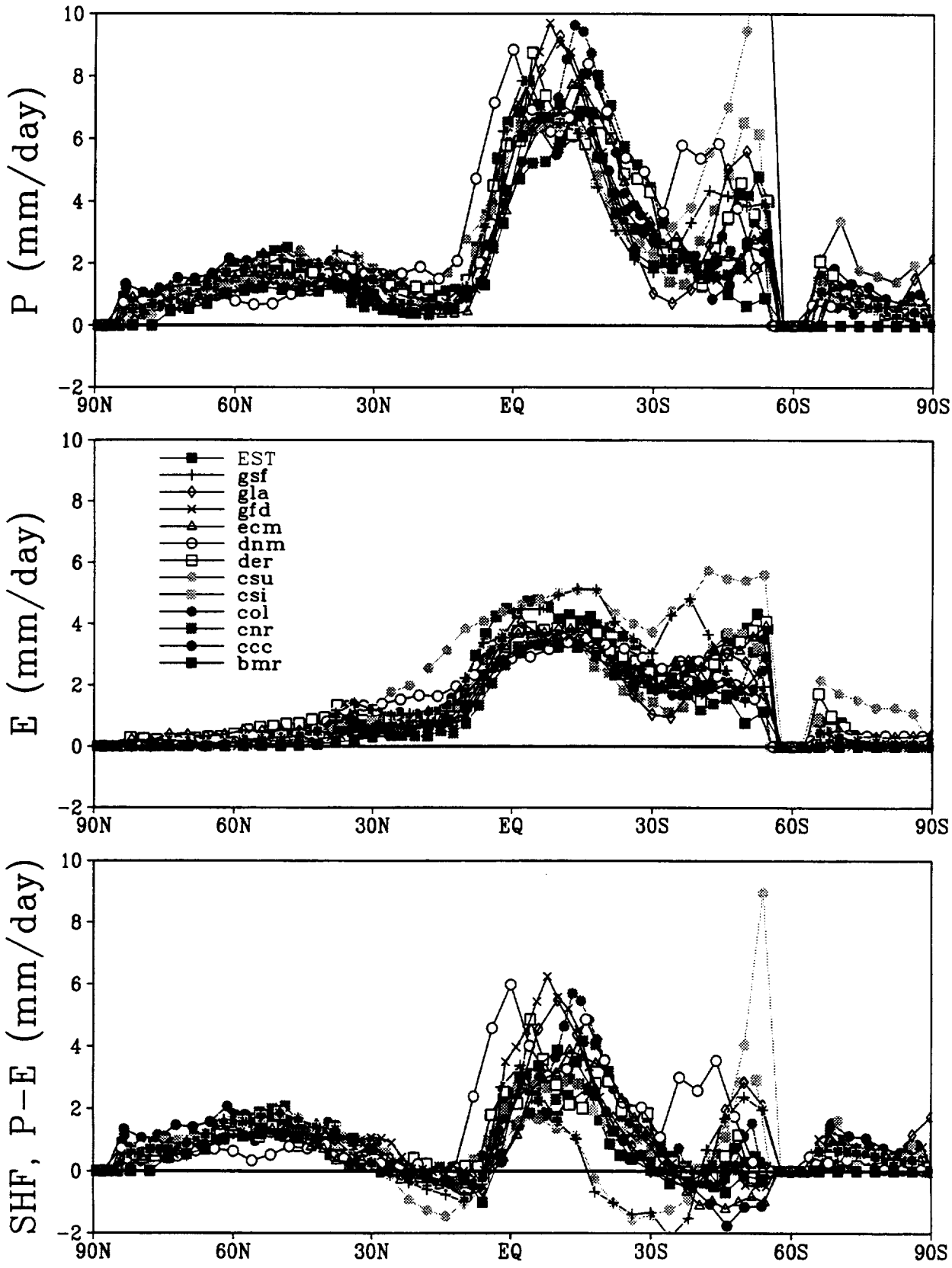

Figure 7.2

Water Budget over Land, DJF

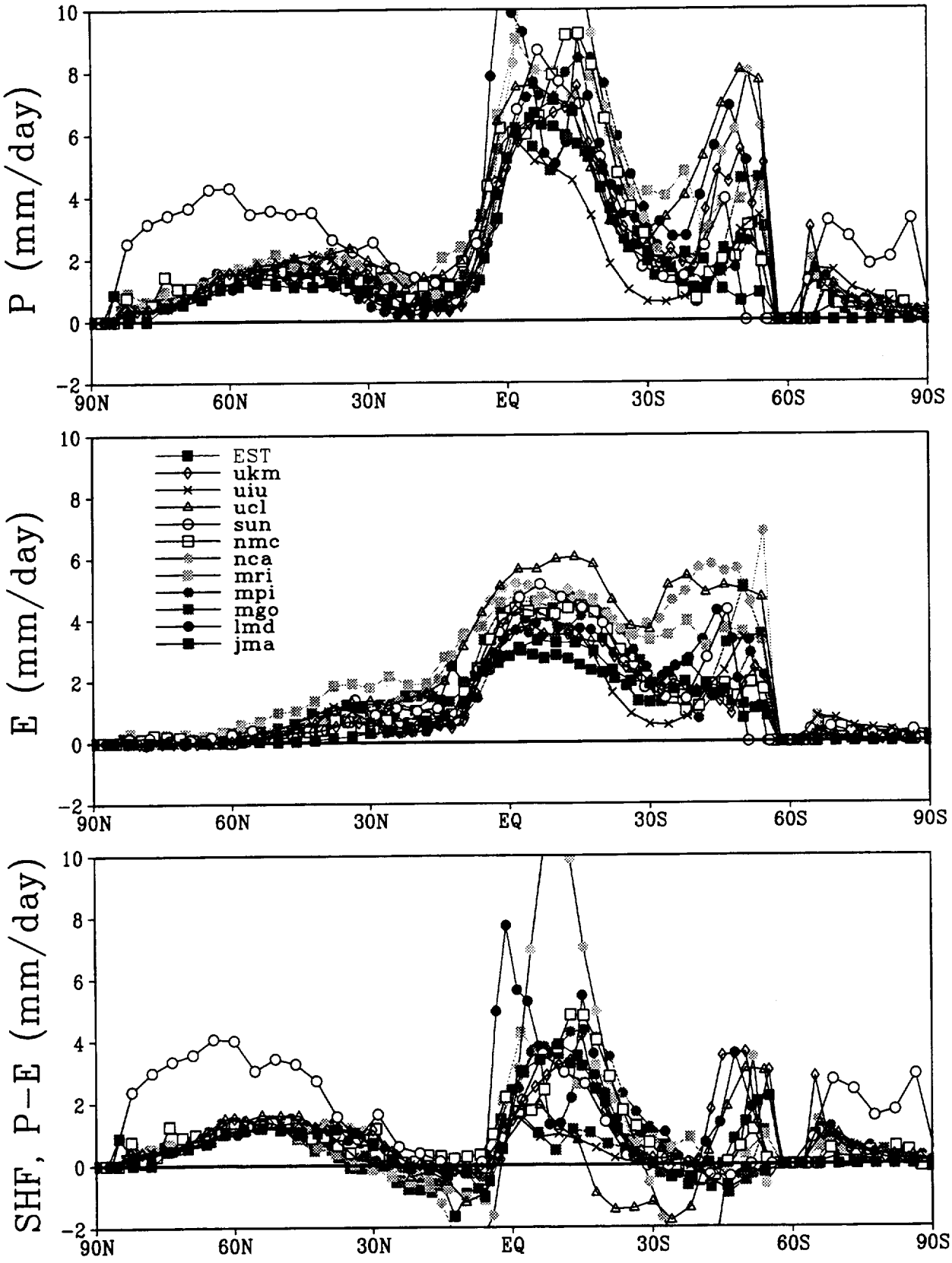

Figure 7.2 (continued)

Water Budget over Land, JJA

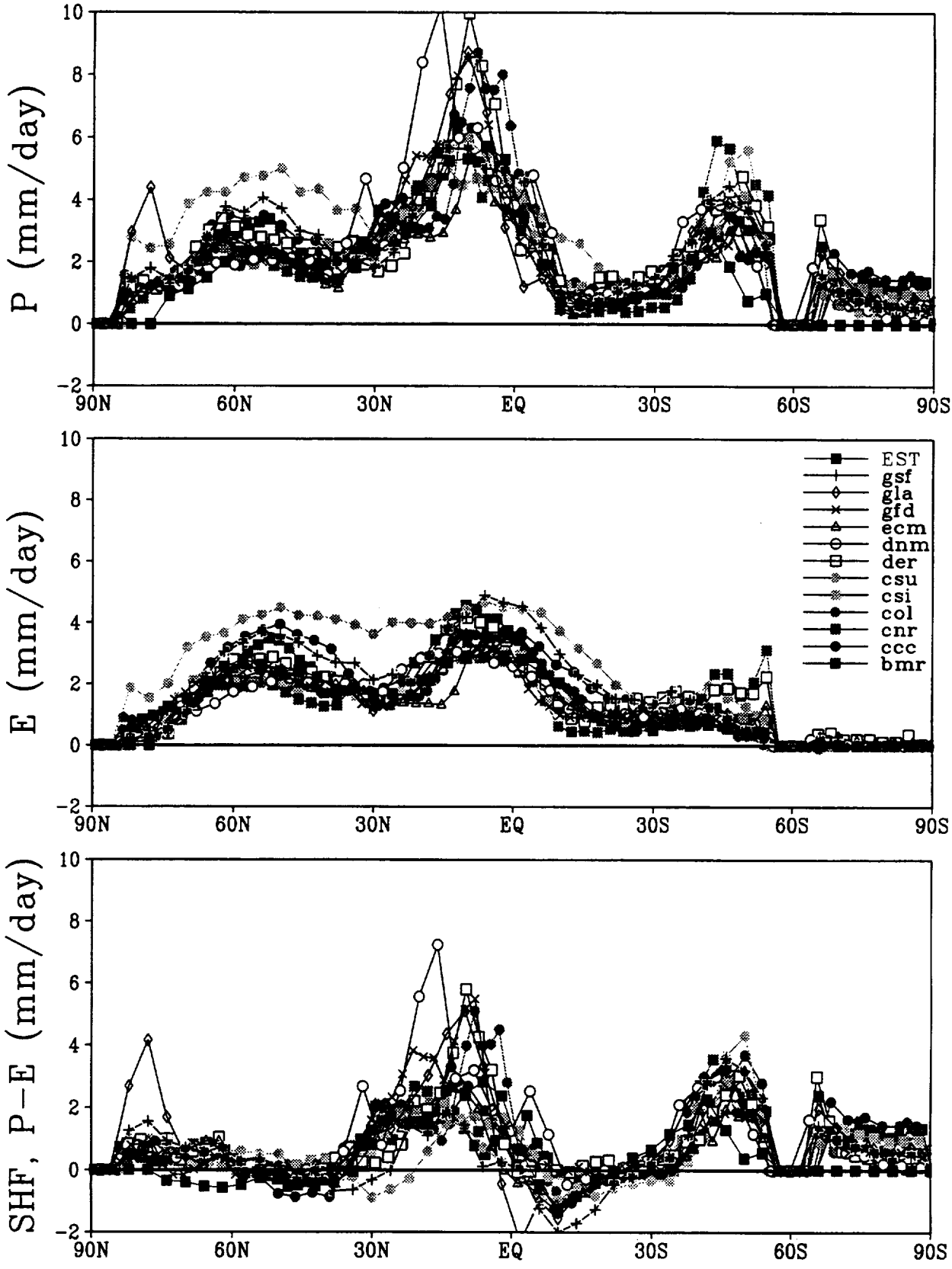

Figure 7.3

Water Budget over Land, JJA

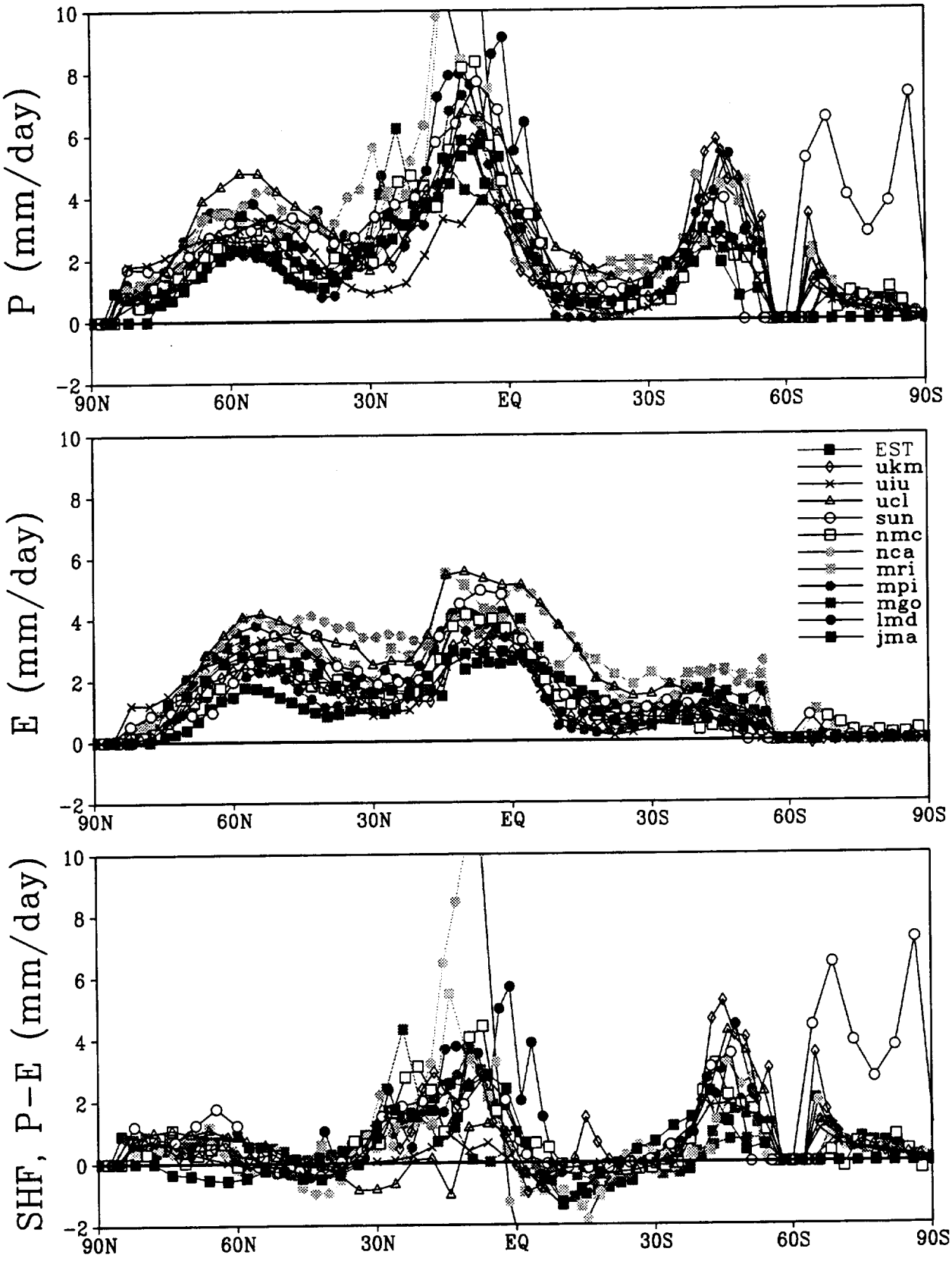

Figure 7.3 (continued)

Water Budget over Ocean, Annual

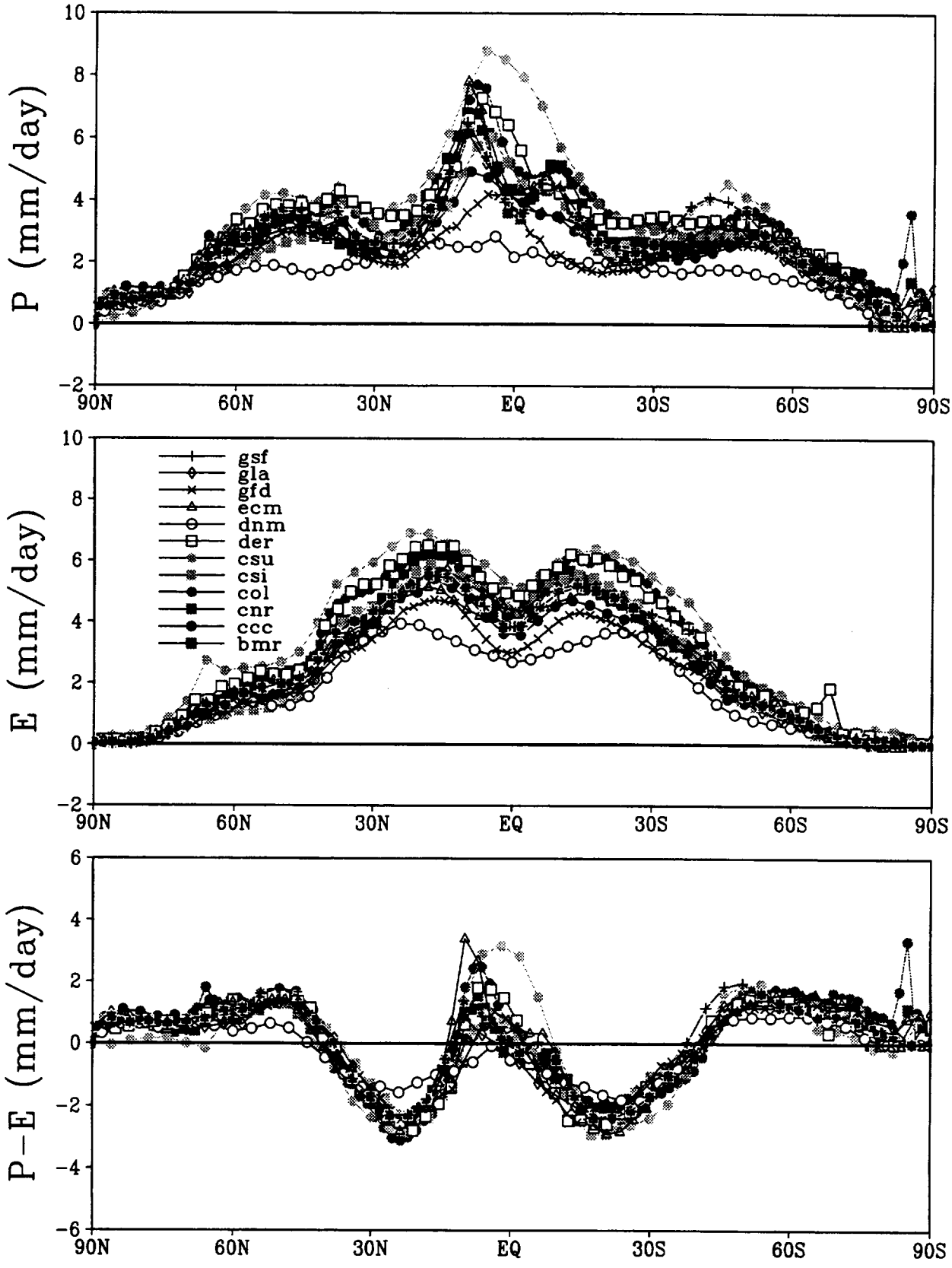

Figure 7.4

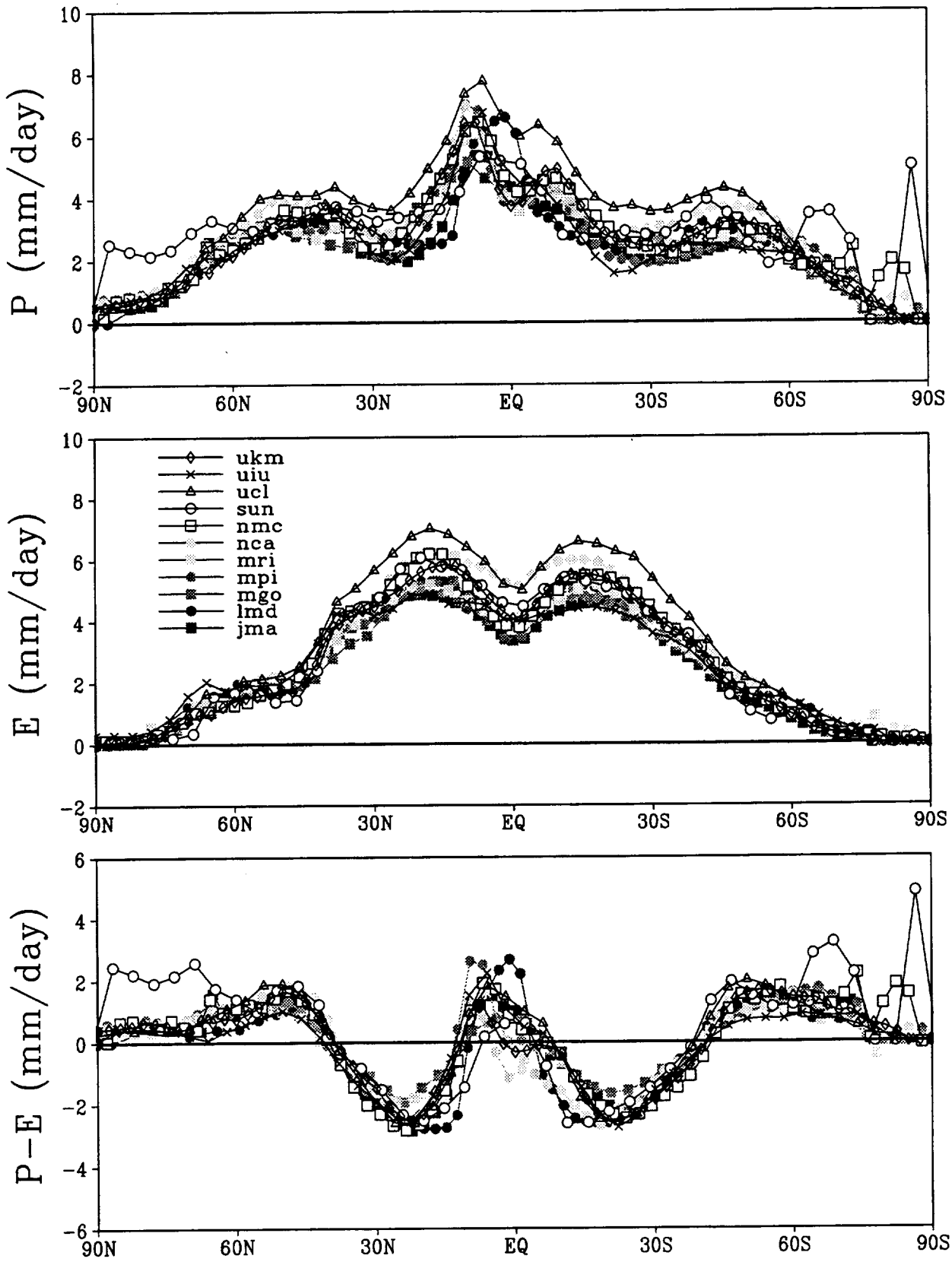

Figure 7.4 (continued)

Water Budget over Ocean, DJF

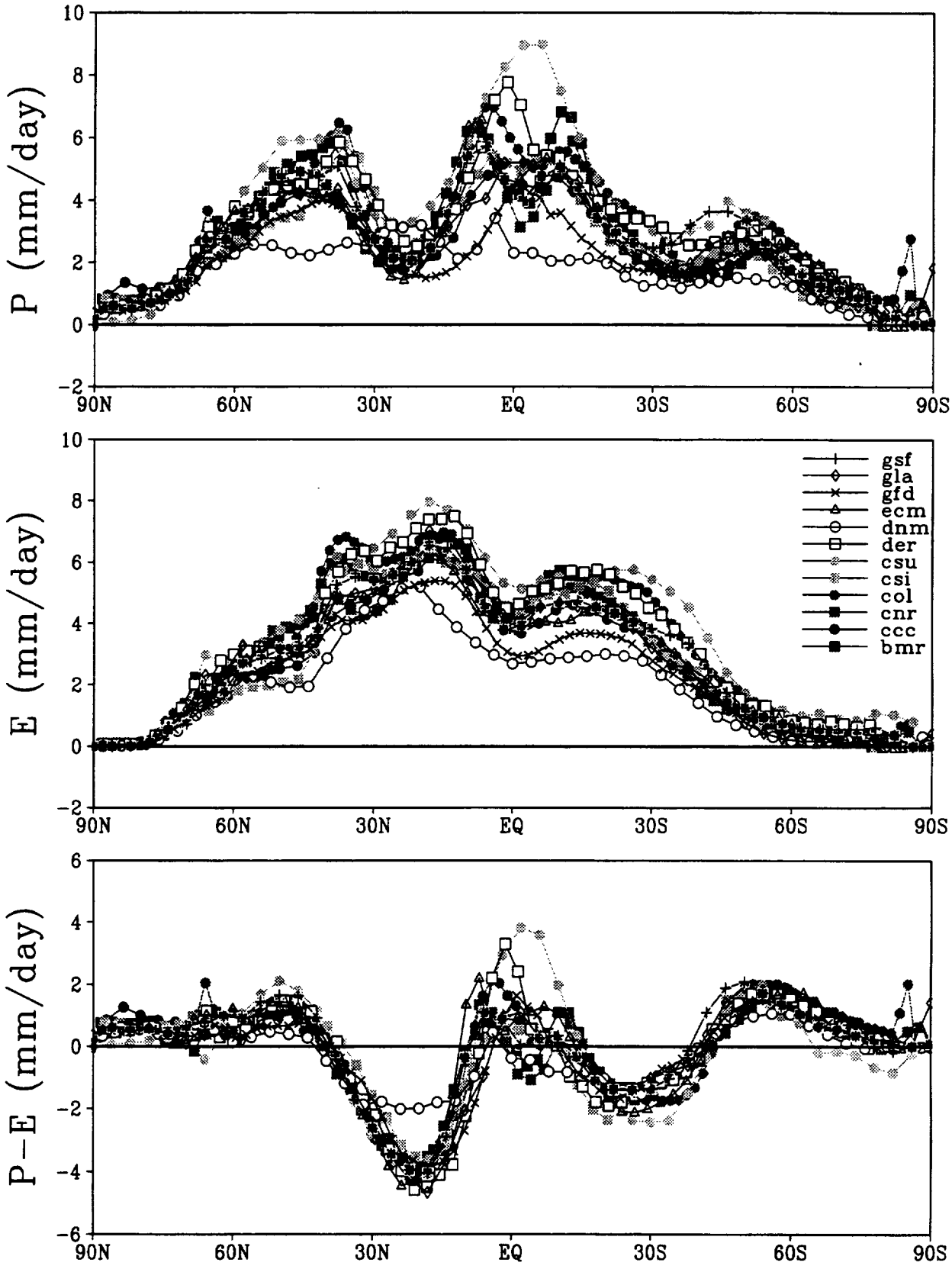

Figure 7.5

Water Budget over Ocean, DJF

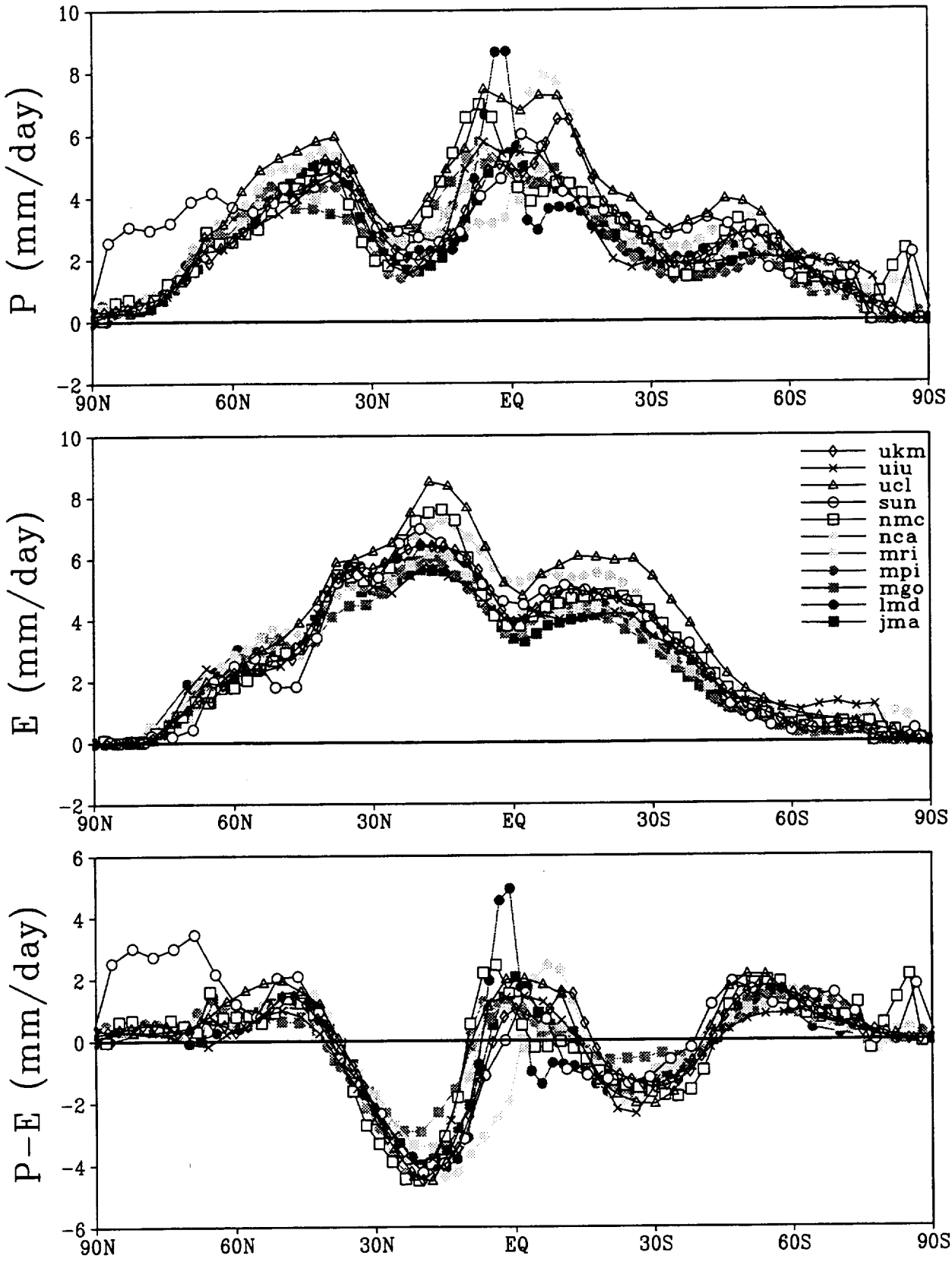

Figure 7.5 (continued)

Water Budget over Ocean, JJA

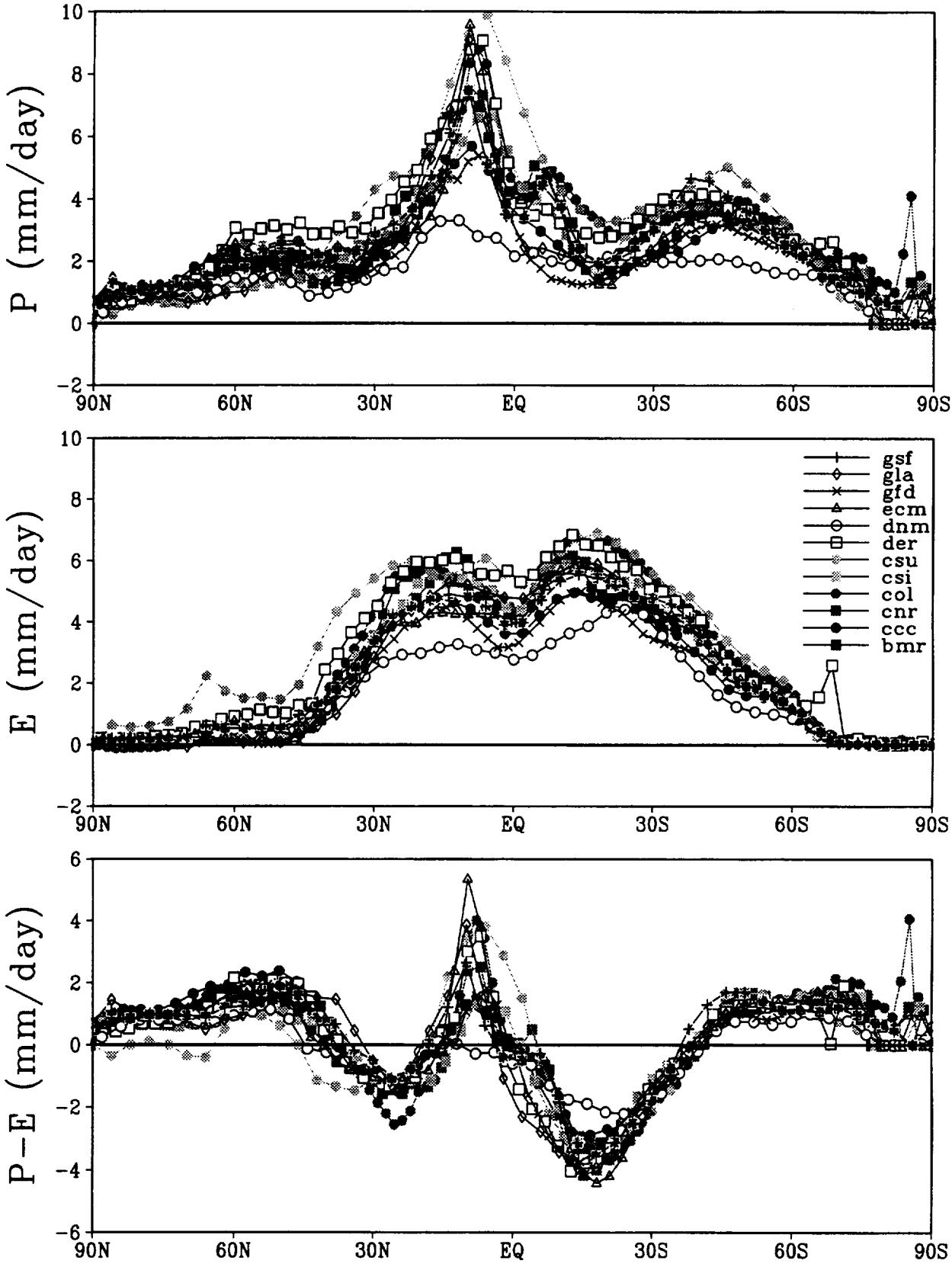

Figure 7.6

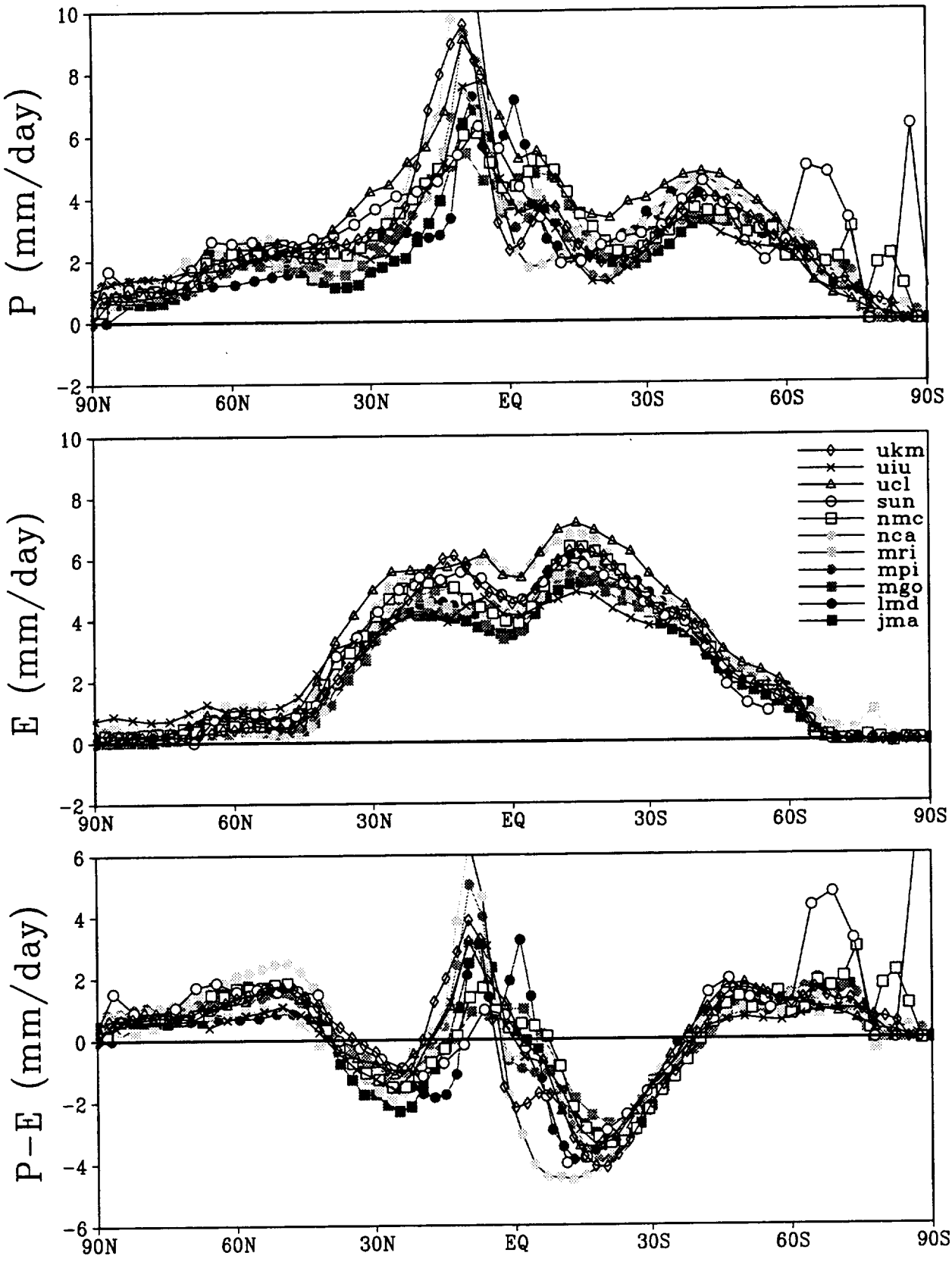

Figure 7.6 (continued)

Precipitation, Mean of 23 AMIP GCMs

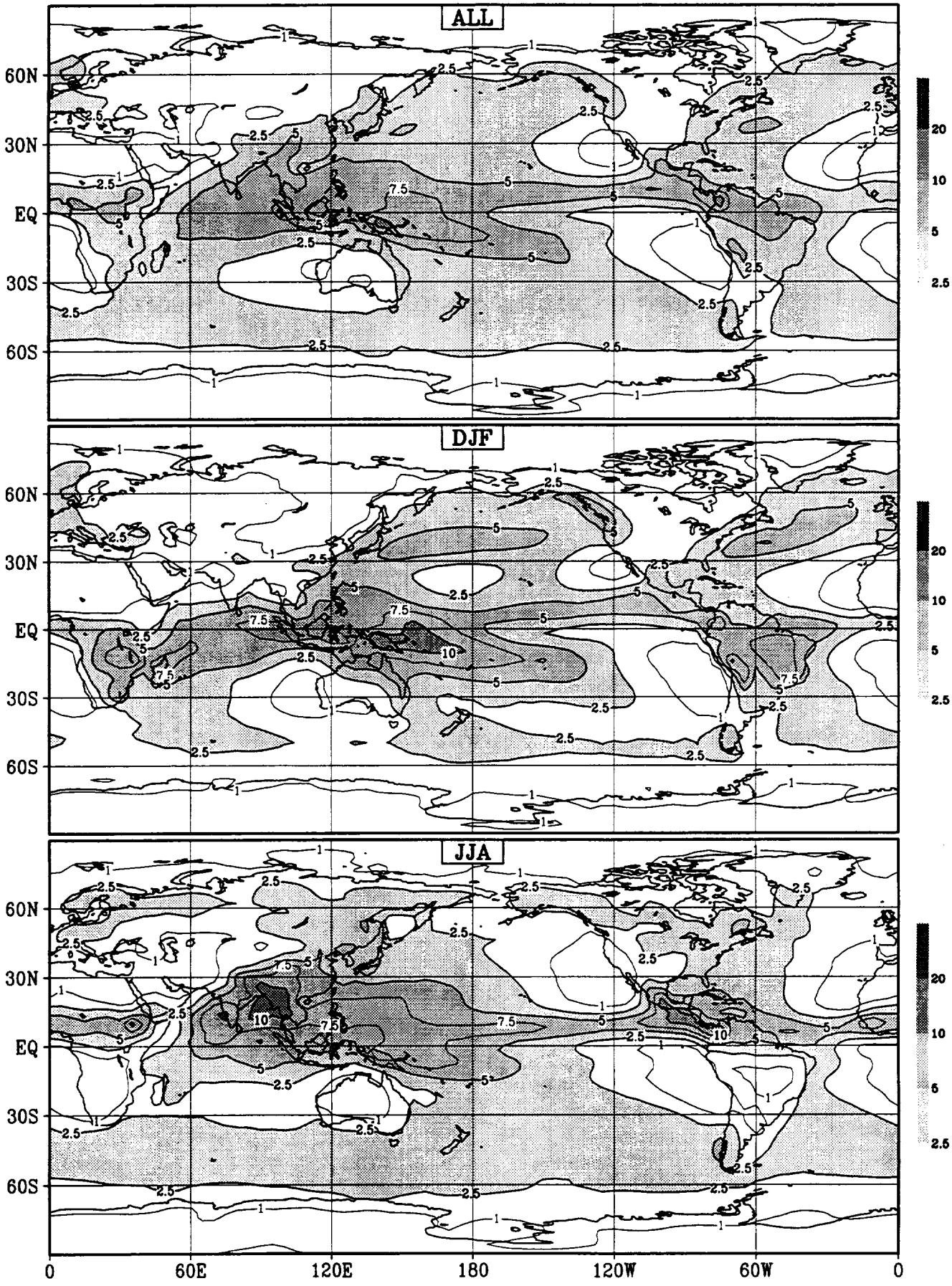

Figure 8.1

Precipitation, Standard Deviation of 23 AMIP GCMs

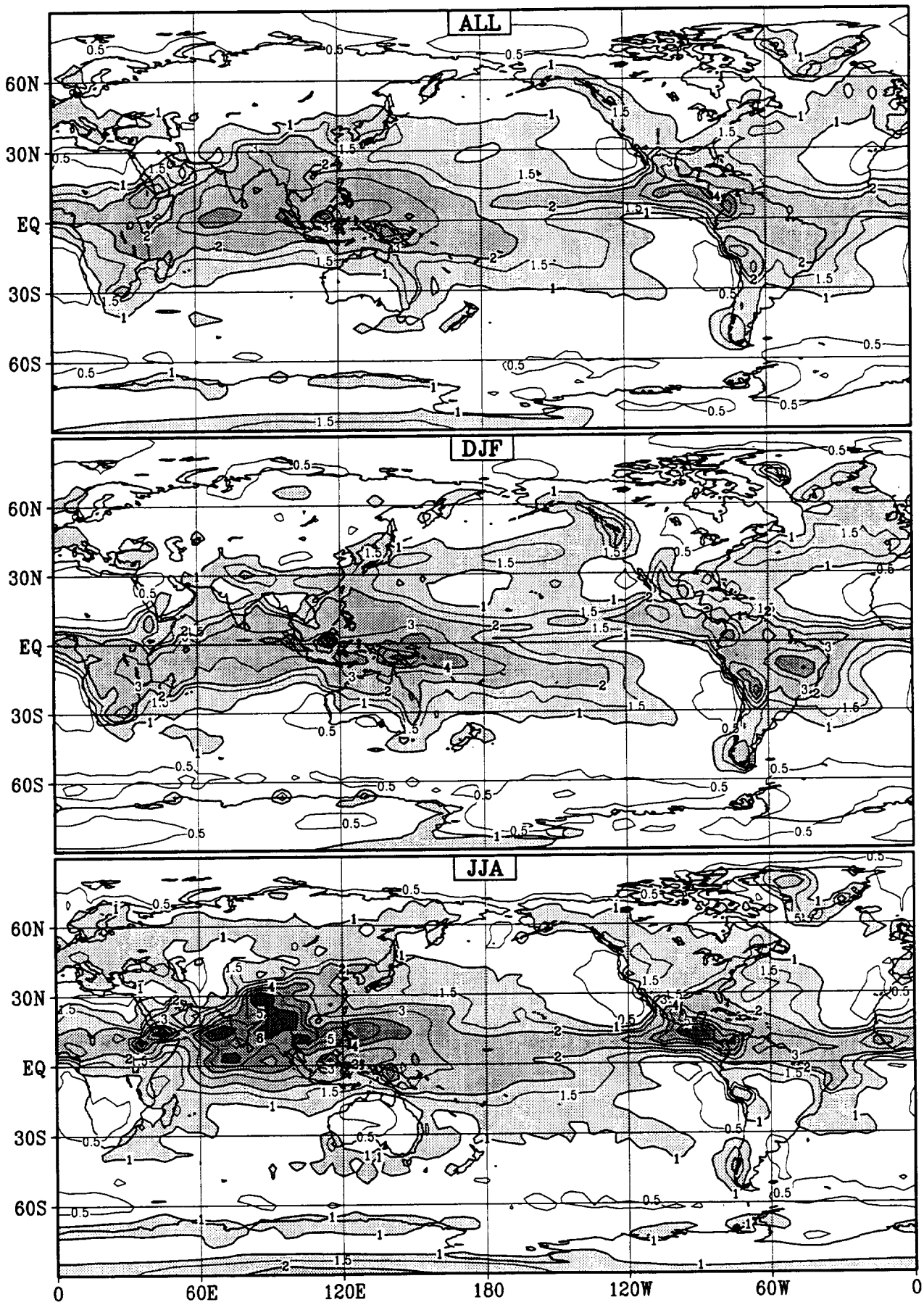

Figure 8.1 (continued)

Precipitation, Mean of 4 Verifications

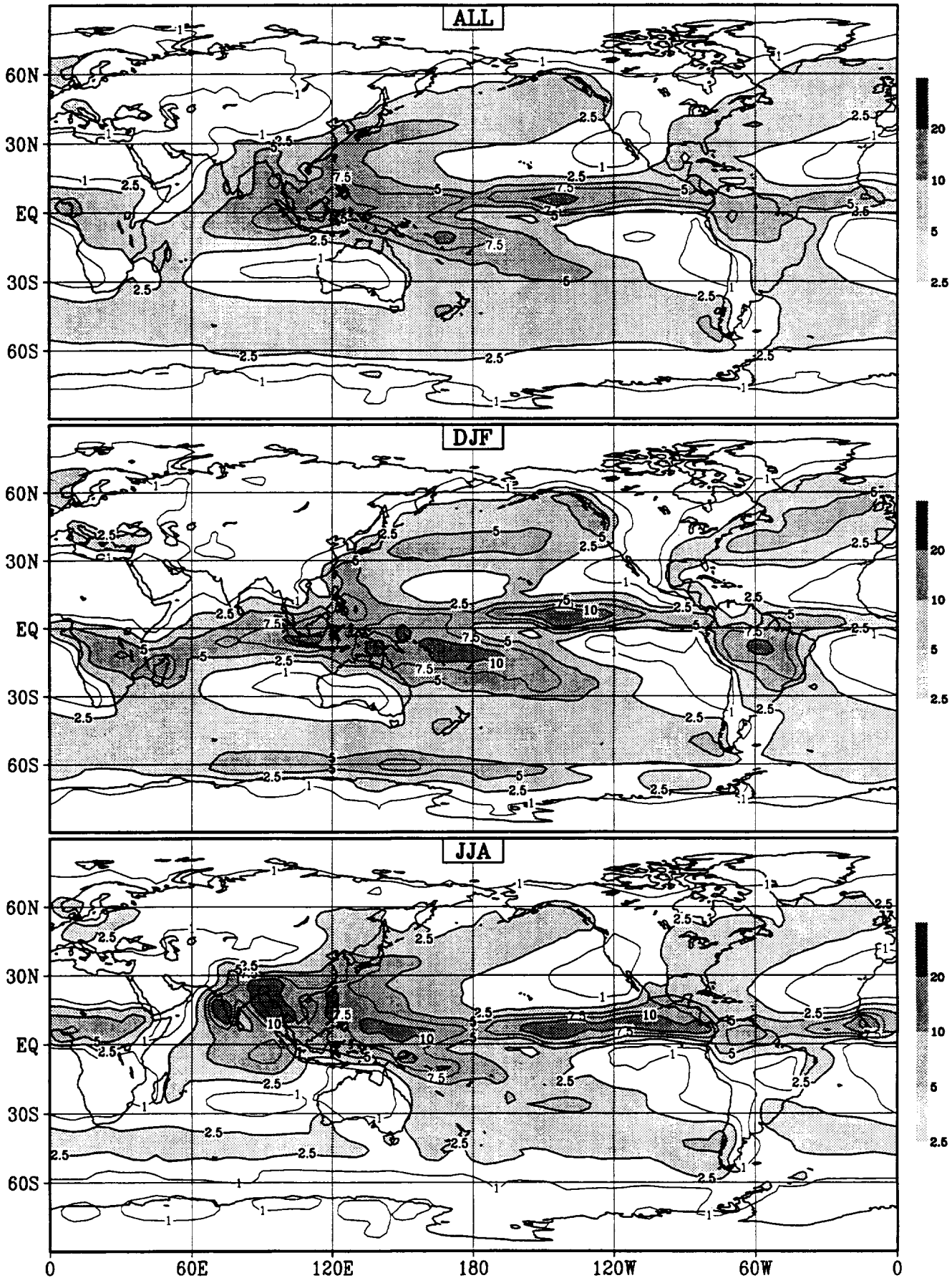

Figure 8.2

Precipitation, Standard Deviation of 4 Verifications

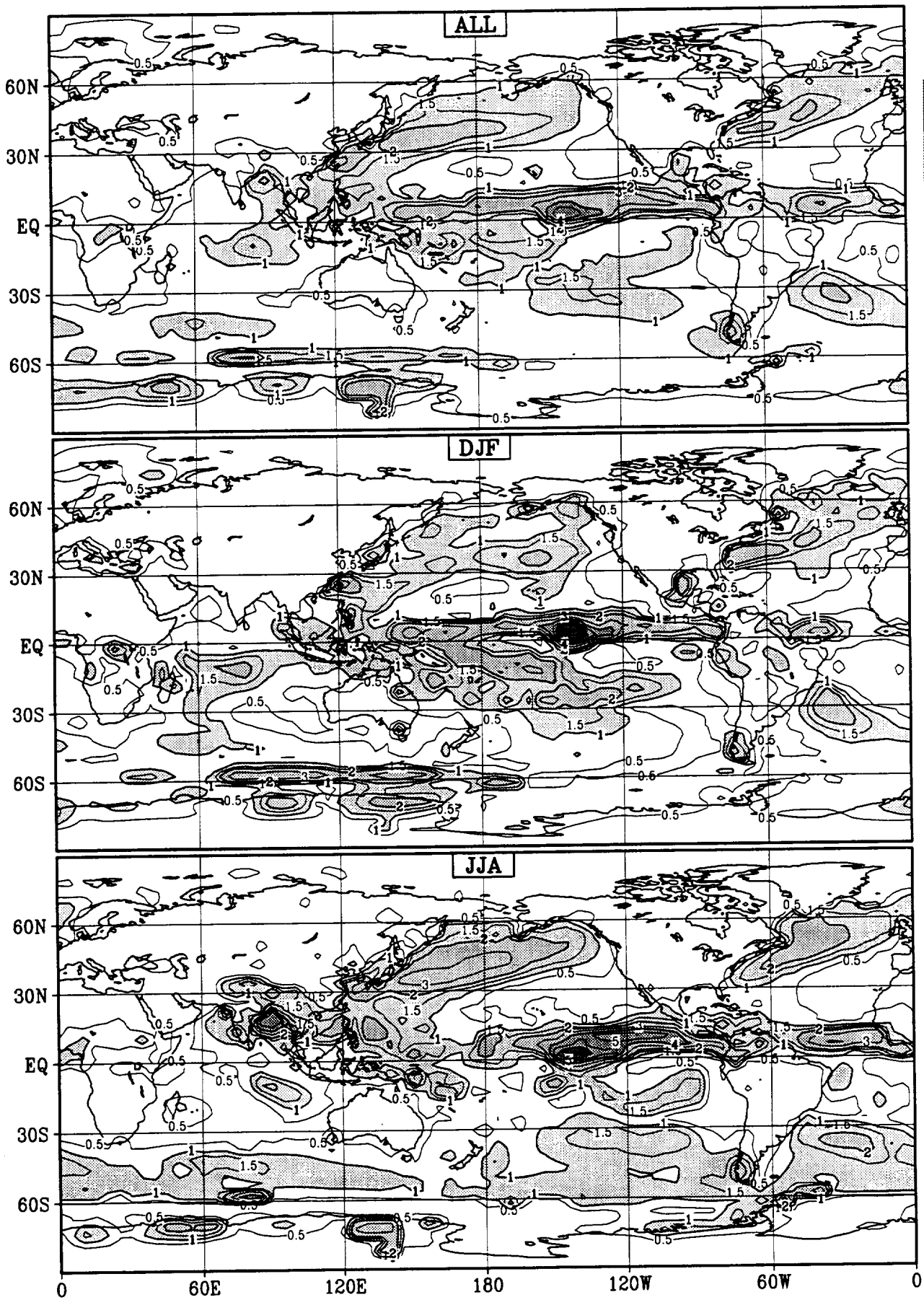

Figure 8.2 (continued)

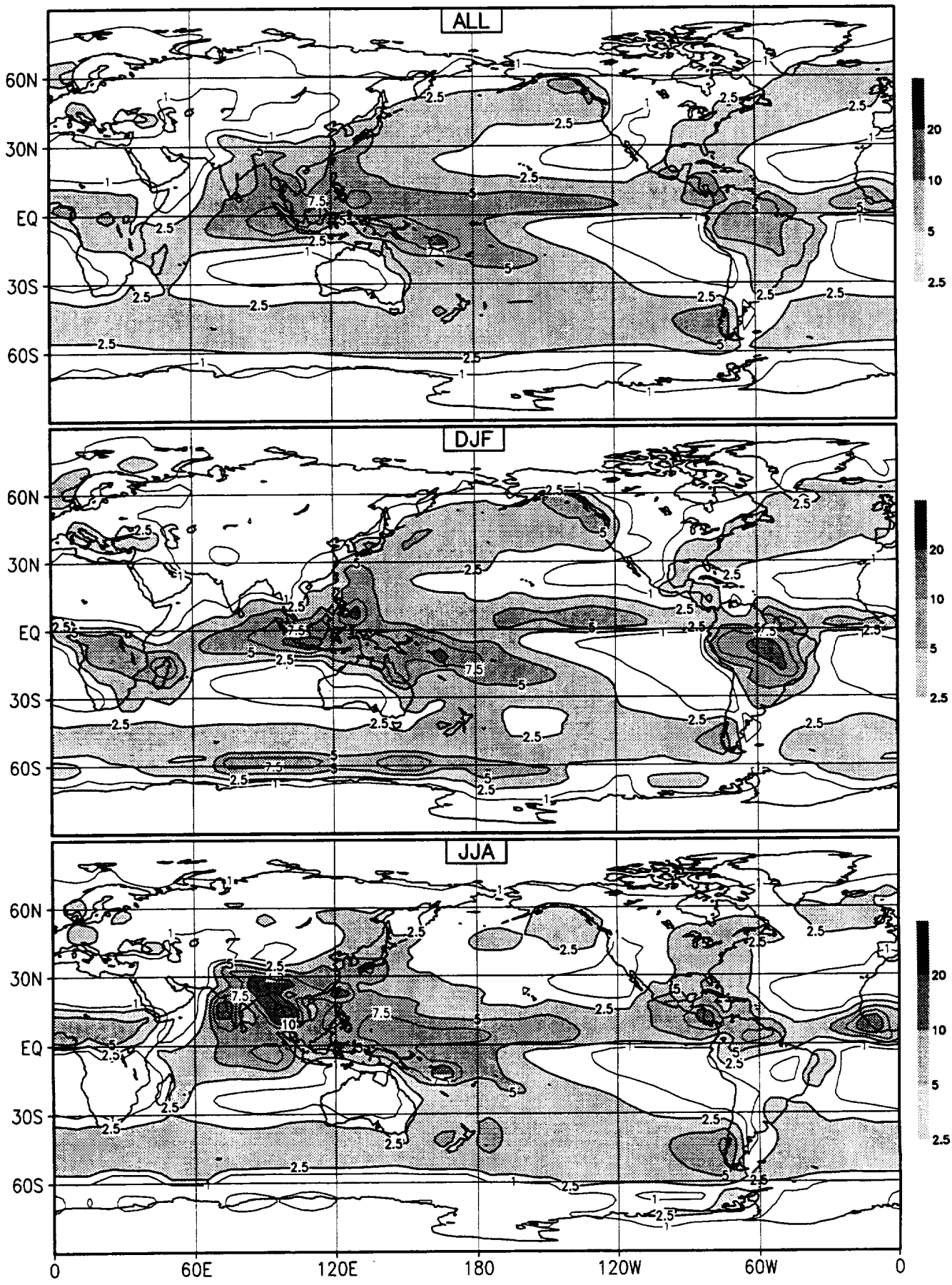
Precipitation OBS; jgr
ALL
DJF
JJA
60N
30N
EQ
30S
60S
0
60E
120E
180
120W
60W
0
20
10
5
2.5

Figure 8.3

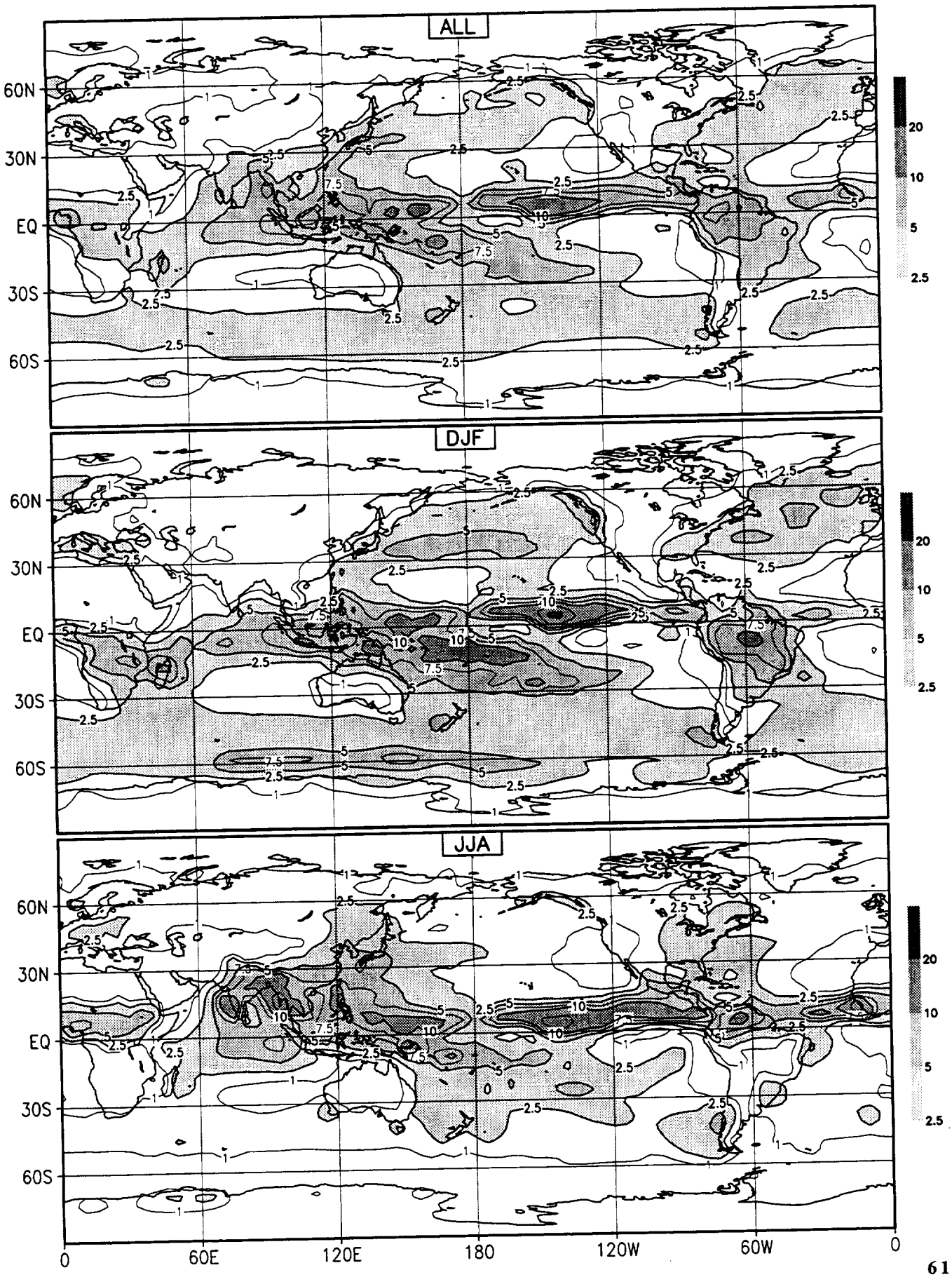

Figure 8.3 (continued)

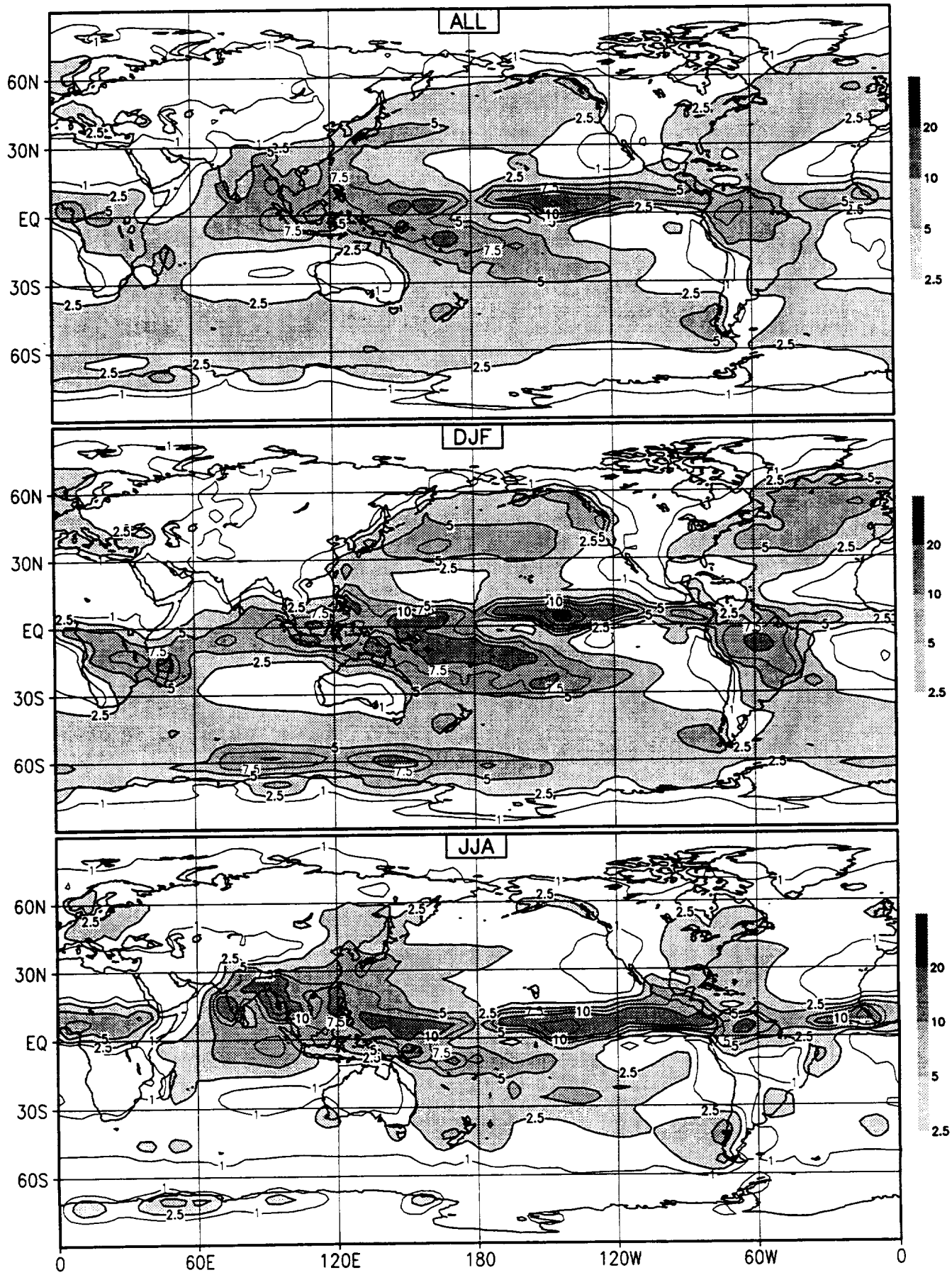

Figure 8.3 (continued)

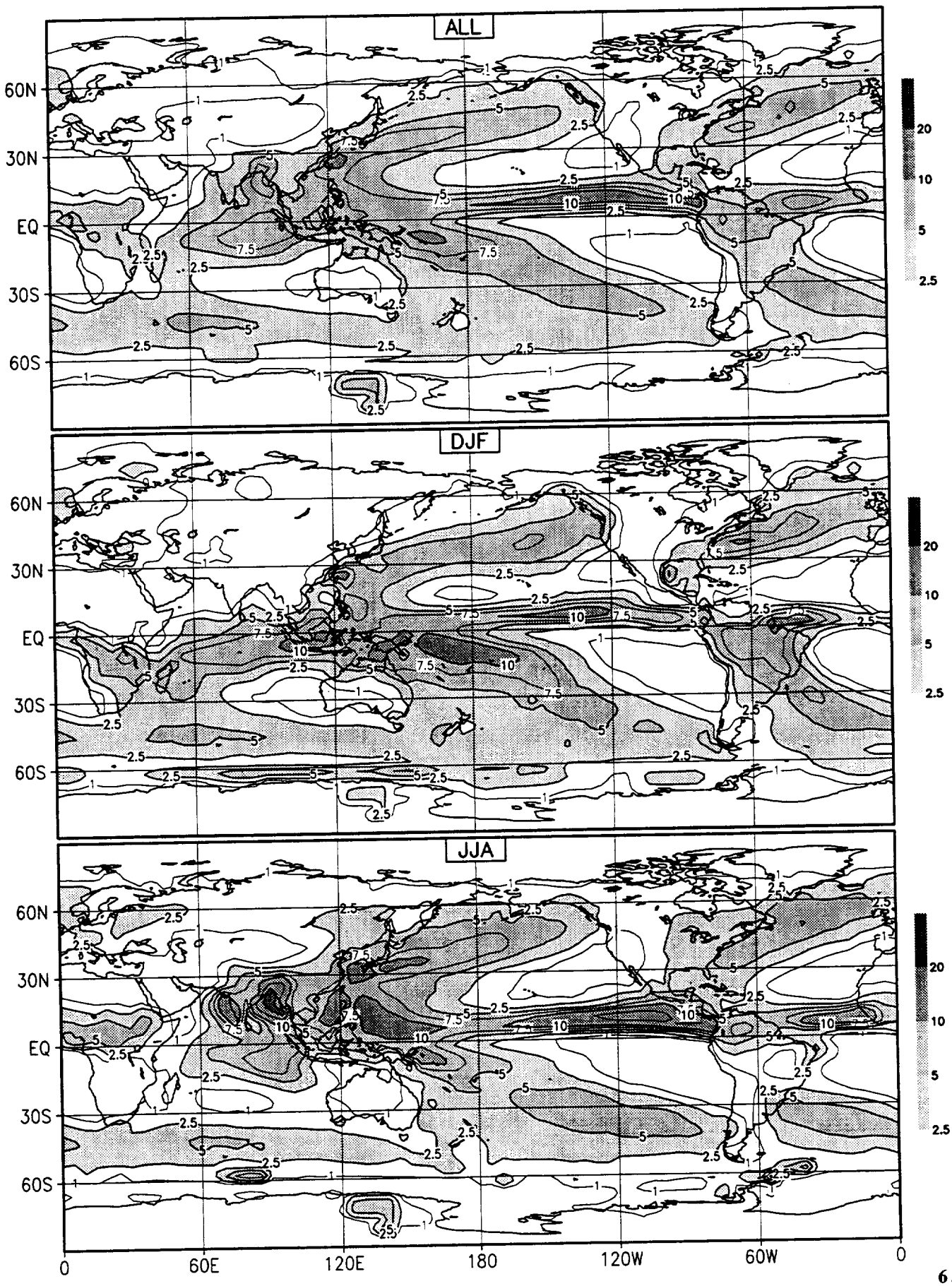

Figure 8.3 (continued)

Precipitation GCM; bmr

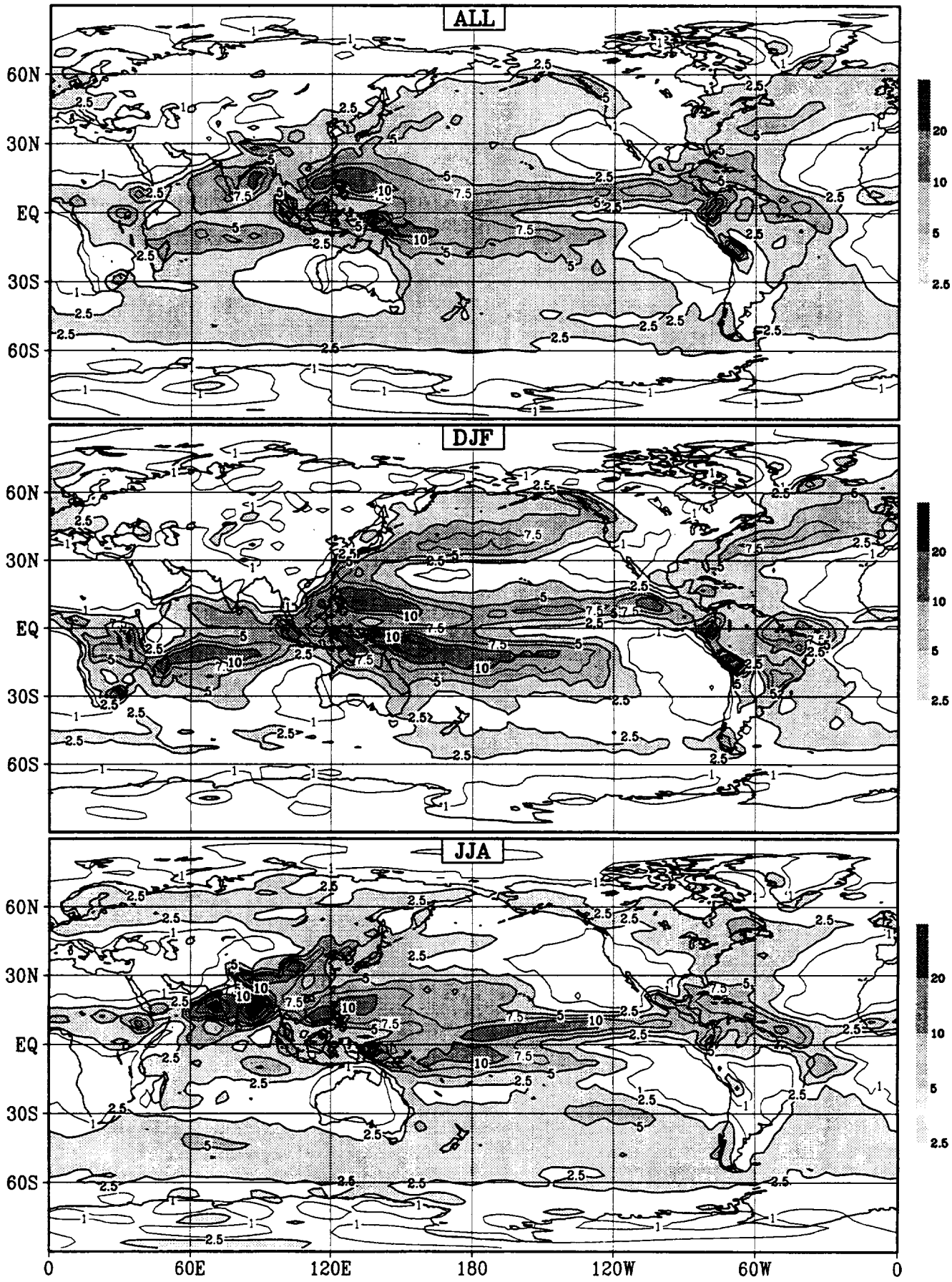

Figure 8.4

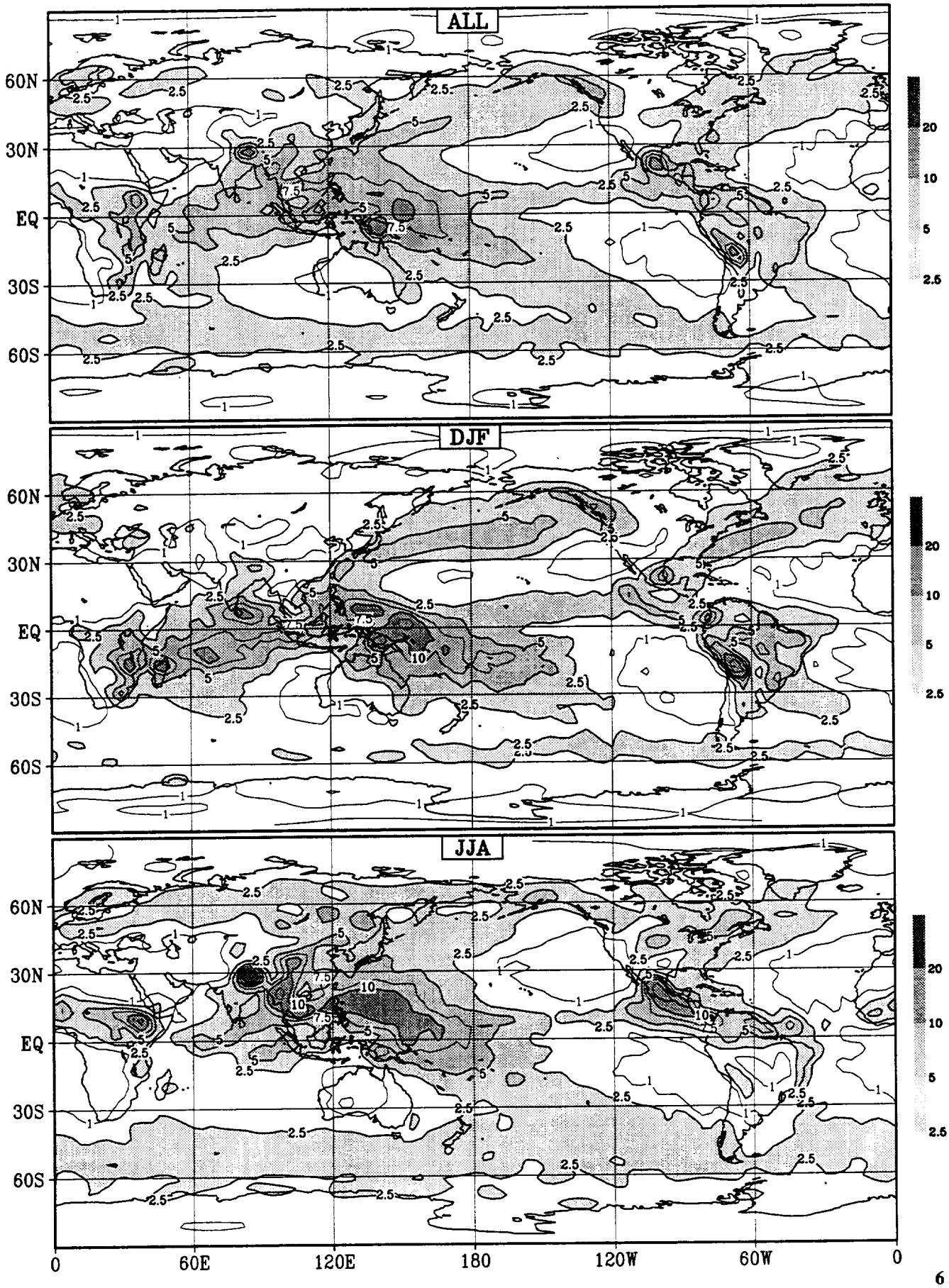

Figure 8.4 (continued)

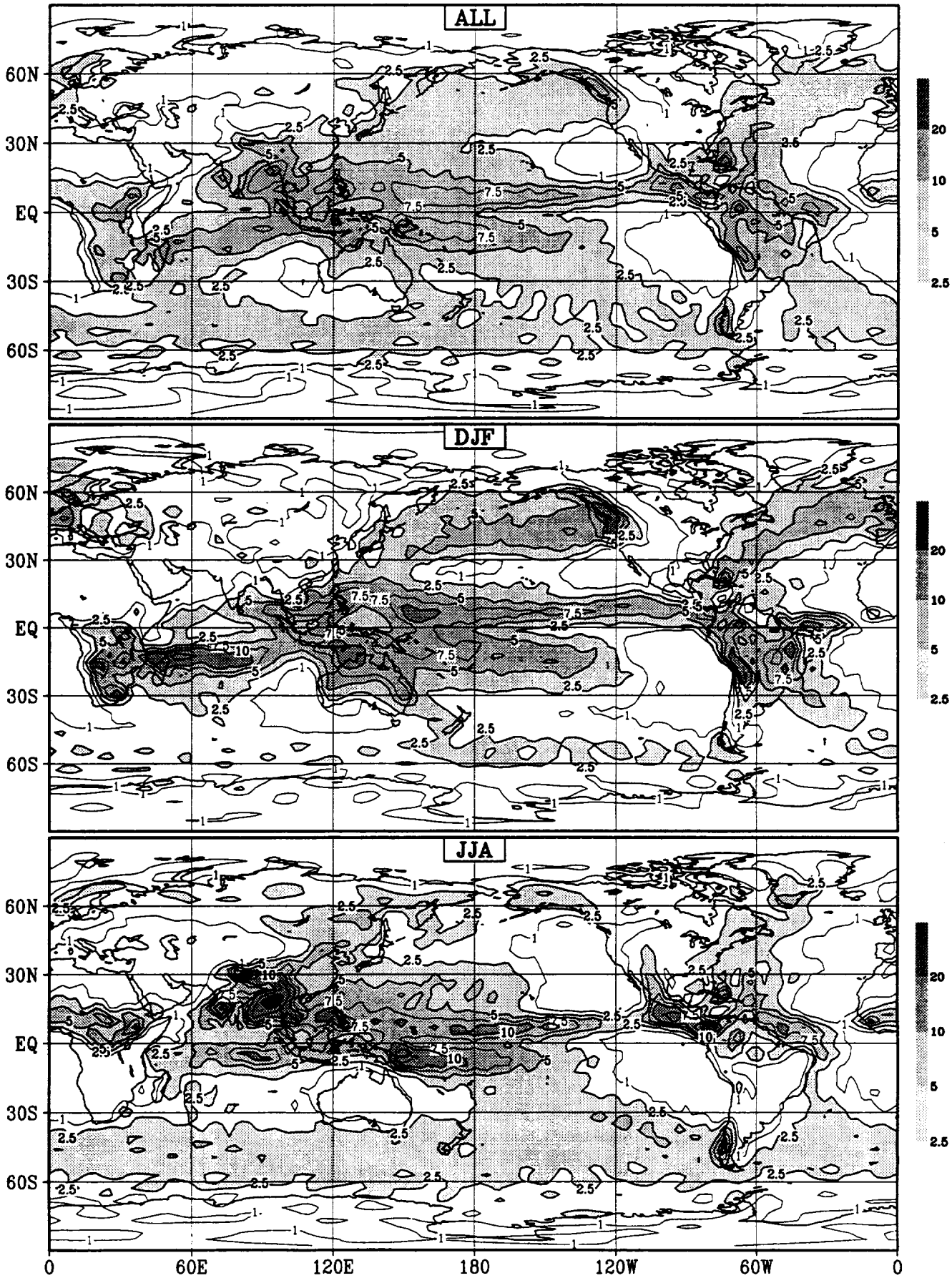

Figure 8.4 (continued)

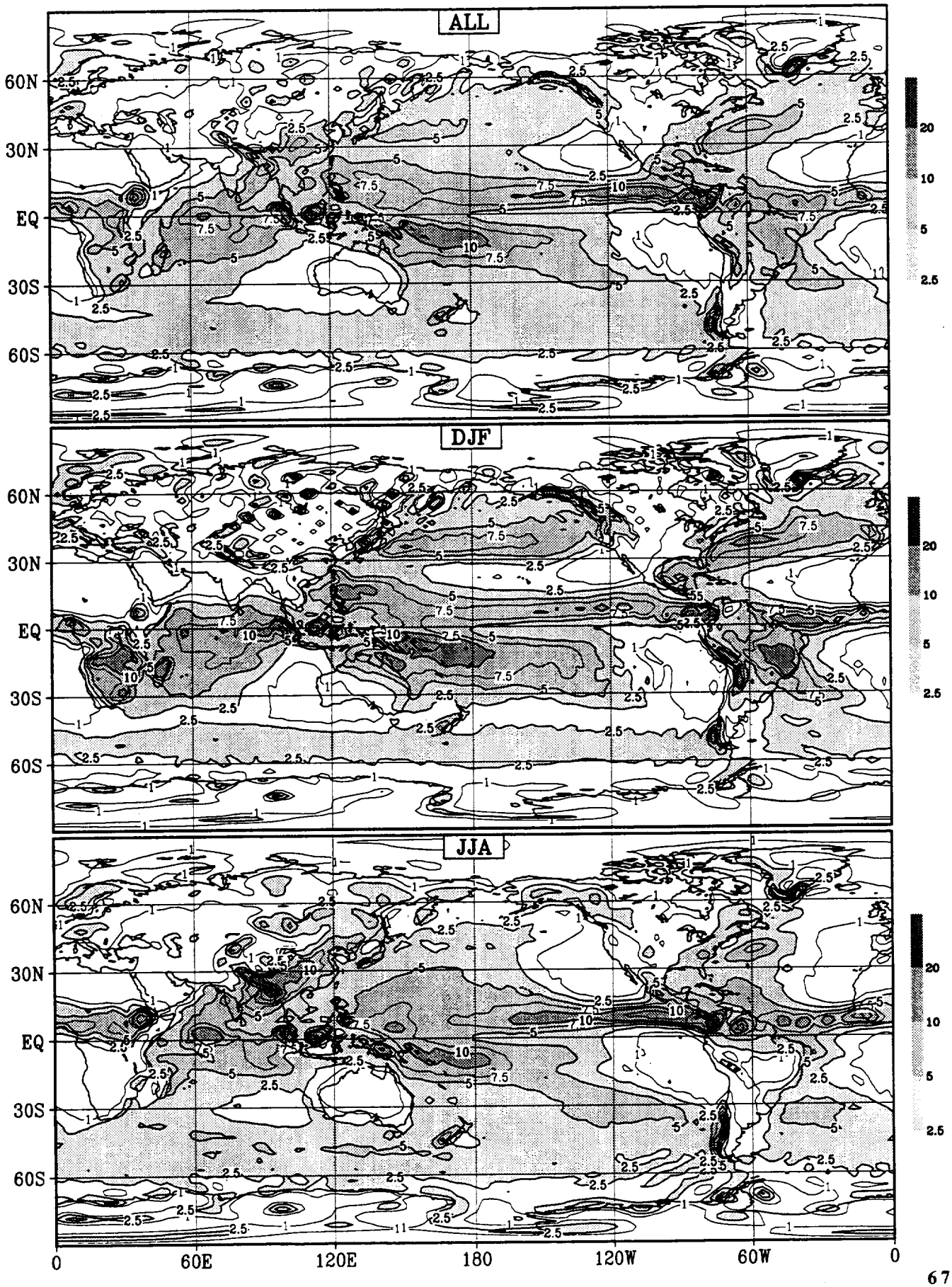

Figure 8.4 (continued)

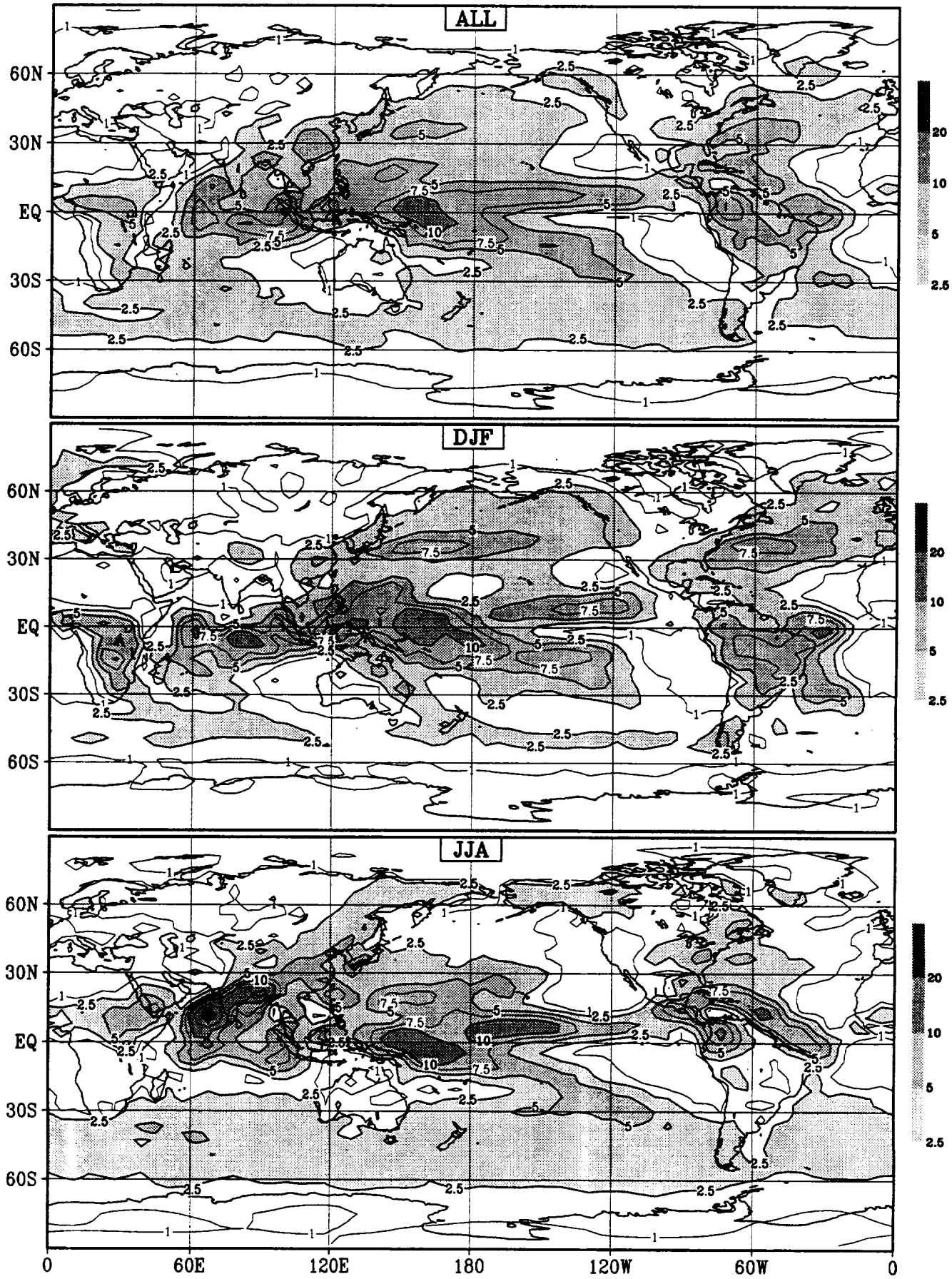

Figure 8.4 (continued)

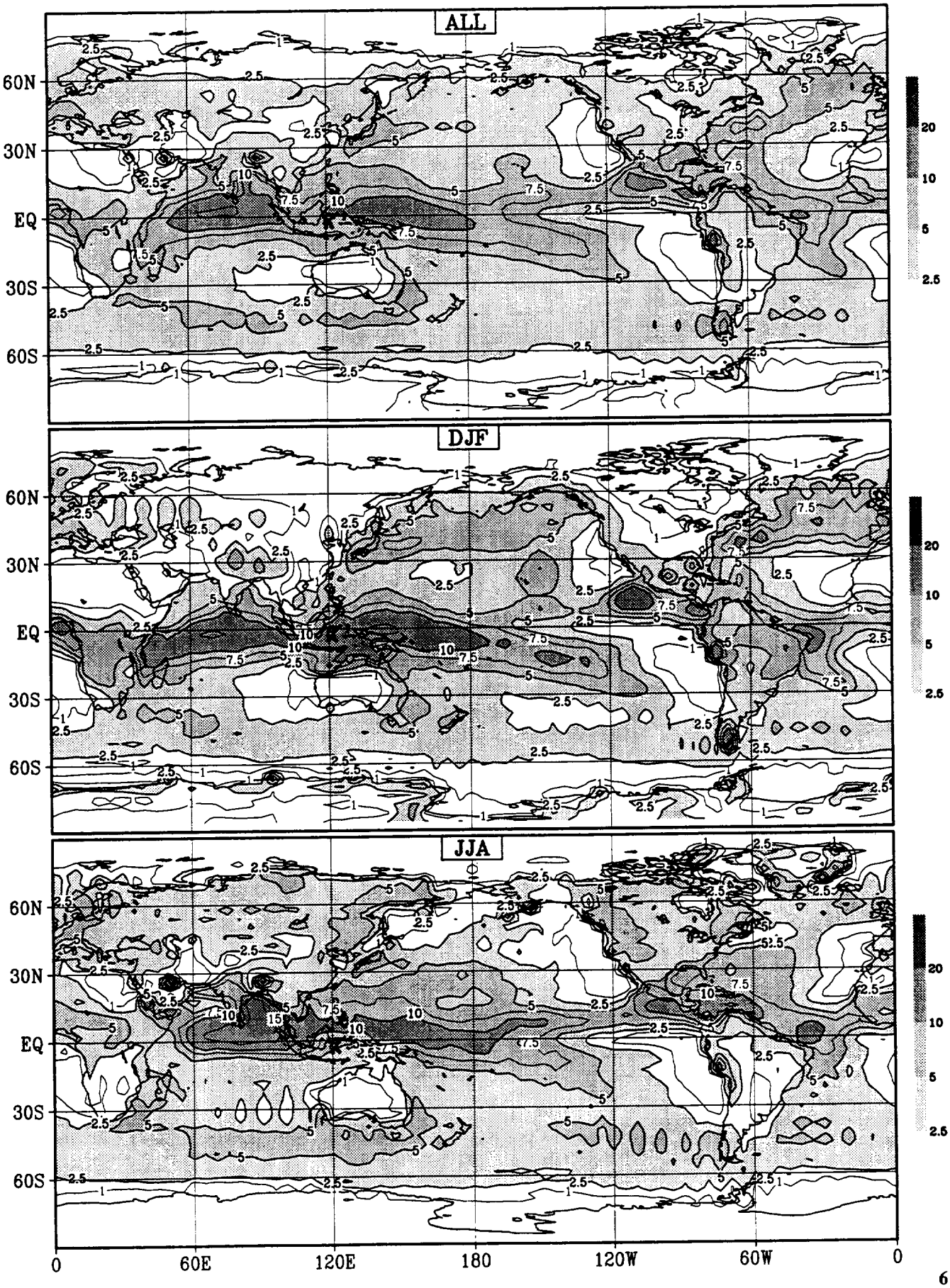

Figure 8.4 (continued)

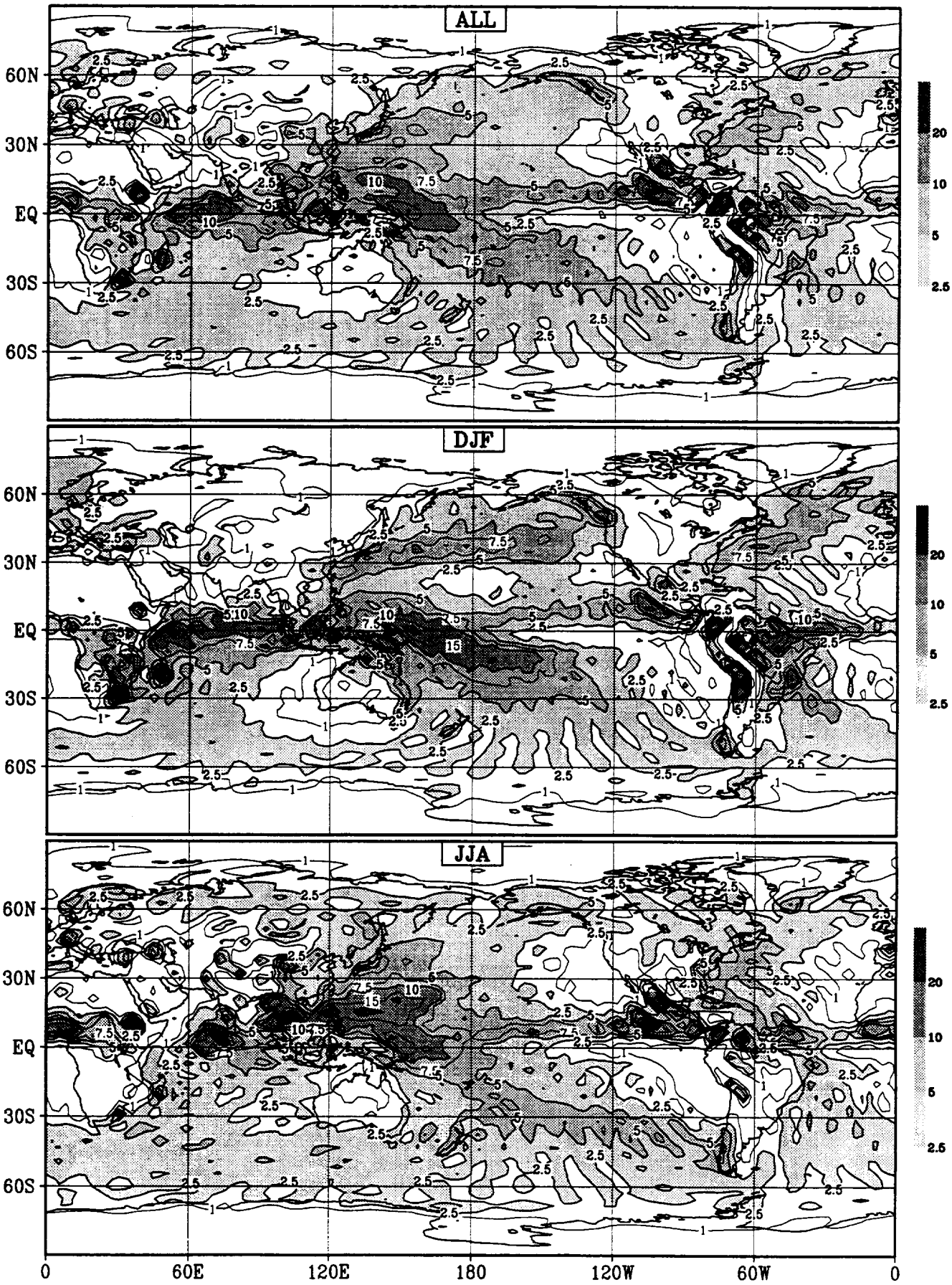

Figure 8.4 (continued)

Precipitation GCM; dnm

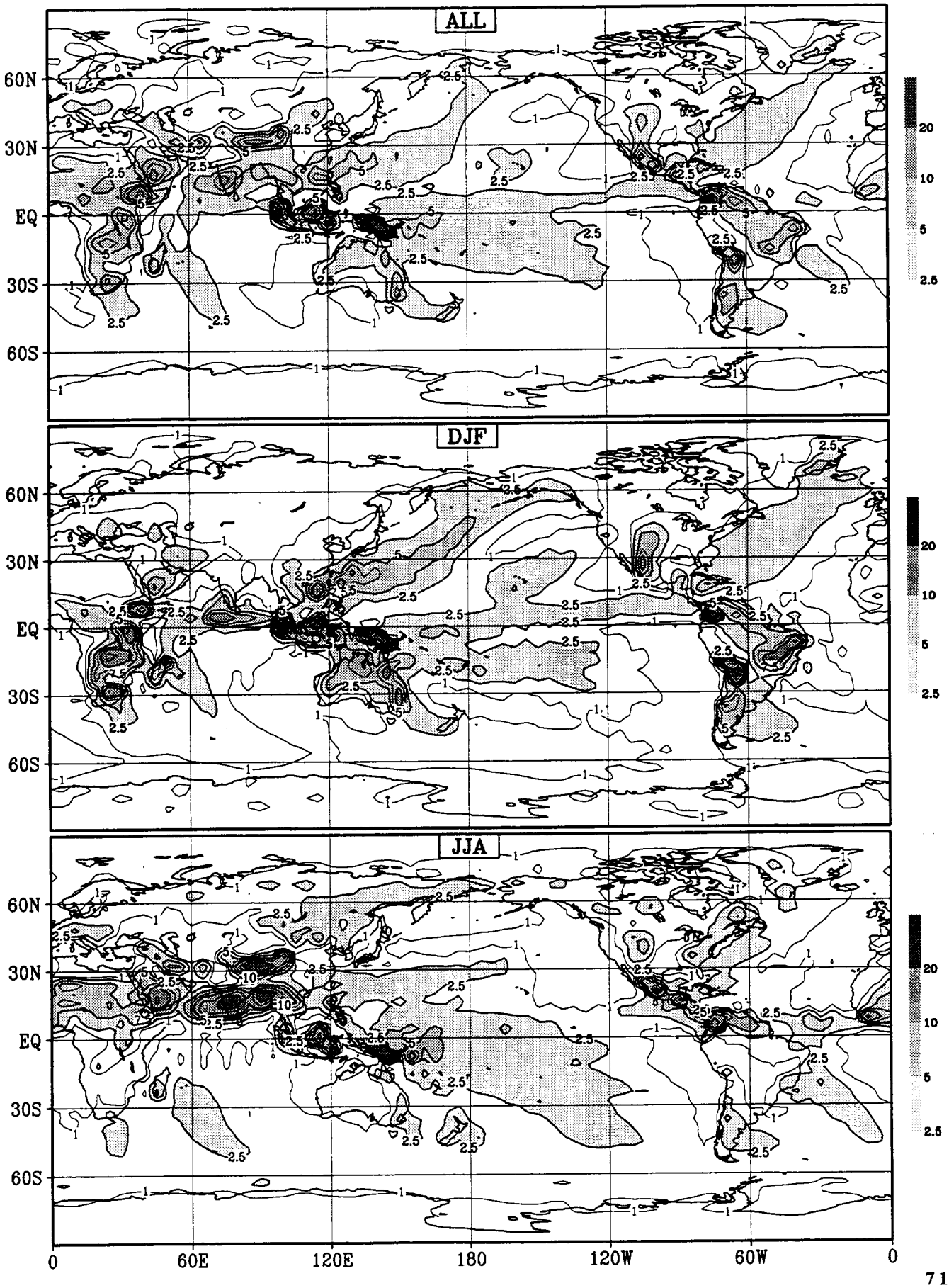

Figure 8.4 (continued)

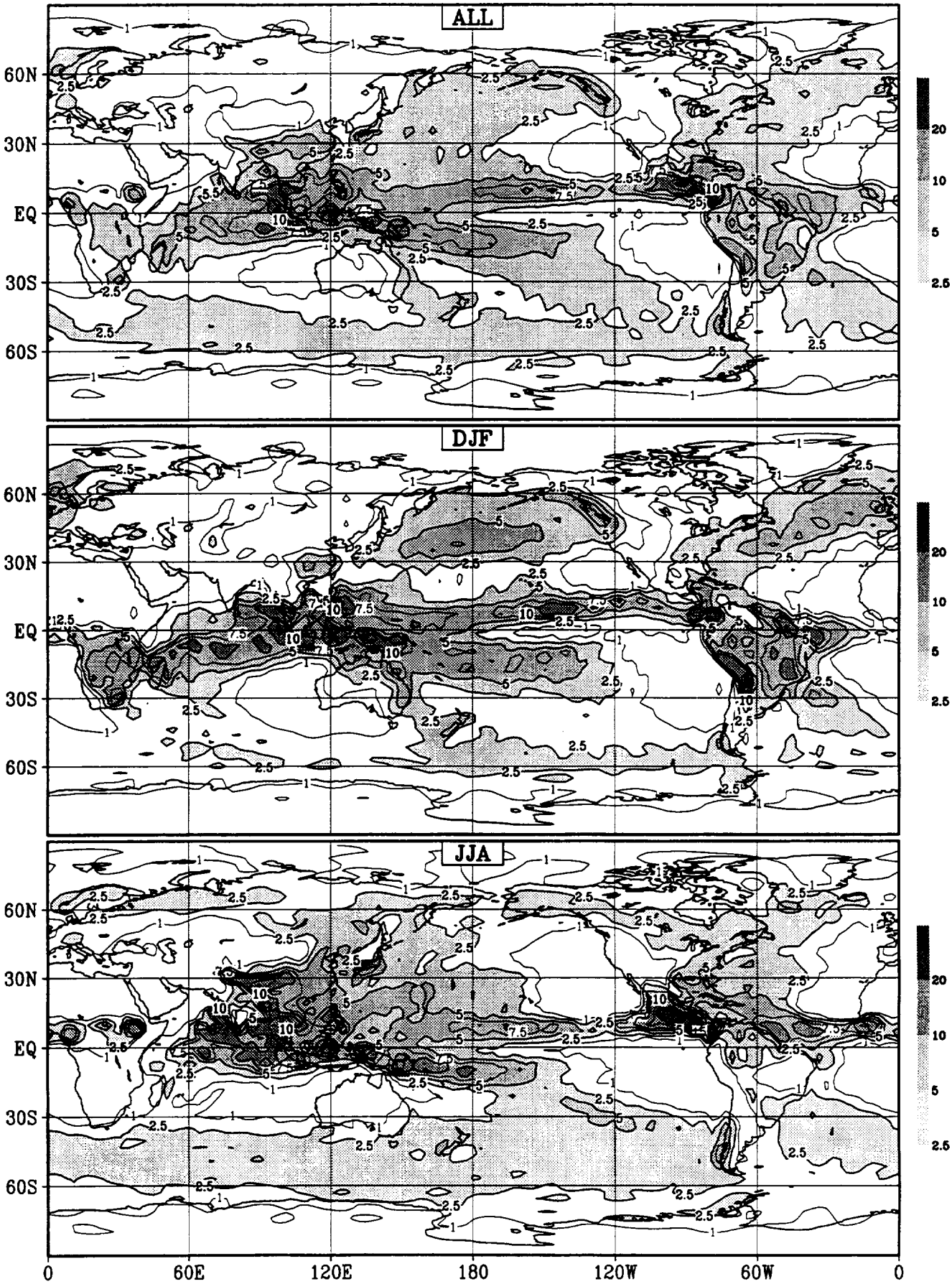

Figure 8.4 (continued)

Precipitation GCM; gfd

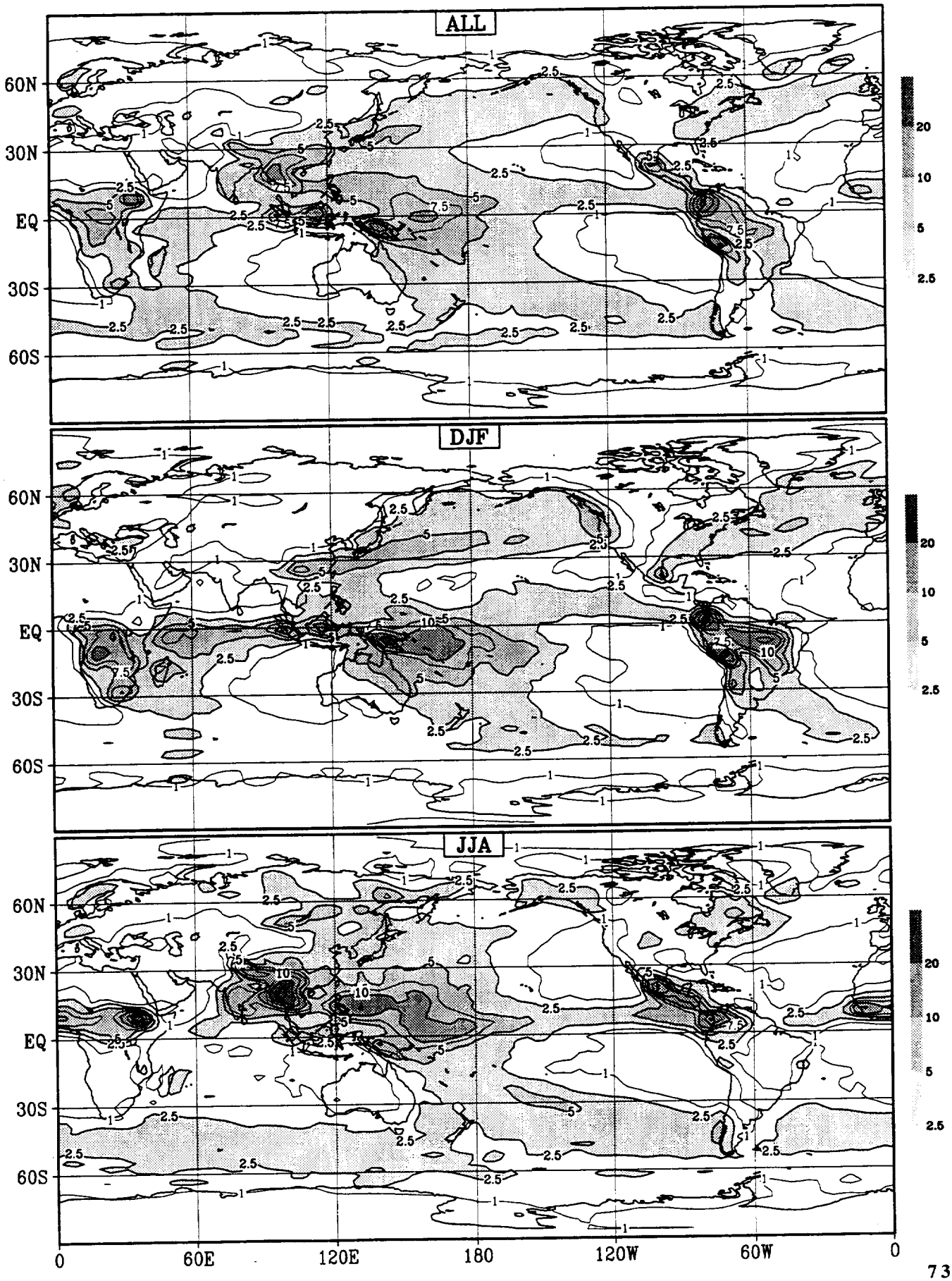

Figure 8.4 (continued)

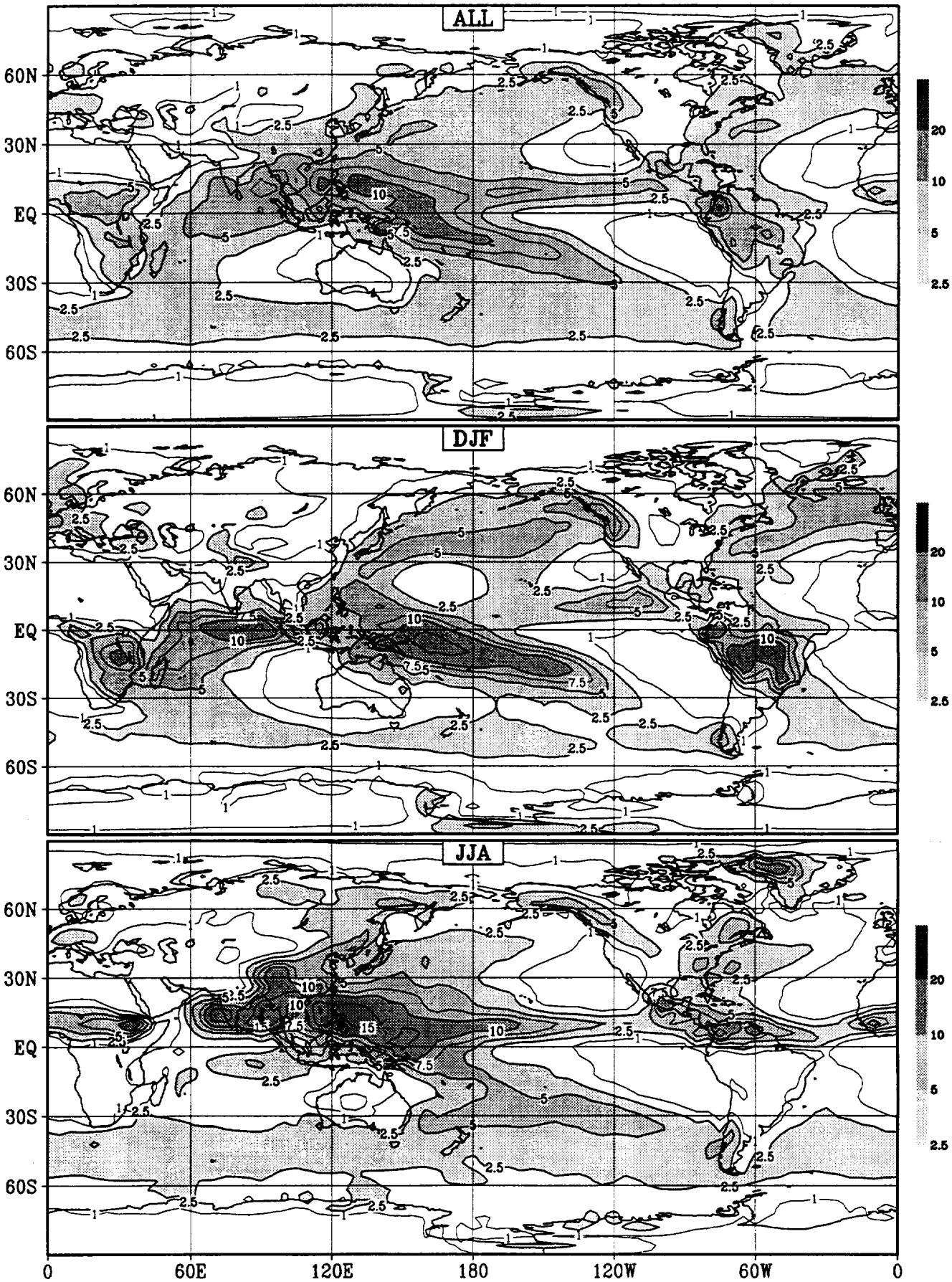

Figure 8.4 (continued)

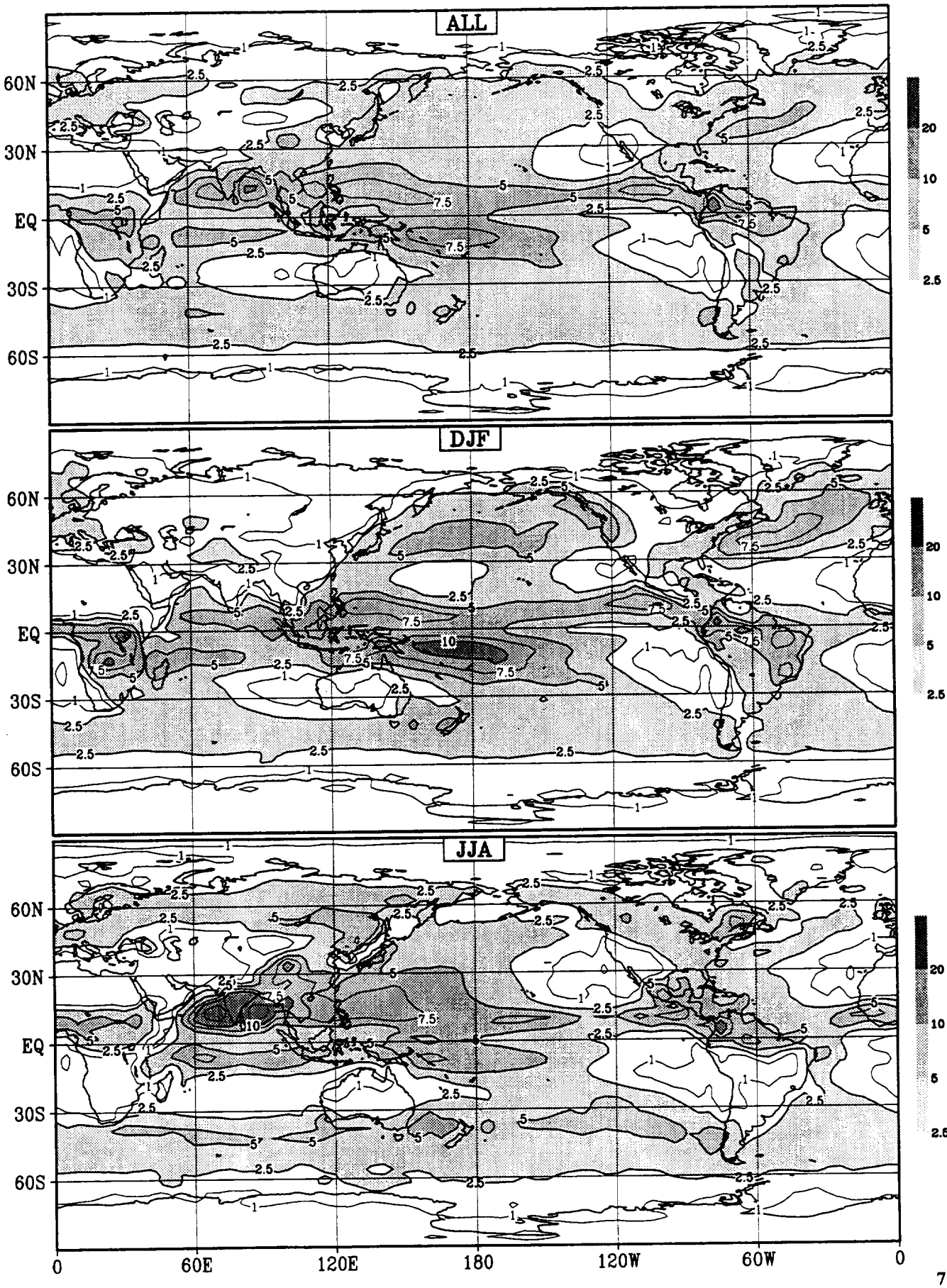

Figure 8.4 (continued)

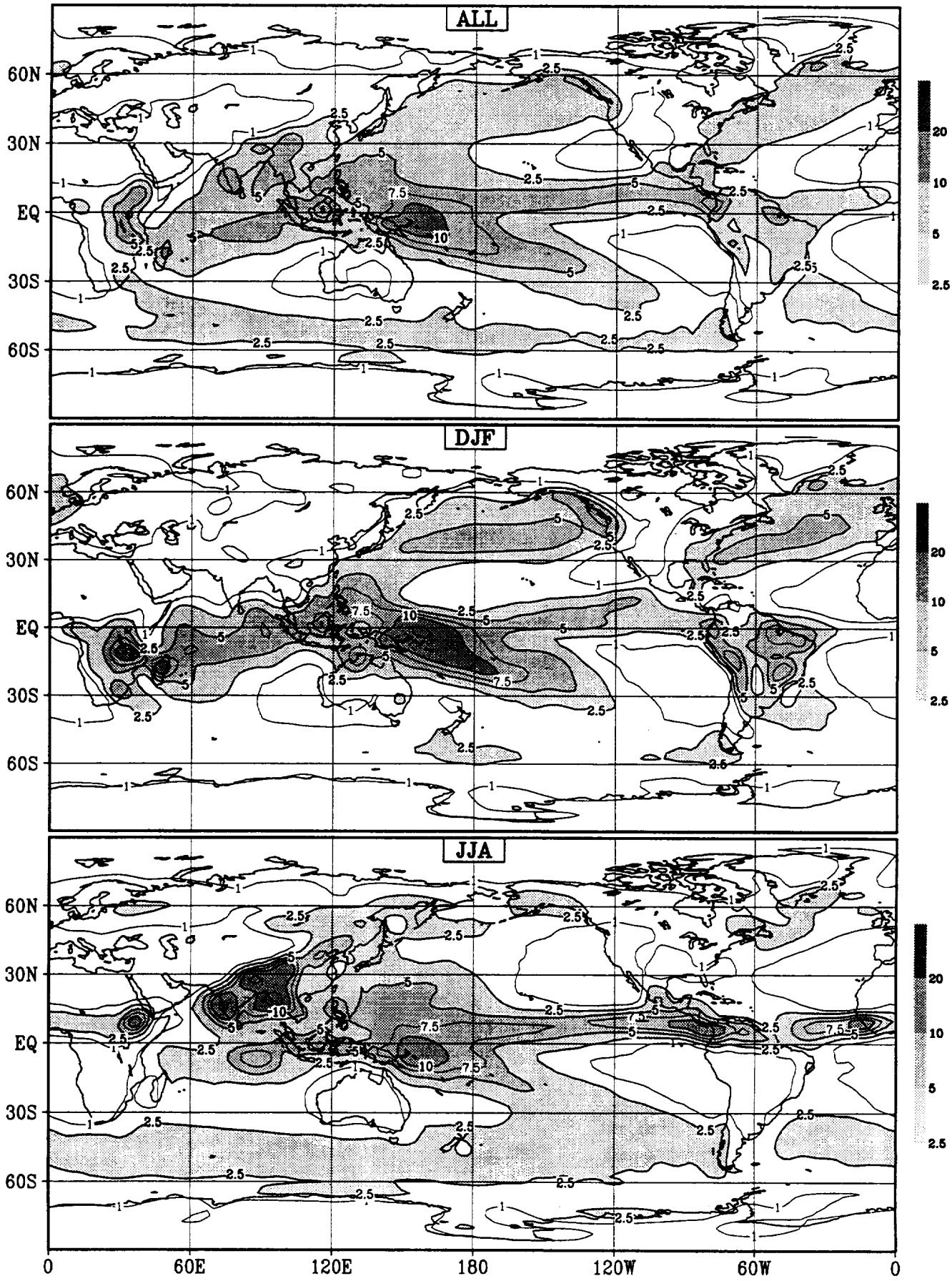

Figure 8.4 (continued)

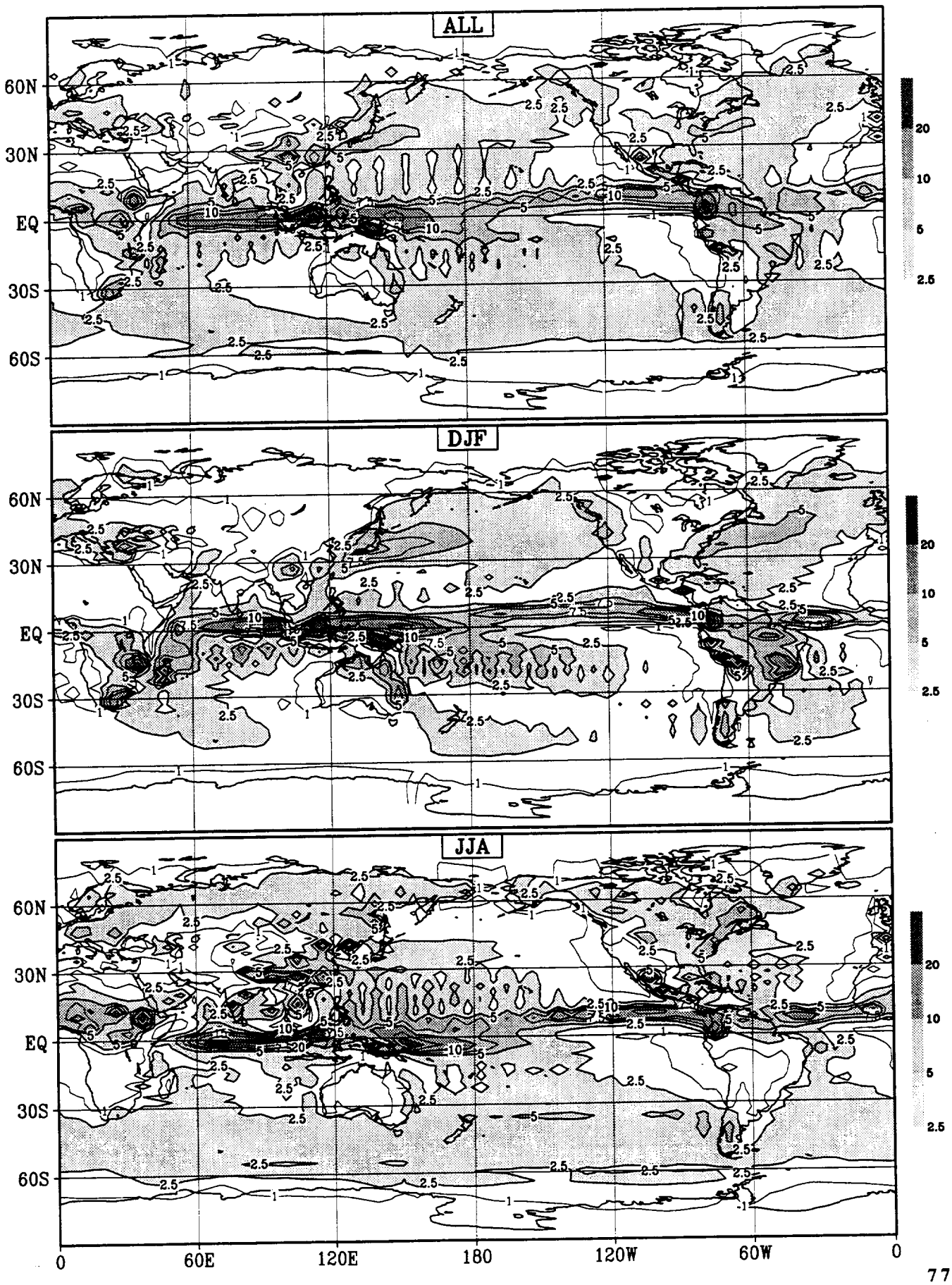

Figure 8.4 (continued)

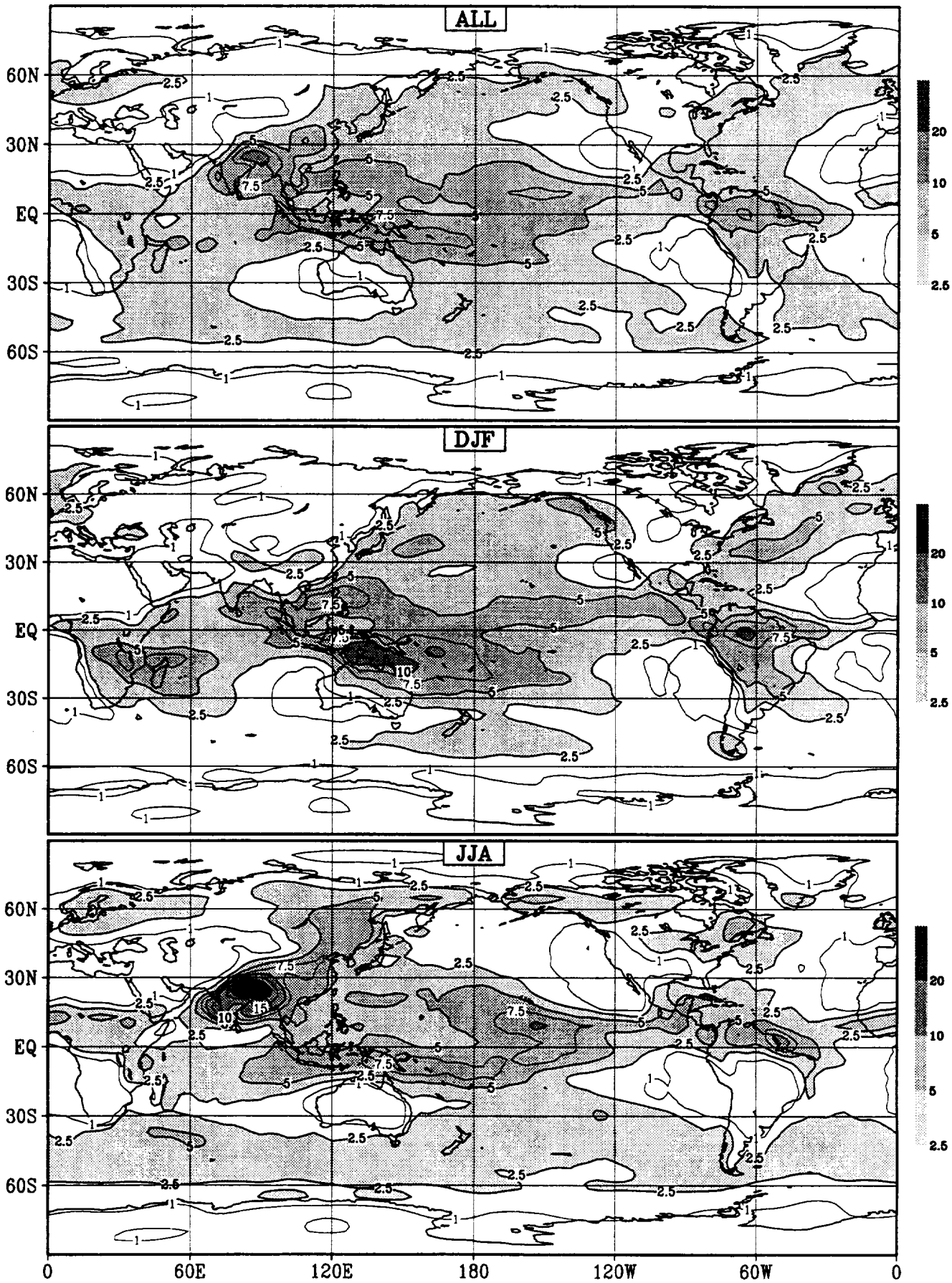

Figure 8.4 (continued)

Precipitation GCM; mpi

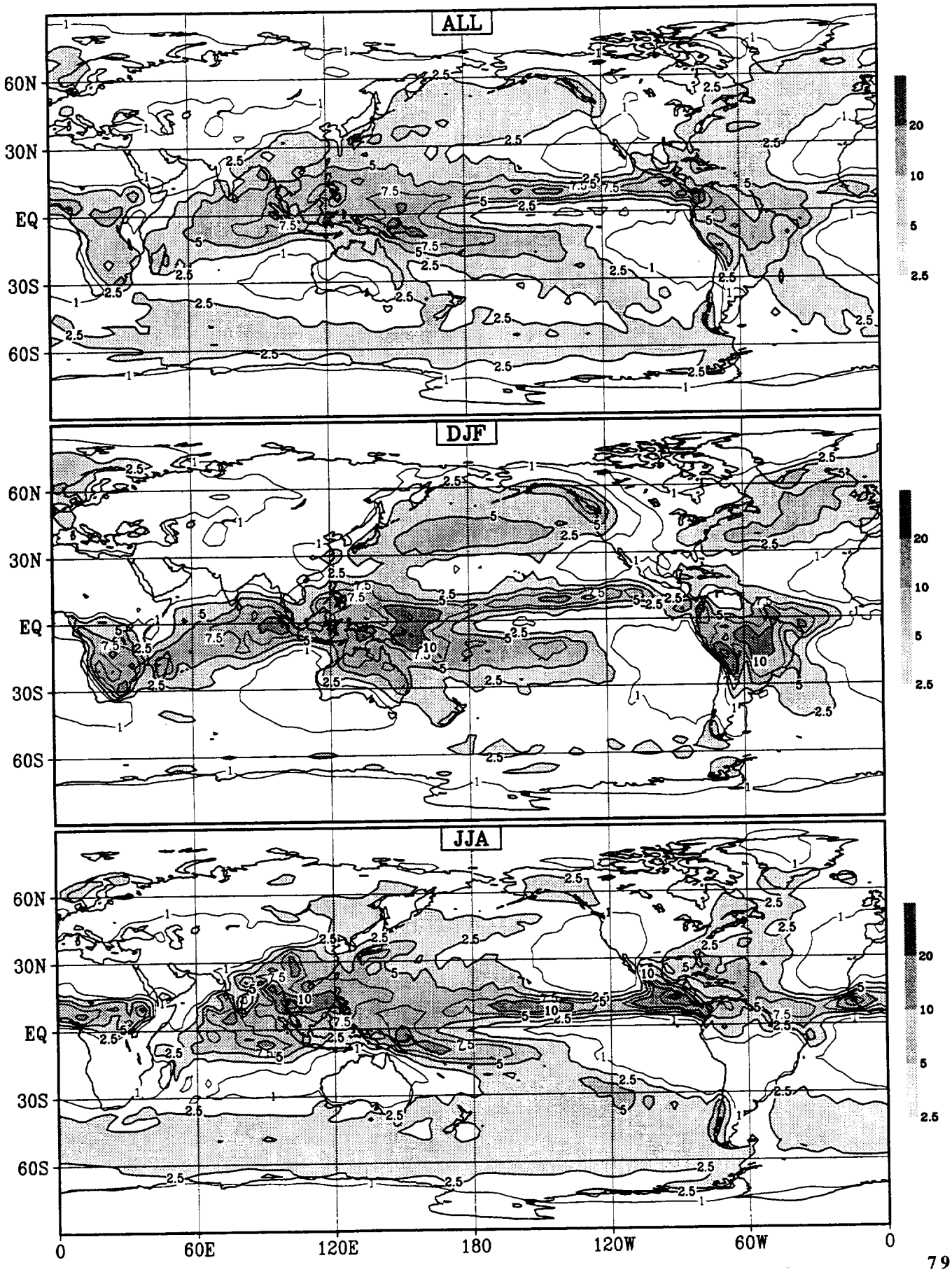

Figure 8.4 (continued)

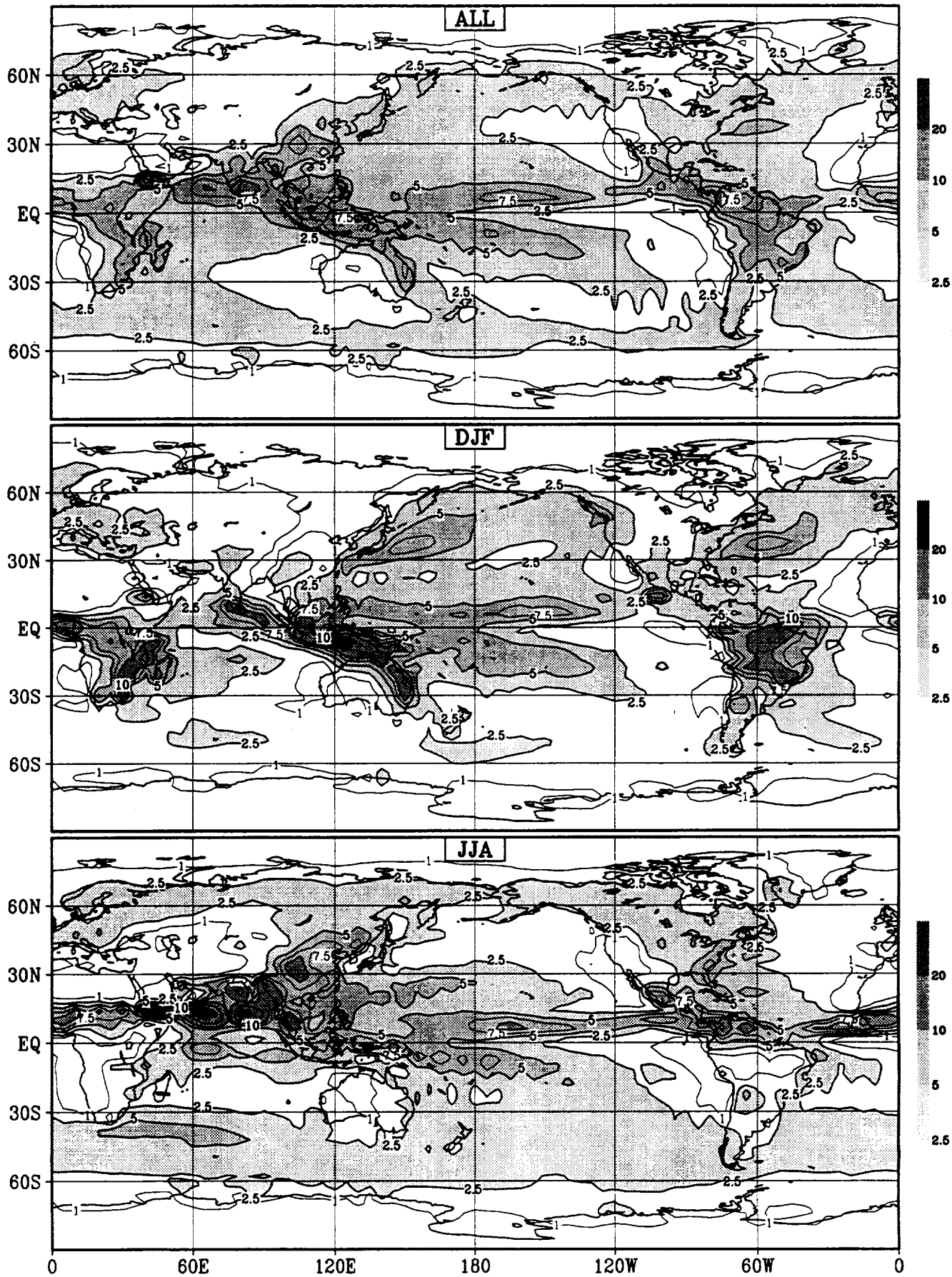

Figure 8.4 (continued)

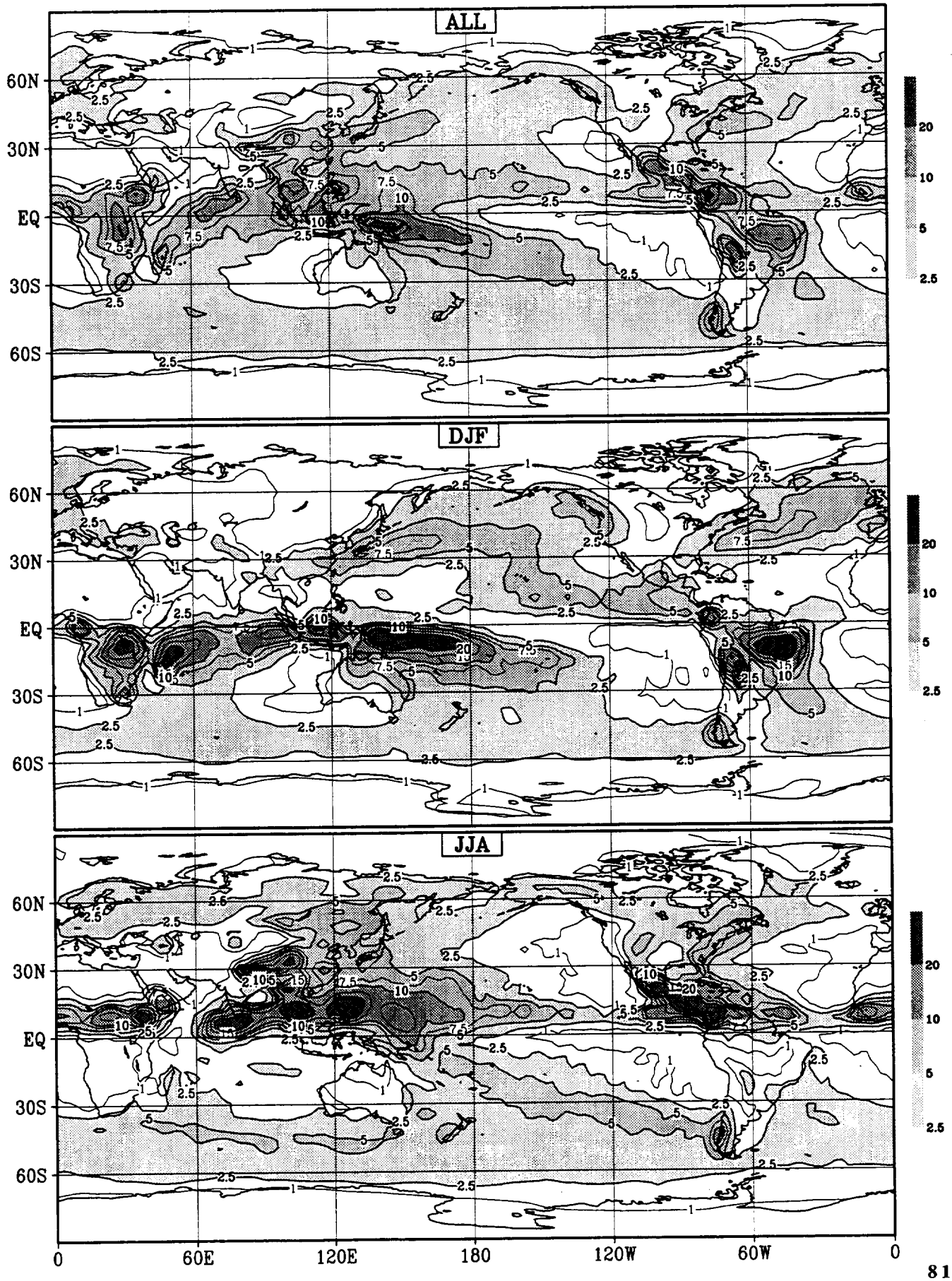

Figure 8.4 (continued)

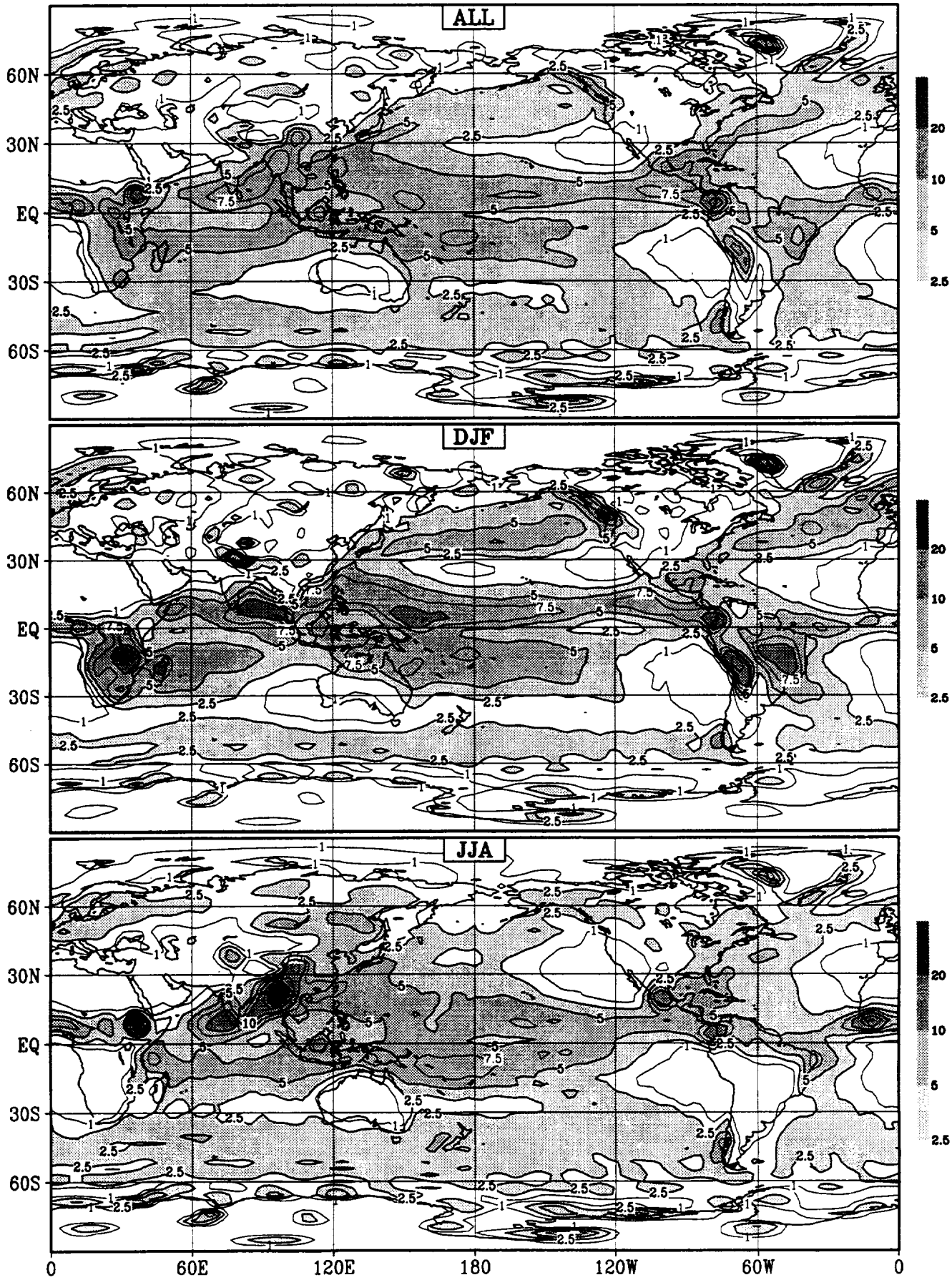

Figure 8.4 (continued)

Precipitation GCM; sun

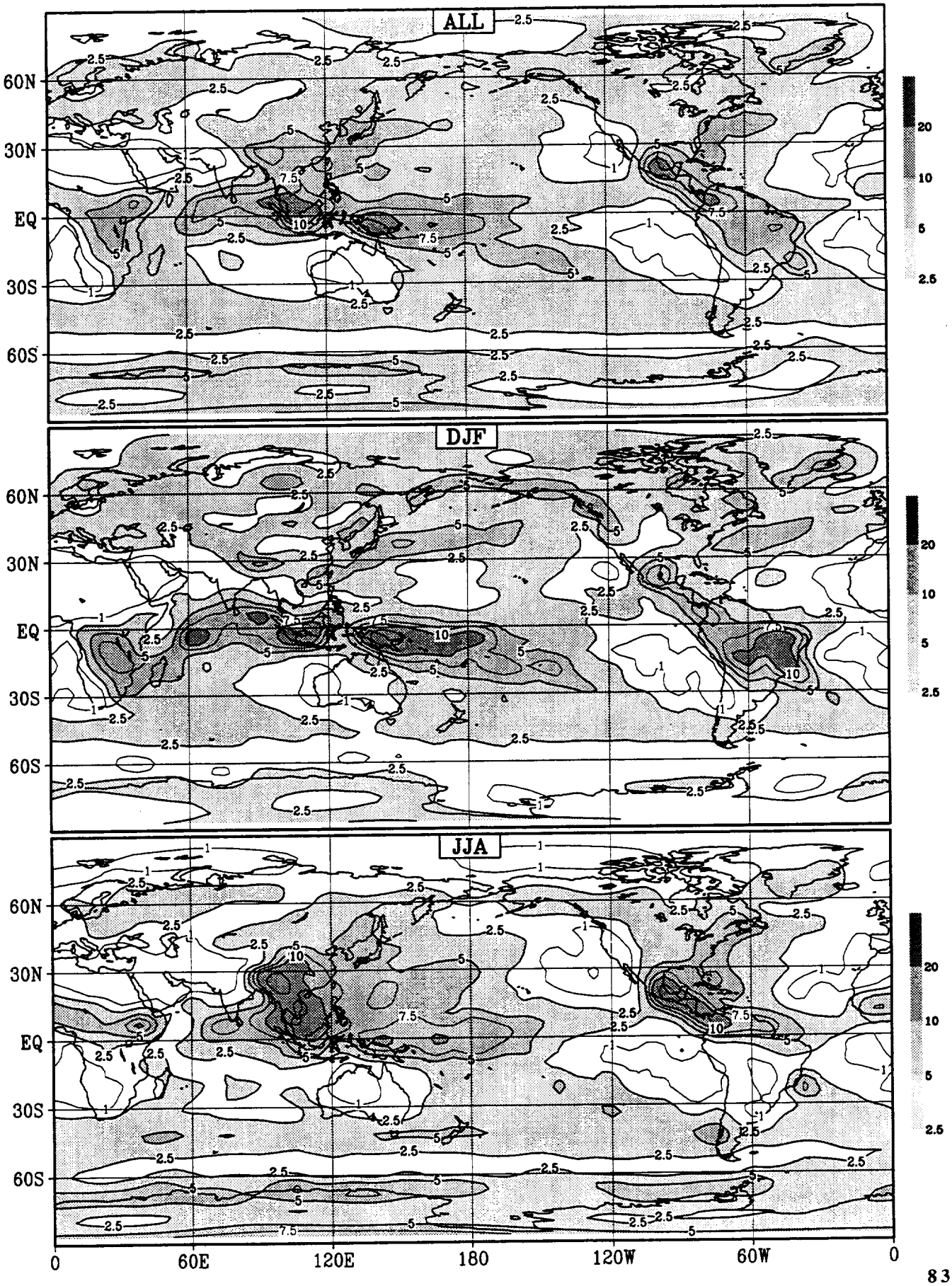

Figure 8.4 (continued)

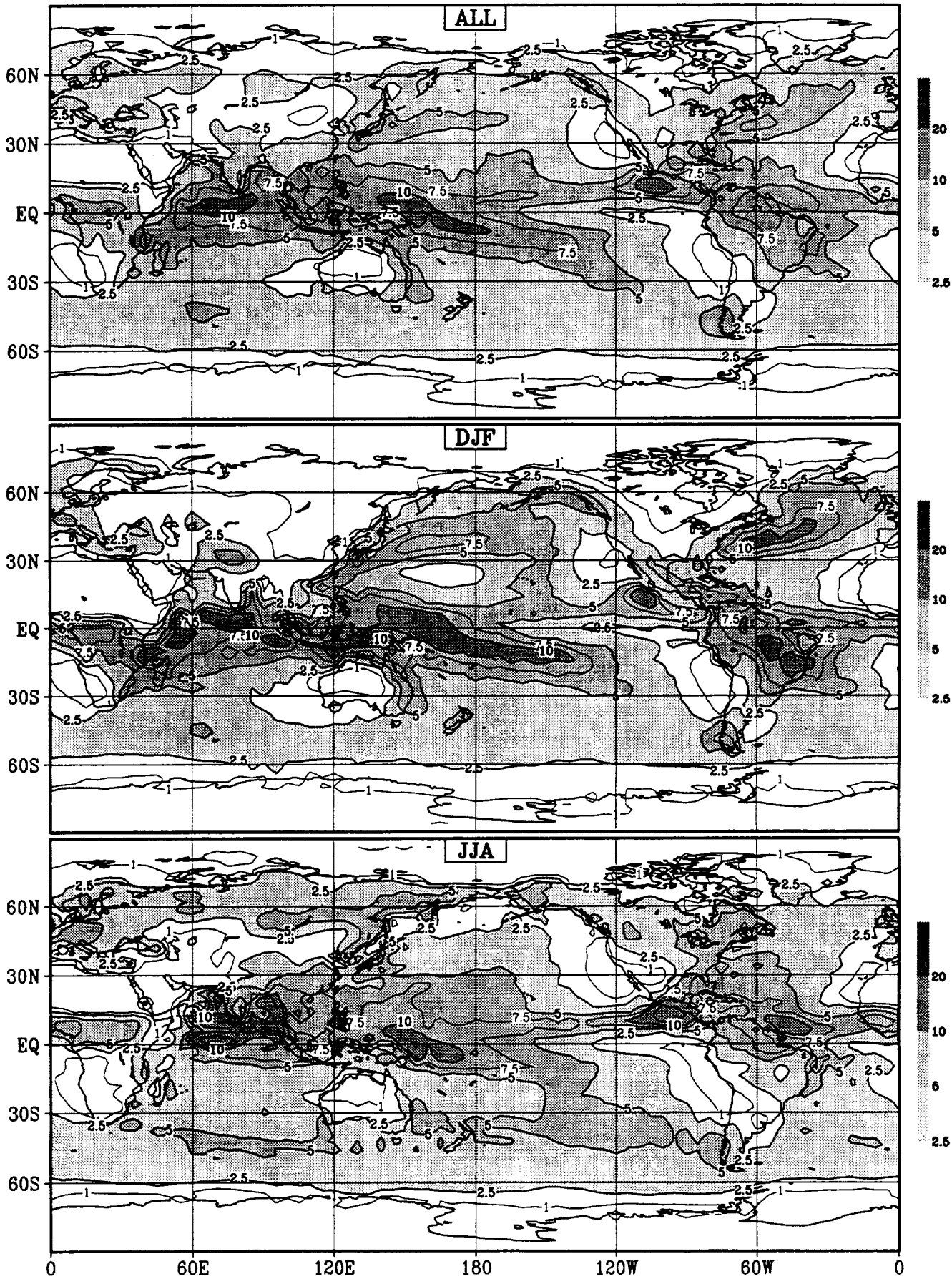

Figure 8.4 (continued)

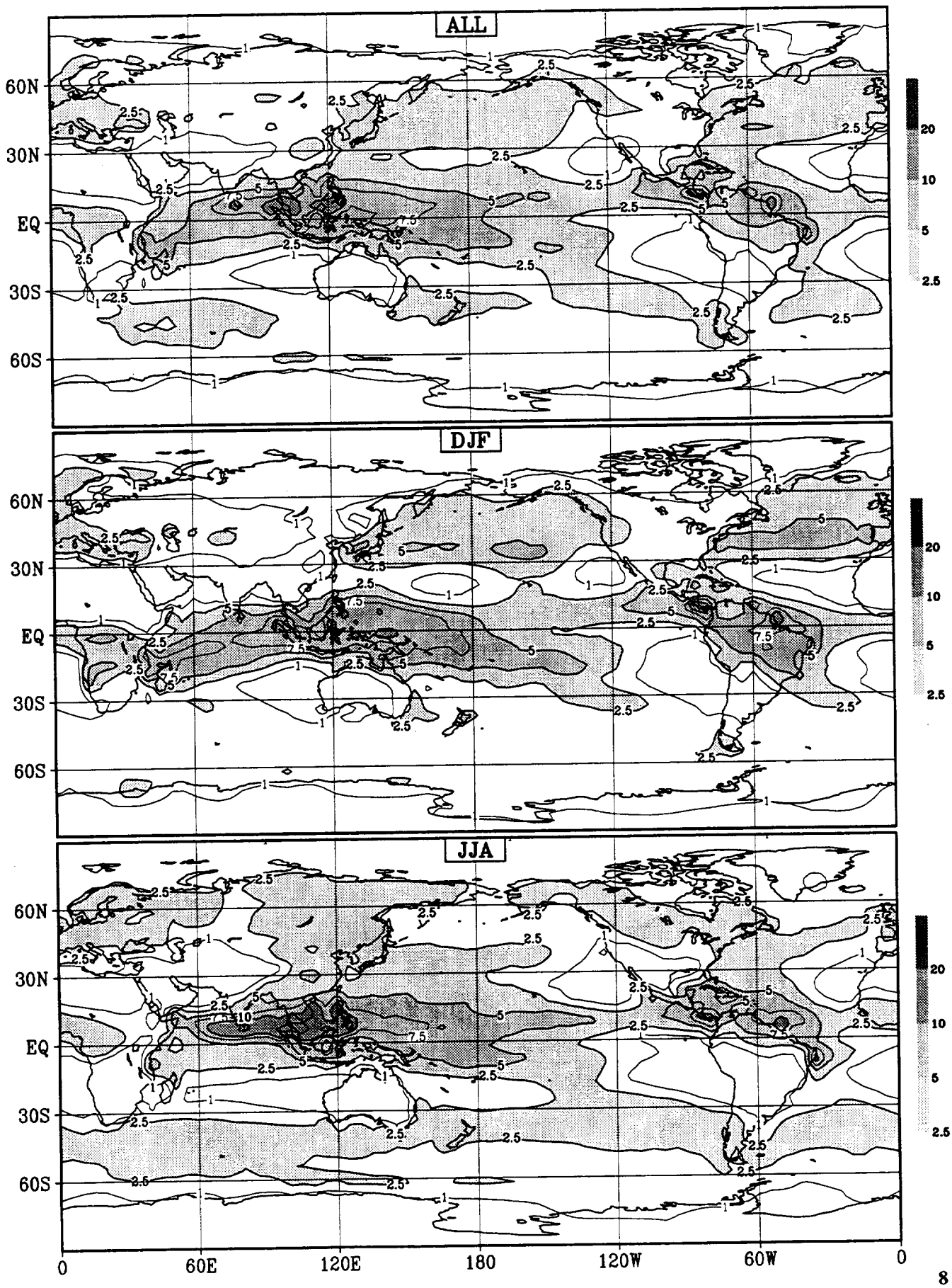

Figure 8.4 (continued)

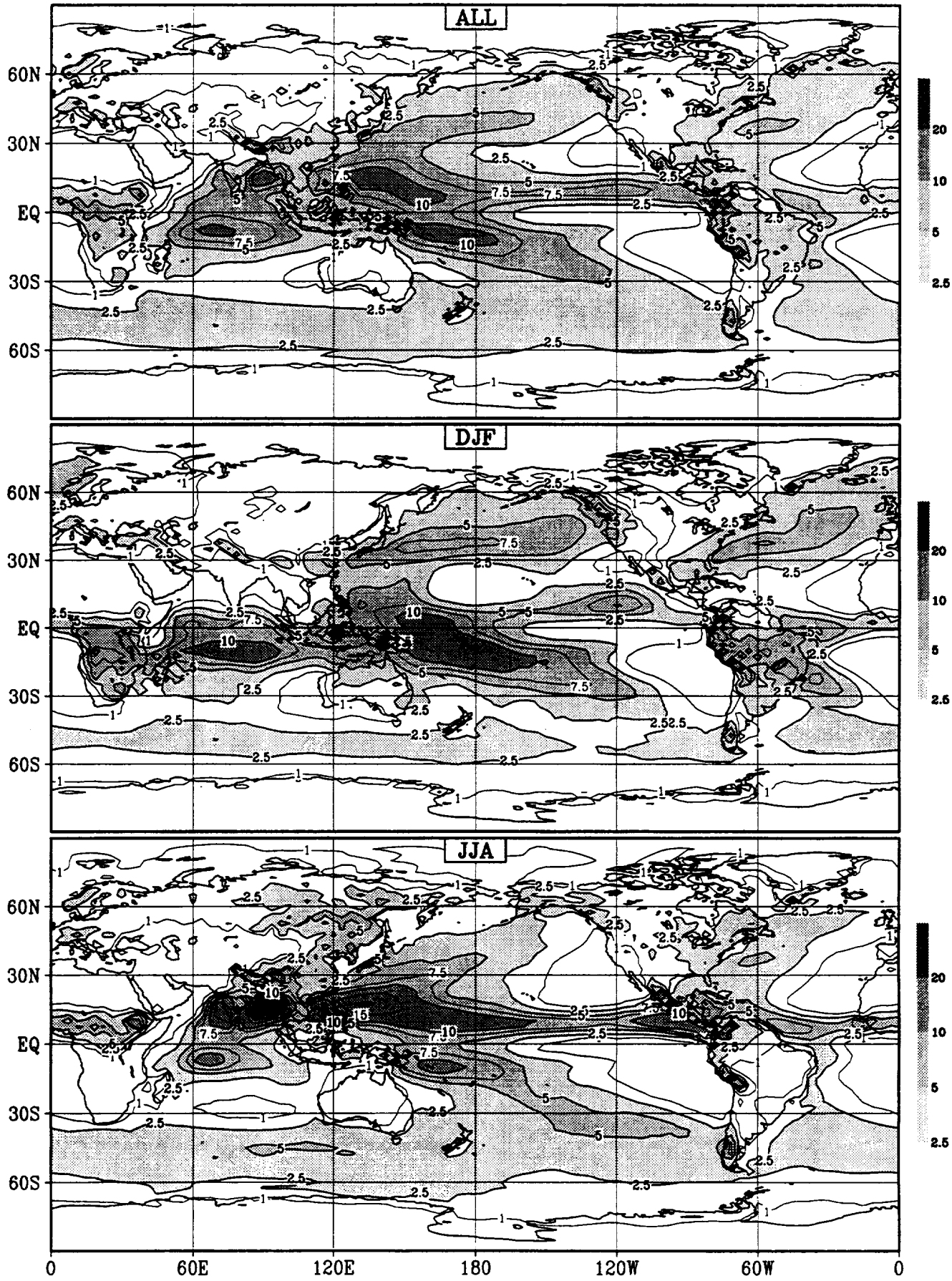

Figure 8.4 (continued)

Evaporation, bmr

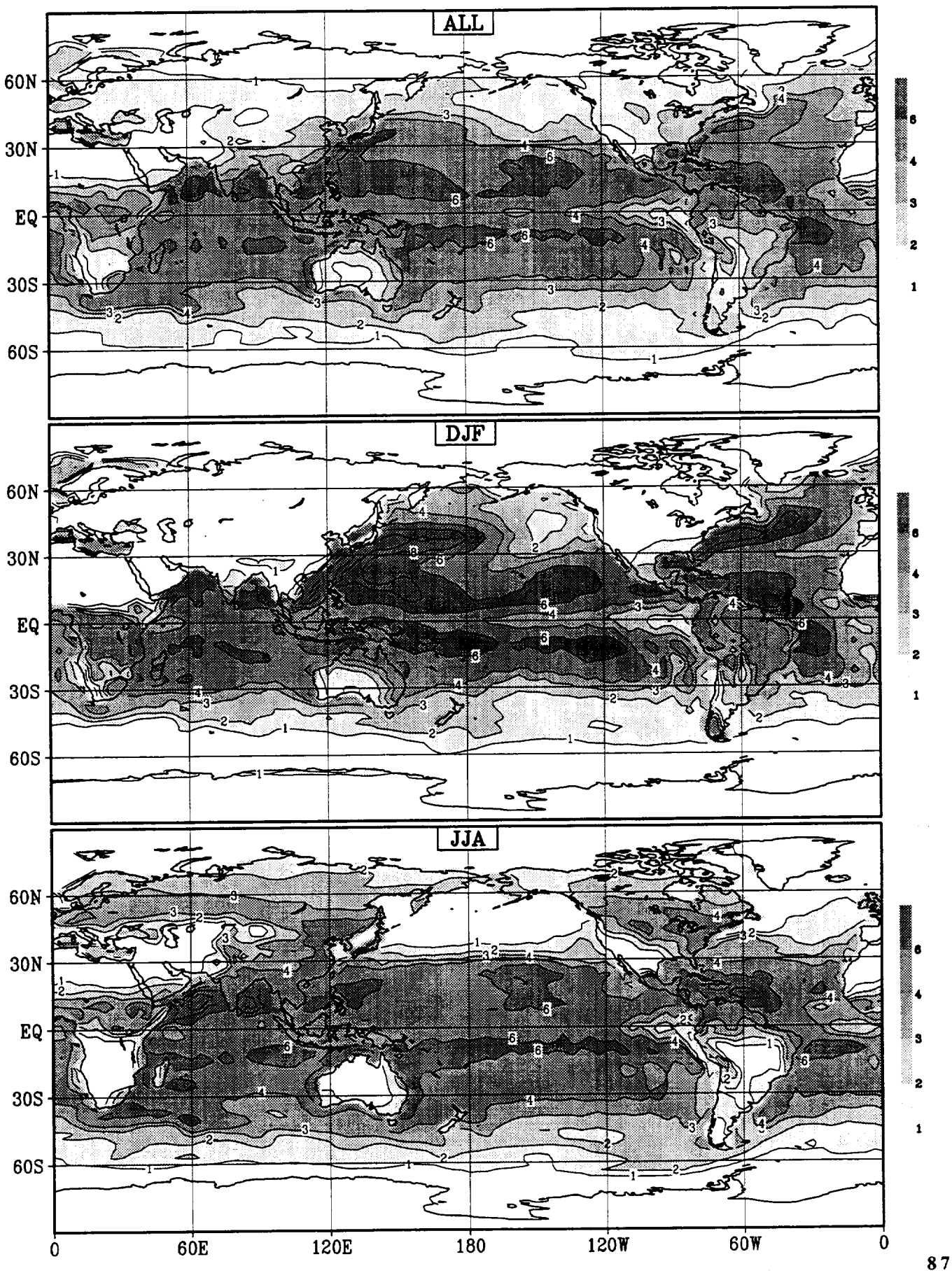

Figure 9

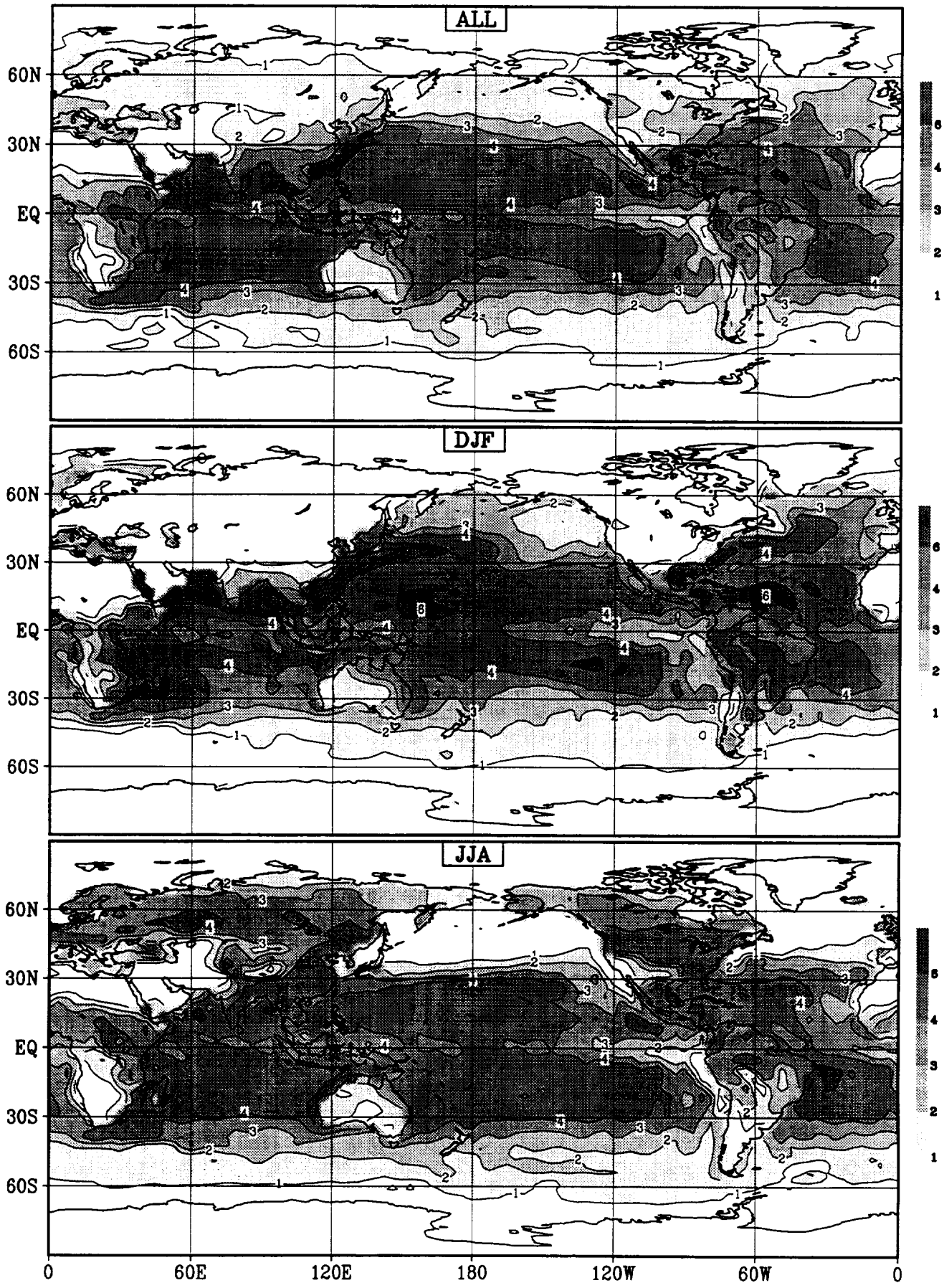

Figure 9 (continued)

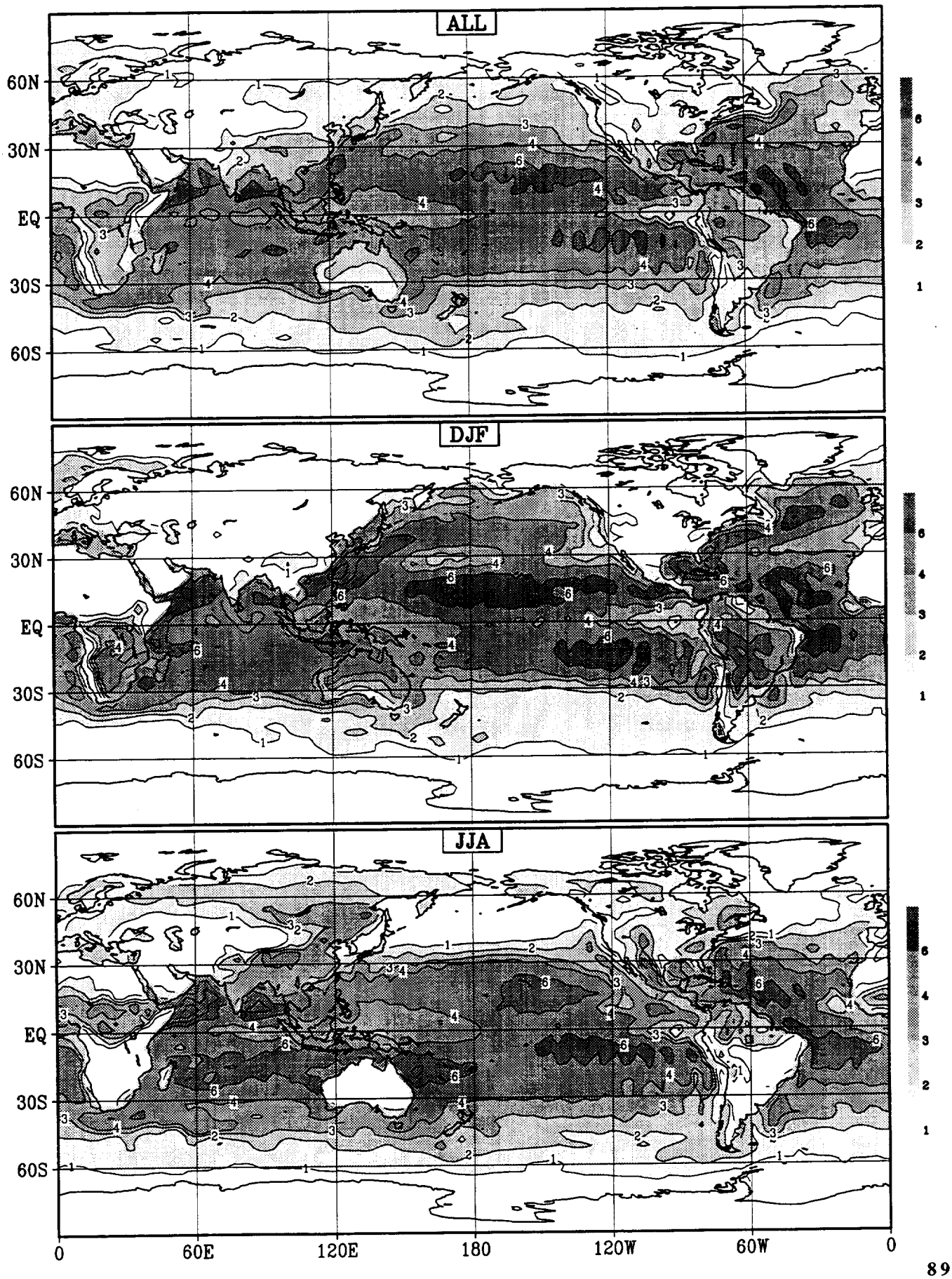

Figure 9 (continued)

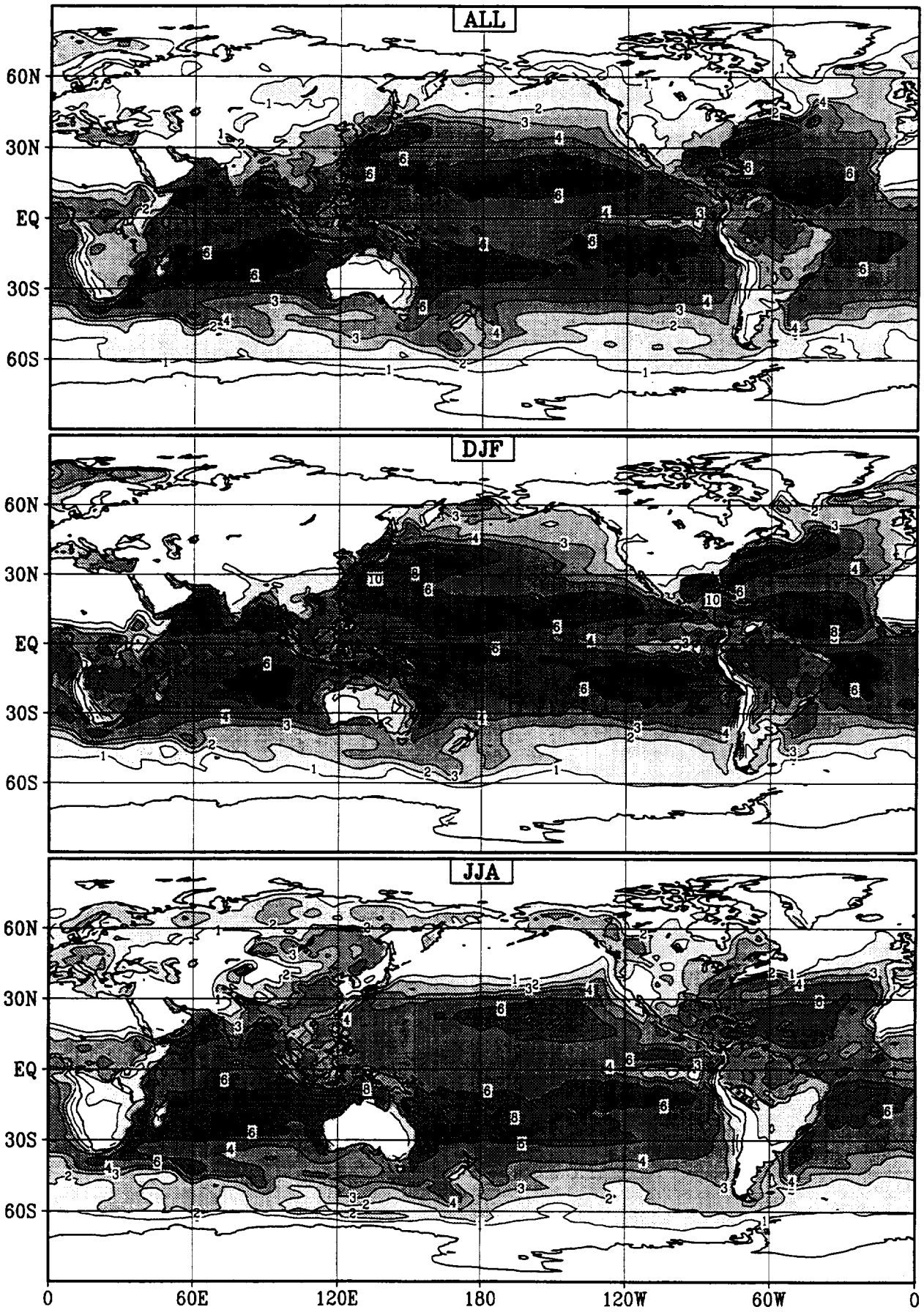

Figure 9 (continued)

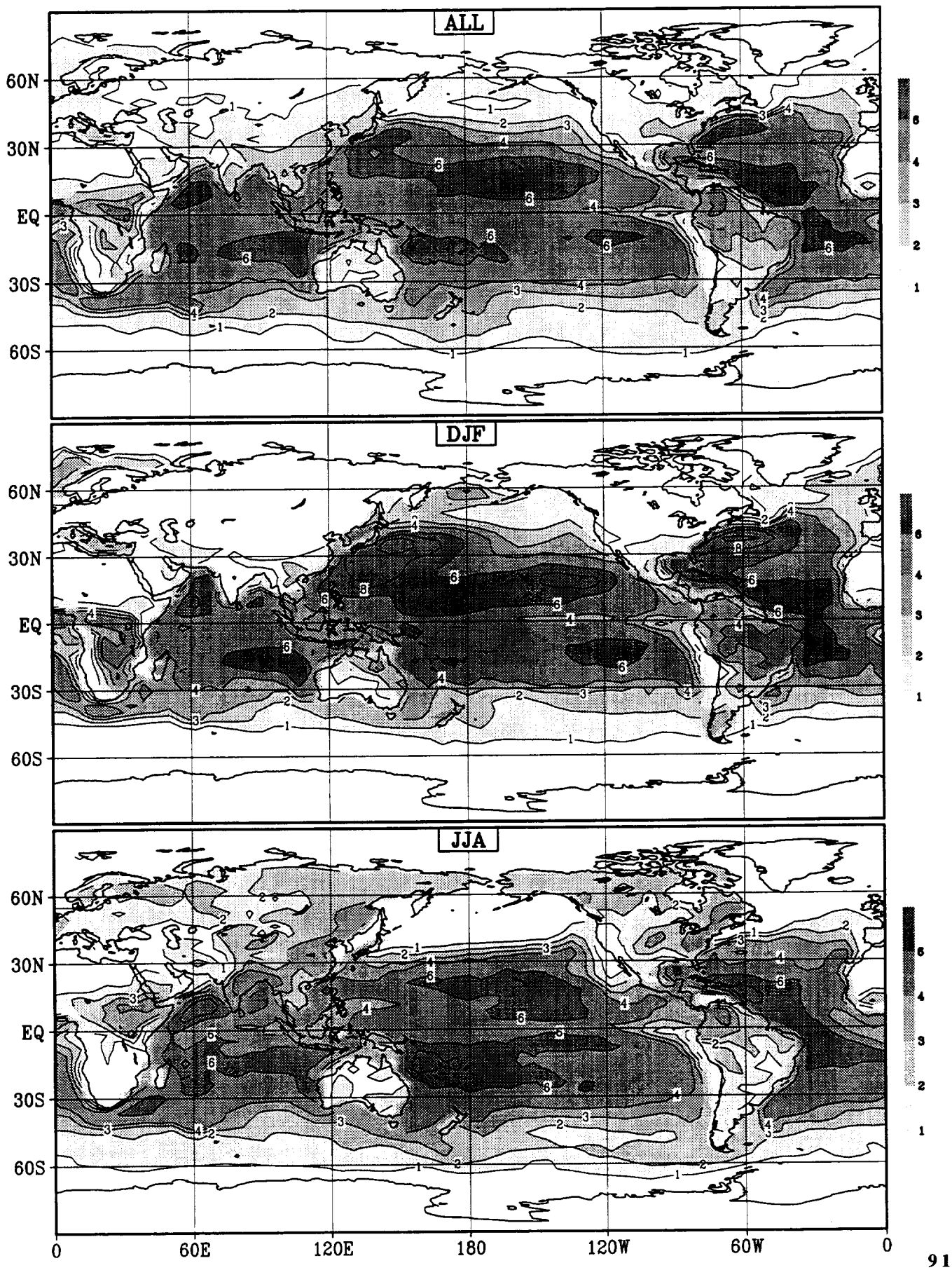

Figure 9 (continued)

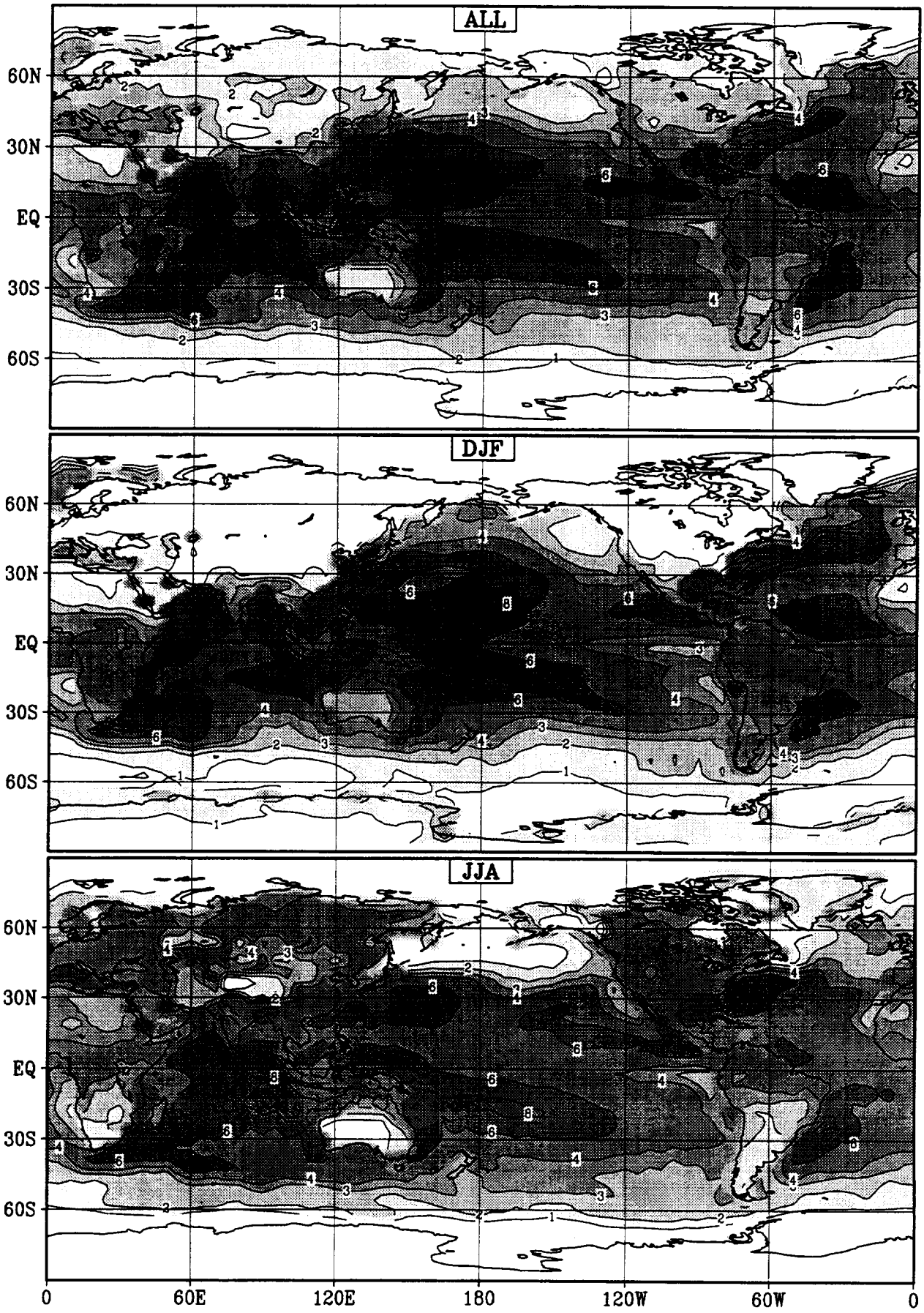

Figure 9 (continued)

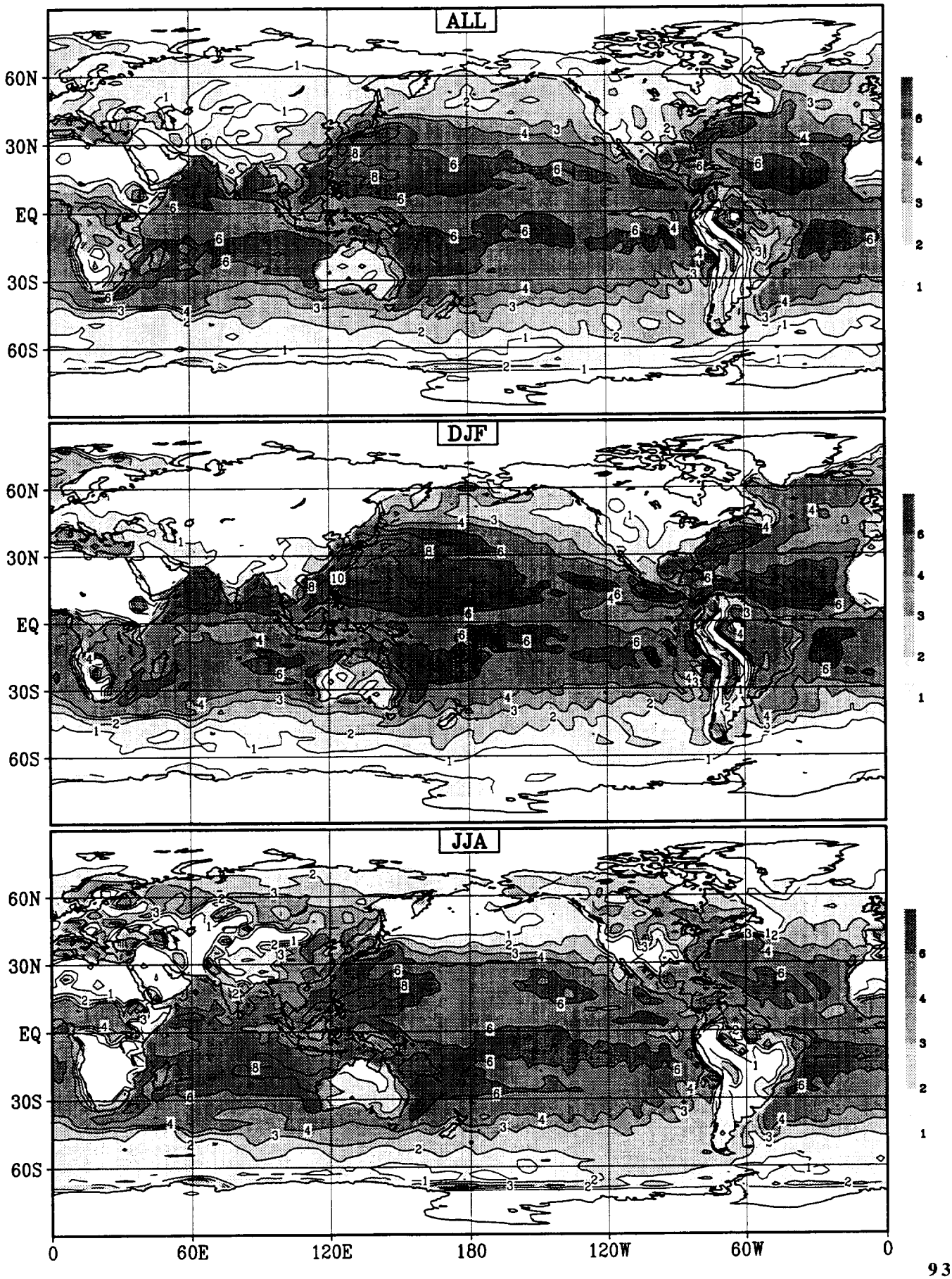

Figure 9 (continued)

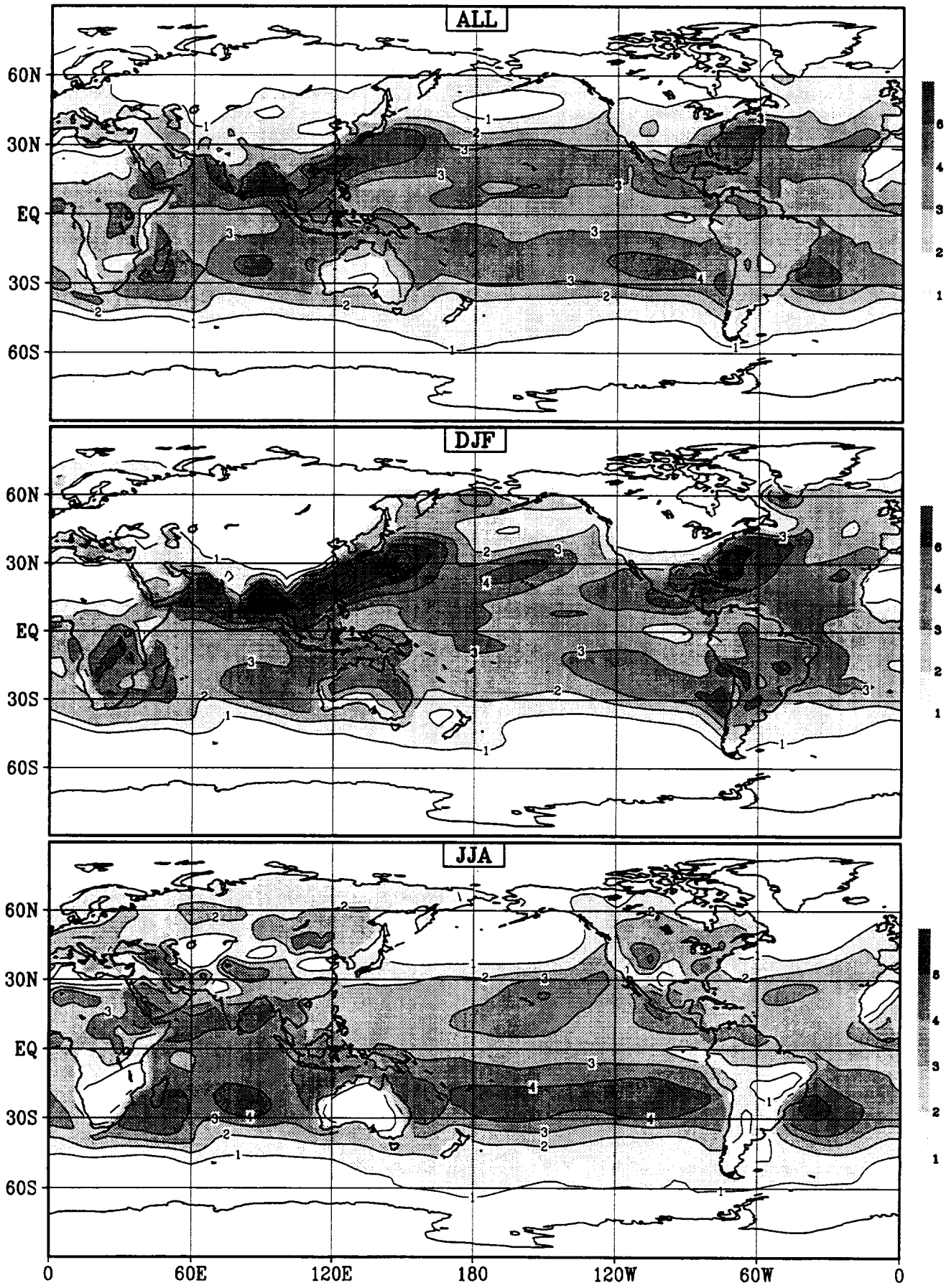

Figure 9 (continued)

Evaporation, ecm

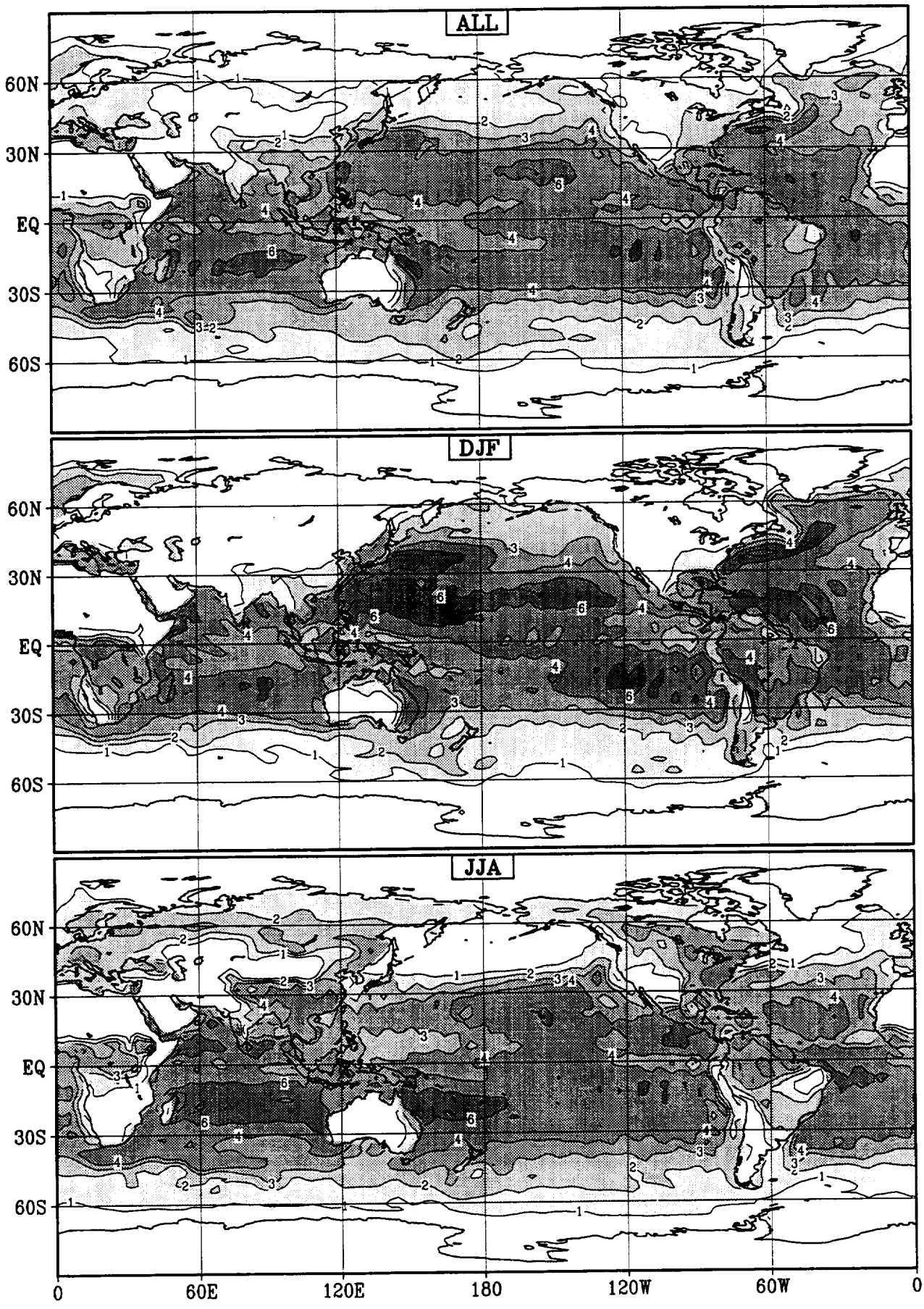

Figure 9 (continued)

C-2

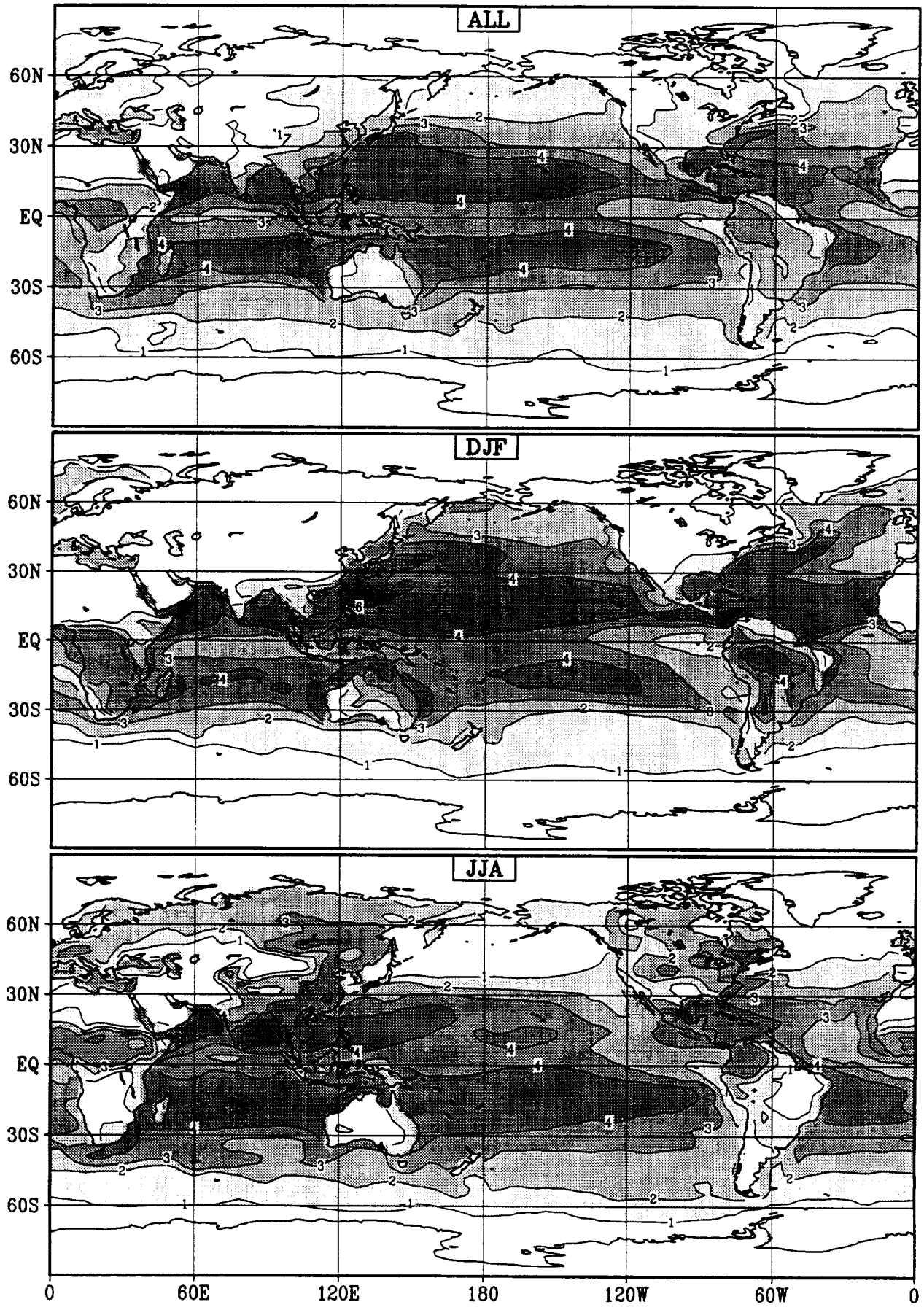

Figure 9 (continued)

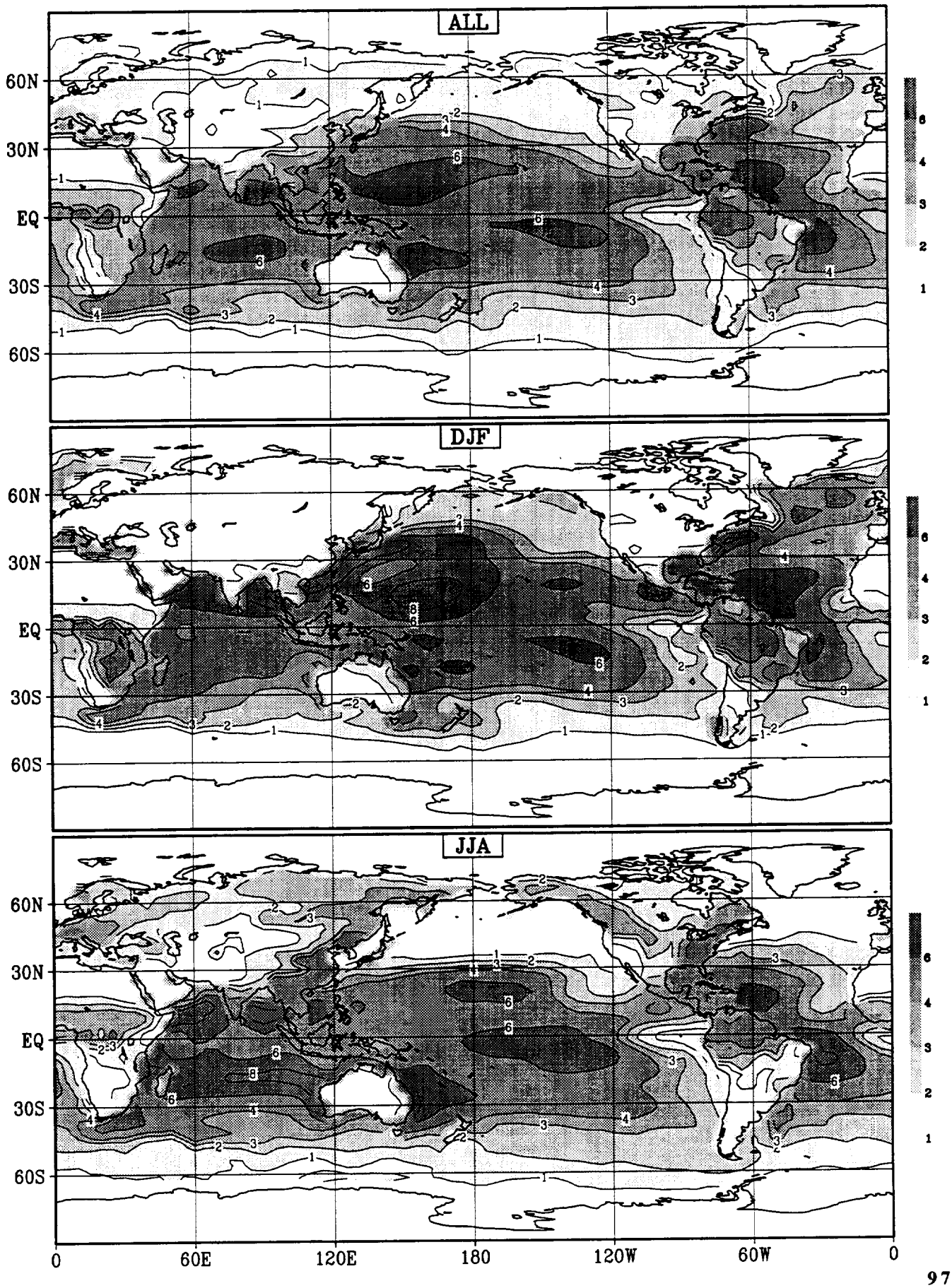

Figure 9 (continued)

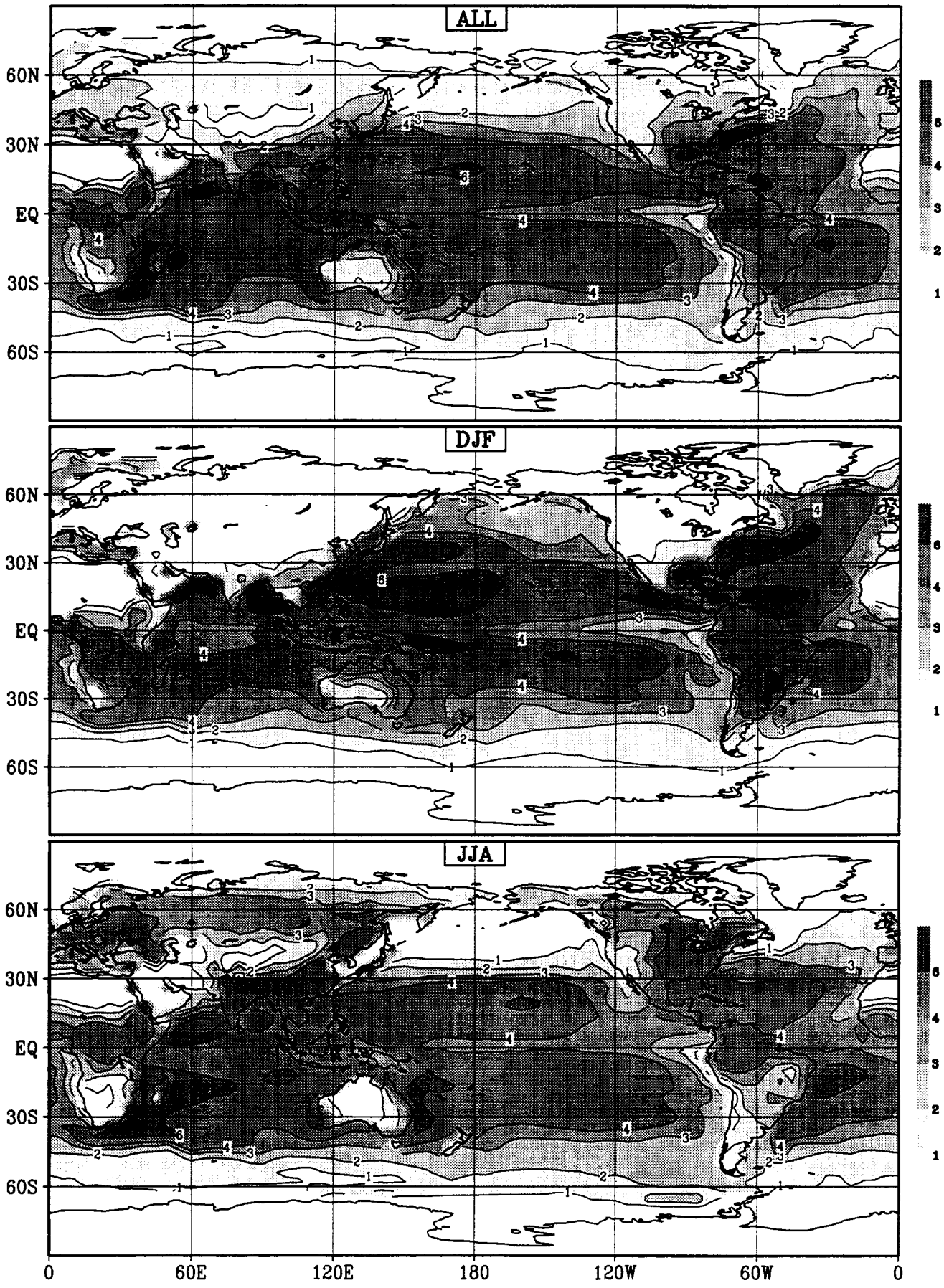

Figure 9 (continued)

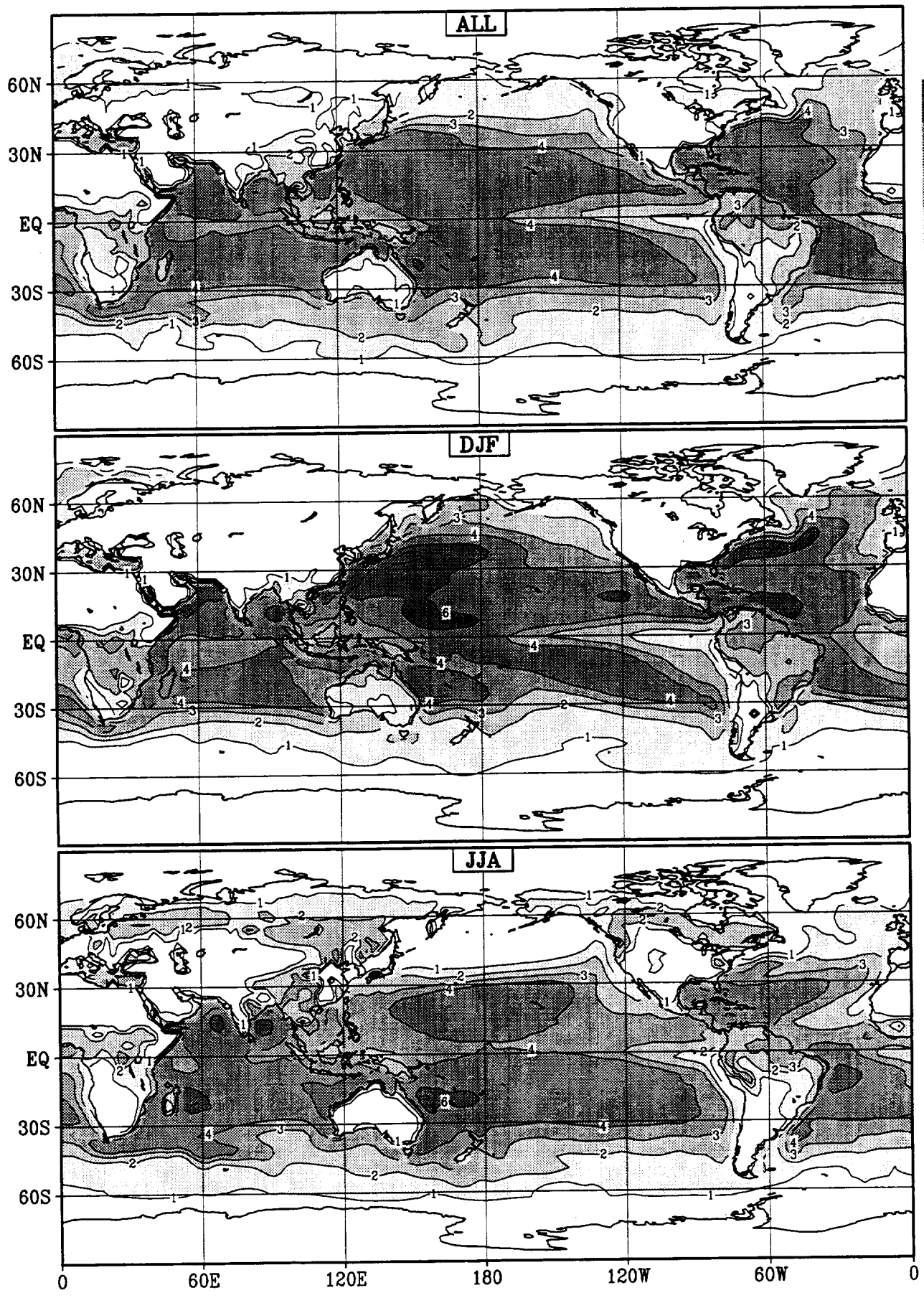

Figure 9 (continued)

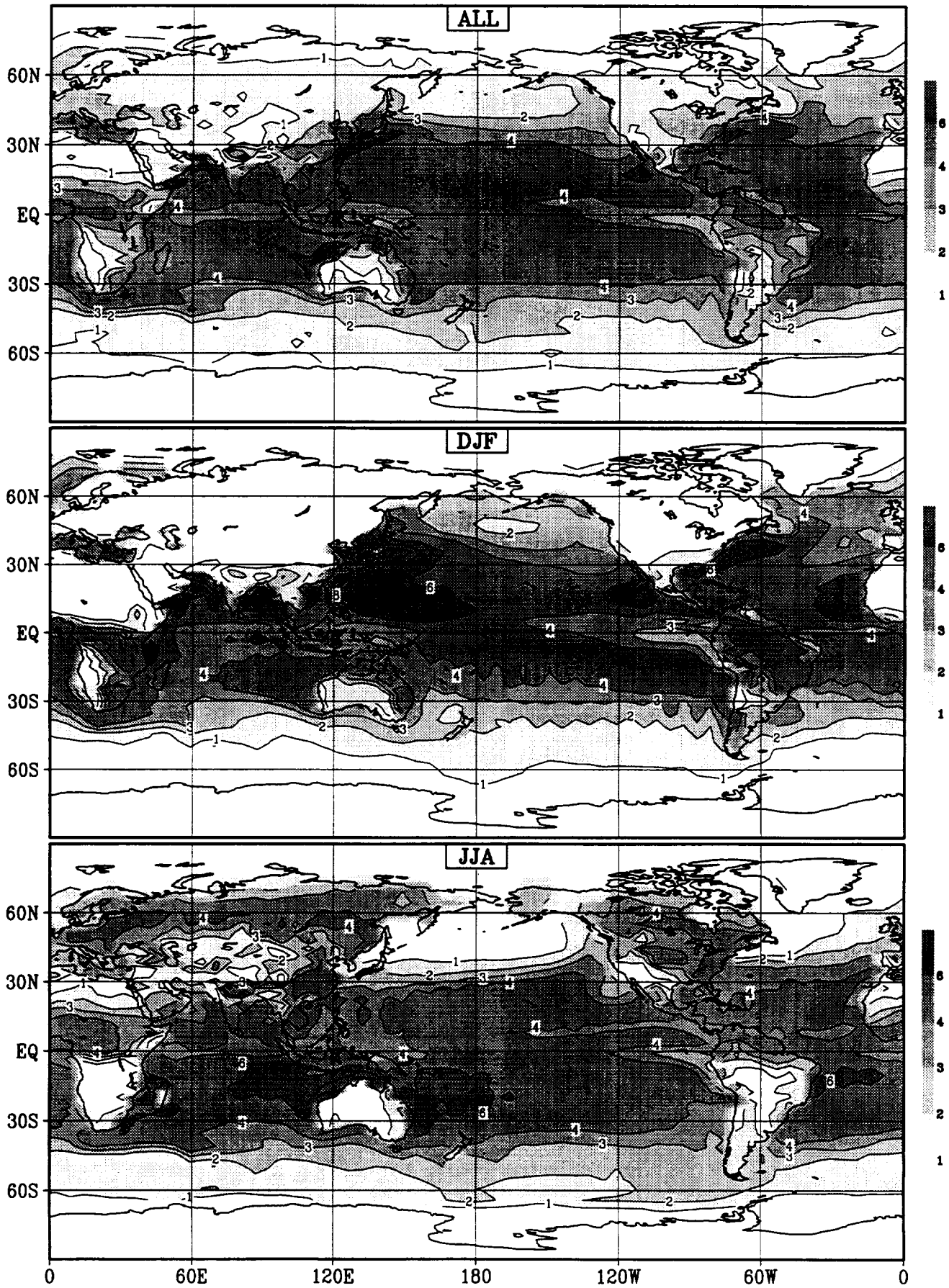

Figure 9 (continued)

Evaporation, mgo

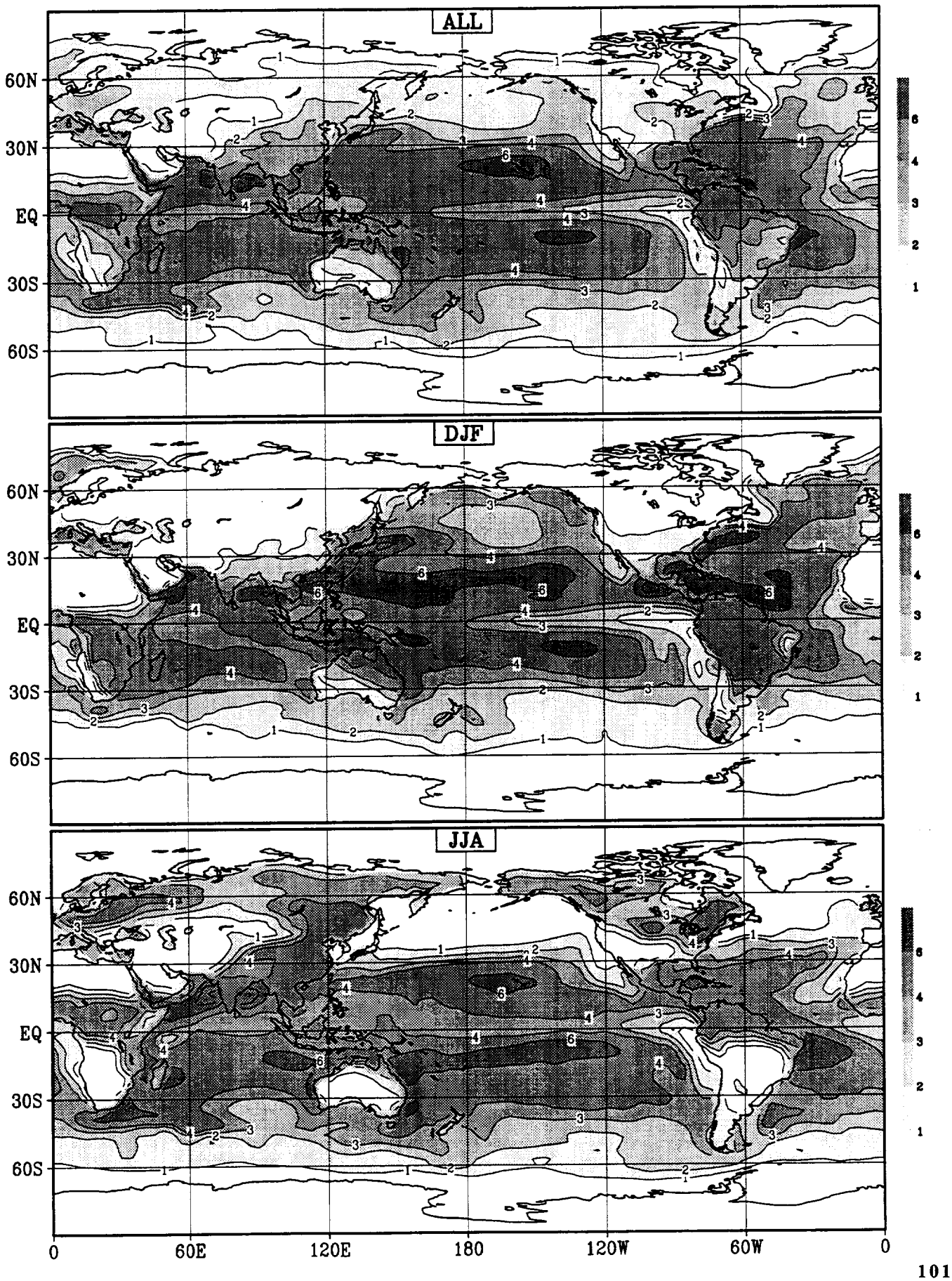

Figure 9 (continued)

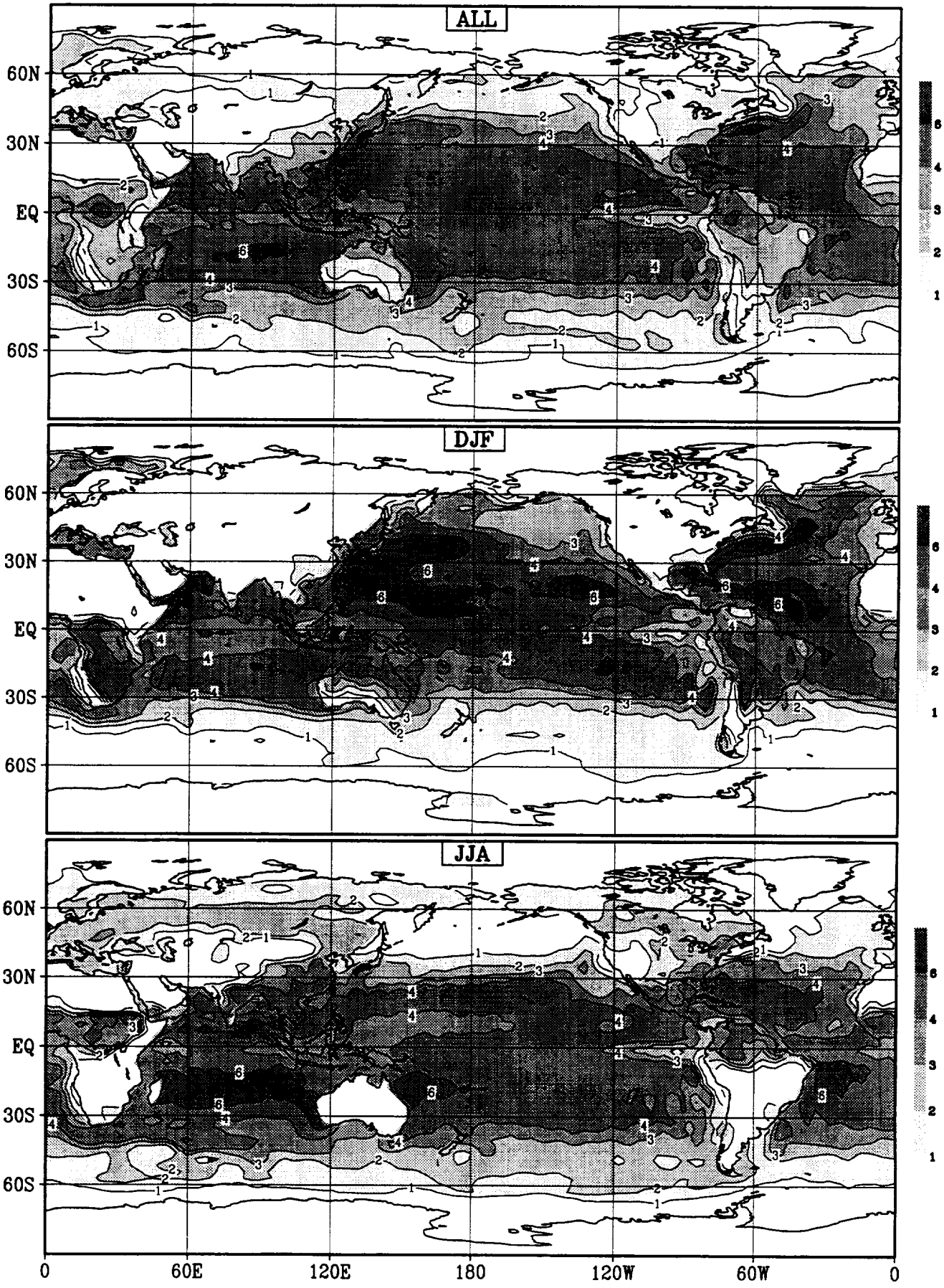

Figure 9 (continued)

Evaporation, mri

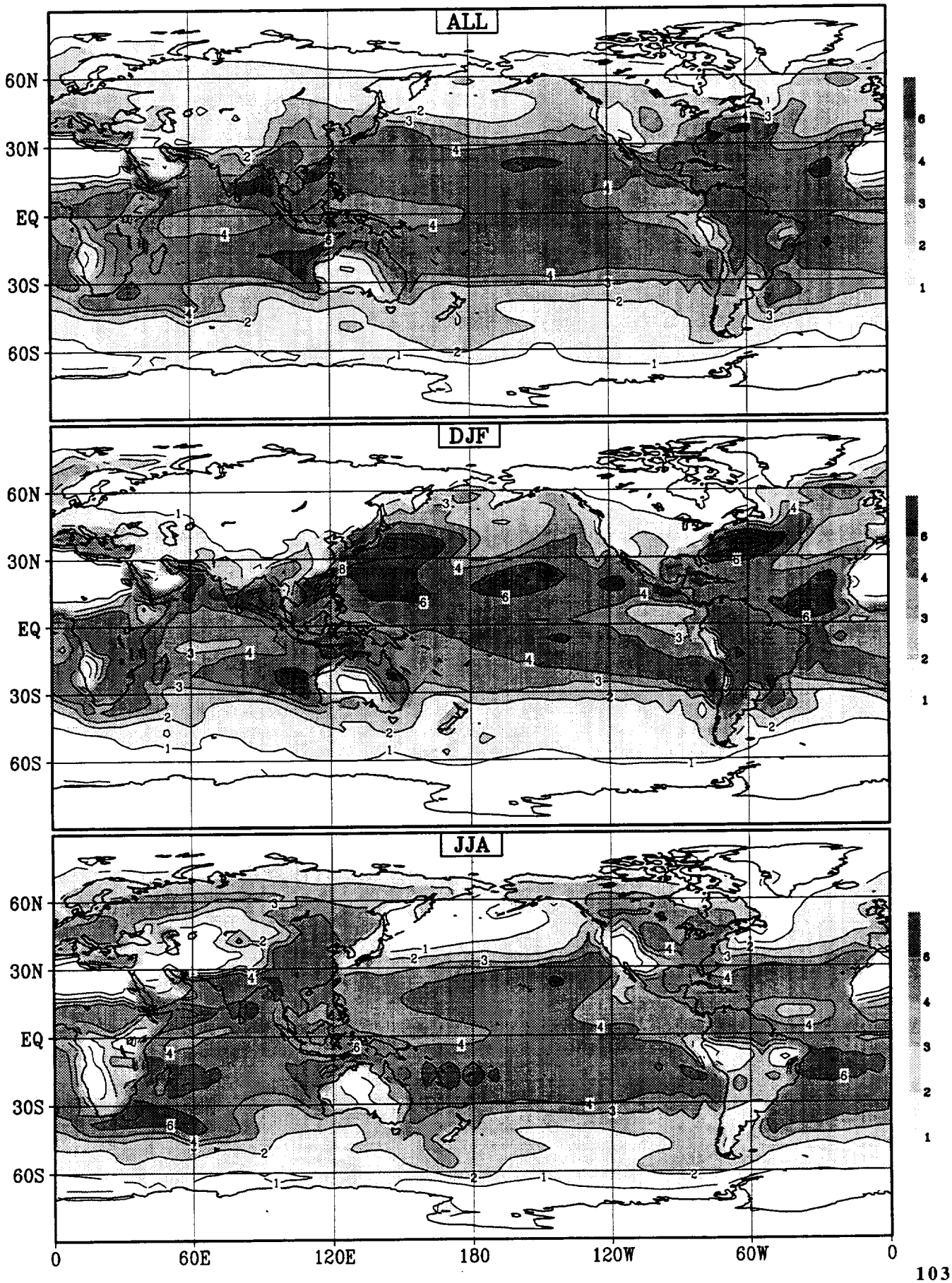

Figure 9 (continued)

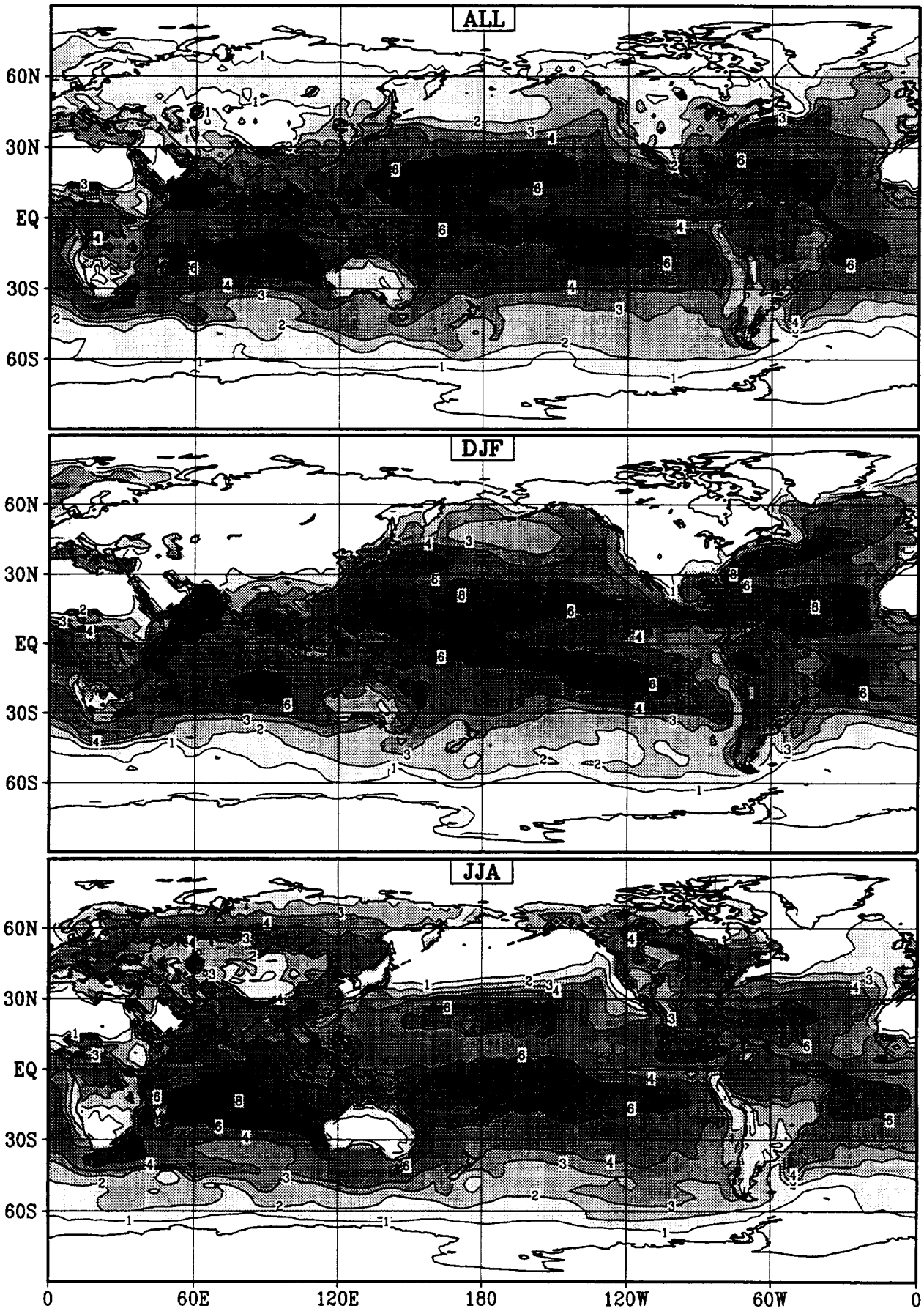

Figure 9 (continued)

Evaporation, nmc

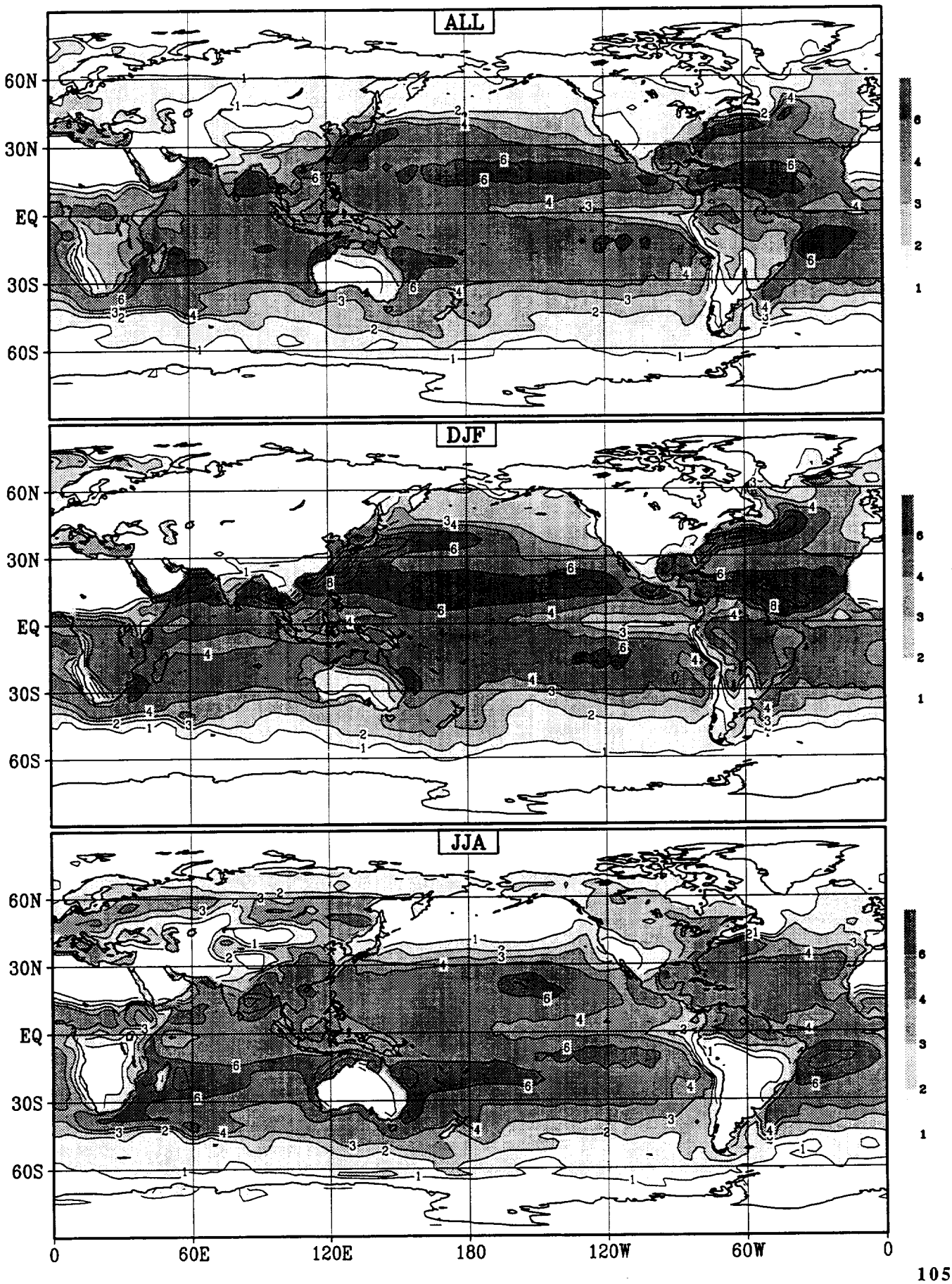

Figure 9 (continued)

Evaporation, sun

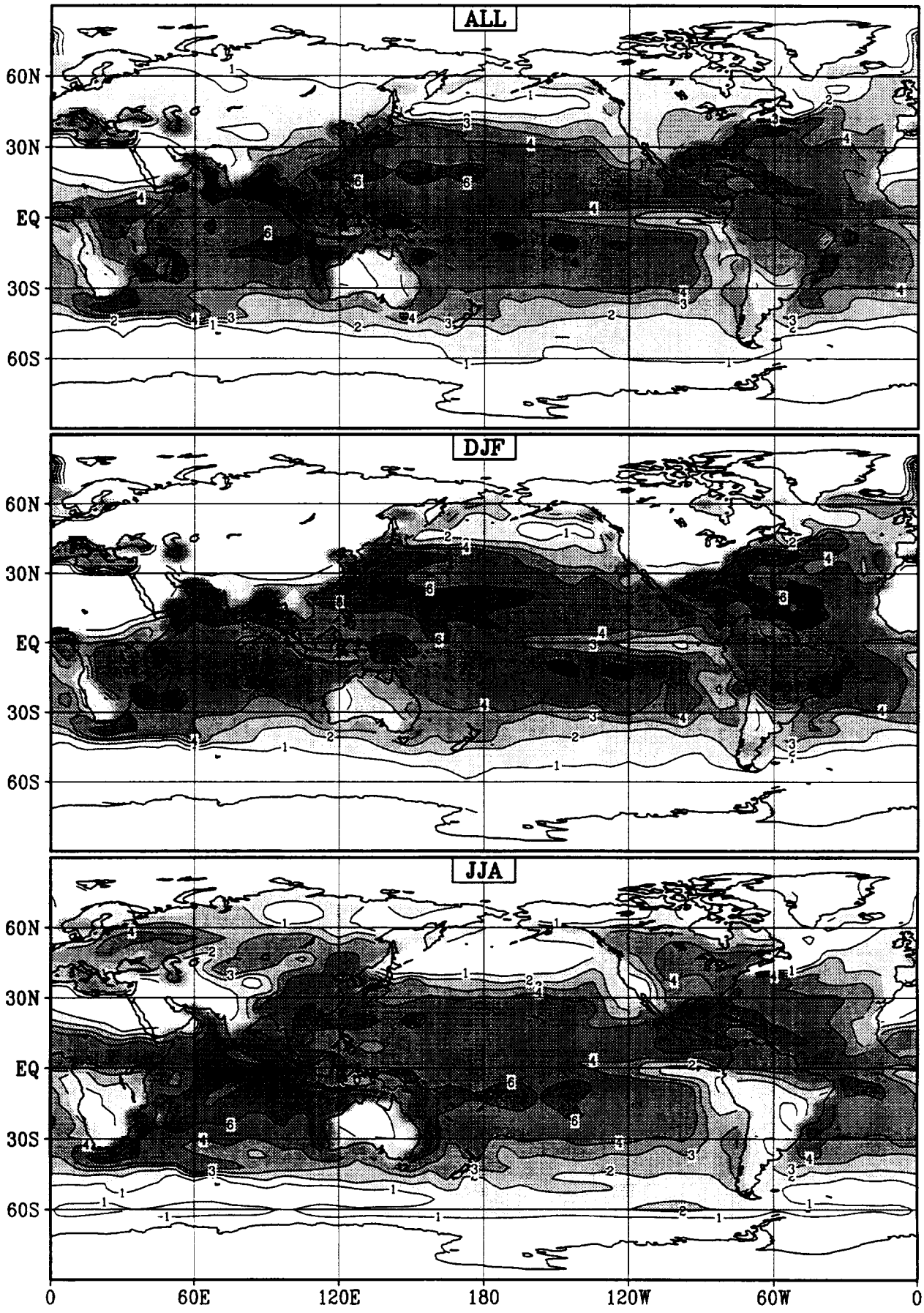

Figure 9 (continued)

Evaporation, ucl

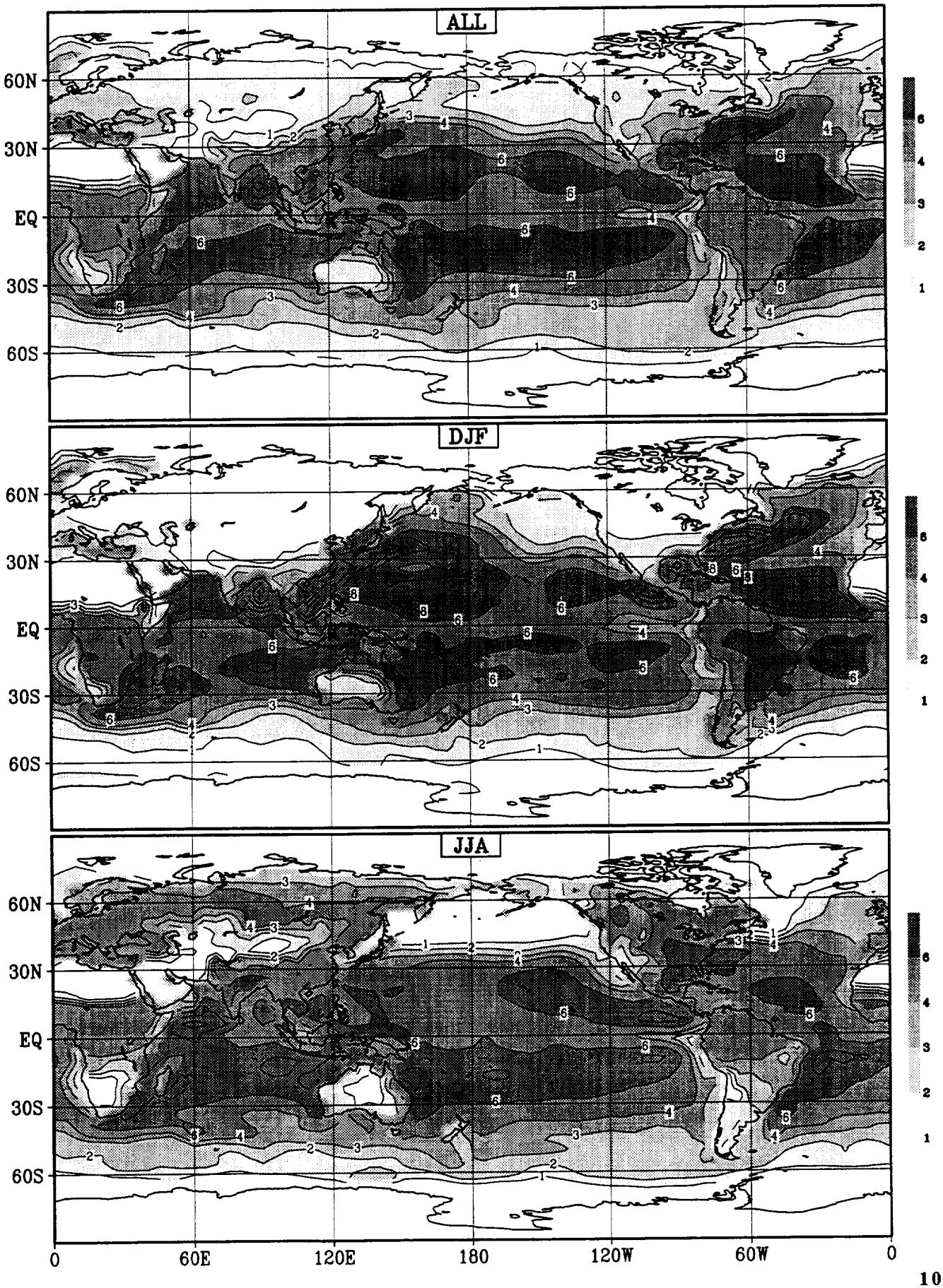

Figure 9 (continued)

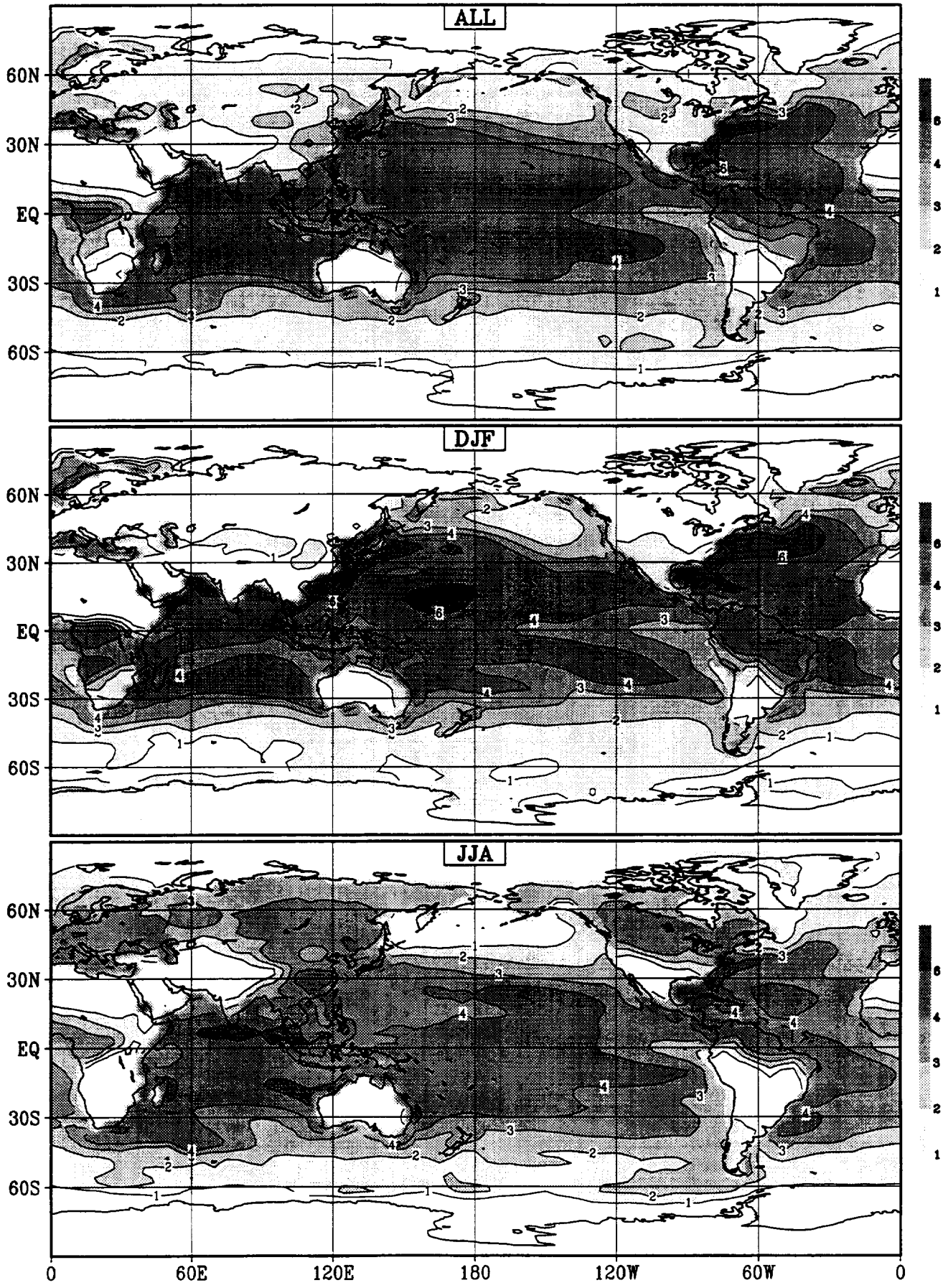

Figure 9 (continued)

Evaporation, ukm

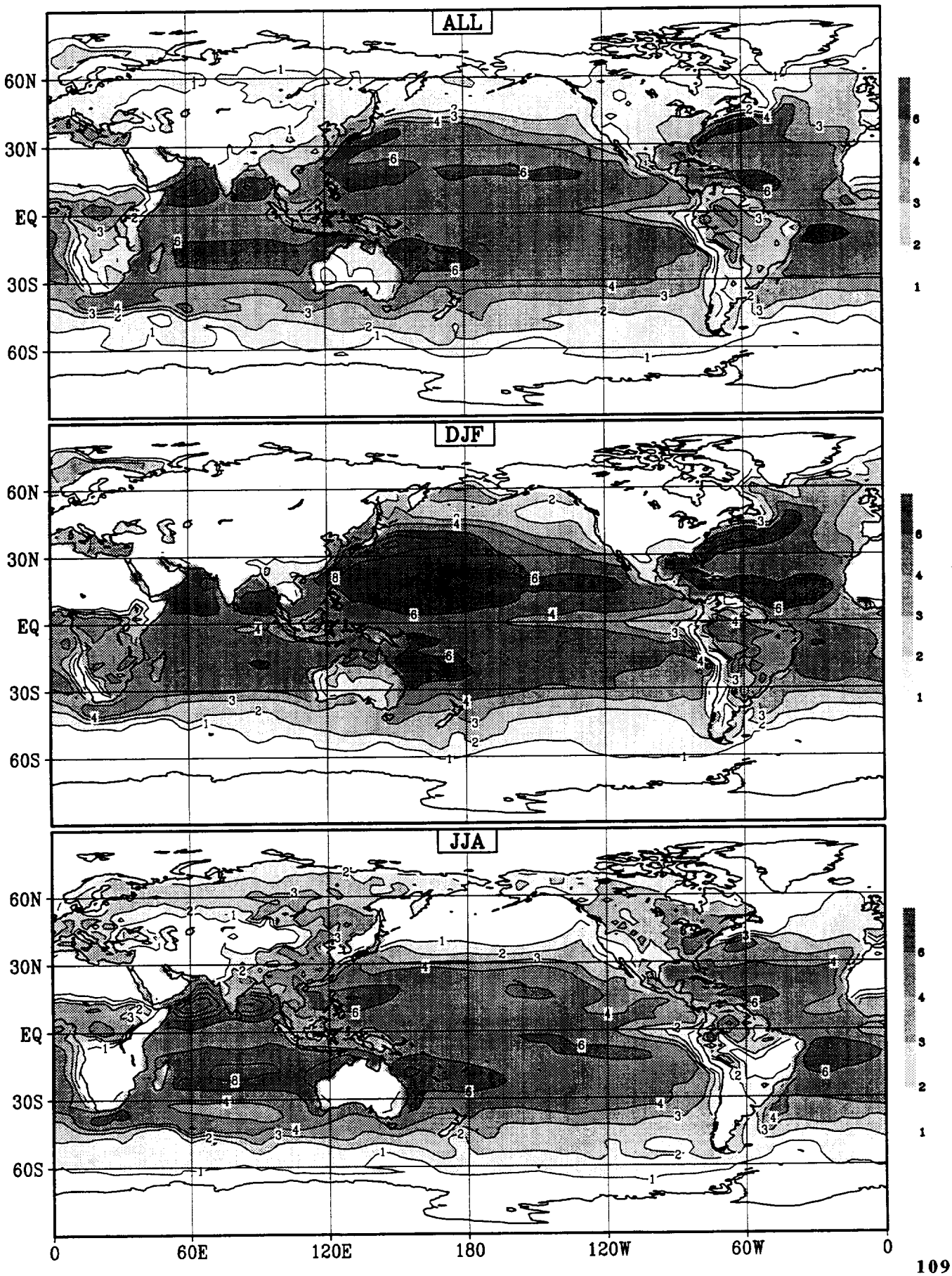

Figure 9 (continued)

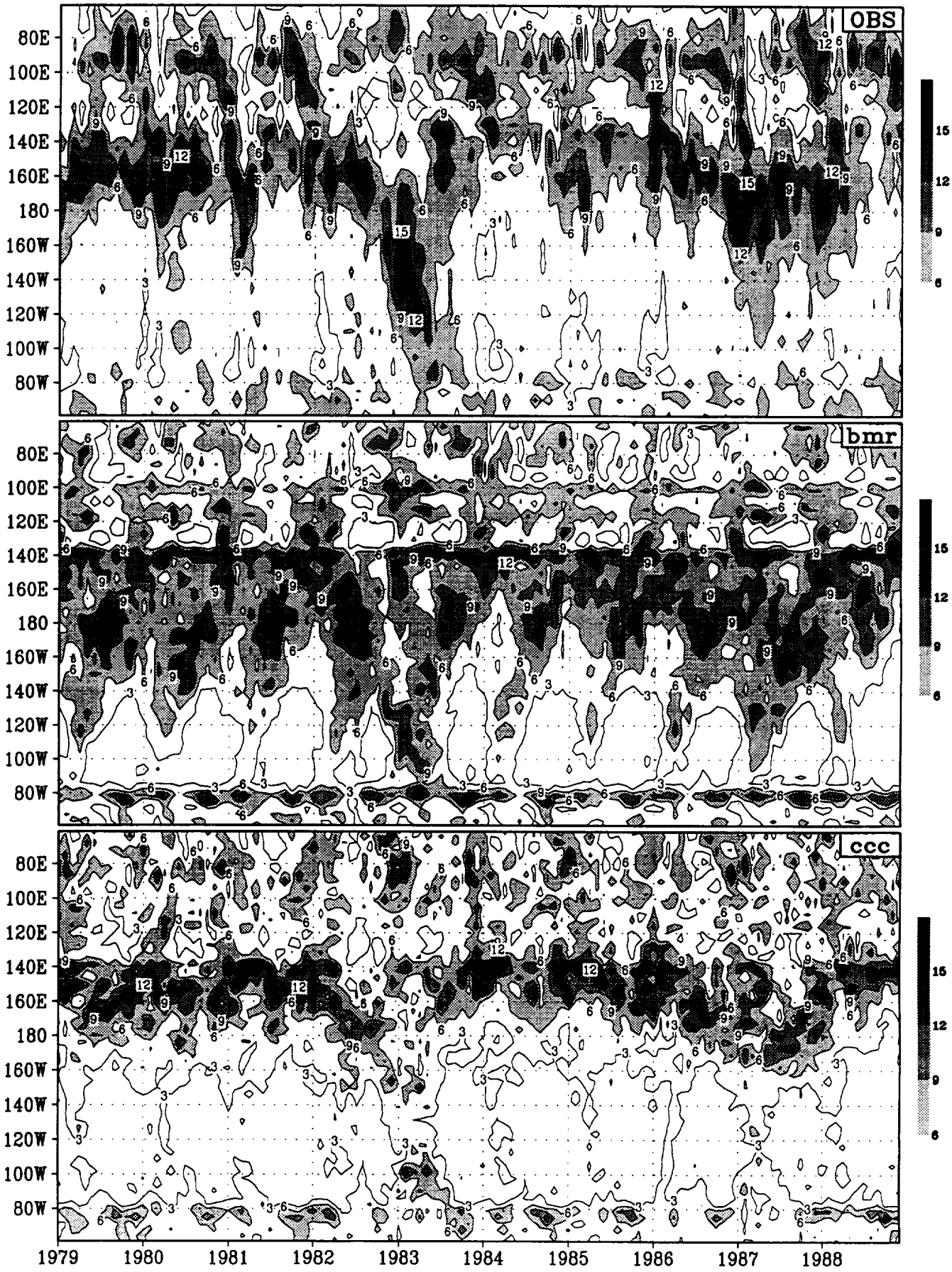
OBS
bmr
ccc
80E
100E
120E
140E
160E
180
160W
140W
120W
100W
80W
15
12
9
6
3
1979
1980
1981
1982
1983
1984
1985
1986
1987
1988

Figure 10

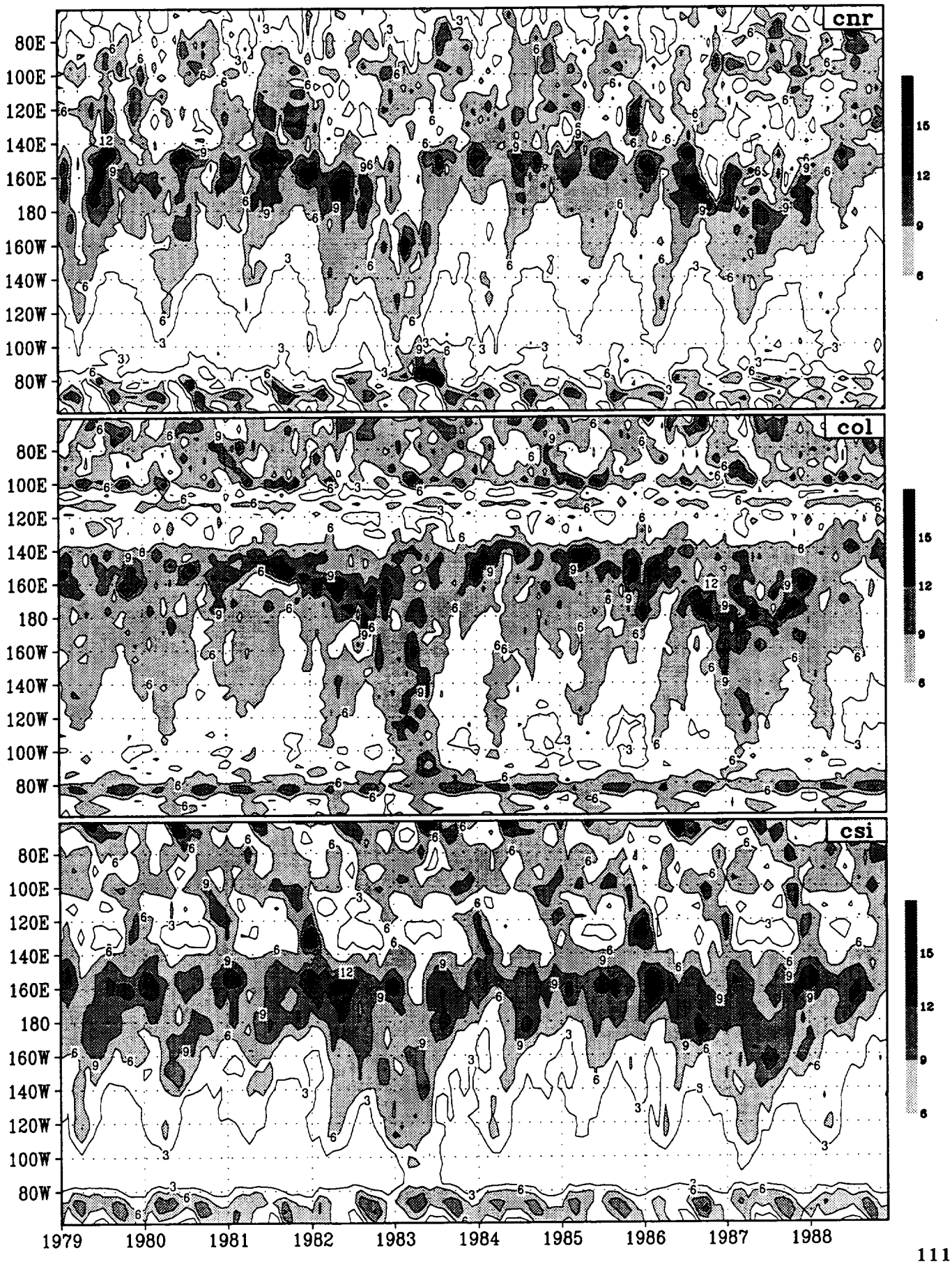

Figure 10 (continued)

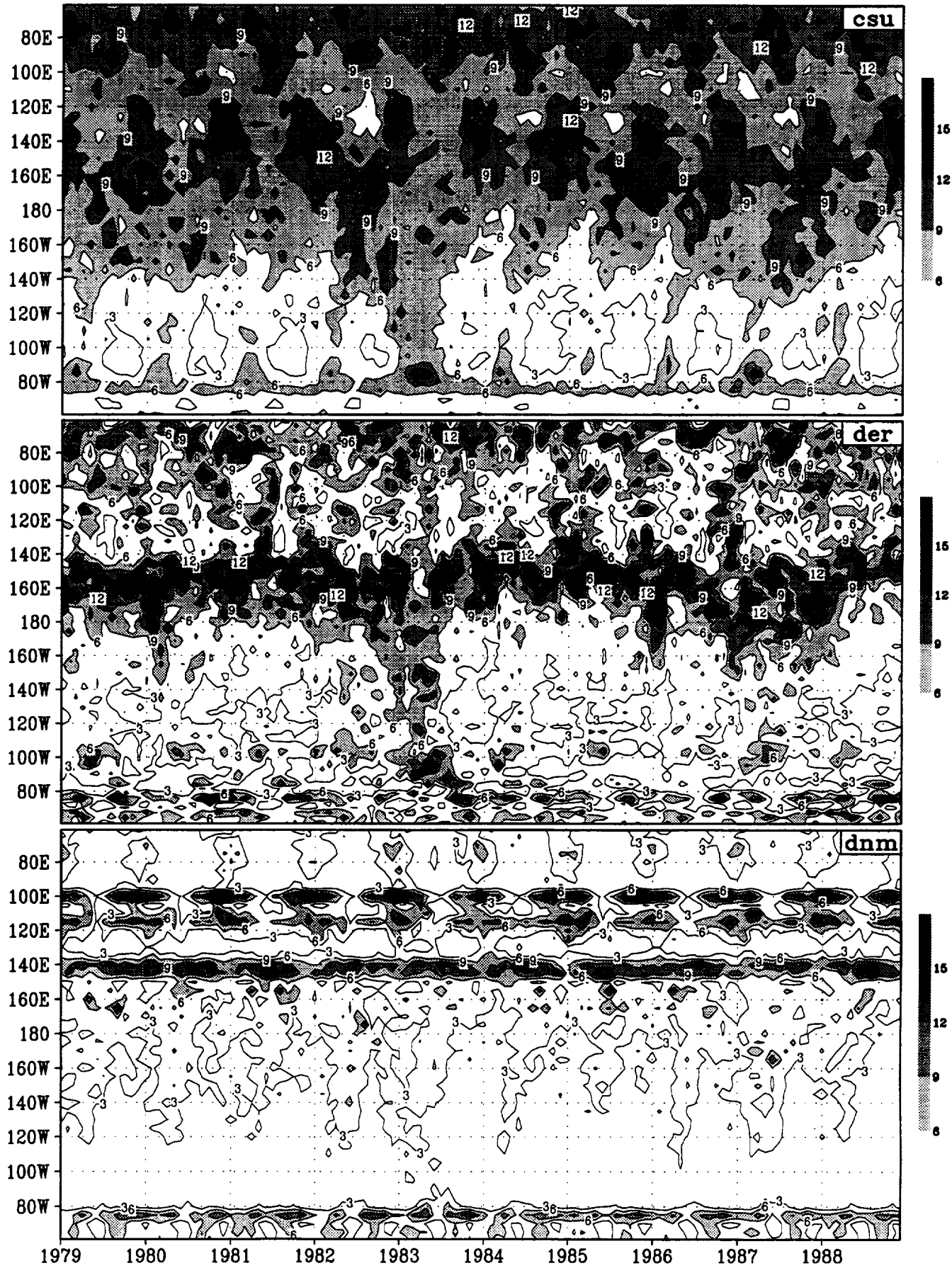

Figure 10 (continued)

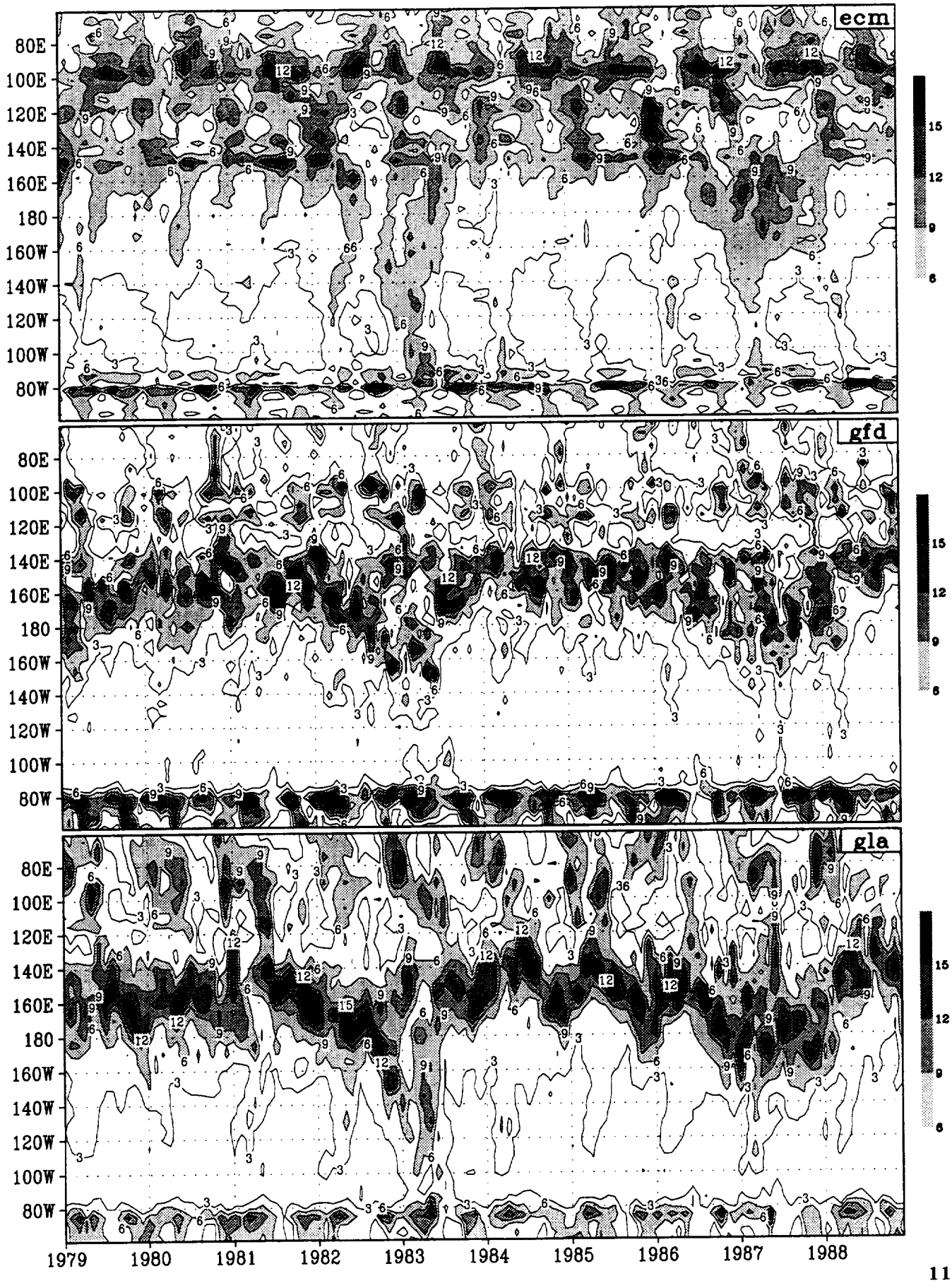

Figure 10 (continued)

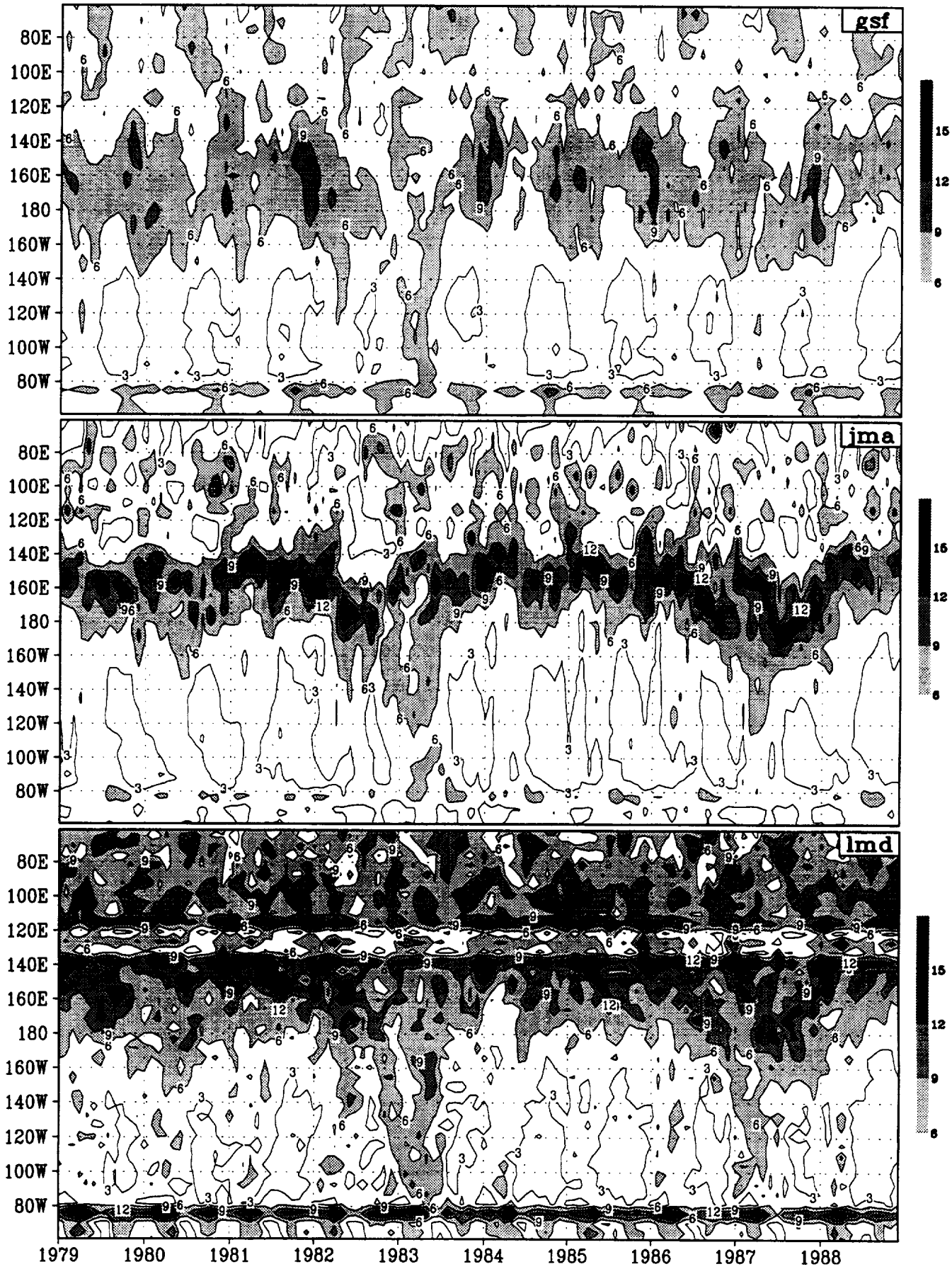

Figure 10 (continued)

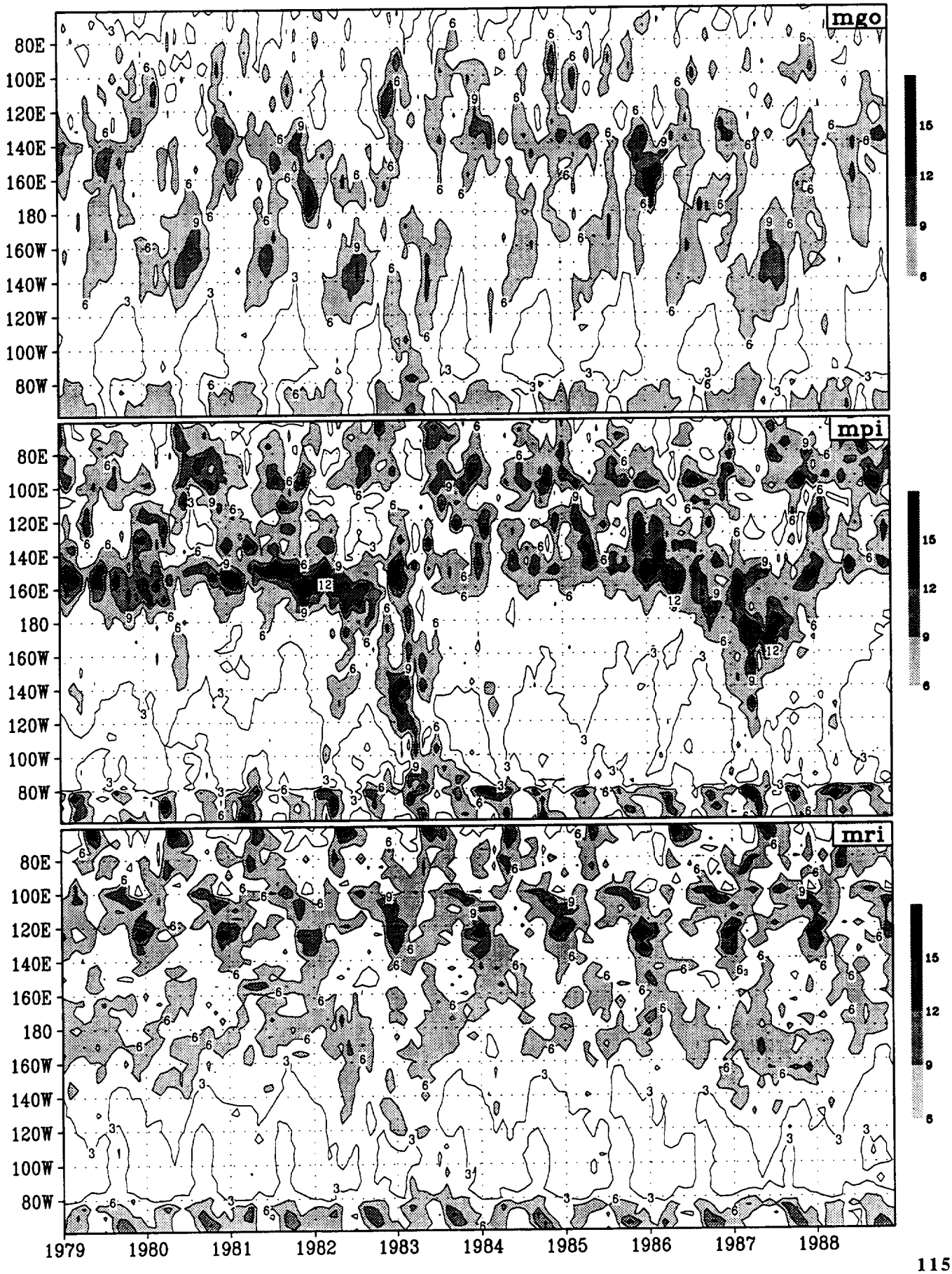

Figure 10 (continued)

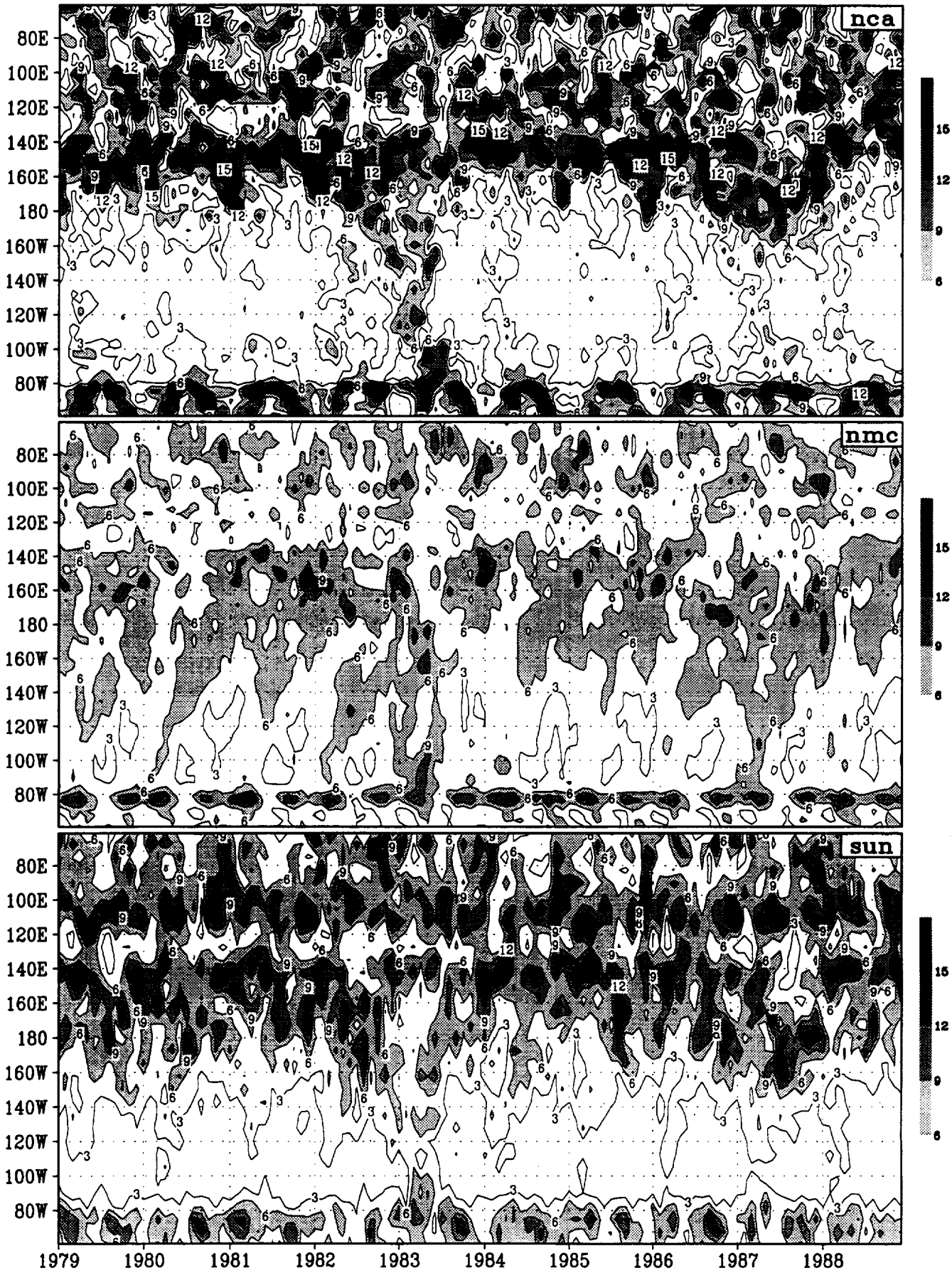

Figure 10 (continued)

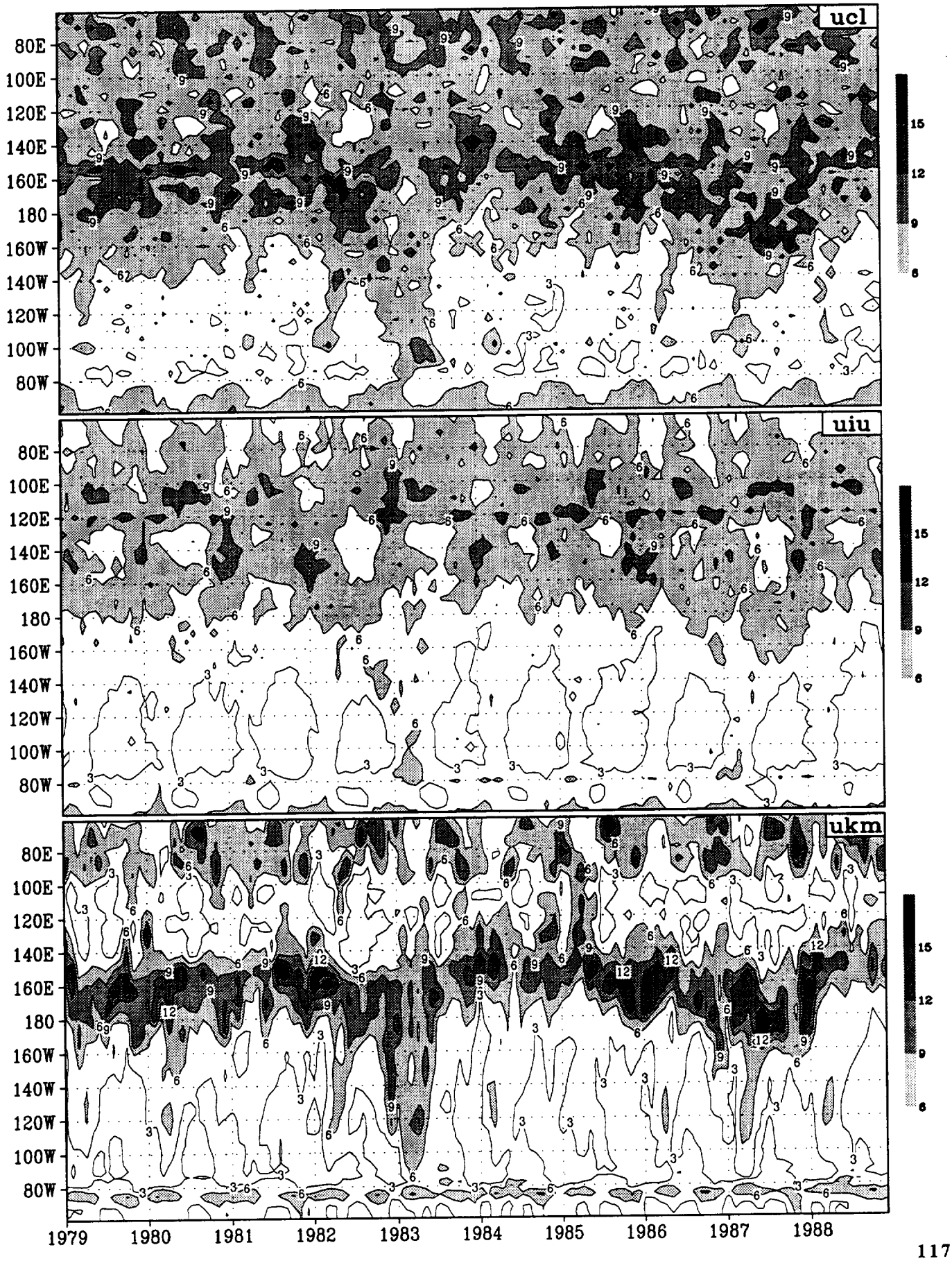

Figure 10 (continued)

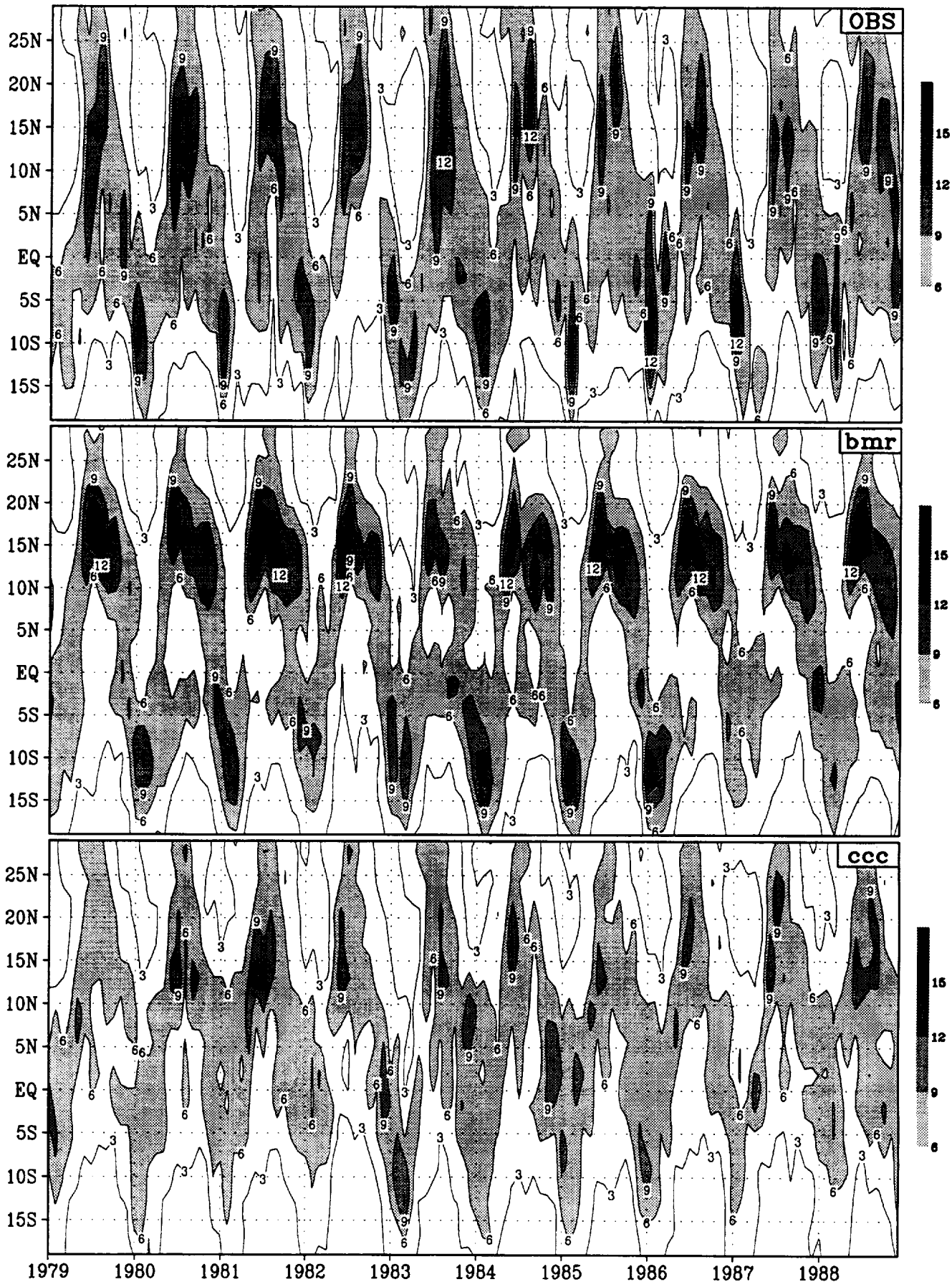
OBS
bmr
ccc
25N
20N
15N
10N
5N
EQ
5S
10S
15S
1979
1980
1981
1982
1983
1984
1985
1986
1987
1988
15
12
9
6

Figure 11.1

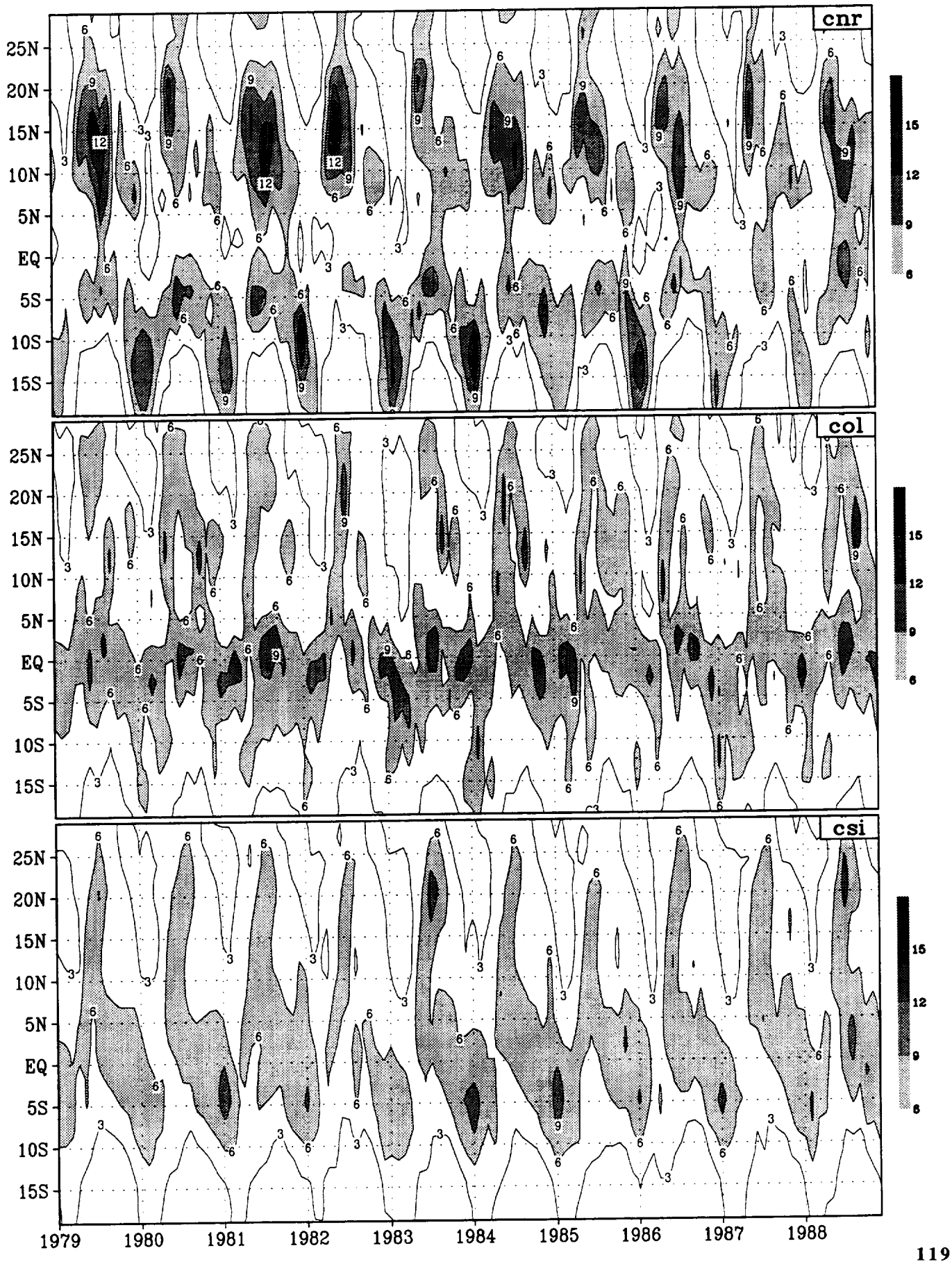

Figure 11.1 (continued)

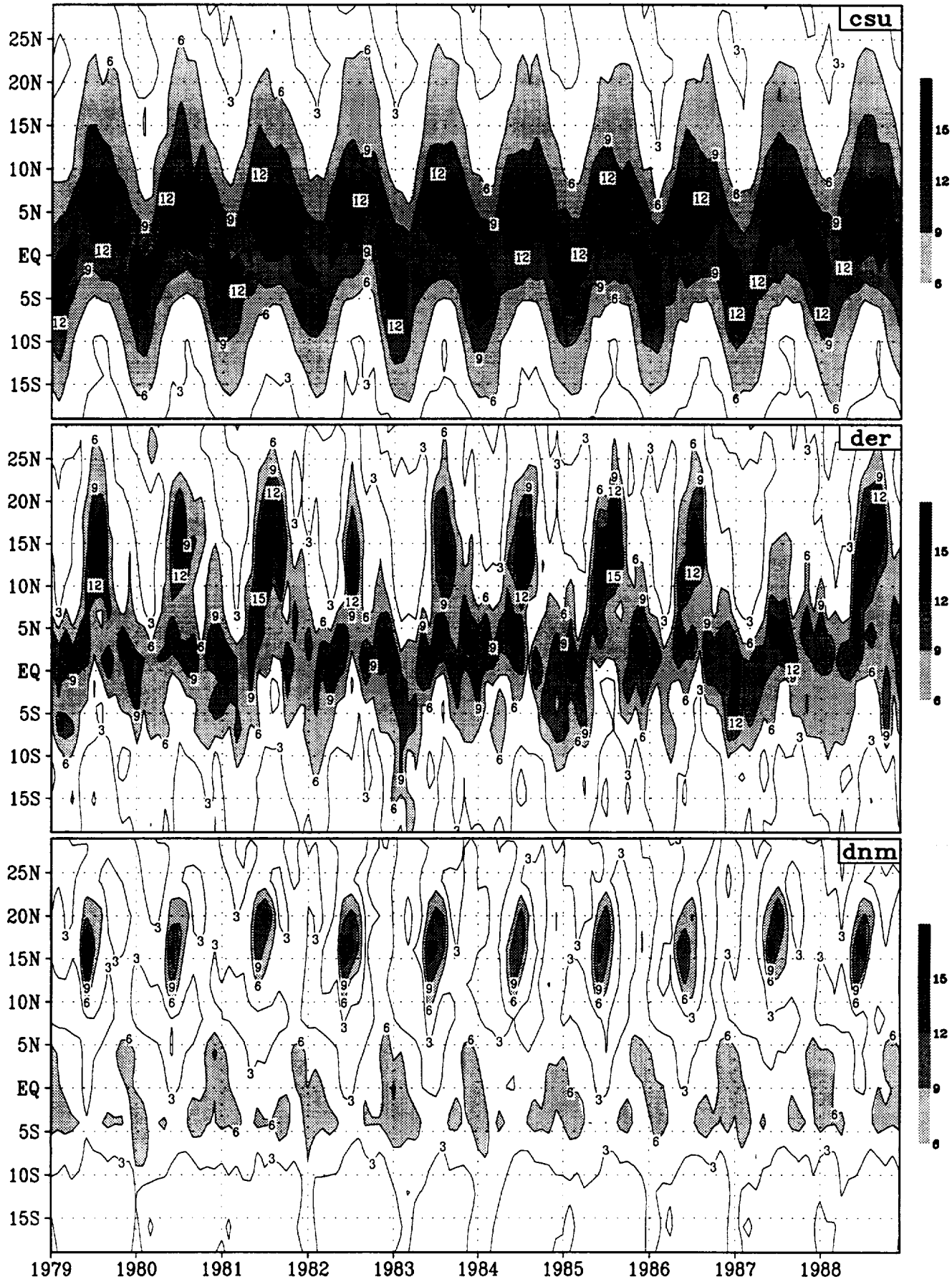

Figure 11.1 (continued

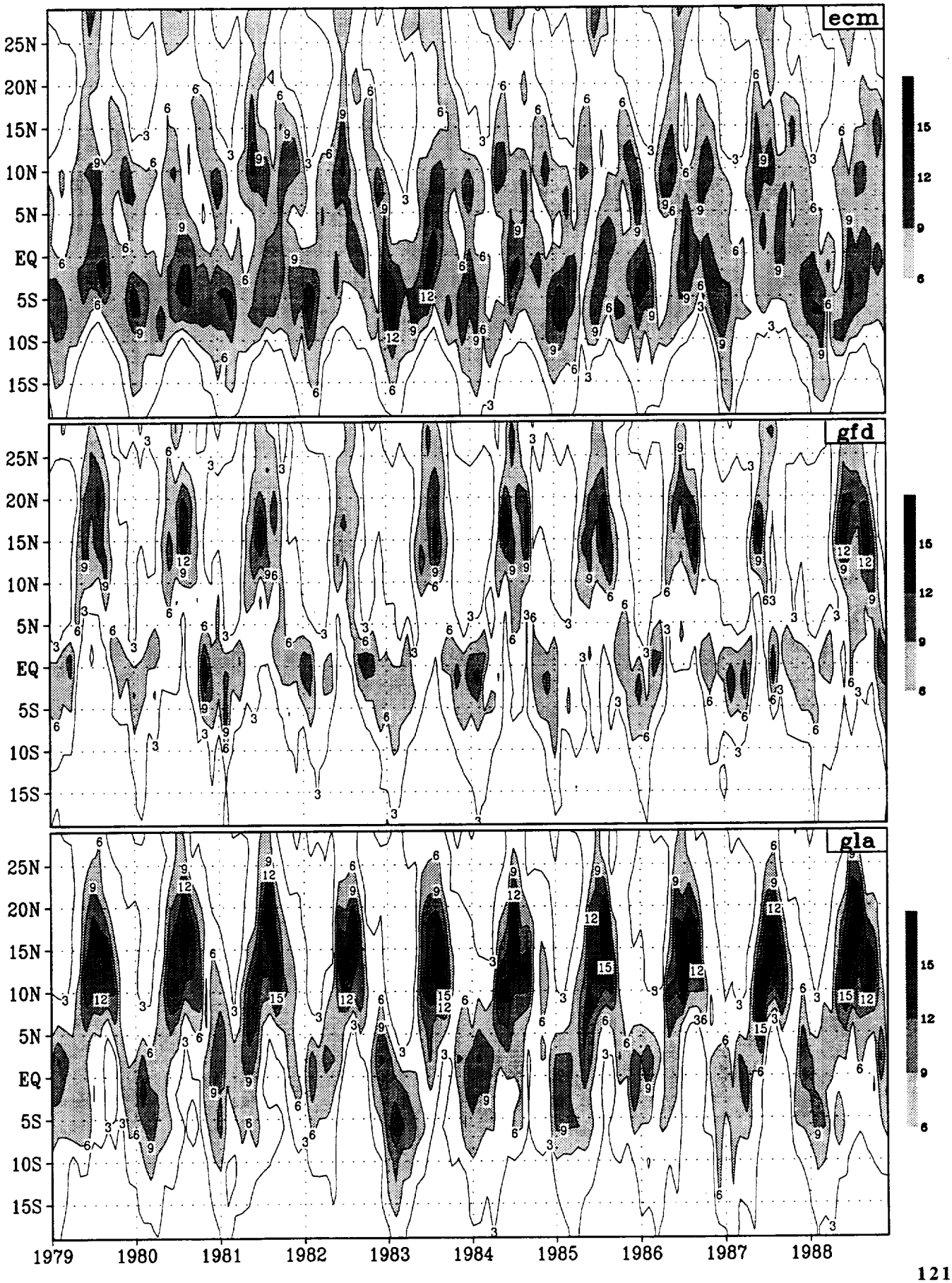

Figure 11.1 (continued)

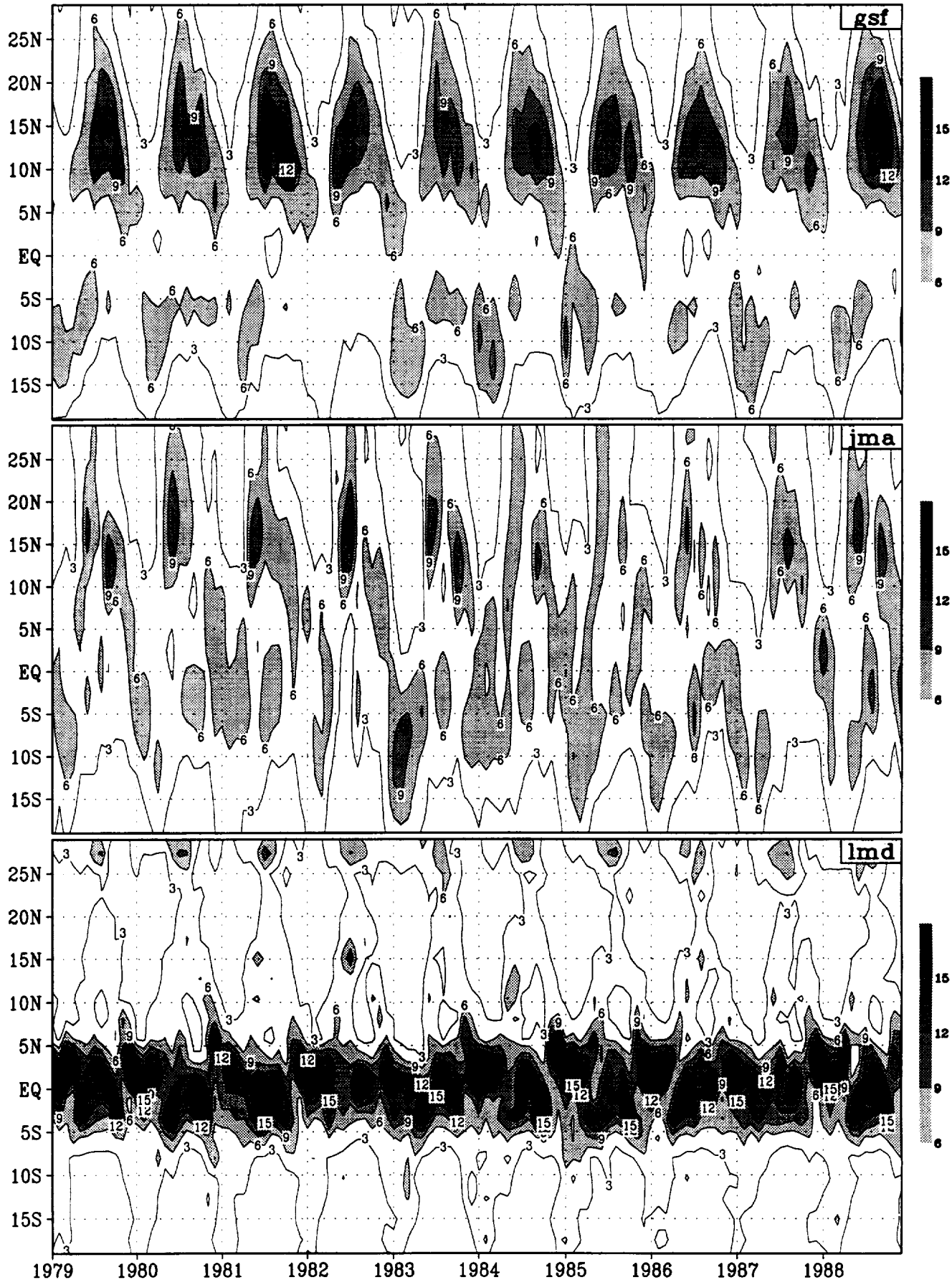

Figure 11.1 (continued)

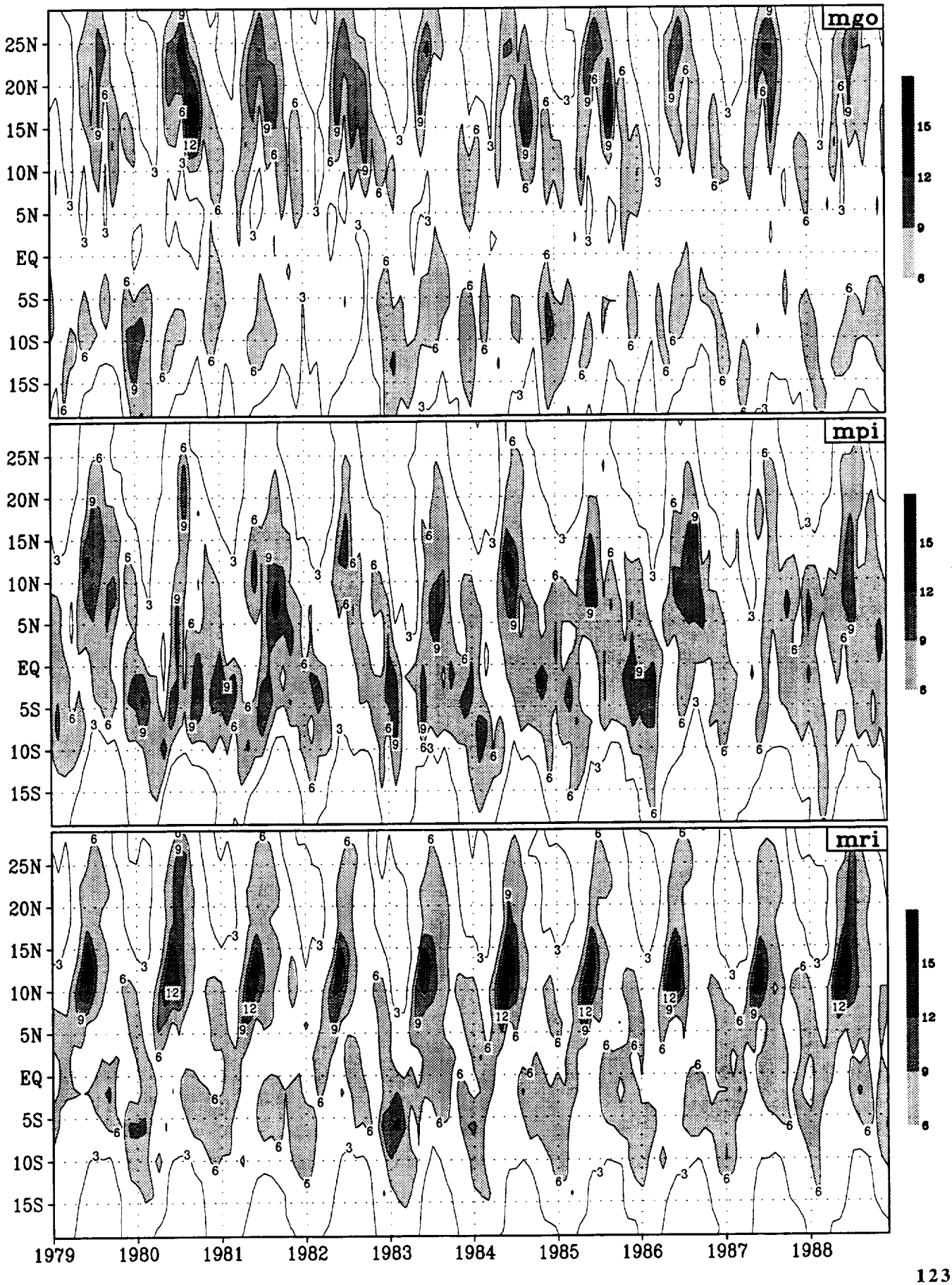

Figure 11.1 (continued)

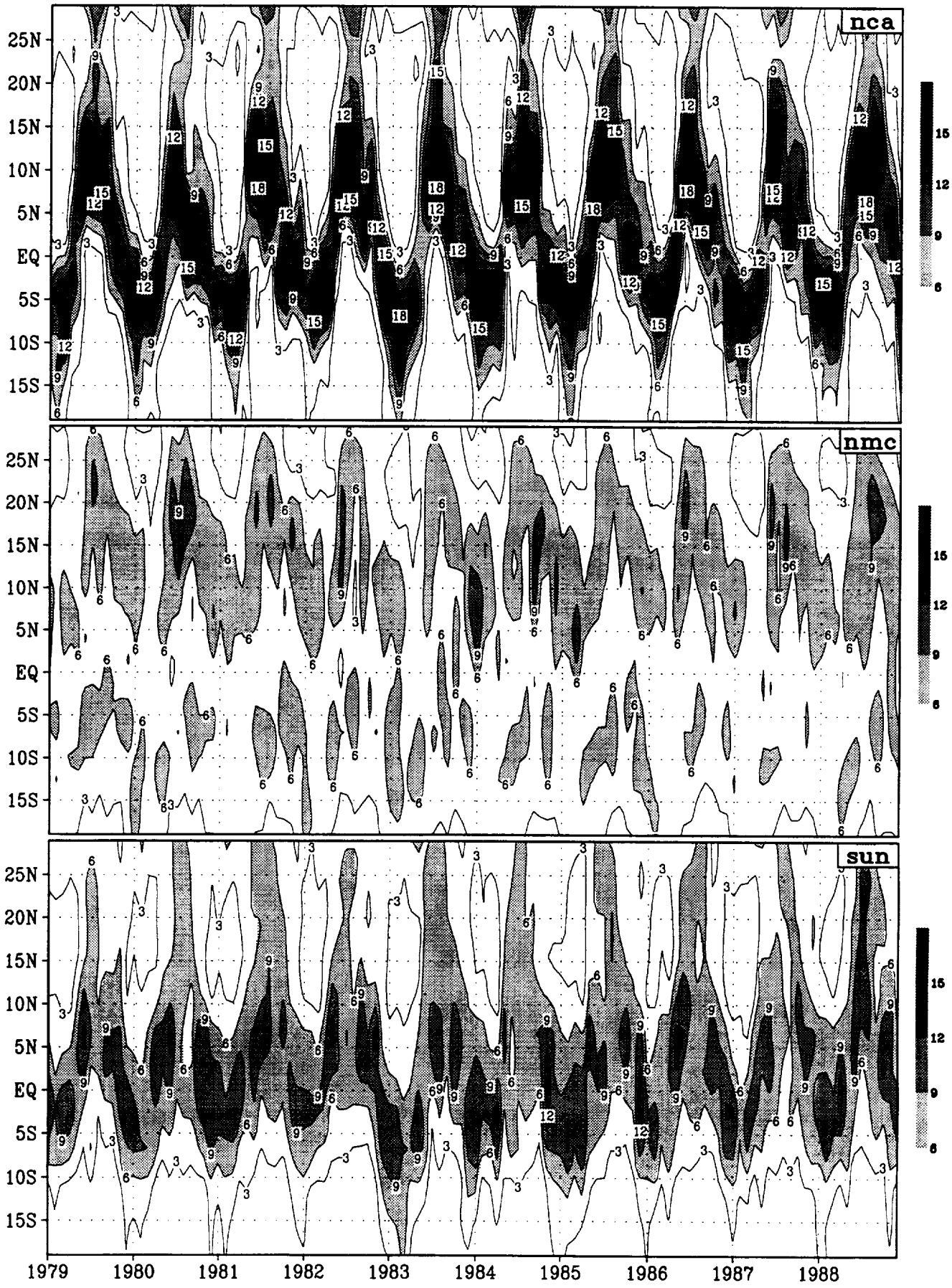

Figure 11.1 (continued)

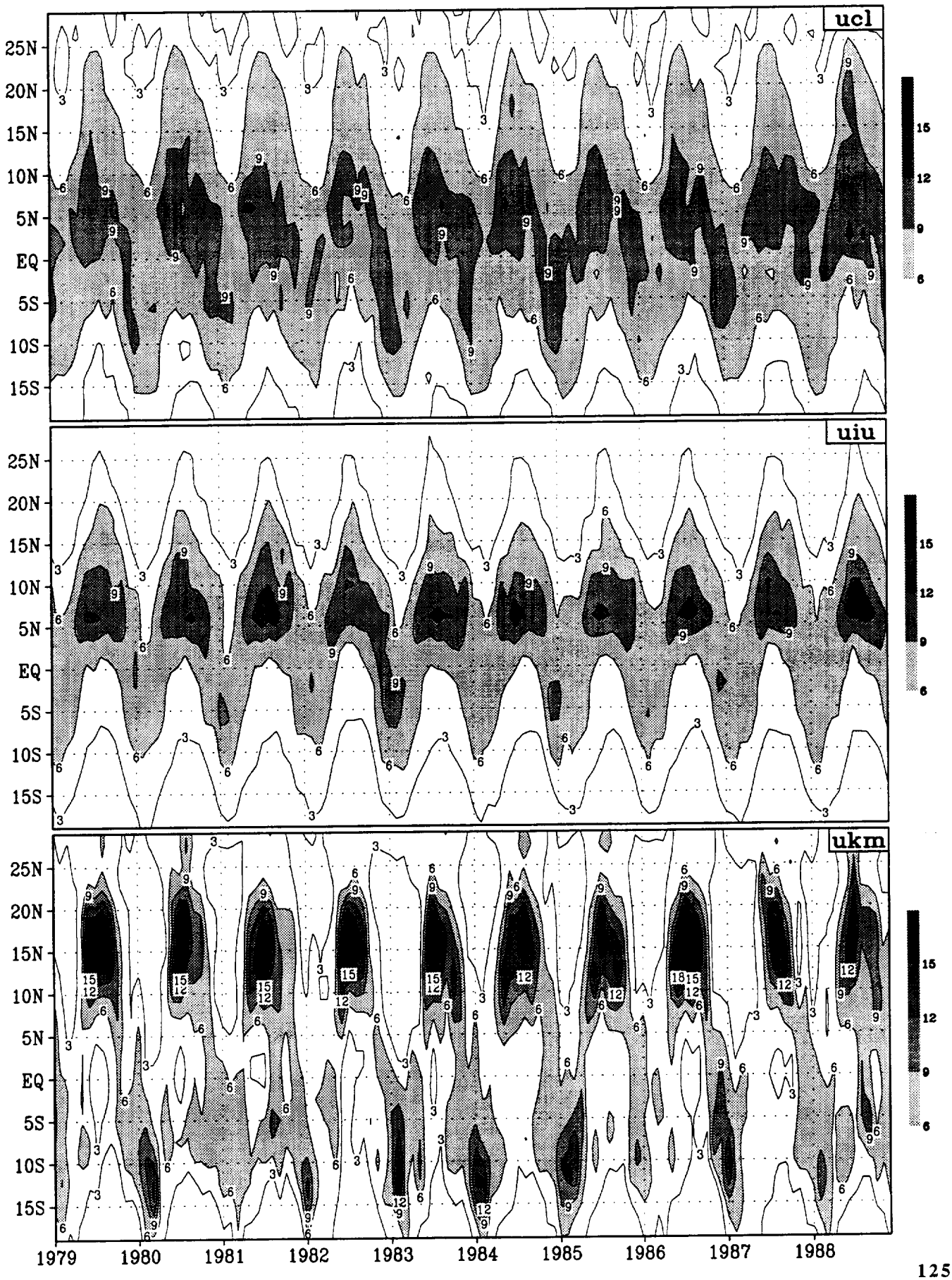

Figure 11.1 (continued)

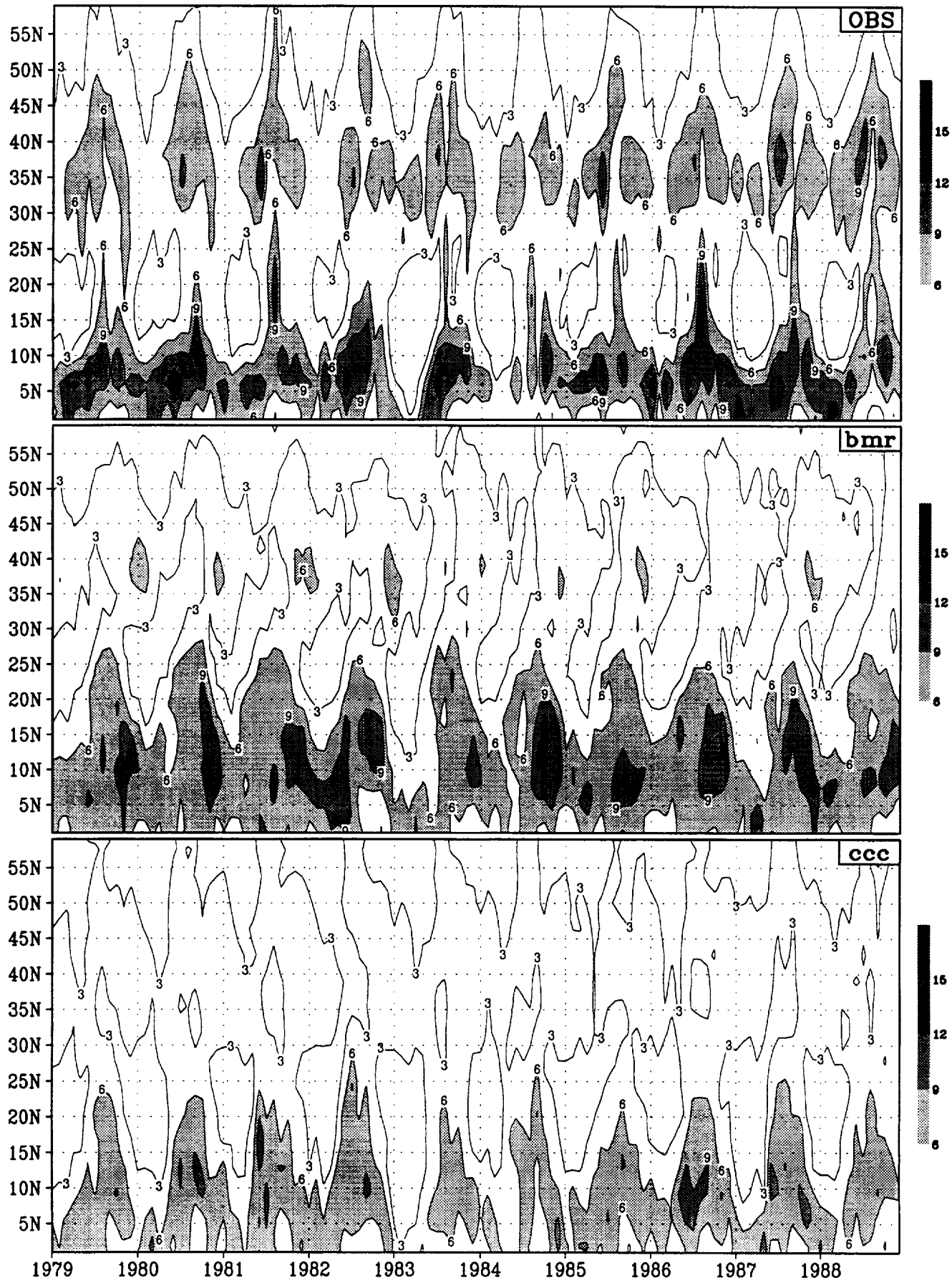
OBS
bmr
ccc
55N
50N
45N
40N
35N
30N
25N
20N
15N
10N
5N
1979
1980
1981
1982
1983
1984
1985
1986
1987
1988
15
12
9
6

Figure 11.2

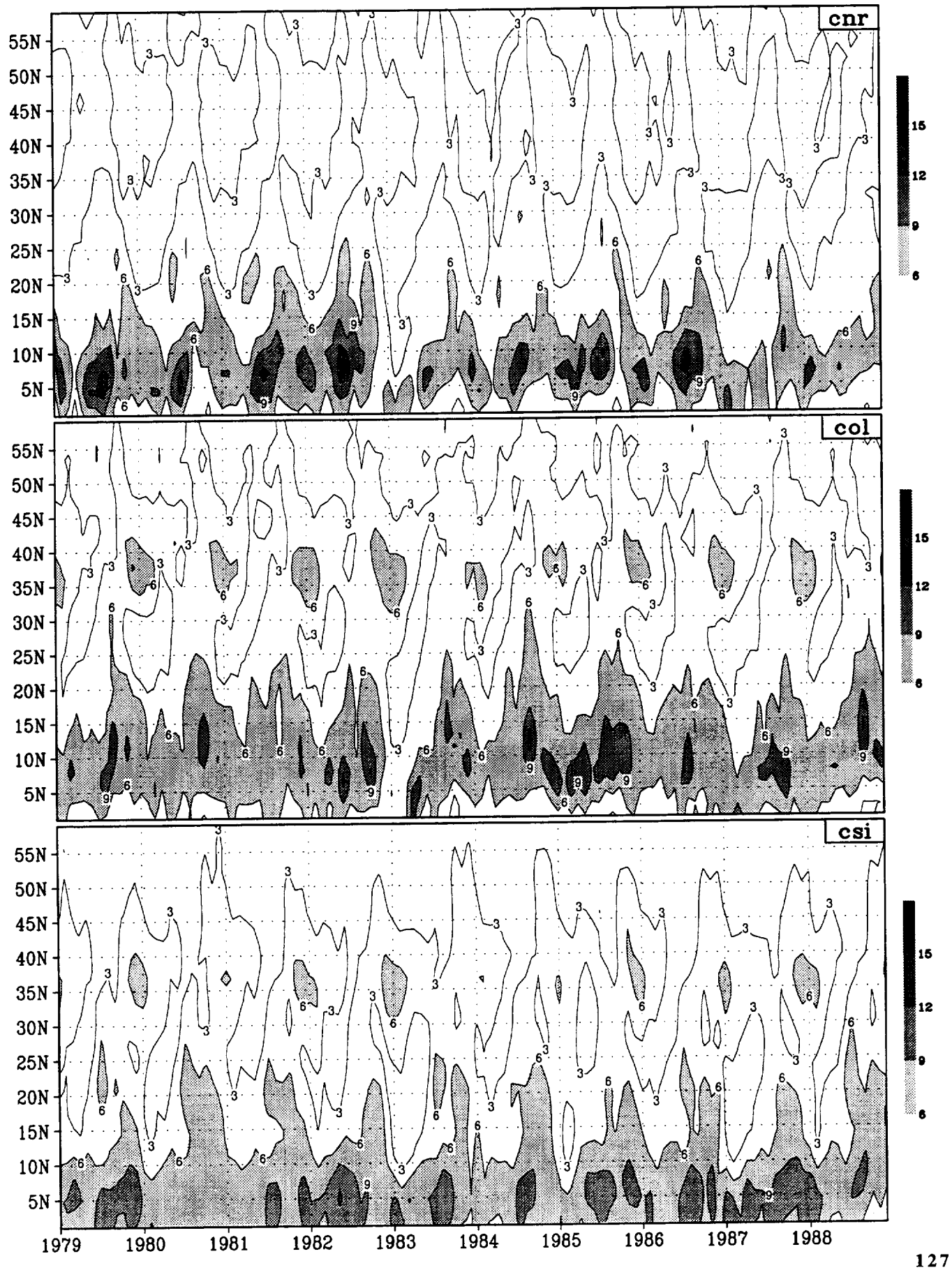

Figure 11.2 (continued)

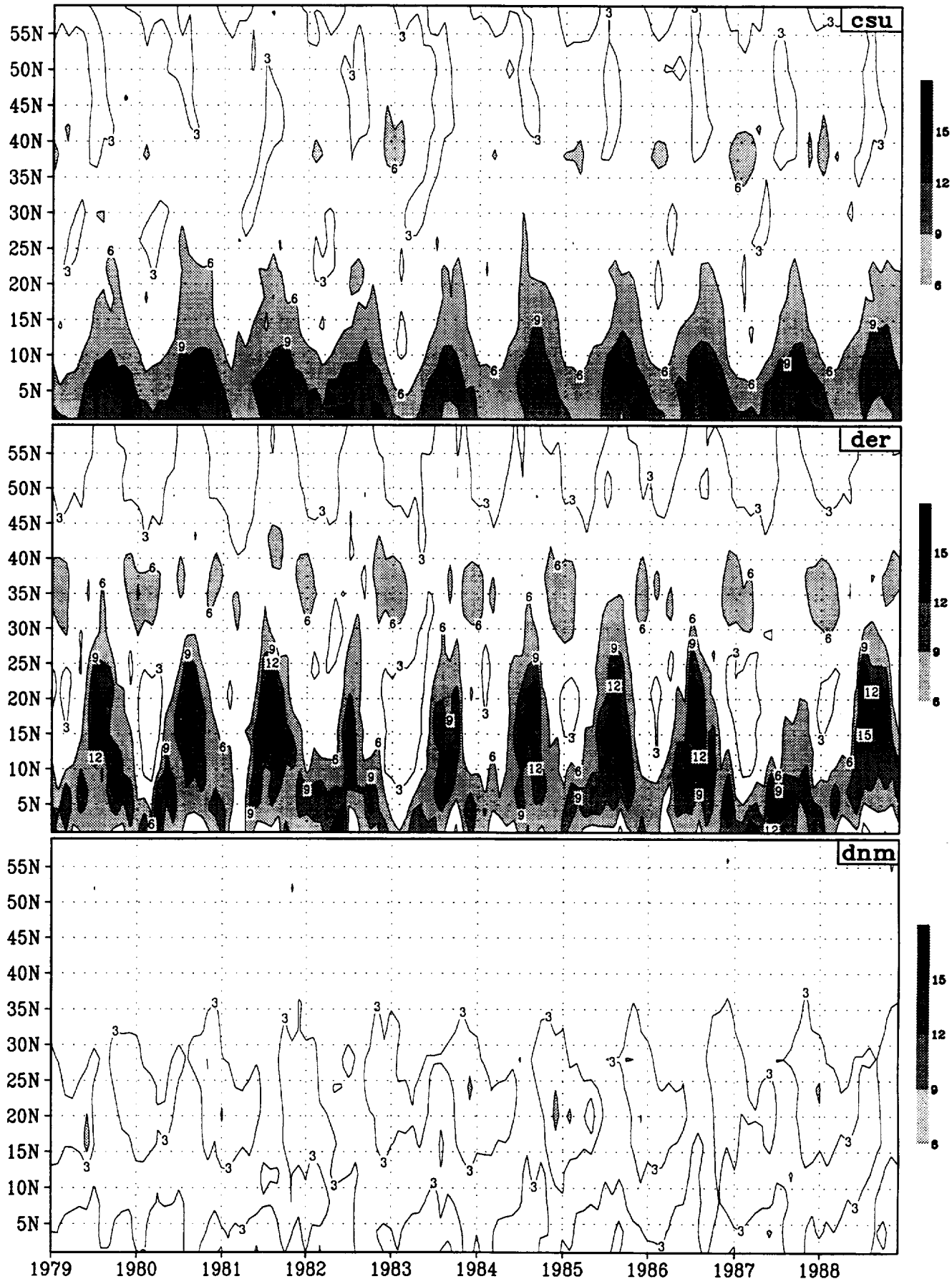

Figure 11.2 (continued)

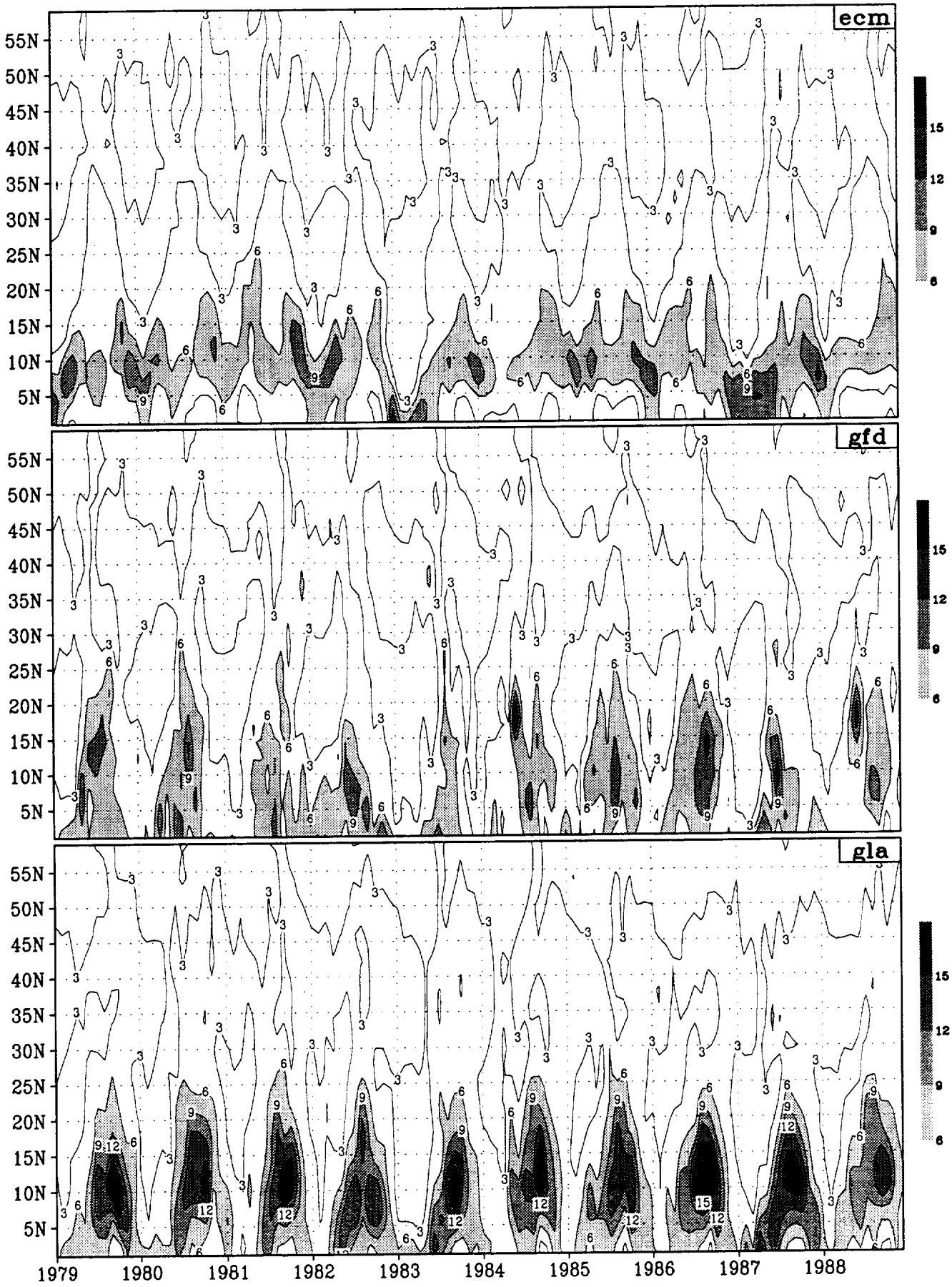

Figure 11.2 (continued)

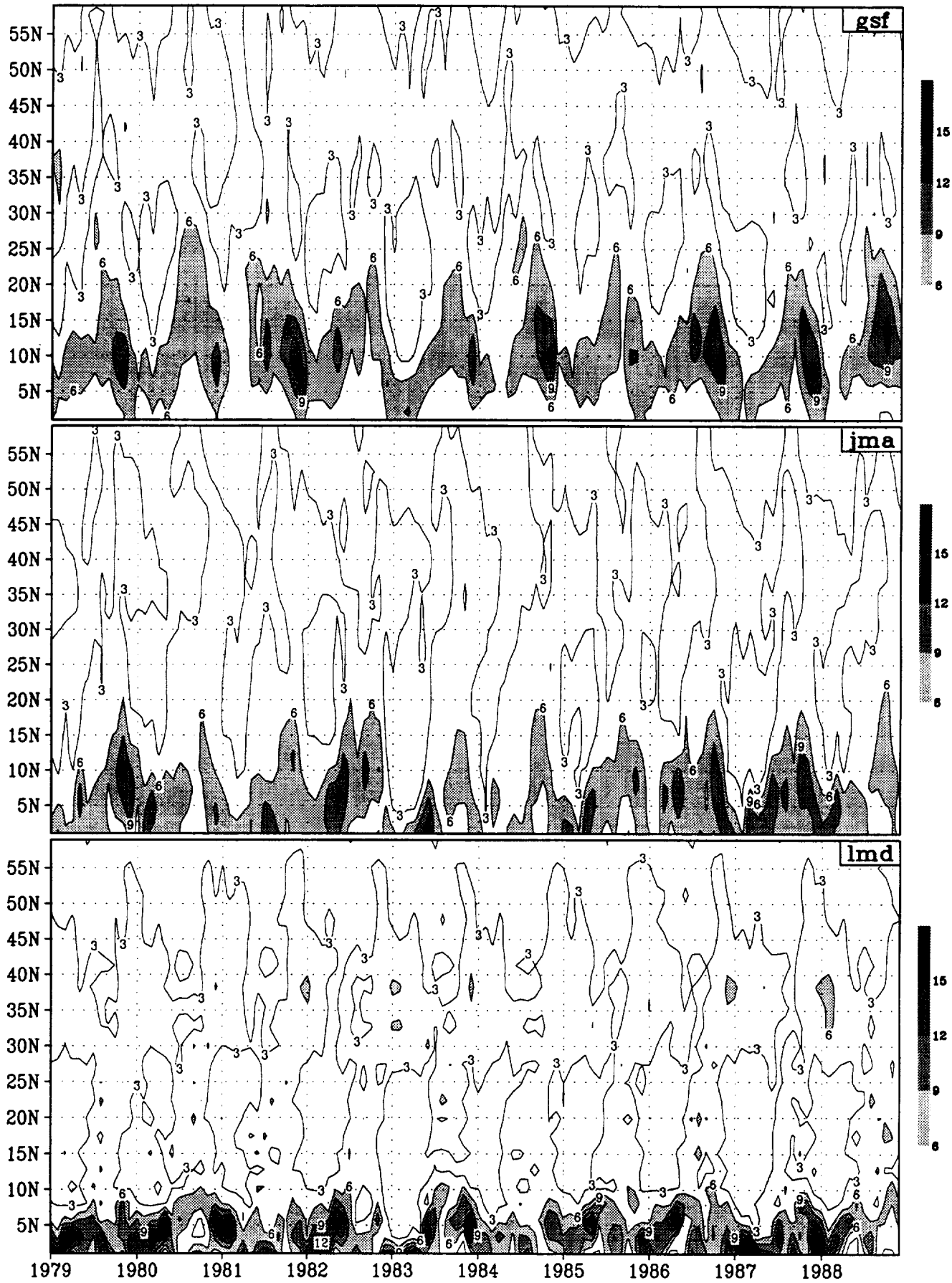

Figure 11.2 (continued)

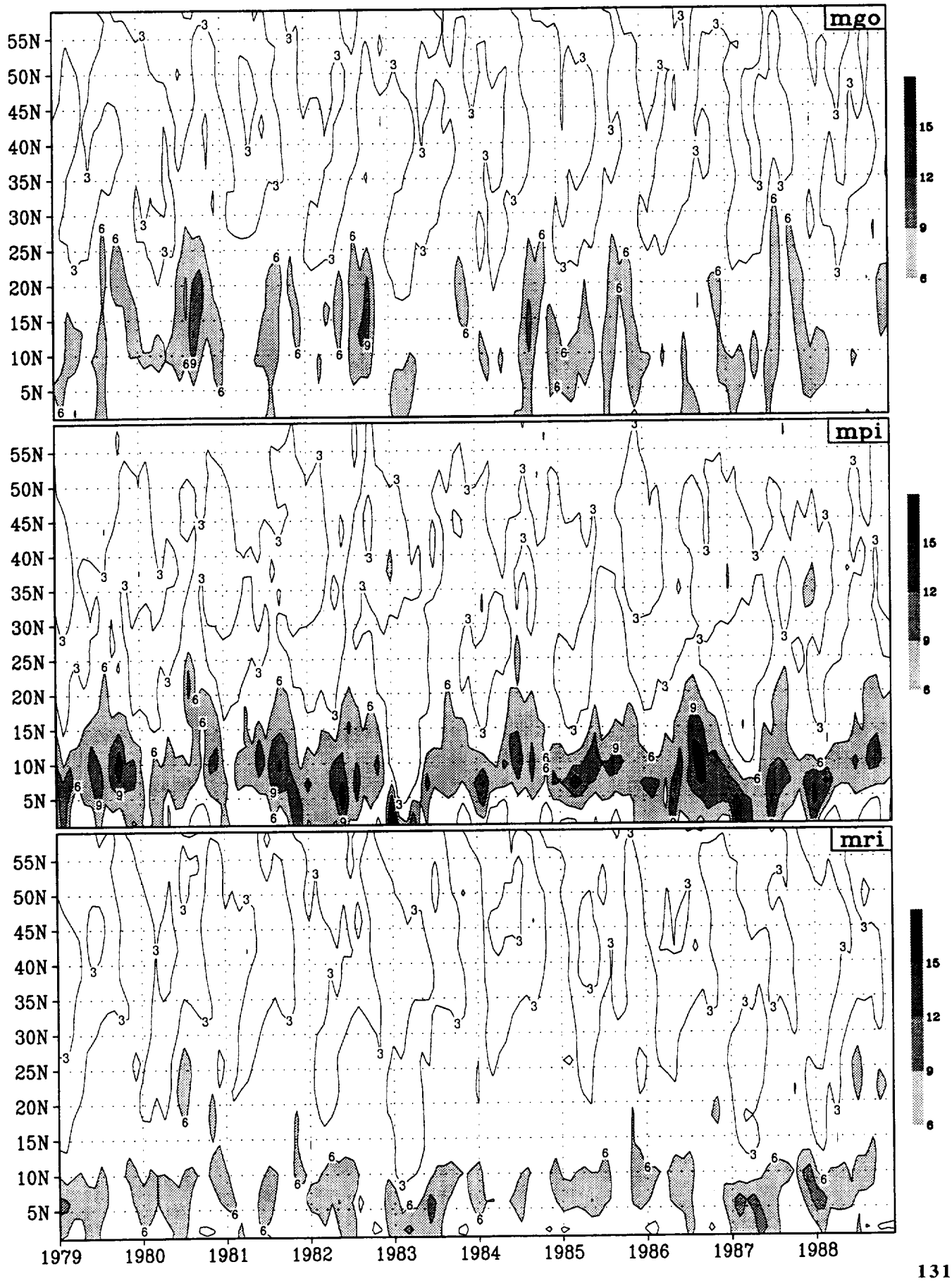

Figure 11.2 (continued)

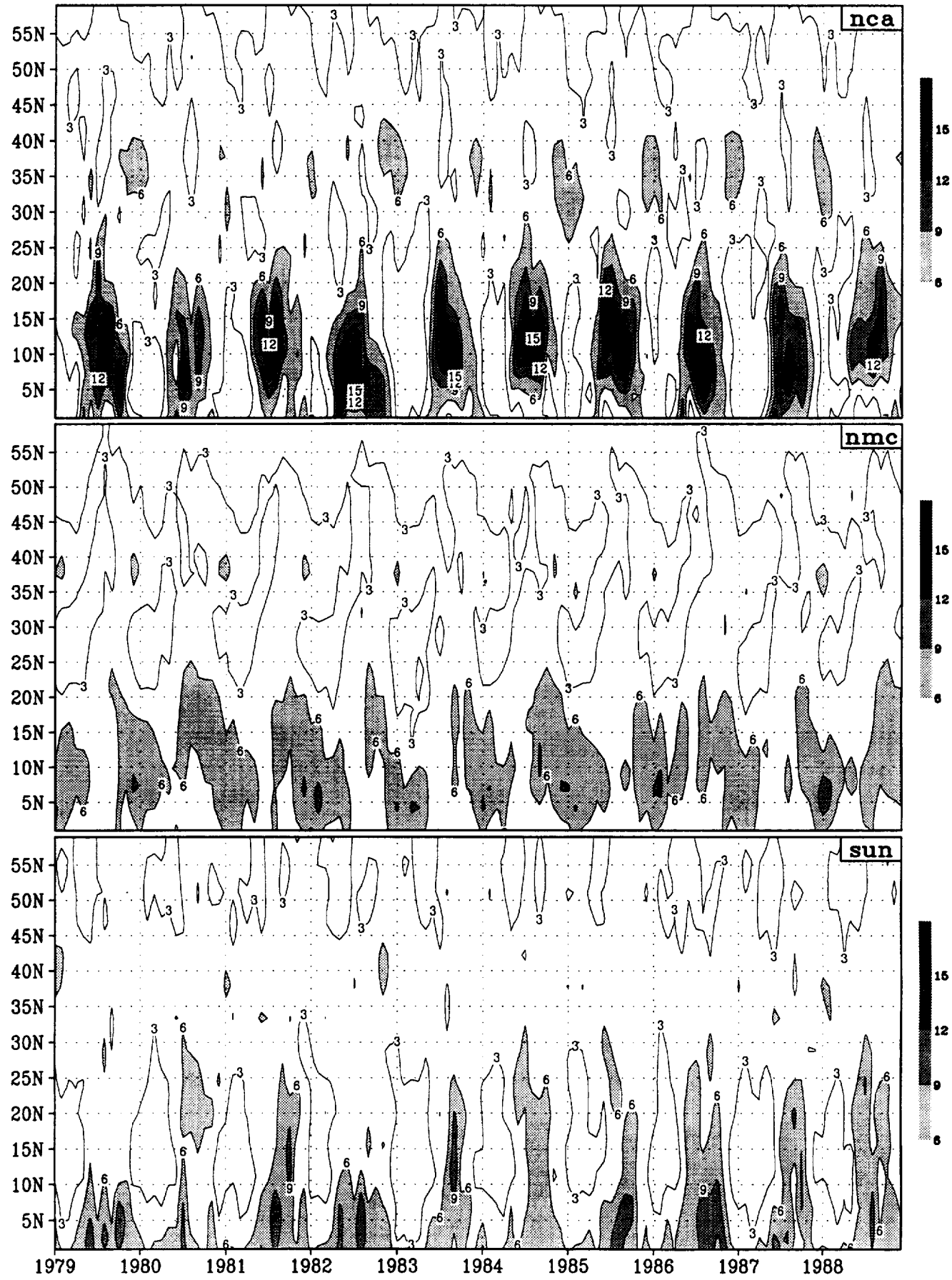

Figure 11.2 (continued)

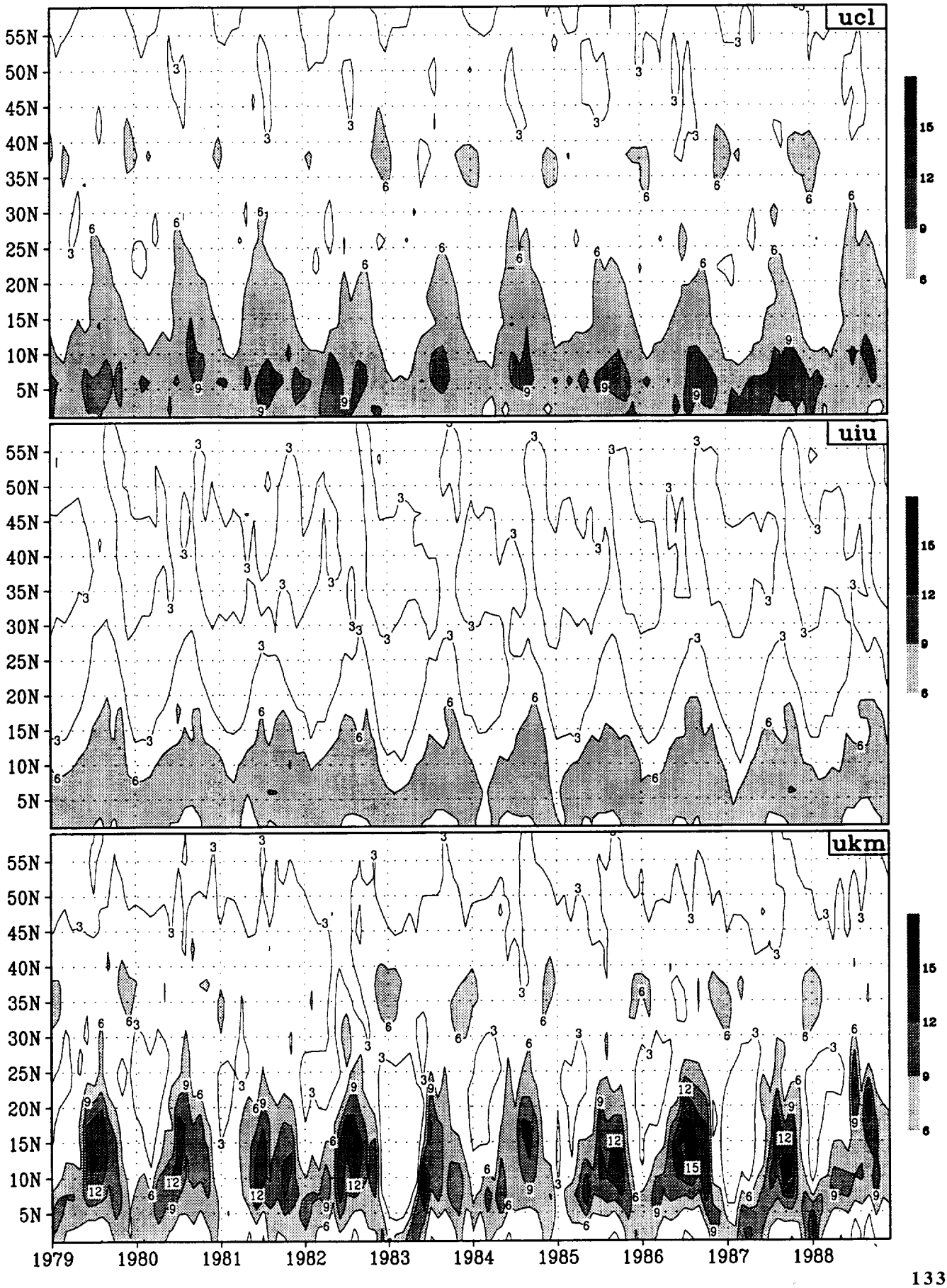

Figure 11.2 (continued)

Pattern Correlation Coefficients in Seasonal Anomaly Rainfall (30SH–30NH)

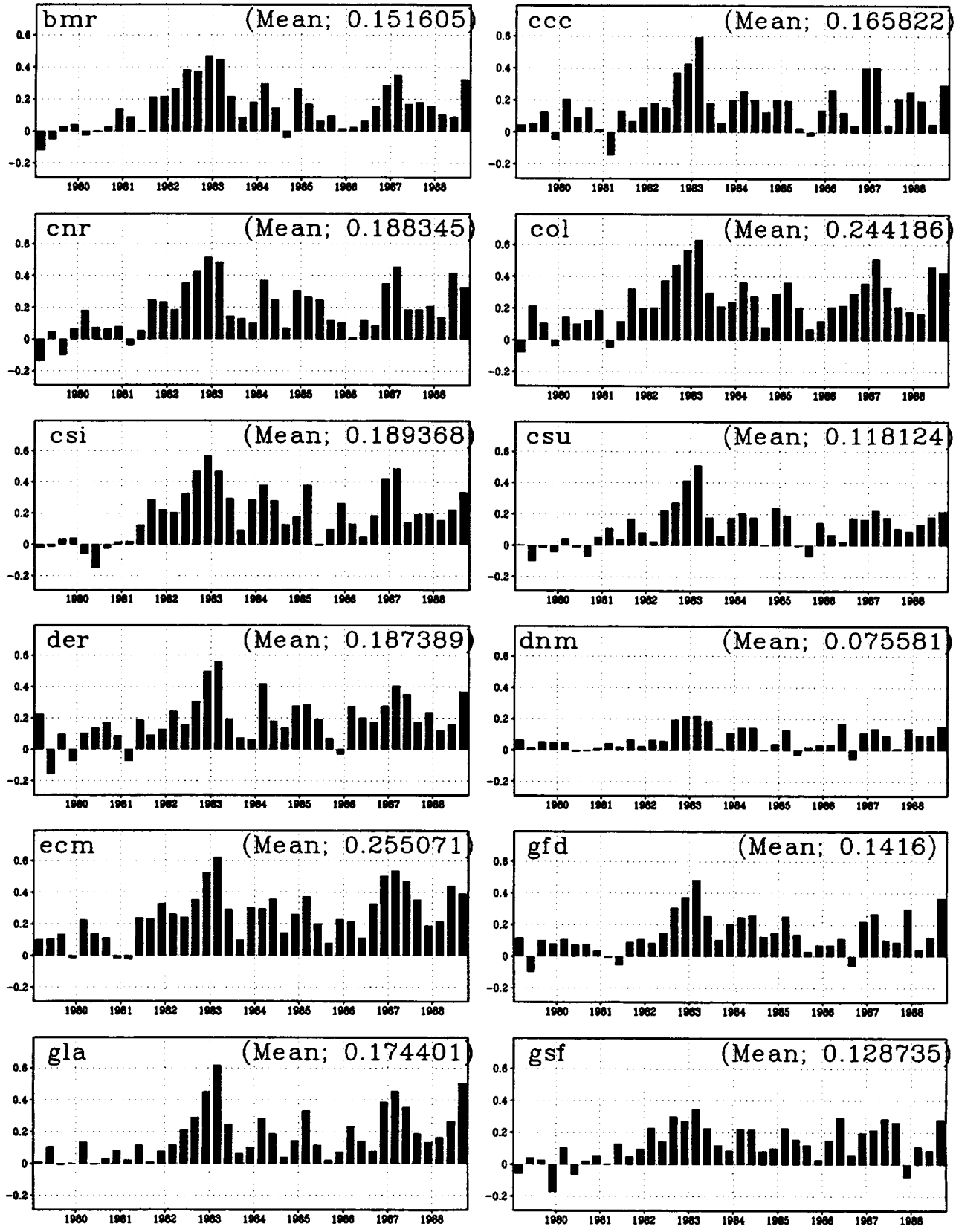

Figure 12

Pattern Correlation Coefficients in Seasonal Anomaly Rainfall (30SH–30NH)

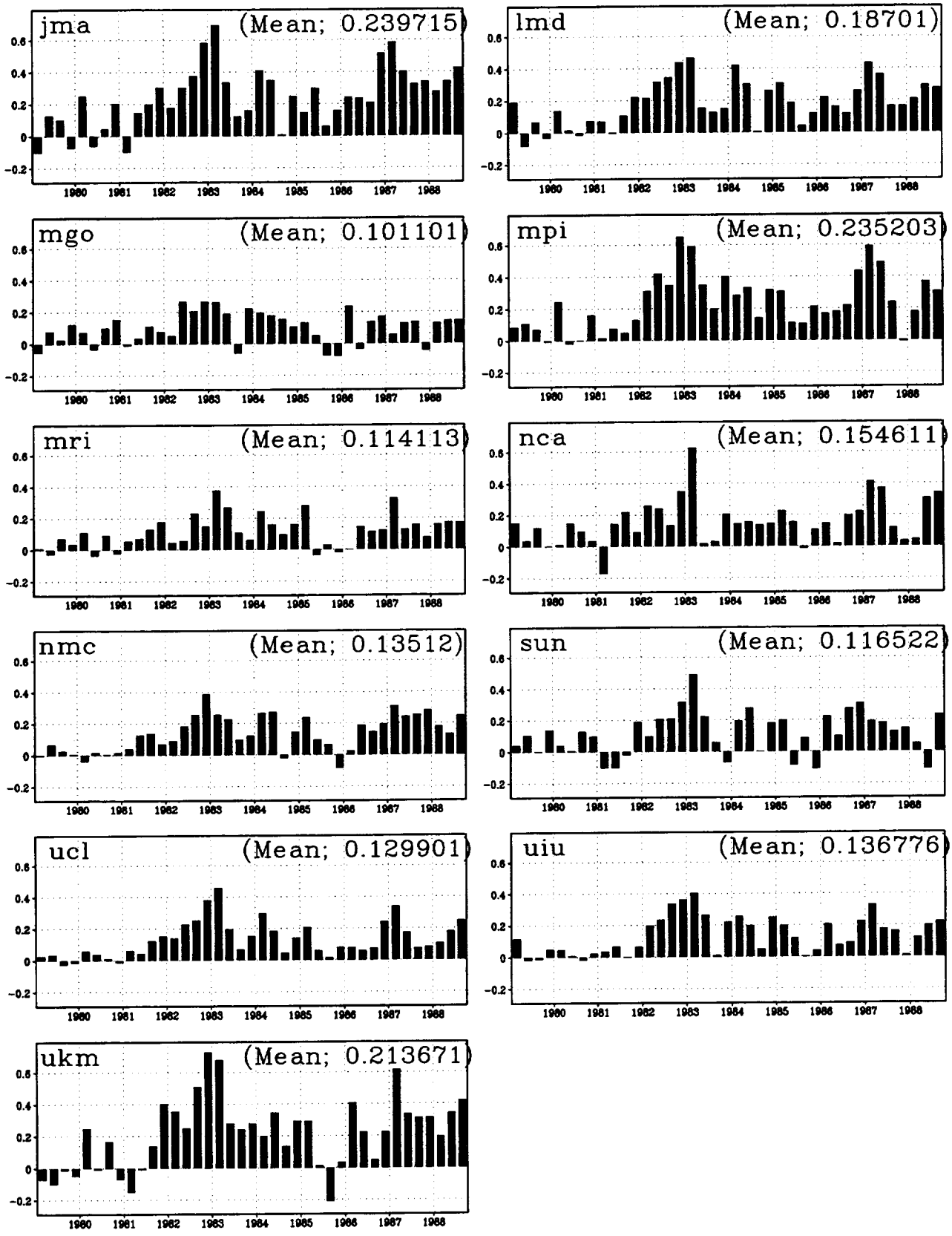

Figure 12 (continued)

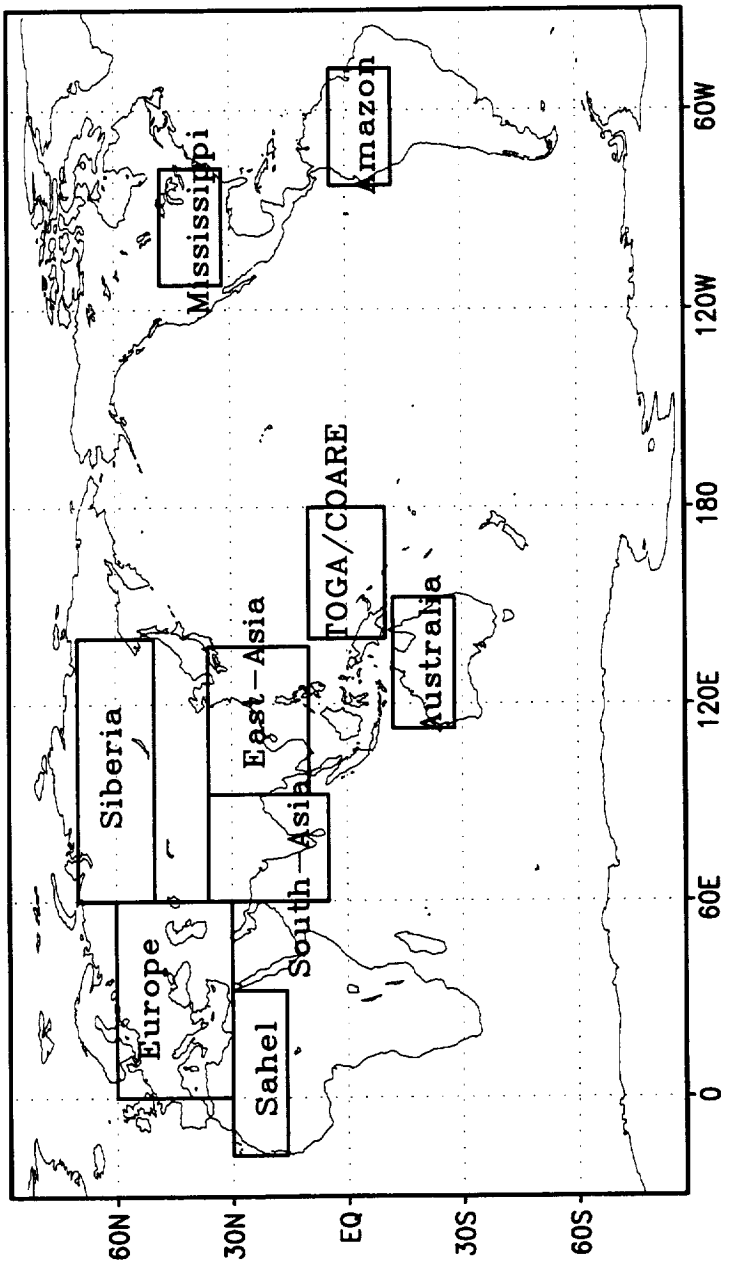

Figure 13.1

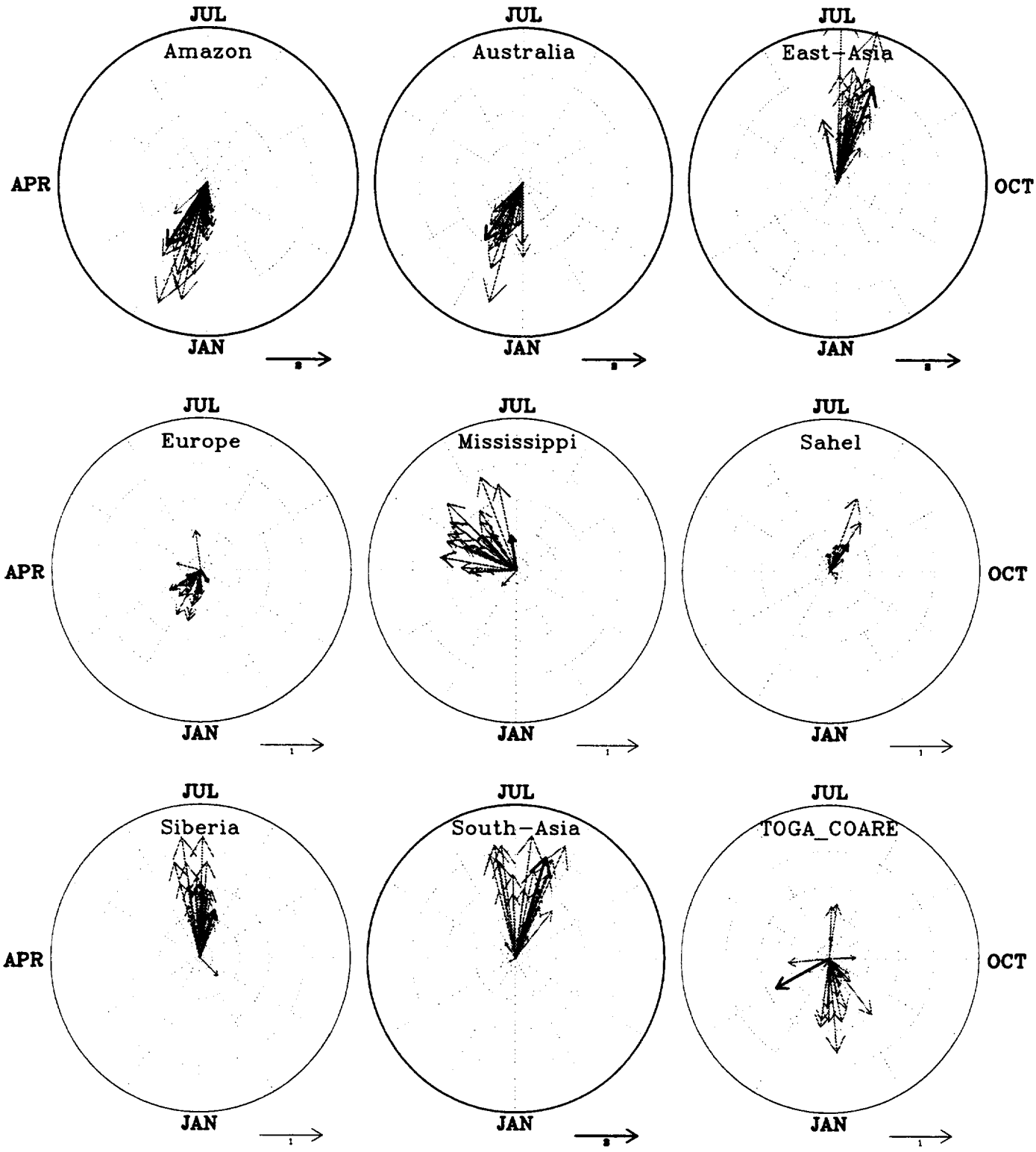
Annual Cycles in Precipitation
unit, mm/day
JUL
Amazon
APR
JAN
JUL
Australia
JAN
JUL
East-Asia
OCT
JAN
JUL
Europe
APR
JAN
JUL
Mississippi
JAN
JUL
Sahel
OCT
JAN
JUL
Siberia
APR
JAN
JUL
South-Asia
JAN
JUL
TOGA_COARE
OCT
JAN

Figure 13.2

Semiannual Cycles in Precipitation
unit, mm/day

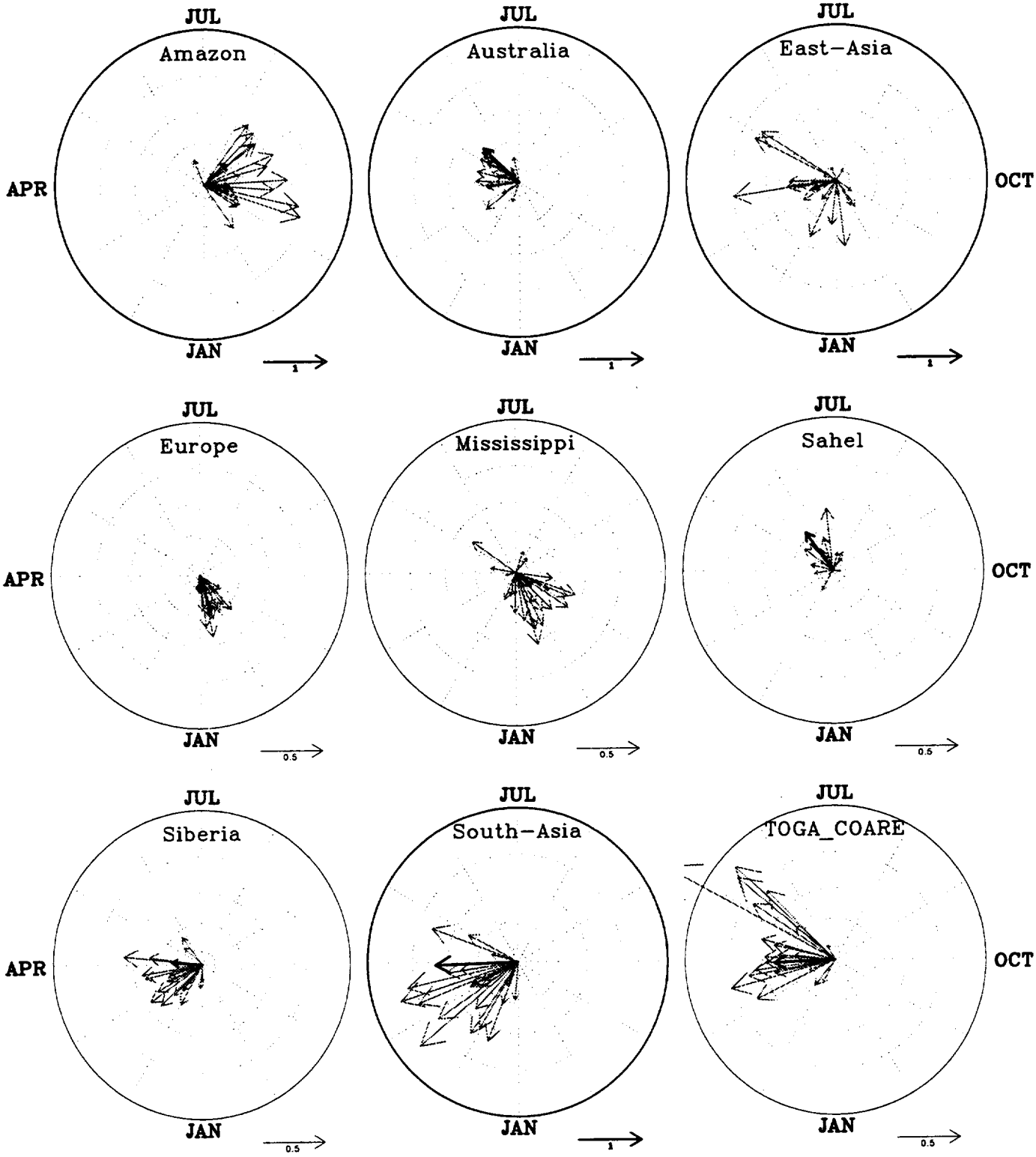

Figure 13.3

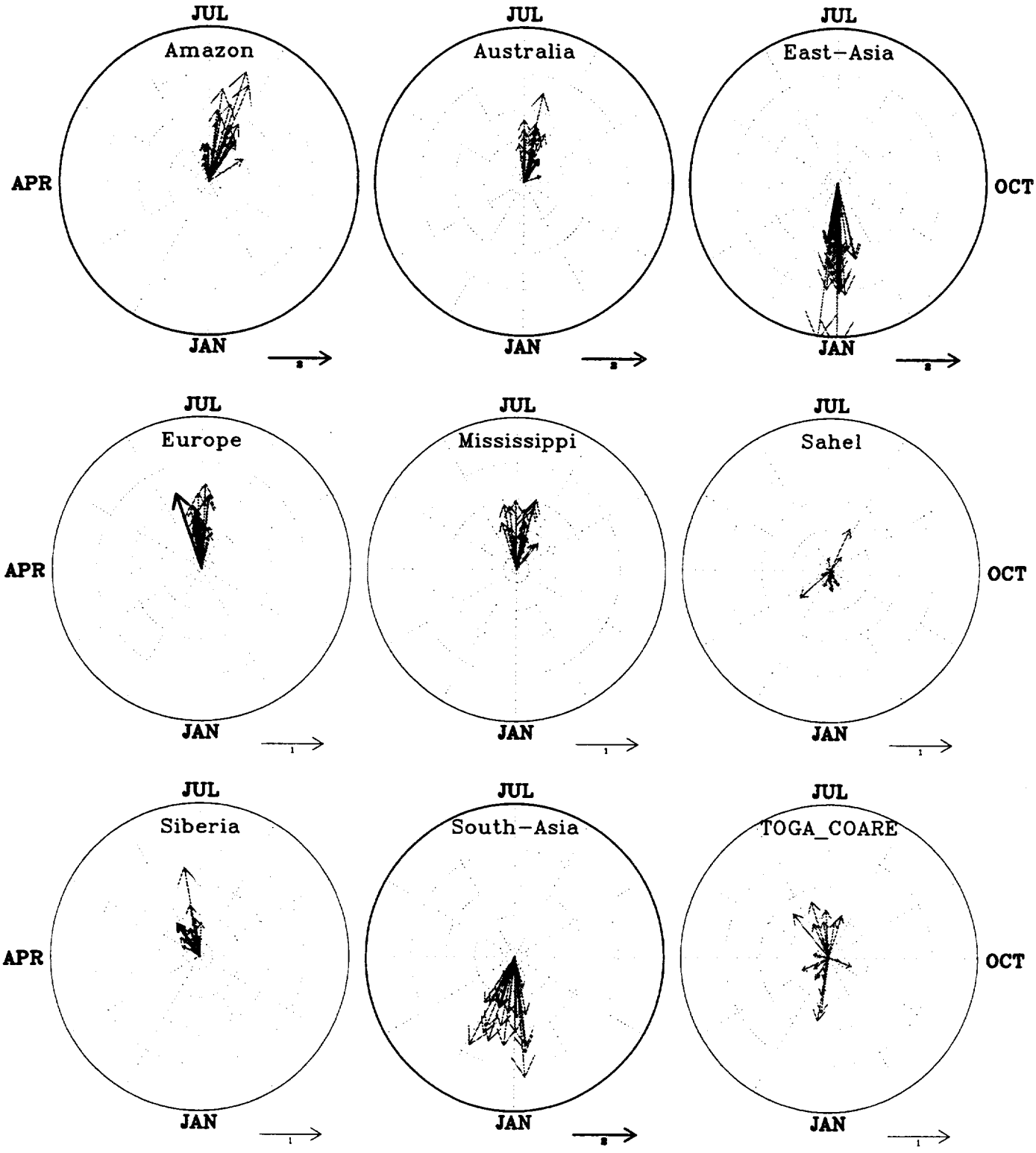
Annual Cycles in E − P
unit, mm/day
JUL
Amazon
APR
JAN
JUL
Australia
JAN
JUL
East−Asia
OCT
JAN
JUL
Europe
APR
JAN
JUL
Mississippi
JAN
JUL
Sahel
OCT
JAN
JUL
Siberia
APR
JAN
JUL
South−Asia
JAN
JUL
TOGA_COARE
OCT
JAN

Figure 13.4

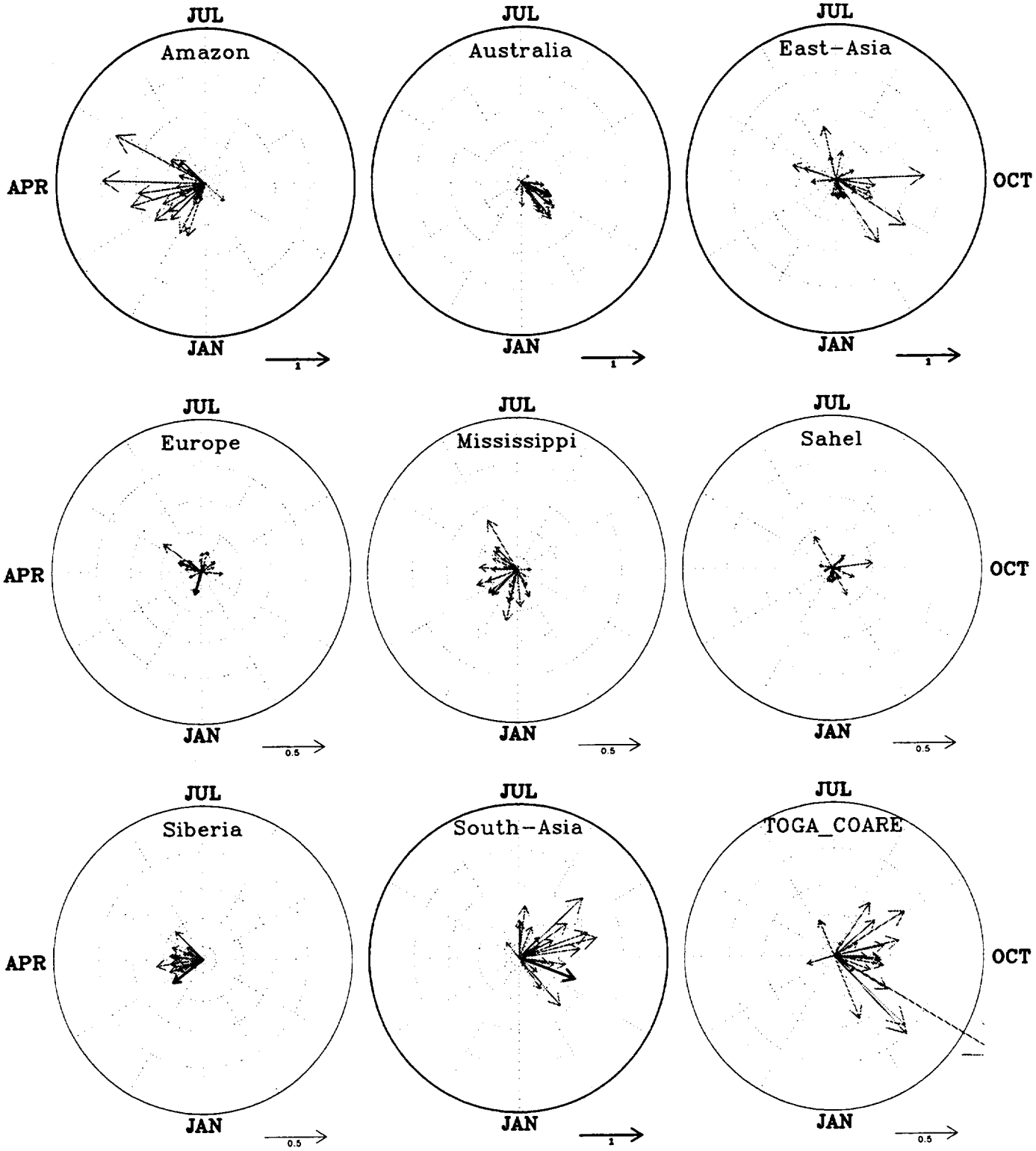
Semiannual Cycles in E − P
unit, mm/day
JUL
Amazon
APR
OCT
JAN
1
JUL
Australia
JAN
1
JUL
East−Asia
OCT
JAN
1
JUL
Europe
APR
JAN
0.5
JUL
Mississippi
JAN
0.5
JUL
Sahel
OCT
JAN
0.5
JUL
Siberia
APR
JAN
0.5
JUL
South−Asia
JAN
1
JUL
TOGA_COARE
OCT
JAN
0.5

Figure 13.5

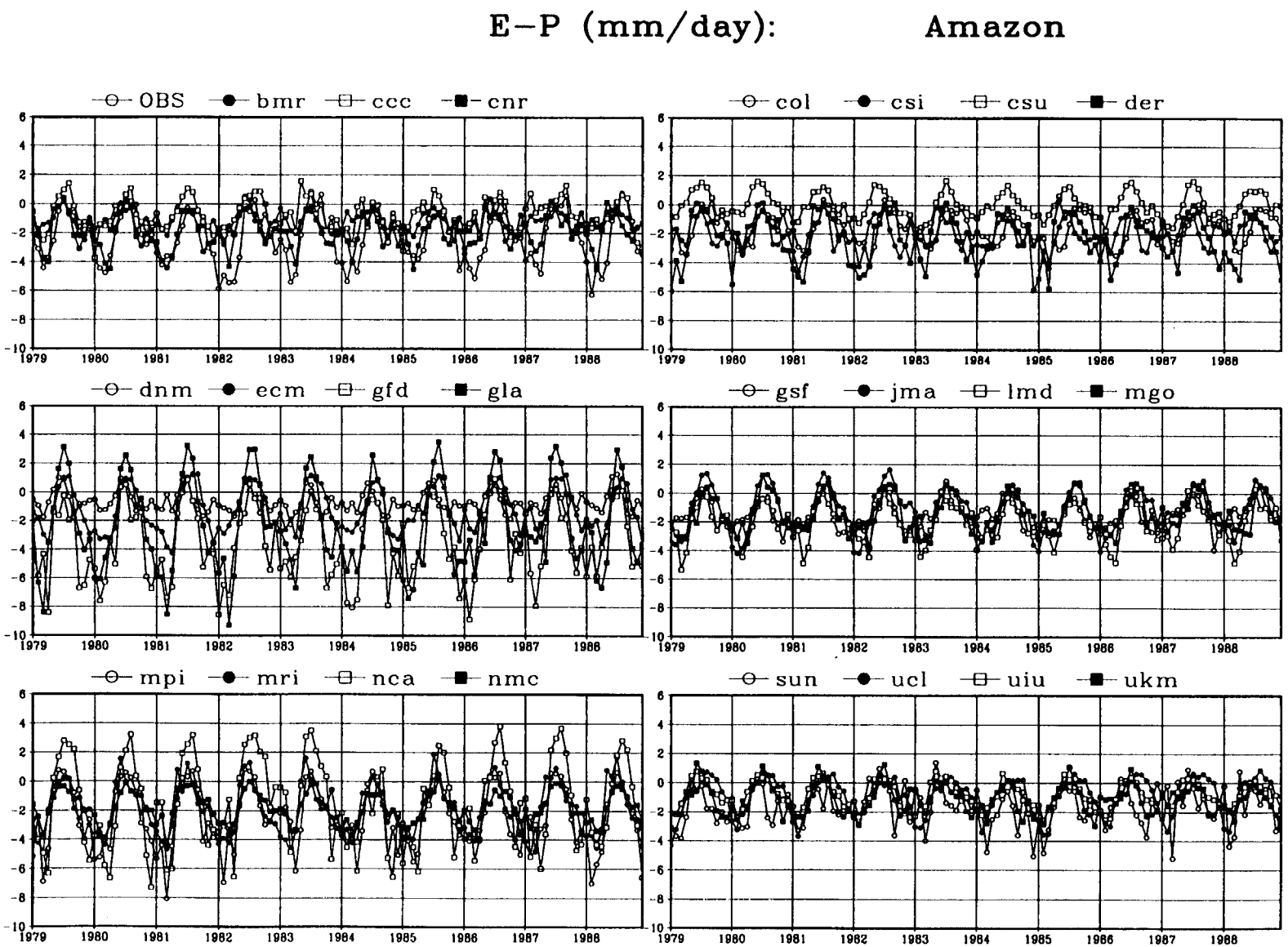
E−P (mm/day): Amazon
OBS bmr ccc cnr
col csi csu der
dnm ecm gfd gla
gsf jma lmd mgo
mpi mri nca nmc
sun ucl uiu ukm
6
4
2
0
-2
-4
-6
-8
-10
1979 1980 1981 1982 1983 1984 1985 1986 1987 1988

Figure 14

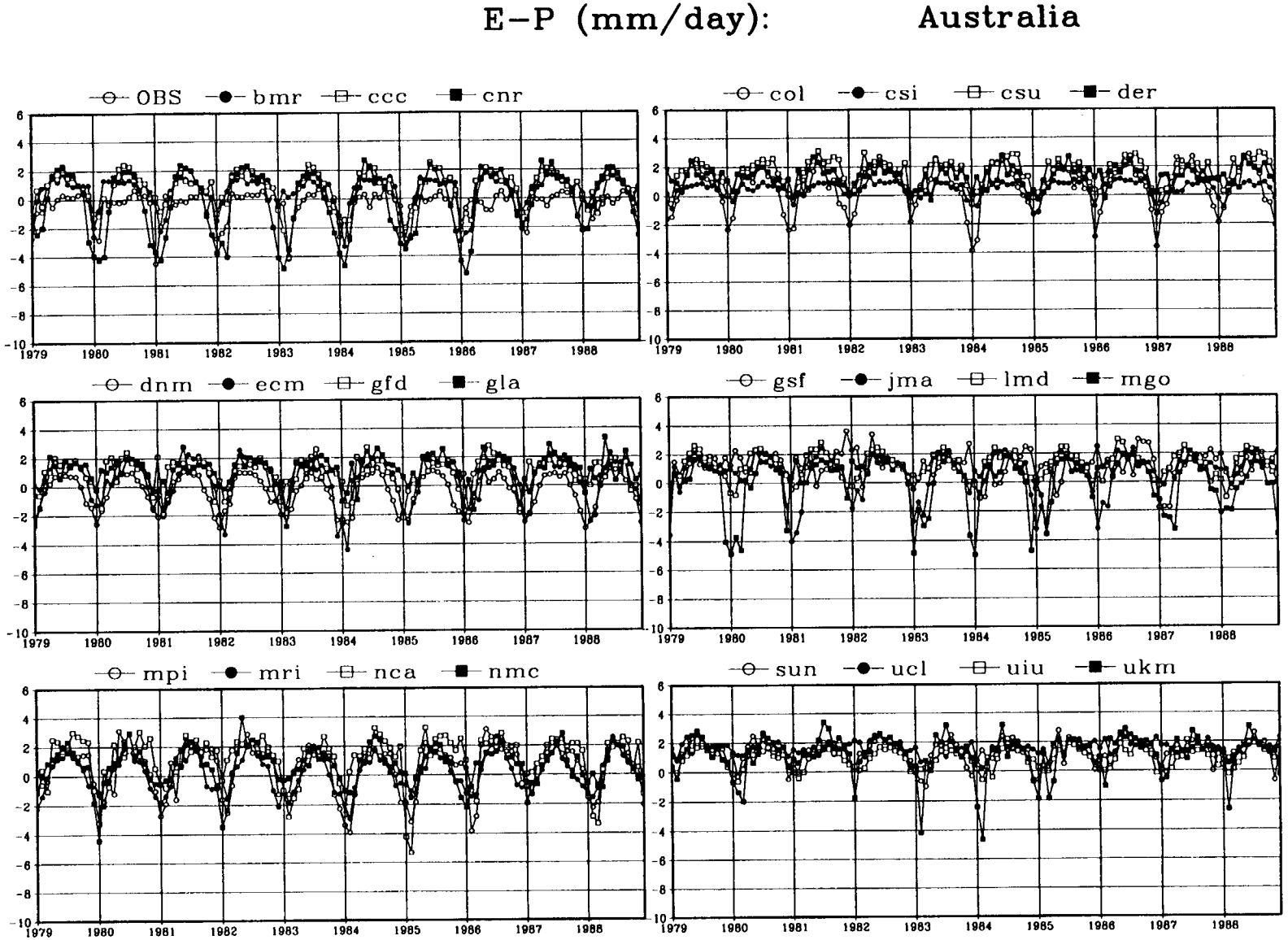

Figure 14 (continued)

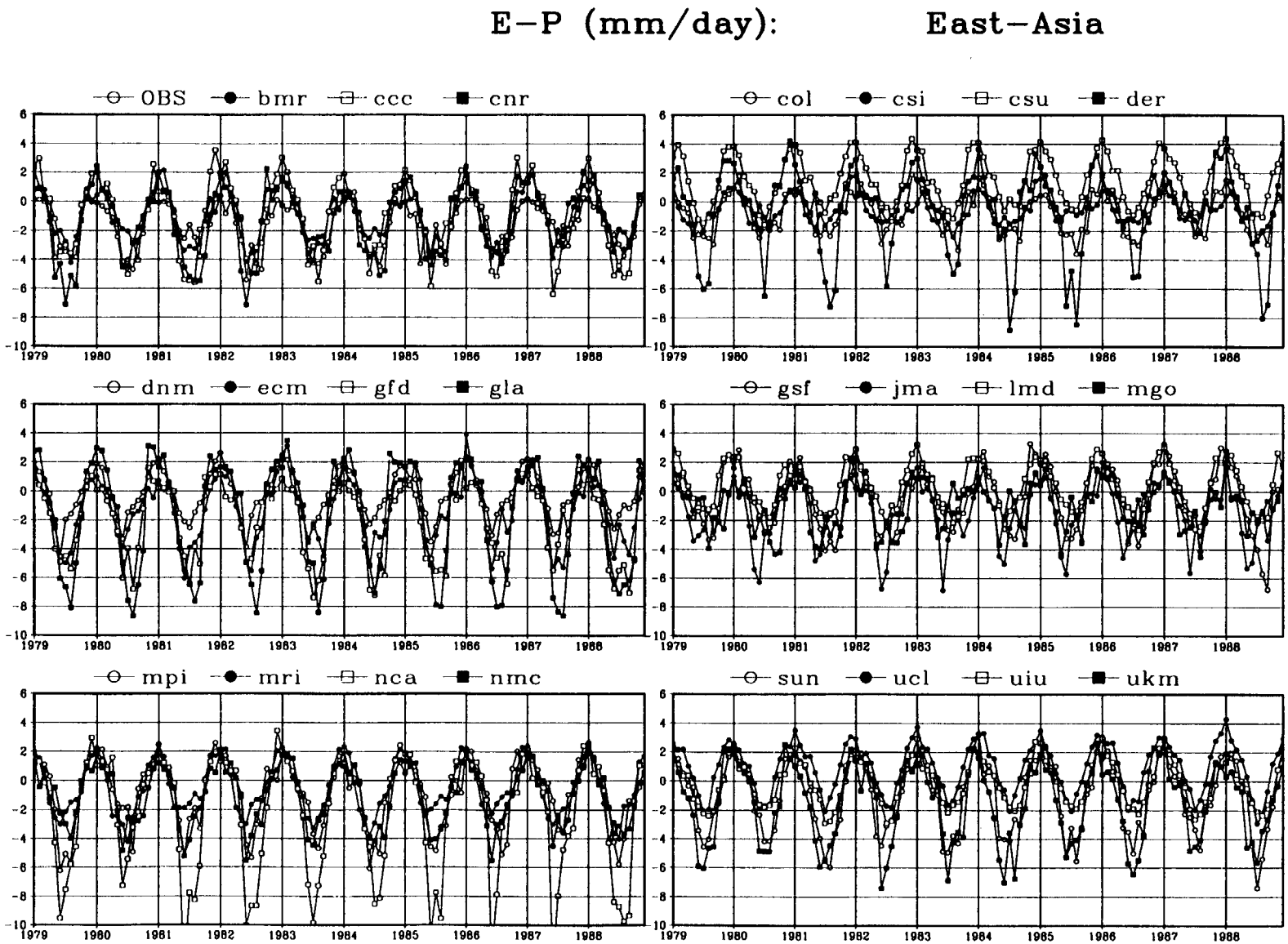

Figure 14 (continued)

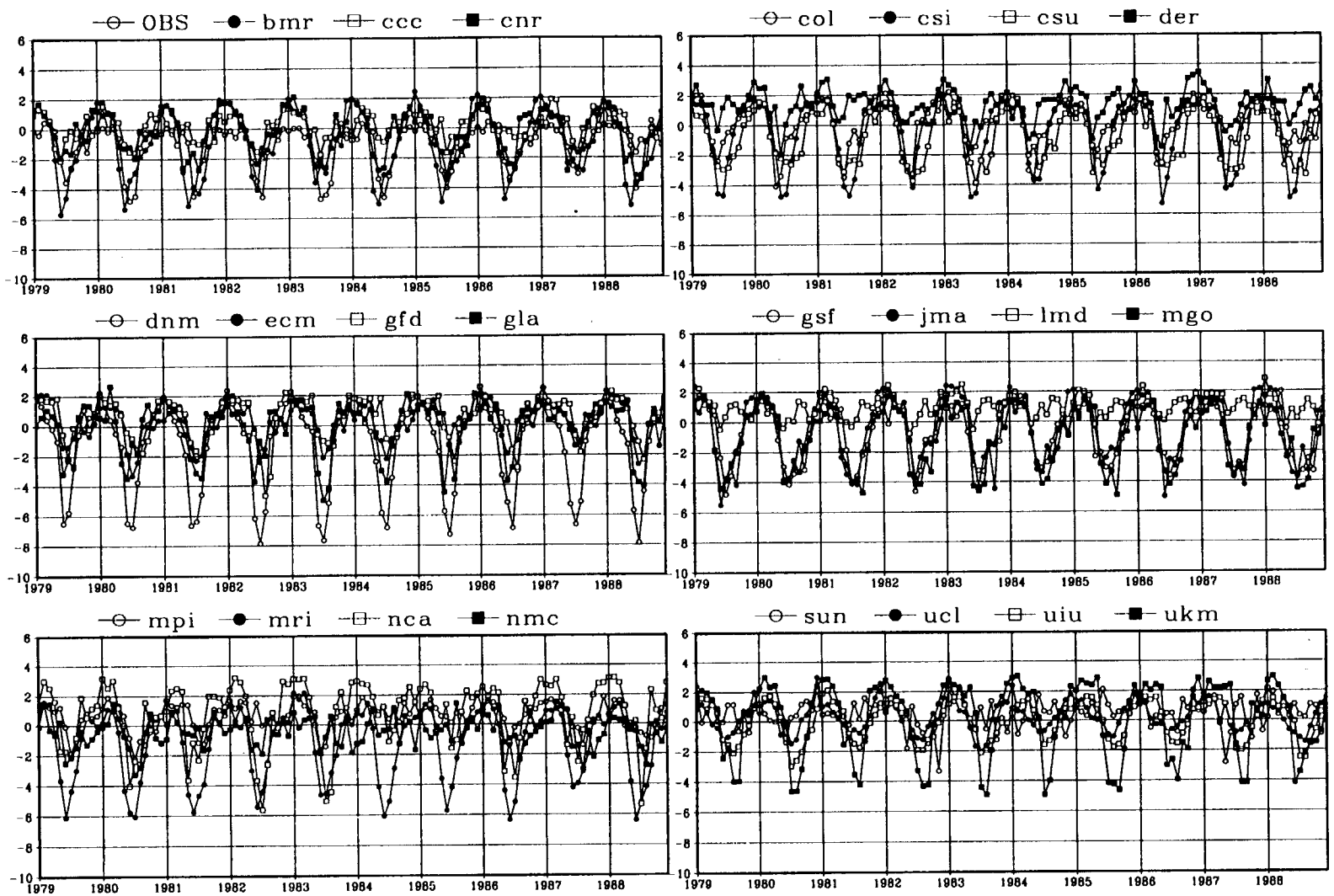

Figure 14 (continued)

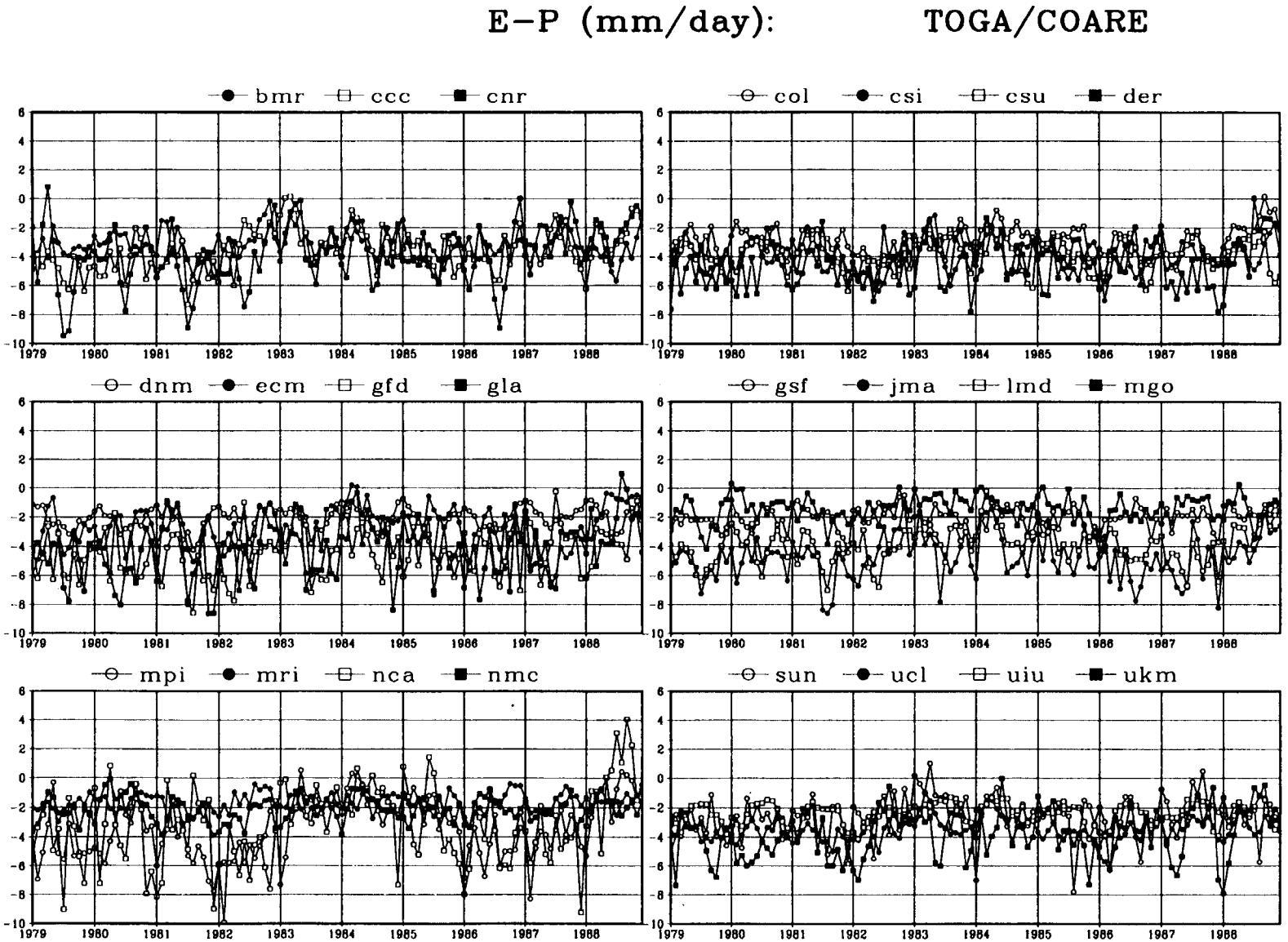

Figure 14 (continued)

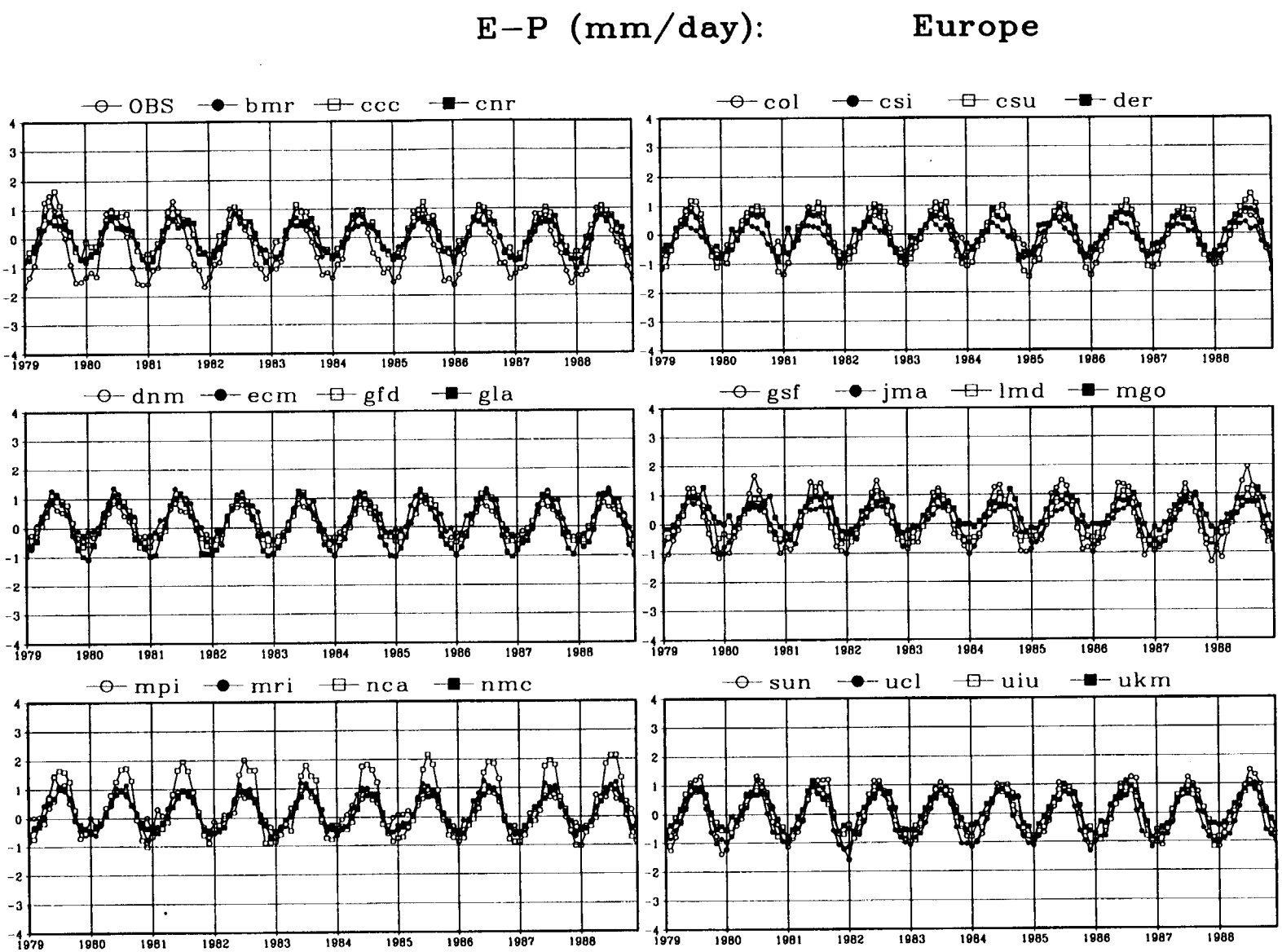

Figure 14 (continued)

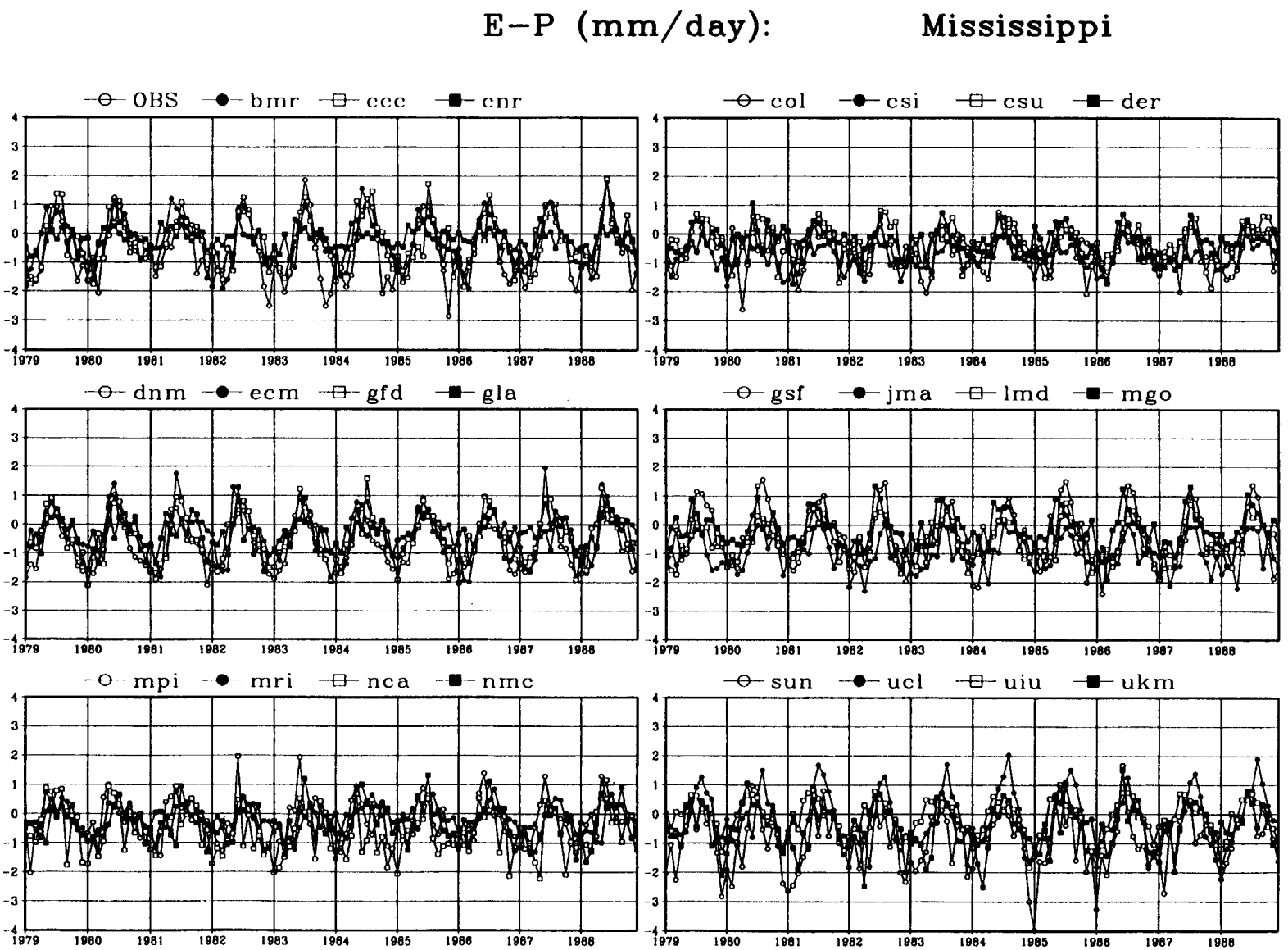

Figure 14 (continued)

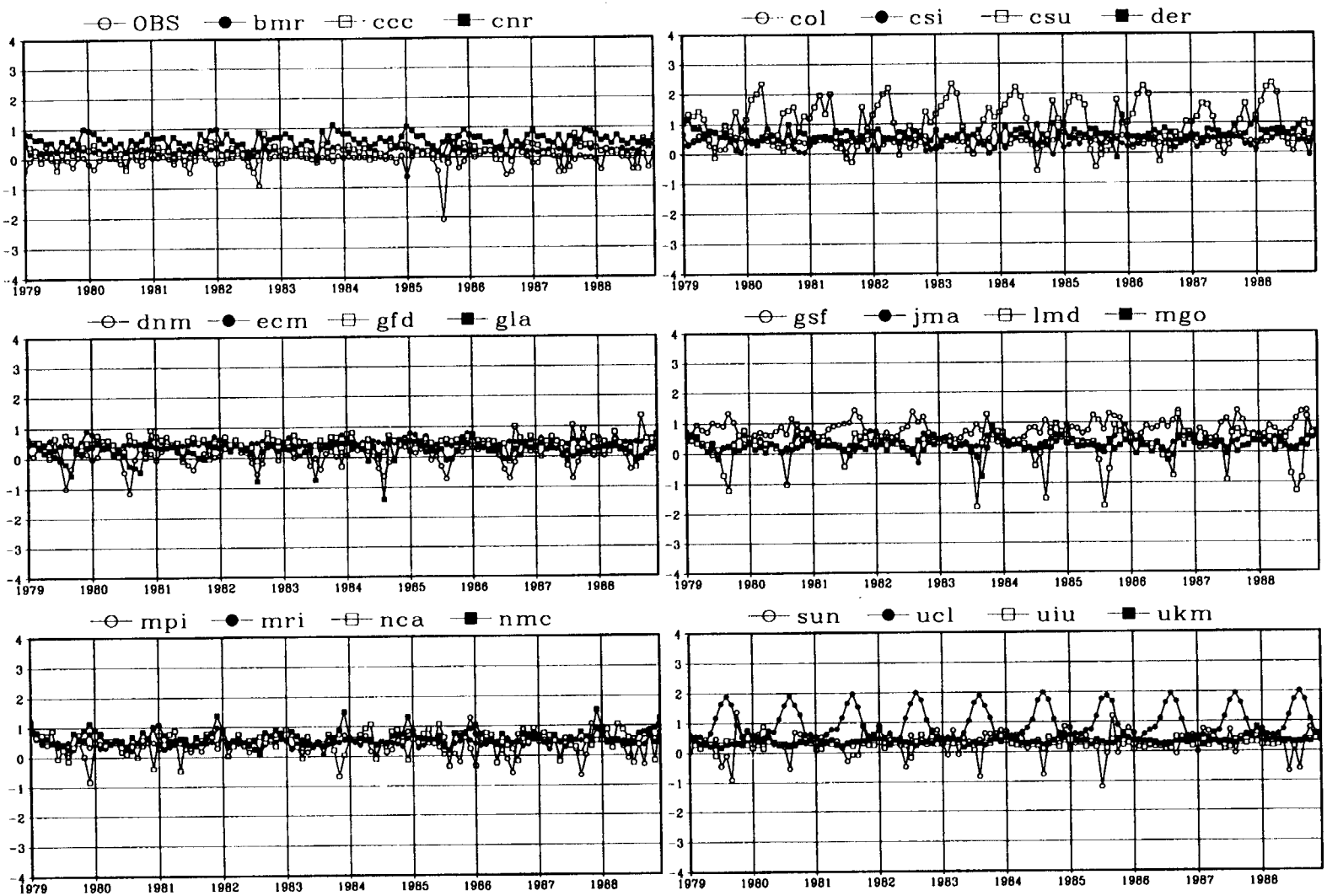

Figure 14 (continued)

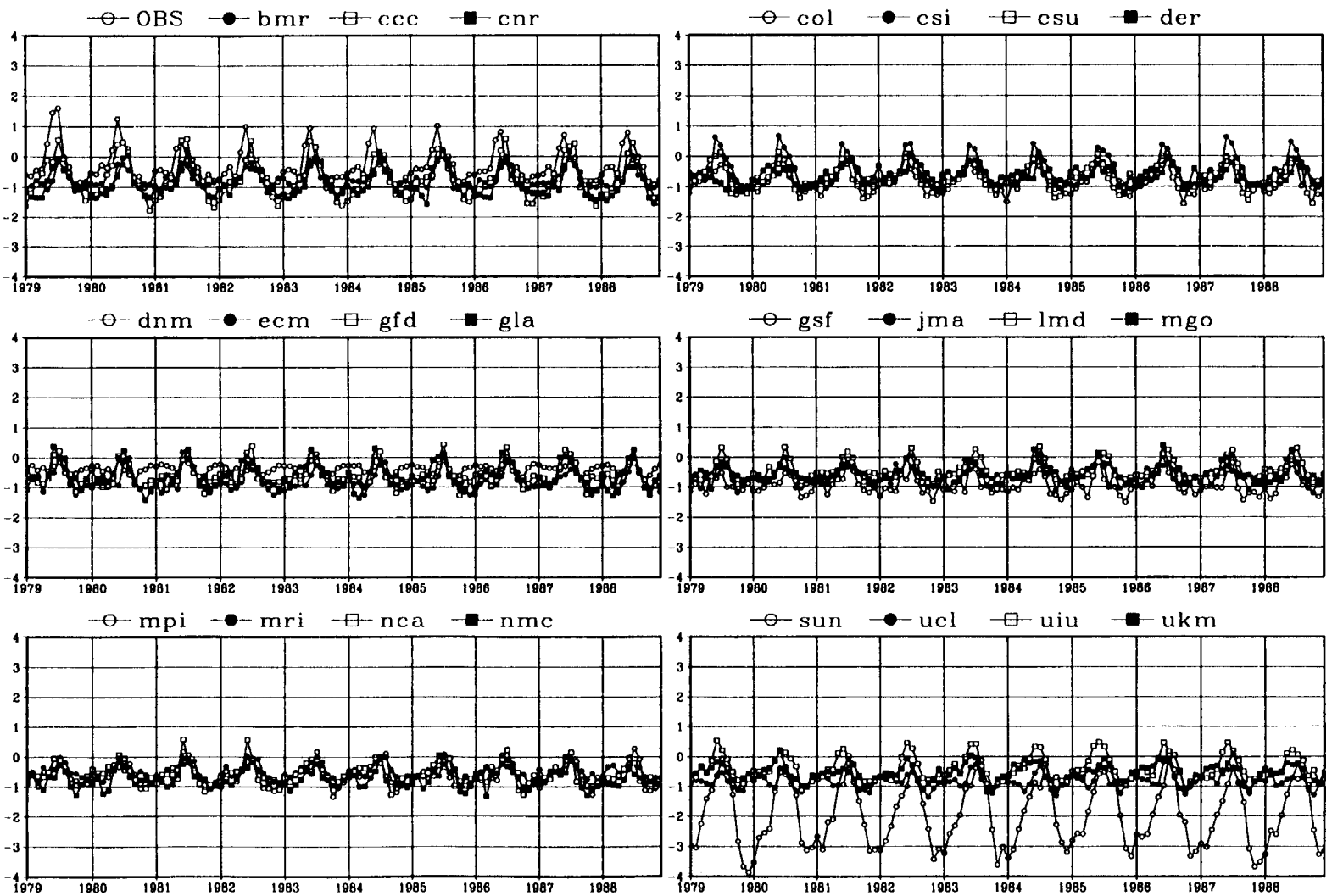

Figure 14 (continued)

Koeppen Climate Classification

by Climatological Monthly Mean Rainfall and Surface Air Temperature

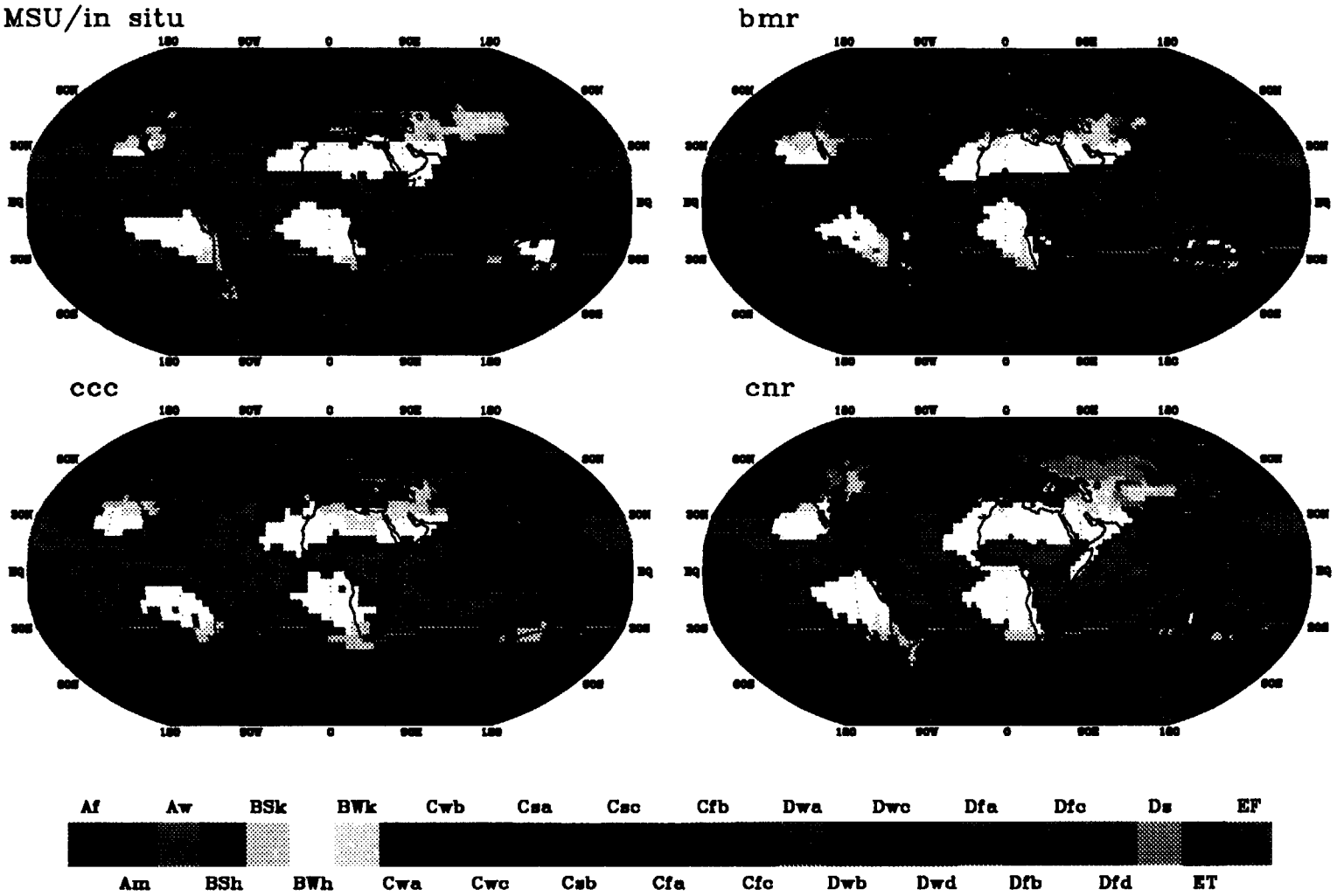

Figure 15

Koeppen Climate Classification

by Climatological Monthly Mean Rainfall and Surface Air Temperature

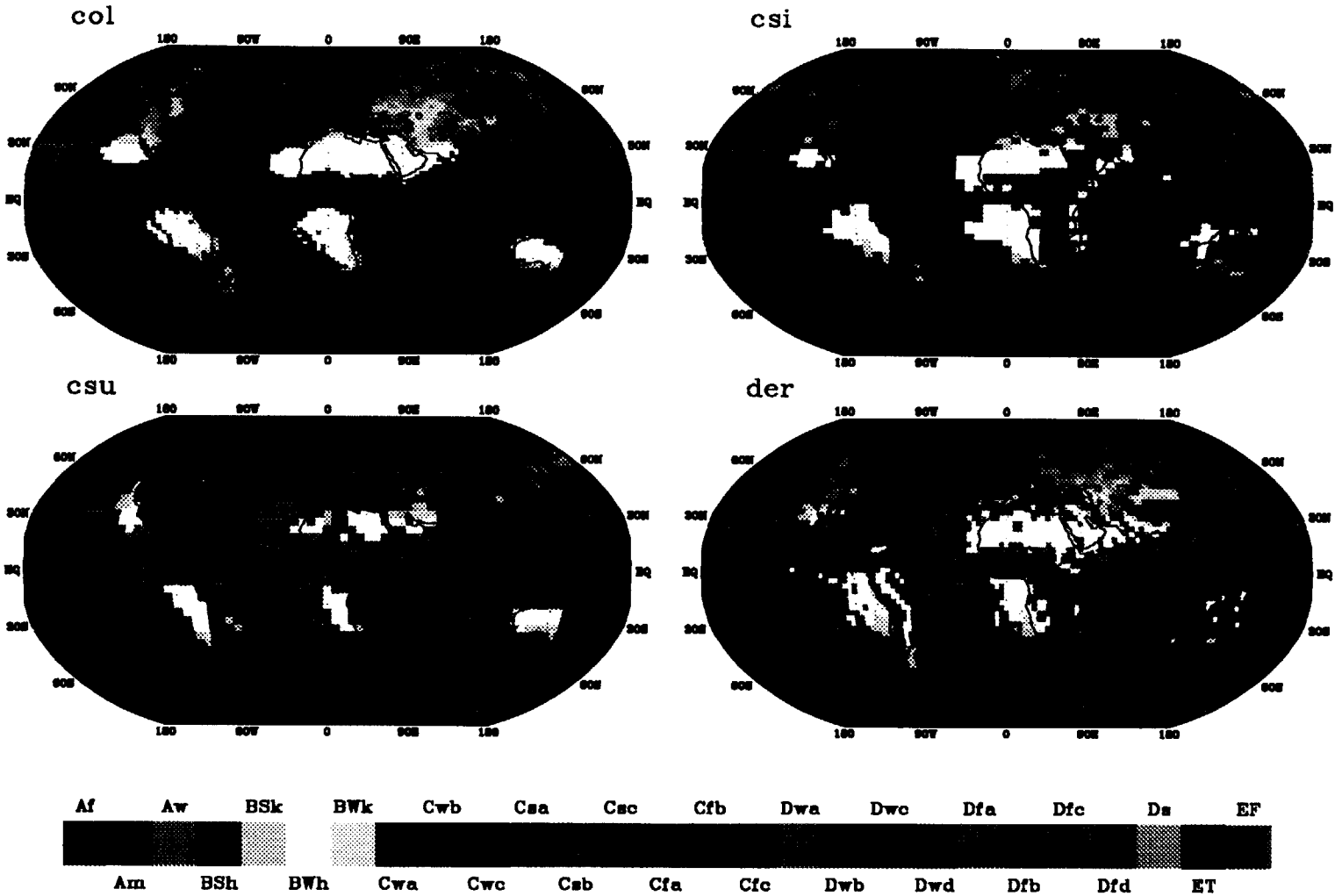

Figure 15 (continued)

Koeppen Climate Classification

by Climatological Monthly Mean Rainfall and Surface Air Temperature

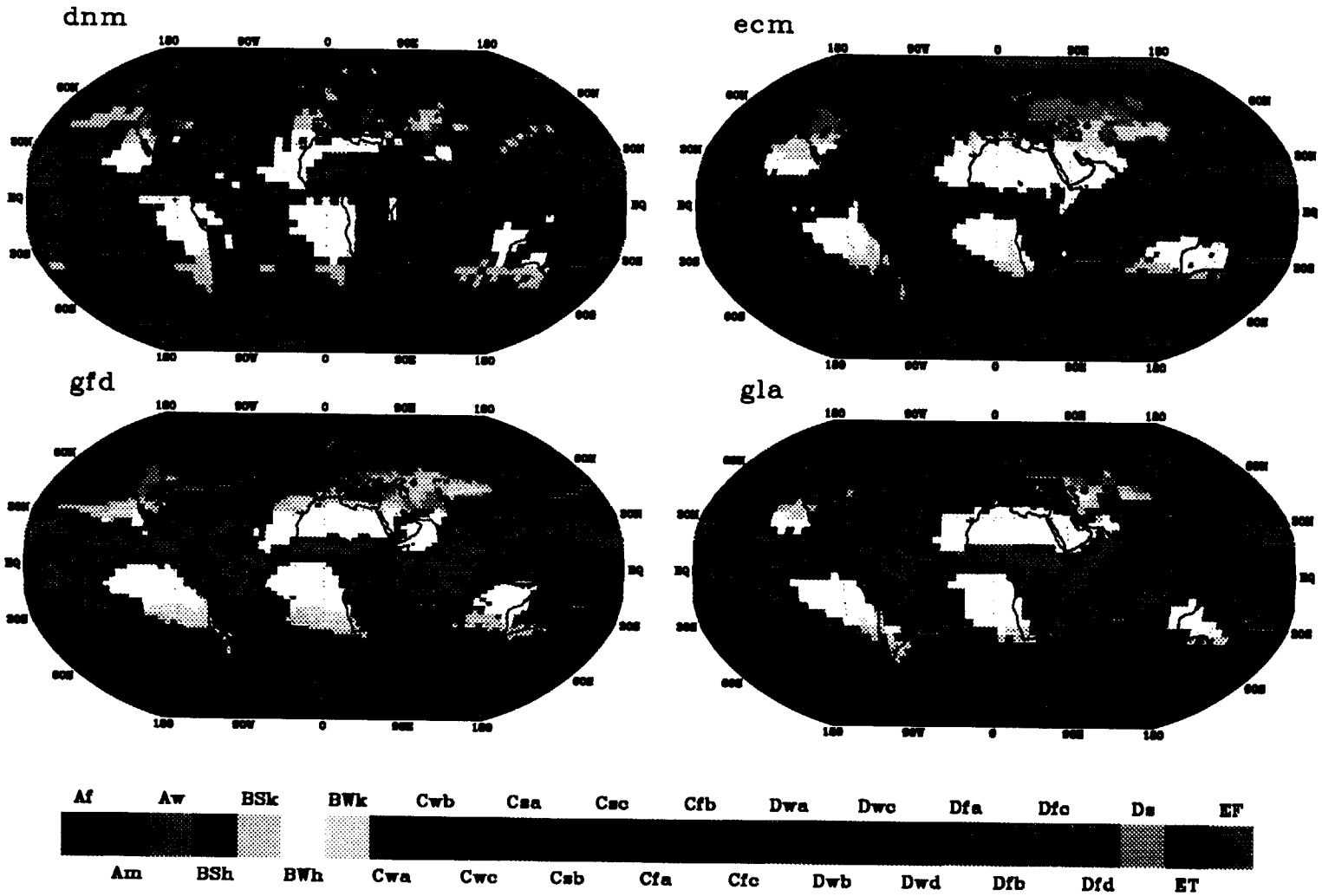

Figure 15 (continued)

Koeppen Climate Classification

by Climatological Monthly Mean Rainfall and Surface Air Temperature

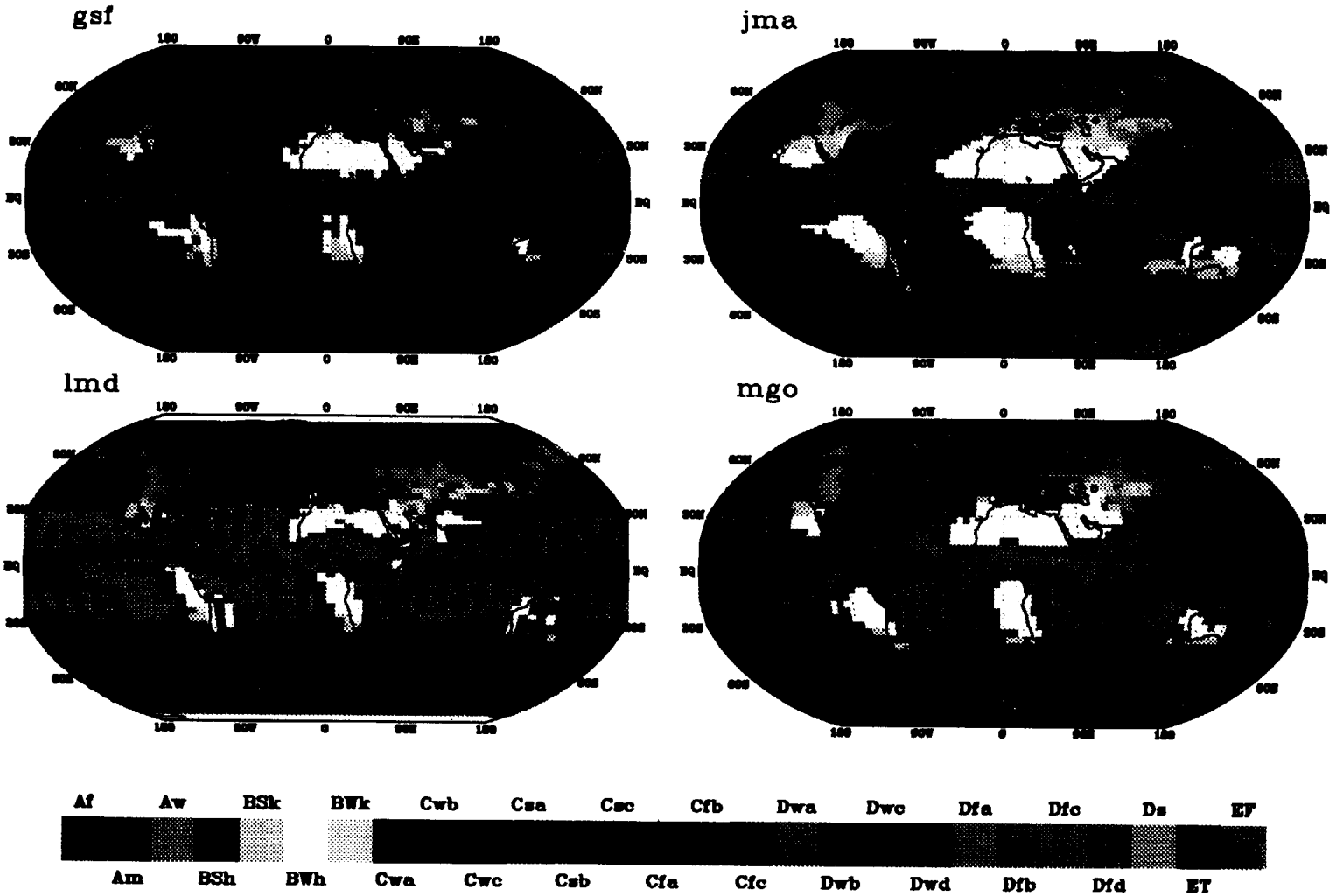

Figure 15 (continued)

Koeppen Climate Classification

by Climatological Monthly Mean Rainfall and Surface Air Temperature

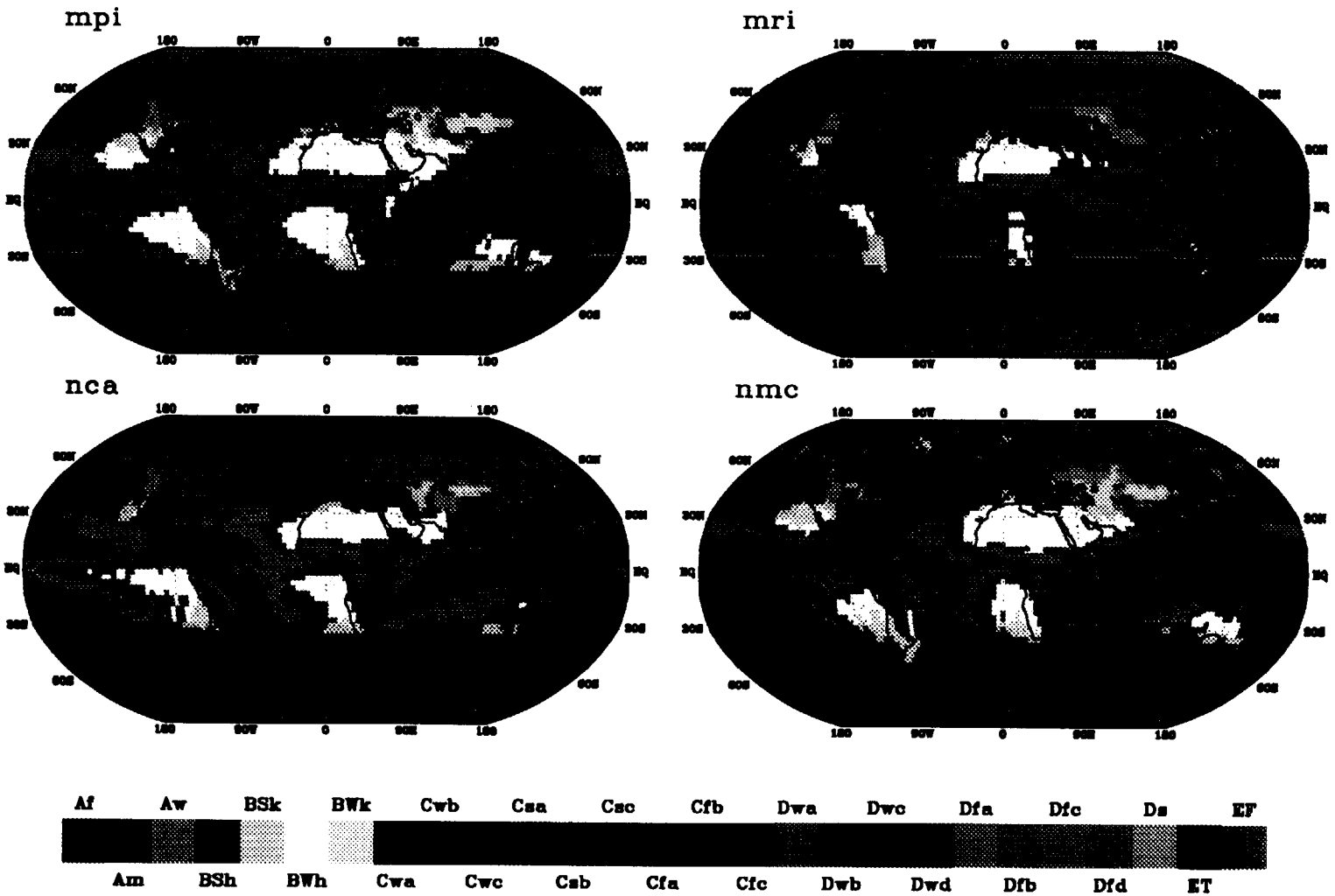

Figure 15 (continued)

Koeppen Climate Classification

by Climatological Monthly Mean Rainfall and Surface Air Temperature

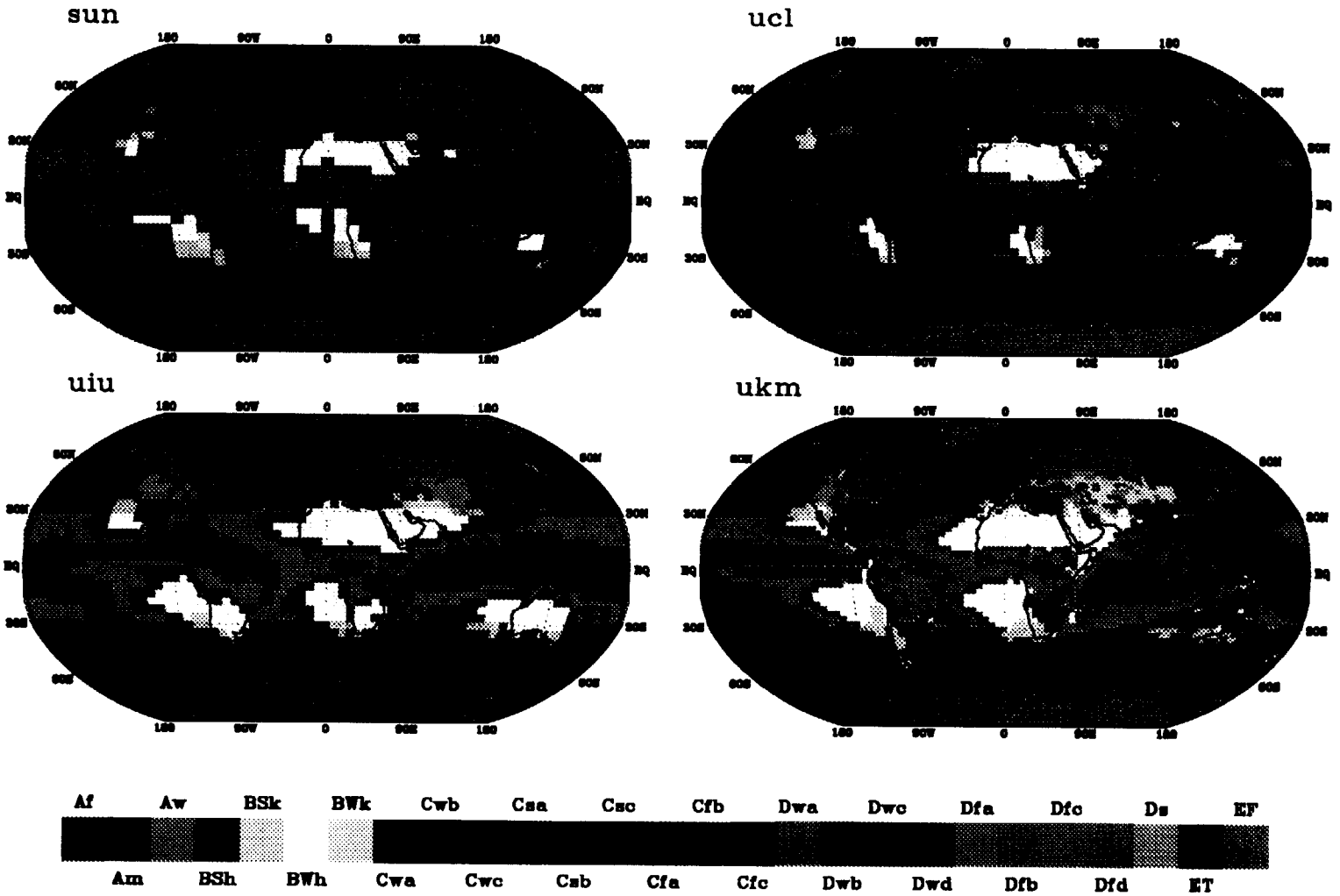

Figure 15 (continued)